Ph.D Thesis Dissertation

Thesis defended on the 12th of September 2016 to obtain the degree of Doctor in Electrical Engineering

by

Vasiliki Klonari

Probabilistic Analysis of Low Voltage Distribution Networks with Distributed Generation

Members of the Jury

Prof. Dr.ir. Francis Moiny (UMONS, Chairman)

Prof. Dr.ir. Bruno François (Ecole Centrale de Lille, External member)

Prof. Dr.ir. Emmanuel De Jaeger (UCL, External member)

Prof. Dr.ir. Pierre-Etienne Labeau (ULB, External member)

Dr.ir. Bart Meersman (UGENT, External member)

Prof. Dr.ir. Sébastien Bette (UMONS, Secretary)

Prof. Dr.ir. Jacques Lobry (UMONS, Co-promoter)

Prof. Dr.ir. François Vallée (UMONS, Promoter)

September 2016

Ph.D. Thesis developed at the Power Electrical Engineering Unit

Summary

This study investigates the problem of long-term analysis and development of Low Voltage (LV) distribution networks with Distributed Generation (DG). The focus is on developing proper methodologies for reliably modeling the operation of LV networks, by taking account of the inherent uncertainties. In this context, the challenge lies in identifying a way for efficiently simulating network operation states on which long-term analysis and design of the network should focus.

For simulating the stochasticity of nodal power exchanges in LV networks (generation- and consumption-wise), probabilistic models have been widely proposed in the related literature. Compared to deterministic worst-case models, probabilistic methods can at the same time identify extreme loading scenarios (in terms of impact on the principal network operation indices) while directing the interest of the analysis on the most possible situations. The accuracy of such models has been up to recently restricted due to the entire lack of observability (historic measurements) in LV networks. The recently launched and upcoming integration of smart metering (SM) devices in LV networks offers a new potential in this direction. Long-term historic measurements recorded at the premises of end-users, connected to LV feeders, can be exploited to enhance probabilistic simulation methods and to allow them to better represent the real operation of the network.

The present study aims at providing a method for taking advantage of the potential of combining probabilistic models with long-term historic measurements. To this end, a probabilistic framework is developed that uses Monte Carlo simulation for assembling a wide range of possible network states, in a given network, based on samplings from Smart Meter (SM) datasets, recorded in the respective network. In this way, the network state variability in a LV feeder can be simulated with time steps of one quarter of an hour. The principal operation indices that affect network planning and development can be statistically characterized based on feeder-specific measurements. Several technical strategies can be modeled, evaluated and refined to the needs of the studied LV networks thanks to the developed tool.

The proposed probabilistic framework has been applied for analyzing an existing three-phase LV feeder with distributed photovoltaic (PV) units equipped with SM devices. The LV feeder has been analyzed considering its actual condition and the integration of different distributed control schemes or technical strategies for increasing the integration of renewable energy resources while ensuring the quality of power supply. The simulated strategies include PV power curtailment for voltage rise mitigation, voltage unbalance mitigation, integration of electric vehicles and residential demand side management.

Plan of the thesis report

This thesis report is divided into two parts. Their contents are summarized hereafter.

Part I: Concepts, state-of-the-art and objectives' formulation

Chapter 1

The introductory Chapter 1 presents the impact of the integration of distributed renewable energy resources, and mainly distributed photovoltaic units, on the operation of Low Voltage networks. The most important operation indices that are affected by this integration are explained and discussed with regard to the existing regulation (European standards or local technical directives). In this way, the impact of volatile renewable energy resources and time-varying consumption loads on the long-term analysis and design of Low Voltage networks is introduced. Based on this analysis, the major modeling challenges concerning the simulation of Low Voltage networks, with distributed generation, are highlighted.

Chapter 2

A literature review about existing and currently applied methodologies for the simulation of Low Voltage networks is presented. The findings of this review are used in order to formulate the problem that will be treated by this thesis. In this way, the focus is set on probabilistic methods developed for the simulation of Low Voltage distribution networks. The strong and weak points of the existing probabilistic methods are discussed. Based on this analysis, Chapter 2 presents the main objectives of this thesis concerning the development of reliable probabilistic algorithms that can exploit the available smart metering measurements in Low Voltage networks.

Part II: Original Contributions

Chapter 3

This chapter presents the collection, treatment and analysis of a principal asset that has supported the development of the present study, namely the historic smart metering measurements of end-users connected to the Low Voltage network of Flobecq (Belgium). The procedure that has been implemented, by our research team, for collecting and treating the available smart metering recordings (to which we had access thanks to ORES support, the local Distribution System Operator) is explained step by step. This information is primordial for under-

standing the development of the probabilistic algorithms proposed in the following chapters.

Chapter 4

This chapter presents the basic structure of a probabilistic algorithm that has been developed for deploying long-term observability analysis of the Low Voltage network with the use of historic smart metering measurements. The developed methodology and the respective algorithm can model Low Voltage network uncertainty and redirect long-term network planning towards the most frequent network states rather than the extreme ones. The application of the developed algorithm in order to analyze an existing Low Voltage network and to compare the obtained outputs with real-case voltage measurements is also presented. This chapter also presents a clustering methodology for exploring the potential correlation of photovoltaic generation and energy consumption of end-users located in a close geographical area. Finally, a statistical load and generation modelling methodology for addressing the presence of sparse metering data, when deploying long-term analysis of Low Voltage networks, is outlined.

Chapter 5

Chapter 5 presents the implementation of the basic structure of the probabilistic methodology, developed in Chapter 4, for simulating the operation of an existing three-phase Low Voltage feeder located in the city of Flobecq (Belgium). The implementation of a probabilistic approach gives a detailed statistical analysis of the values that the various network operation indices can take. In this way, extreme worst-case values are computed and probability functions are constructed for each studied time step at each node of the network. Critical nodes are identified and statistically characterized in terms of technical constraints' violation.

Chapter 6

Chapter 6 presents a probabilistic methodology for estimating the photovoltaic hosting capacity of a given feeder, considering a set of predefined photovoltaic units' location scenarios, with the use of models based on feeder-specific measurements. The outputs of the methodology are compared to the ones of a typical deterministic approach that also uses feeder-specific historic measurements.

Chapter 7

Chapter 7 presents the adaptation of the basic probabilistic algorithm of Chapter 4 in such a way that it can simulate the action of different distributed time-varying control schemes against voltage rise and voltage unbalance. Five control schemes are modeled and compared. In this way, a reliable long-term assessment of the evaluated control schemes, which considers an extensive range of possible system states rather than a set of deterministically defined ones, is pre-

sented. The stochasticity of nodal loads and generation and their interaction with the respective control schemes is modeled, leading to a more refined design of each control strategy for a given feeder.

Chapter 8

Chapter 8 presents the restructuring of the basic probabilistic algorithm of Chapter 4 so that it can simulate three "load modification" strategies. The first two strategies concern the integration of electric vehicles in Low Voltage feeders (one plug-in hybrid electric vehicle charging station, in section 8.1, and several e-bike charging stations, in section 8.2). The third one deals with the integration of demand side management actions implemented by residential end-users as a response to a specially tailored distribution tariff scheme. The probabilistic modeling of time-varying electric vehicles' charging profiles and demand side management actions in Low Voltage feeders allows considering the volatility of the Low Voltage network state in the long-term evaluation of such schemes. Moreover, the use of feeder-specific historic measurements increases the accuracy of the assessment.

Chapter 9

The general conclusions of the presented thesis and the future perspectives are presented in Chapter 9.

Table of contents

List of figures

List of tables

List of acronyms

AC	Air Condition
CBA	Cost Benefit Analysis
CD	Clothes Dryer
CDF	Cumulative Distribution Function
CW	Clothes Washer
DER	Distributed Energy Resource
DG	Distributed Generation
DR	Demand Response
DSM	Demand Side Management
DSO	Distribution System Operator
DW	Dish Washer
EDSO	European Distribution System Operators
EU	Europe/ European
EV	Electric Vehicle
IEEE	Institute of Electrical and Electronics Engineers
LC	Load Curtailment
LS	Load Shifting
LV	Low Voltage
MC	Monte Carlo
MPP	Maximum Power Point
MPPT	Maximum Power Point Tracking
MV	Medium Voltage
NSMC	Non Sequential Monte Carlo
OPEX	Operational Expenses
OV	Overvoltage
P/V	Active Power/Voltage
PCC	Point of Common Coupling

PDF	Probability Distribution Function
PF	Power Flow
PHEV	Plug-in Electric Vehicle
PLF	Probabilistic Load Flow
PMU	Phasor Measurement Unit
PQ	Power Quality
PV	Photovoltaic
Q/V	Reactive Power/Voltage
QSMC	Quasi Sequential Monte Carlo
RMS	Root Mean Square
RTP	Real-time Pricing
SLP	Synthetic Load Profile
SM	Smart Meter/ Smart metering
SMC	Sequential Monte Carlo
SoC	State of Charge
TDP	Typical Day Profile
ToU	Time-of-Use
UV	Undervoltage
VBD	Voltage-based Droop
VUF	Voltage Unbalance Factor
3ph-DPC	Three-phase Damping Control
3ph-SI	Three-phase Symmetrical Injection

List of symbols

a	voltage angle
$a_{d,q}$	load of appliance *d* in time step *q*
$a_{d,q}^{DSM}$	desired load of appliance *d* in time step *q*
AER	total distance that PHEVs can cover running on an all-electric mode (km)
b	constant-power band width in the P/V control (p.u.)
c	class interval
$\boldsymbol{c_D}$	number of demand components in a LV feeder
$\boldsymbol{c_G}$	number of dispersed generation components in a LV feeder
C_q	optimal length of class interval at time step q
C^{PHEV}	energy obtained from PHEV charging (Wh)
C_{max}^{PHEV}	maximum capacity of PHEV battery (Wh)
CDF_{ref}	standardized reference CDF for PV generation in a specific feeder, based on the measurements of the available SM devices in the feeder
$\underline{CDF_s^{\text{q}}}$	cumulative distribution function of probability for *s* Monte Carlo iterations computed for time step *q*
$\text{cosphi}_{\text{cons}}$	power factor of power withdrawal from the LV network
$\text{cosphi}_{\text{inj}}$	power factor of PV power injection to the LV network
d^{PHEV}	energy given from PHEV discharging (Wh)
e^n	cost of energy absorbed from the grid, at time slot *q*, according to a pricing scheme ($)
E	droop convergence tolerance [W]
$E_{\text{curt.mean}}$	daily average curtailed energy [Wh]

$E_{\text{bikes,i}}$	total ¼-hourly required charging energy by the e-bikes charging station connected to node *i* [Wh]
$E_{\text{cons,grid,q,i}}$	total ¼-hourly energy withdrawal from the network at time step *q* at node *i* [Wh]
$E_{\text{i,d}}$	total ¼-hourly PV energy generation recorded at node *i*, during a given time step *q*, of day *d* [Wh]
$E_{\text{i,j}}$	total ¼-hourly energy flow of end-user *j* pertaining to network component *i* [Wh]
$\overline{E_{i,j}}$	normalized total ¼-hourly energy flow of end-user *j* pertaining to network component *i* [Wh]
$E_{i,j}^{tot}$	total annual energy consumption of end-user *i* pertaining to network component *i* [Wh]
$E_{\text{i,q}}$	total ¼-hourly consumed or injected energy at node *i* during time step *q* [Wh]
$E_{\text{inj,grid,q,i}}$	total ¼-hourly injected PV energy at node *i* during time step *q* [Wh]
$E_{\text{inj,i,s}}$	total ¼-hourly injected PV energy at node *i* in simulated network state *s* [Wh]
$E_{\text{inj,pv,q,i}}$	total ¼-hourly generated PV energy at node *i* during time step *q* [Wh]
$E_{n_g}^{tot}$	annual consumed energy for node $n_g \in N_g$, with N_g the set of nodes assigned to cluster $g = 1, \dots, n_{c_G}$
$E_{n_d}^{tot}$	annual generated energy for node $n_d \in N_d$, with N_d the set of nodes assigned to cluster $d = 1, \dots, n_{c_D}$
E_{m_g}	vector of ¼-hourly consumed energy flows for node $m_g \in M_g \subseteq N_g$ equipped with SM device
E_{m_d}	vector of ¼-hourly generated energy flows for node $m_d \in M_d \subseteq N_d$ equipped with SM device
$E_{\text{load,q,i}}$	total ¼-hourly net energy consumption at node *i* during time step *q* [Wh]

$E_{\text{pv battery to bikes,i}}$	total ¼-hourly injected energy from PV battery to e-bikes charging station at node *i* [Wh]
$E_{\text{pv bikes,i}}$	total ¼-hourly generated energy from PV unit connected to e-bikes charging station at node *i* [Wh]
$E_{\text{tot,mean}}$	total daily injected energy [Wh]
$E_{\text{cons,grid}}$	total ¼-hourly consumed energy from the LV network [Wh]
$E_{\text{cons, grid,sm}}$	total ¼-hourly recorded by the SM energy consumption at node *i* [Wh]
$E_{\text{inj,pv}}$	total ¼-hourly generated PV energy [Wh]
$E_{\text{inj,grid}}$	total ¼-hourly injected PV energy to the grid [Wh]
$E_{\text{inj, grid,sm}}$	total ¼-hourly recorded by the SM energy injection at node *i* [Wh]
$E_{\text{inj, grid,sm}}$	total ¼-hourly recorded by the SM energy generation at node *i* [Wh]
$E_{\text{load,wd}}$	total ¼-hourly net energy generation on a weekend day, during a given time step [Wh]
epsilon	error between two consecutive droop attempts [W]
f	network frequency [Hz]
f_i	reference factor for scaling the normalised CDF_{ref} in function of $P_{\text{rated,l}}$
G_1	fundamental output conductance
G_d	damping conductance
h	matrix of differences of cumulative probabilities $P(X \leq x)$ that a computed value falls within each one of the defined classes [x_1, $x_2 \ldots x_n$].
I_{abc}	matrix of line currents (phase components) [A]
$I_{\text{load,012}}$	matrix of nodal currents (sequence components) [A]

$I_{\text{load,abc}}$	matrix of nodal currents (phase components) [A]
$I_{\text{j,j+1}}$	line current between nodes *j* and *j+1* [A]
k	coefficient defining the slope of P/V droop control
k_t	total number of values, recorded at a given time step *q*, which belong to interval *c*
N	total number of nodes in a LV feeder
N_d	number of end-users in a LV feeder equipped with SM device
N_q	number of values recorded by the SM during a given time step *q*
N_d	number of days in a month
N_{PV}	number of end-users in a LV feeder equipped with a PV unit
N_{tdp}	number of values in a TDP profile
N_{SM}	number of end-users in a LV feeder equipped with SM device
N_y	number of years for which SM historic measurements at given node or feeder are available
$P_{\text{bikes,i,q}}$	total required charging power for the currently present bikes at node *i* [W]
$P_{\text{i,s}}$	active power flow at node *i* in network state *s* [W]
p_F^q	overall building energy demand in time step *q*
$P_{\text{MPP,i,s}}$	maximum active power point at node *i* in network state *s* [W]
$P_{\text{network to bikes, i}}$	active power withdrawal for charging the e-bikes station connected to node *i* [W]
$P_{\text{j,d}}$	active power flow at node *j* on day *d* at a given time step [W]
$P_{\text{j+1,N}}$	sum of active loads $P_{\text{load,i}}$ (simple end-user without PV generation) and active PV power injections $P_{\text{inj,pv,i}}$ flowing between node *j+1* and node *N* [W]
$P_{\text{load,i}}$	active load at node *i* [W]

$P_{load,MC,i}$	active power withdrawal sampled from the MC algorithm at node *i* [W]
$P_{loss,\ i+1}$	active power losses in the line segment connecting nodes *i* and *i+1* [W]
$P_{rated,l,i}$	new installed PV power at node *i* in configuration *l* [W]
$P_{rated,ref}$	installed rated power of the PV unit that has been used to normalize CDF_{ref} [W]
$P_{step,i}$	increase step of the installed rated power of the PV unit at node *i* [W]
P_{12}	active power that flows between nodes 1 and 2 [W]
p_c	the probability that a recorded item belongs to a specific energy interval *c*
P_i^{DSM}	the final curtailed load that can be applied at node *i* in the context of a DSM strategy without resulting in any technical parameters violation in the feeder [W]
$P_{overvoltage}$	overvoltage probability
$P_{unbalance}$	Probability of exceeding voltage unbalance limit
$P_{undervoltage}$	undervoltage probability
Q_{ev}	number of time slots in the scheduling periods for PHEVs charging
$Q_{j+1,N}$	sum of reactive loads $Q_{load,i}$ (simple end-user without PV generation) and reactive power injections from PV inverters $Q_{inj,pv,i}$ flowing between node *j+1* and node *N* [Var]
$Q_{loss,\ i+1}$	reactive power losses in the line segment connecting nodes *i* and *i+1* [W]
$Q_{pv,i}$	reactive power injection from PV inverter at node *i* [W]
Q_{12}	reactive power that flows between nodes 1 and 2 [W]
q	index of the simulated ¼-hourly time step [1→96]

R	line resistance (Ohm)
R’	line resistance per kilometer (Ohm/km)
R_q	range of recorded values at time step *q*
RV	number of random variables
s	index of simulated network state
S	total number of simulated system states
s_l	total distance that PHEVs can cover running on an all-electric mode (km)
$\boldsymbol{S}_{lateral,i}$	total transited power by each unbalanced lateral (per phase) [VA]
$\underline{\boldsymbol{S}}_{load,abc}$	Matrix of initial nodal loads (phase components) [VA]
$\underline{\boldsymbol{S}}_{load,012}$	Matrix of initial nodal loads (sequence components) [VA]
$\boldsymbol{S}_{load,x,i}$	nodal load at phase *x* at node *I* [VA]
$\boldsymbol{S}_{loss,i}$	power loss along line segment [VA]
SoC_Max	battery capacity [Wh]
SoC_i	state of charge of the battery connected to node *i* [Wh]
t	index of droop iteration
$t_{q,i}$	time repartition factor of $E_{inj,pv,q,i}$ or $E_{load,q,i}$ at node *i* during time step *q*
U_i	[*Dx96*] sized matrix of ¼-hourly energy use of *D* domestic appliances [Wh]
U_i^{DSM}	[*Dx96*] sized matrix of ¼-hourly energy use of *D* domestic appliances within the context of a DSM strategy [Wh]
U_i	voltage at the slack node [V]
$u_{inj,pv,i}$	randomly sampled value in the interval [0,1] for PV generation at node *i*

$u_{\text{load,we}}$	randomly sampled value in the interval [0,1] for load on a week day
$\underline{\boldsymbol{V}}_{\text{abc}}$	matrix of computed nodal voltages (phase components) [V]
$\underline{\boldsymbol{V}}_{012}$	matrix of computed nodal voltages (sequence components) [V]
$\underline{\boldsymbol{V}}_{\text{initial,abc}}$	matrix of initial nodal voltages (phase components) [V]
$\underline{\boldsymbol{V}}_{\text{initial,012}}$	matrix of initial nodal voltages (sequence components) [V]
$\boldsymbol{V}_{\text{MV/LV,q}}$	voltage at the MV/LV transformer node at time step *q* [V]
V_{n}	negative voltage sequence component [V]
V_{nom}	nominal voltage [V]
V_{p}	positive voltage sequence component [V]
V_{up}	upper reference of voltage in the P/V control [V]
X	line reactance [Ohm]
X’	line reactance per kilometer [Ohm/km]
$[Y_{012}^{z}]$	sequence components admittance matrix [S]
$\underline{y}_0^z, \underline{y}_1^z, \underline{y}_2^z$	zero, positive and negative sequence admittance matrices [S]
Z0,Z1,Z2	matrices of zero, positive and negative line impedance [Ohm]
$\underline{\theta}_{x,i}$	voltage angle at node *i* at phase *x* (°)
$\underline{\theta}_{abc}$	[3xN] vector of nodal voltage angles in a three-phase feeder with *N* end-users (°)

Chapter 1 Distributed Generation: Impact and Challenges in Low Voltage Networks

Highlights

- *The high volatility of distributed photovoltaic generation affects the operation of the Low Voltage network*
- *The variation of voltage magnitude and unbalance is the main concern even though other operation metrics are also affected.*
- *The EN 50160 standard deals with voltage magnitude and unbalance in the Low Voltage network with statistical or probabilistic terms.*
- *The volatility of network operation states should be reliably modeled to allow a cost-effective design that focuses on the most expected network states rather than the extreme ones.*
- *The available smart metering data can drastically enlarge the potential for reliable and cost-effective network planning and development.*
- *Long-term LV network models are subject to the following requirements: ability to balance the trade-offs of the various end-users' objectives and perspectives and flexibility to evolve with the changing mix of resources*

1.1 Impact on Operation Indices

During the recent years, a major challenge in the design of the energy system worldwide has been to maximize the share of renewable resources in the electric energy supply. In 2015, 28.9 GW of new power generating capacity was installed in the European Union (EU), 2.4 GW more than the one installed in 2014 (Figure 1.1) [1]. Wind power was the energy technology with the highest installation rate in 2015: 12.8 GW, accounting for 44% of all new installations. Solar photovoltaic (PV) came second with 8.5 GW (29% of 2015 installations) and coal third with 4.7 GW (16%). During 2015, Member States decommissioned 8 GW of coal capacity, 4.3 GW of gas, 3.3 GW of fuel oil, 1.8 GW of nuclear energy capacity, 518 MW of biomass and 281 MW of wind energy. The main driver for this trend is to increase the self-sufficiency of the network, based on local resources, while responding to the climate change. Concerning the Low Voltage (LV) distribution network in Europe, distributed PV generation is the mostly met Distributed Energy Resource (DER) [2].

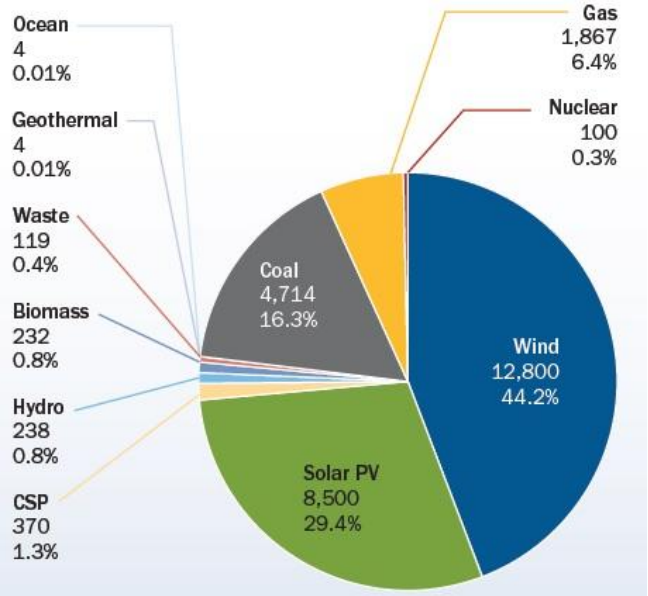

Figure 1.1: Repartition of new power generating capacity that was installed in the EU in 2015 [1]

So far, the biggest share of distributed PV units came with no strategic design or reinforcement of the network while monitoring data in the small-usage sector (residential or small business) were absent almost everywhere in Europe. Given the lack of visibility and controllability in common LV networks, the uncoordinated integration of distributed PV generation currently leads to power quality issues. In this evolving framework, illustrated in Figure 1.2, Distribution System

Operators (DSOs) are called to safeguard a stable and secure power supply in all possible demand conditions while fostering a massive DER integration. This task becomes even more complex in view of the upcoming integration of electric vehicles (EVs) and the development of flexibility services, both seen as basic components of the future electric energy system. The principal concerns regarding power quality in actual LV networks are thoroughly explained in the following paragraphs.

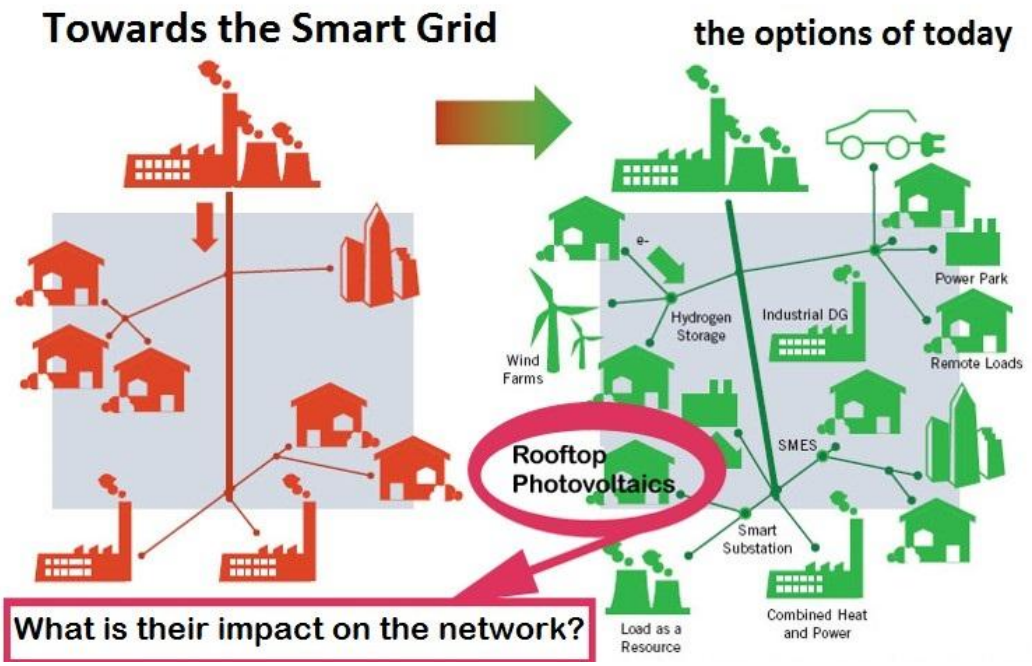

Figure 1.2: The numerous distributed PV units, dispersed in LV networks, result nowadays in power quality and cost-effectiveness problems [3]

1.1.1 *Voltage profile variation*

Concerning steady operation conditions, the main concern in LV networks with distributed PV generation is voltage profile. Traditionally, in the electric power networks, the power generated by large generation plants was delivered to the end-users through distribution networks. Therefore, the flow of power was from the higher towards the lower voltage levels. With the introduction of the Distribution Generation (DG) units, the power flows may be reversed. The LV distribution network is no longer a passive circuit supplying loads but an active system with the power flow and voltage determined by the DG units as well as by the loads [6]. When a DG unit injects active power at a certain point of the system, the voltage of that node can be raised. This fact is explained as follows. Consider the radial system shown in Figure 1.3 [6].

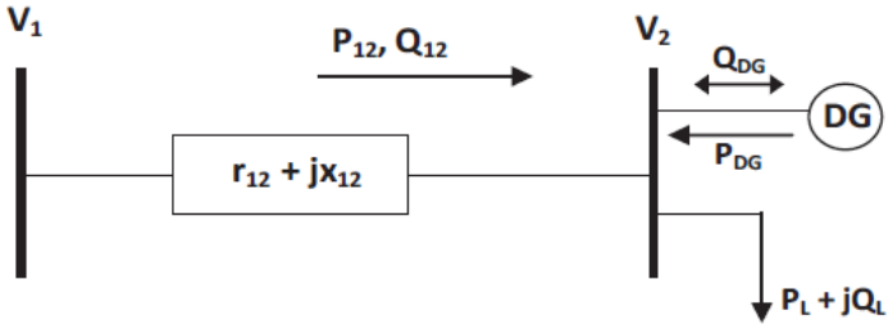

Figure 1.3: Part of a distribution system [6]

In case of no DG unit, the power flow between nodes 1 and 2 (P_{12} and Q_{12}) is equal to the load demand at node 2 (P_L + jQ_L). The voltage drop in per unit at node 2 can be given approximately by expression (1.1) [6]:

$$V_1 - V_2 = P_{12} \cdot r_{12} + Q_{12} \cdot x_{12} \tag{1.1}$$

where r_{12} and x_{12} are the resistance and reactance of the line between nodes 1 and 2. If the DG unit injects power at node 2, the power flow between nodes 1 and 2 is changed. In this case, expression (1.1) must be modified as follows:

$$V_1 - V_2 = (P_L - P_{DG}) \cdot r_{12} + (Q_L \pm Q_{DG}) \cdot x_{12} \tag{1.2}$$

where P_{DG} and Q_{DG} are active and reactive powers of the DG unit. Based on expression (1.2), when the active power injected by the DG unit increases, the term $(P_L - P_{DG})$ can become sufficiently negative so that the right side of expression (1.2) becomes negative that means V_2 is greater than V_1. In such cases, the injection of DG power can cause a voltage rise problem, especially when the x/r ratio is low, which is the case in distribution systems.

Consequently, as it can be observed, the amount of voltage variations depends on the amount of DG units' active and reactive powers, the demand of loads and the impedance of the system lines. Due to the fact that demand of loads and DG units' active powers are changing during the day, both voltage rise and voltage drop problems are possible to occur. The voltage control problem is known as one of the biggest obstacles for increasing the integration of DG units in LV distribution networks. If this problem can be solved efficiently, then higher DG levels could be allowed for connection to LV feeders.

Therefore, the extremely high volatility of PV generation has a severe impact on the variation of voltage profile in such networks (Figure 1.4). According to the European standard EN 50160 [4], [5], the DSO is responsible for maintaining voltage profile within certain limits (within the range of V_{nom} ± 10 %) during at least 95% of the weekly operation time. If the RMS voltage at a certain PV node exceeds the upper limit suggested in the EN 50160 standard, an overvoltage

event takes place and the PV unit must be temporarily cut off [7]. Such cut-offs induce a loss of generated PV power which means a loss of income for the PV system owner. Furthermore, this hard curtailment of PV generation deteriorates the delivered power quality, due to significant voltage and current transients, and accelerates the degradation of the PV inverters [2], [8], [9].

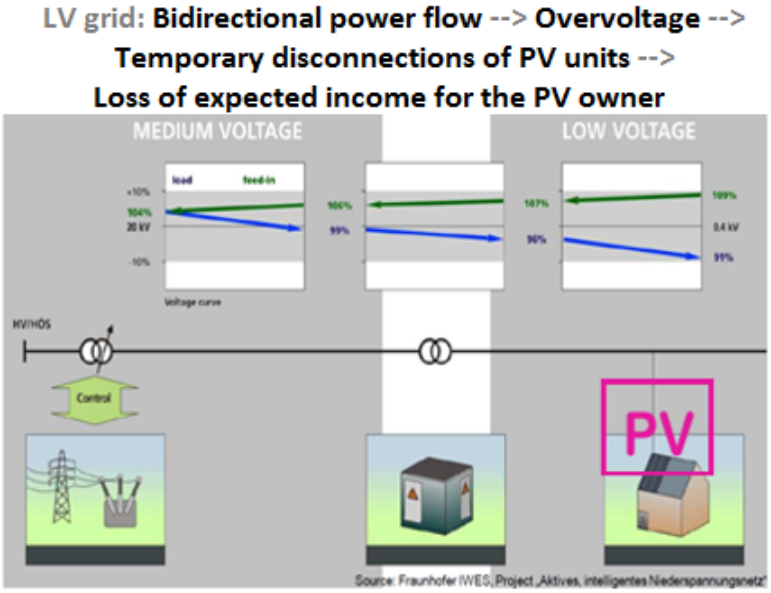

Figure 1.4: Voltage rise is the main concern in LV networks with distributed PV generation

1.1.2 *Voltage phase unbalance*

Voltage magnitude variation is the key issue in LV networks with PV units. However, this is not the only concern. In three-phase LV networks, unbalanced loading and generation lead to unequal voltage magnitudes over the three phases of the network. This can be explained as follows. Let's consider the very simple case of the three-phase LV distribution feeder of Figure 1.5(a) [10], with only one 5 kVA PV unit connected at its end, in single-phase mode. The distribution feeder can be modeled by its series resistance and reactance while the PV unit is modeled by a current source, as illustrated in Figure 1.5(a). The power factor of PV injection is considered equal to one.

As explained in [10], the current injected in the feeder by the PV unit flows in the phase to which it is connected (i.e. phase *b*, in this particular case) and in the neutral conductor, causing voltage variations which are actually observed on all the three phases, according to the phasor diagram shown in Figure 1.5(b). In this simple illustrative case, it can be seen that the phase-to-neutral voltage level is increased for two of the phases (especially the one to which the PV unit is connected), while decreased for the third one, due to the phasor voltage drop on the neutral conductor.

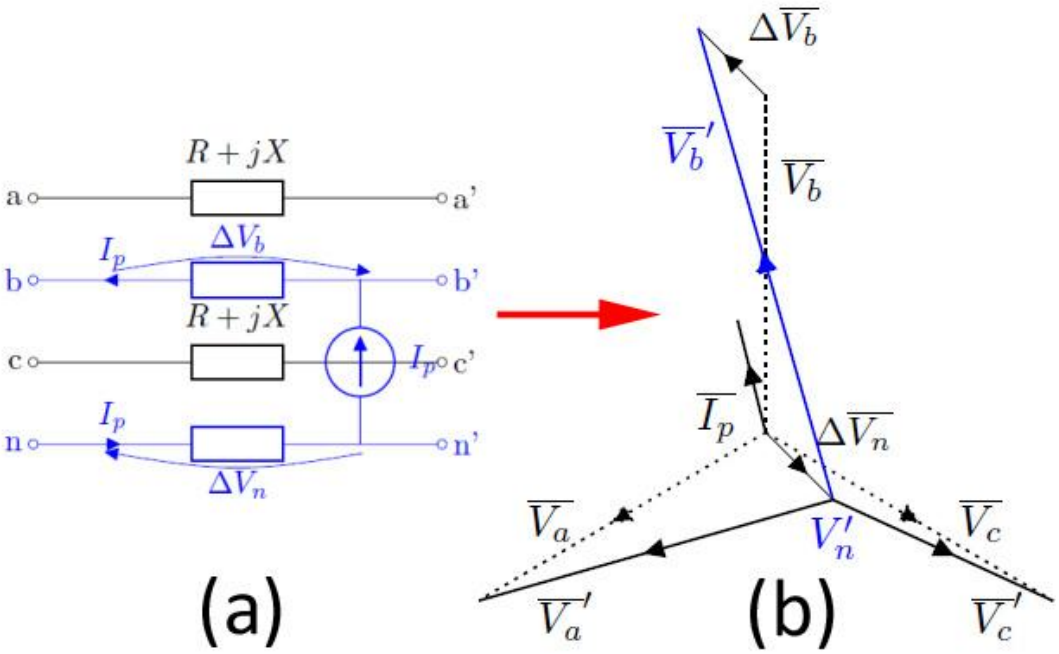

Figure 1.5: (a) Simplified version of a three-phase feeder with a single-phase PV unit connected at its end, (b) Phasor diagram of the three-phase voltage at the end of the feeder

Consequently, the increased current in the neutral conductor, due to unbalance, results in neutral-point shifting which can be disadvantageous for the voltage profile [11]. Voltage unbalance adversely affects network elements and connected equipment [12]–[17]. Under unbalanced conditions, the network induces more losses and heating effects. A small unbalance in phase voltages can result in a disproportional unbalance in phase currents which can overheat connected equipment, reduce its efficiency and shorten its life. Although restrictions on unbalance of assets are imposed since the 1950s [12], [13], it has always been a challenging issue which emerges nowadays due to the on-going single-phase connection of DG sources.

1.1.3 *Congestion risk*

Overvoltage mainly affects the power quality of rural LV networks. Rural LV feeders are characterized by much longer lines with a reduced number of powered households. In case of urban grids the maximum loading current is a significant power quality concern given that they supply many households in a small area; the transformer capacity and the number of connected users are high and the length of lines is short. As a result, congestion risk may grow during periods of high PV injection coming from multiple end-users. Furthermore, in case of EVs

and demand response (DR) integration in LV networks, this phenomenon could continue to increase, especially during peak consumption periods in a day.

1.1.4 *Other concerns*

At the same time, reverse power flows due to high PV injection can significantly increase line losses [18], [19]. Line losses are practically an economic index since the cost that they induce has to be covered by the DSO as part of the operational expenses (OPEX) of the distribution network. The cost of line losses can be monetized as energy consumption that can only be partially included in the network use tariff, in most EU countries. Indeed, in most cases, the volumetric component of the network use tariff is a function of the energy consumption of the user, without incorporating line losses. Consequently, the DSO has a clear economic interest in reducing this parameter, especially in countries that have adopted a "Revenue cap" methodology framework for the use of the distribution network [20].

Finally, the introduction of distributed PV sources increases the risk of protection failure. Types of protection failure that can occur due to DG integration are thoroughly described in [8]. From a longer term perspective, occasional protection failure might be accepted by the DSO to allow more DG integration. However, quality of service must still be guaranteed from the end-user's point of view. Consequently, risk evaluation has to be addressed in the long-term LV network planning.

For increasing the PV hosting capacity of LV networks, it is highly recommended that policy and regulation bodies investigate the aforementioned operation metrics in an overall manner, giving equal honor to technical, long-term strategic and economic parameters. The problem is multidimensional and very challenging. The objective includes managing a fair allocation of costs while ensuring benefits and revenue opportunities to the multiple involved stakeholders, given that the reliability and quality of energy supply towards all end-users of the distribution network is not compromised in any manner.

1.2 Technical Standards

Among the previously mentioned steady-state operation metrics, only few are directly addressed by international or EU standards. The principal EU standard that focuses on the characteristics of electricity at the point of supply of the end-user (mainly in terms of voltage) is the EN 50160 standard [4]. According to this standard, electrical energy is a unique product because it is consumed at the moment of its generation. Consequently, measurement and evaluation of power quality (PQ) issues must also be instantaneous. The magnitude of the supply voltage for an individual network user at any instant is also a function of the current flows due to other network users. Therefore, voltage magnitude is determined both by the individual user's demand and by the simultaneous demand of other network users. Since the demand of every network user and the degree of coincidence between them constantly varies, so does the supply voltage seen by each user [5].

Based on this consideration, EN 50160 standard deals with voltage characteristics in statistical or probabilistic terms. It recommends that, for a percentage of measurements (e.g. 95%) over a given operation time, the studied value must be kept within specified limits. Under normal operating conditions during each weekly period, 95% of the 10-min mean RMS values of the supply voltage must stay within the range of $V_{nom} \pm 10$ %; similarly 100% of the 10-min mean RMS values of the supply voltage must be kept within the range of V_{nom} +15% / -15%. Also, under normal operating conditions, during each weekly period, 95% of the 10-min mean RMS values of the negative sequence component of the supply voltage shall be within the range of 0 to 2% of the positive-sequence component. The majority of international documents and regional or national standards give guidance for determining LV network unbalance in function of the negative-sequence component. The latter is considered to have a bigger influence on the network and the connected equipment compared to zero-sequence currents that can be mostly controlled by system design and maintenance [21], [22]. According to IEEE, the definition of voltage unbalance is the ratio of the negative-sequence voltage component to the positive-sequence voltage component [23], [24].

Regarding congestion management, there is no common EU legislation for the moment. However, the European Distribution System Operator's for Smart Grids (EDSO) recommends that the relevant EU legislation should be amended to include a new article on general principles of congestion management for distribution systems [25]. Meanwhile, international recommendations such as [26] or other customized technical specifications are applied by each DSO for respecting maximum line capacities in steady network operation.

Finally, concerning protection of LV networks, the EN 50160 standard requires that the network operator maintains short-circuit power at a sufficient level, without giving more detailed recommendations. Calculations and protection coordination are deployed based on established national and international practices [27]. The IEC Standard 60909 covers a large variety of voltage levels and configurations. However, it remains focused on the traditional power system paradigm without DG units. Recent studies propose methodologies that account for the impact of DG on short circuit capacity [28], [29].

The task of the DSO is to supply energy within the requirements of the EN 50160 standard unless there are more restrictive national or local regulations. **For facilitating the application of these standards along with the integration of DG in LV networks, reliable modeling tools are required.** The following paragraph defines the basic needs that such modeling methodologies should cover for achieving cost-effective network planning and development.

1.3 Modeling Challenges

The large deployment of smart metering (SM) devices and the automation of the distribution network are the upcoming milestones regarding power distribution. Long-term historic measurements (of 10-min or 15-min latencies) in the residential and commercial sector can drastically enlarge the potential of cost-effective distribution network analysis and planning approaches. Given the massive dispersed nature of distribution networks, the integration of automation will be undoubtedly stepwise while utilities will need to hierarchize the overall implementation. Indeed, the upcoming distribution automation will largely depend on reliable real-time state estimation techniques [30]–[32]. Considering that an operational system providing low-latency real-time state estimation by using Phasor Measurement Units (PMU) specifically tailored to the MV level has been only recently developed [33], one can assume that the automation of LV networks will not come for the foreseeable future.

Currently, the complete lack of real-time monitoring in LV networks and the very restricted deployment of "delayed" SM measurements has prompted the development of long-term modeling methodologies for characterizing the operation of these networks. Such methods are usually based on load flow computations using the sparsely available SM data or typical load patterns. Considering the volatility of small end-users electricity consumption and generation and the fact that DSOs are called to safeguard a stable and secure power supply in all possible demand conditions, the adoption of a streamlined planning approach for analyzing the current energy system becomes urgent. In cost-effectiveness terms, this fact highlights the necessity of leaving behind worst-case design.

As a matter of fact, it is in the economic interest of distribution utilities and of the network user that power supply relates to normally expected conditions rather than to extreme cases [5]. The traditionally applied deterministic approach focuses on the least favorable network operation states, which are very rare. Naturally, this approach may lead DSOs to high initial investments with low amortization rates as well as to very restrictive decisions in terms of DER hosting capacity. Given the current uncertainty of DSO costs and revenues, new planning tools are required for considering the constant time-variability of the energy network [34]. This argument becomes even more solid in view of the upcoming integration of electric vehicles and the development of flexibility services. According to the argument that network design should focus on the most expected conditions rather than on the extreme ones, the optimal design of a technical solution in a given network could be roughly determined by a graph similar to the one of Figure 1.6.

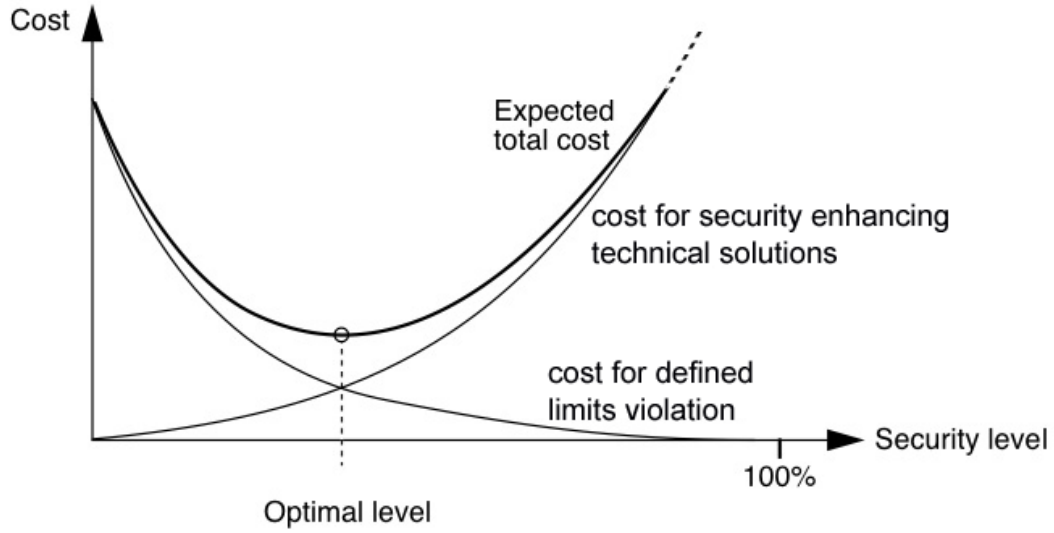

Figure 1.6: Cost-Security rough diagram

For considering the constant variability of the LV network state, caused by the volatility of residential loads and of distributed PV generation, probabilistic methods, tailored for the LV network, are highly recommended. The outputs of such methods can be used for computing statistical distributions and determining the boundary values of LV network operation indices. This information is very useful not only for long-term observability analytics of the network but also for the preprocessing phase of state estimation techniques focusing on the MV level [30]. **The upcoming large deployment of SM devices will increase the reliability of such modeling methodologies.** Indeed, user-specific data can offer a better insight of the power distribution system. Even in a deterministic approach, such data can be used to create accurate absolute worst-case scenarios (maximum recorded generation-minimum recorded load over a long period of time) or load/PV time-of-day coincident worst-case scenarios for all end-users. Feeder-specific data are therefore anyway recommended for a reliable steady-state analysis of LV feeders, even in a deterministic context. Besides, deterministic analysis that is based on really recorded worst-case values is much more realistic than focusing on PV rated power or other assumed generation or demand values.

However, even based on real recorded data, deterministic approach does not consider the fact that the time-of-day in which worst-case values apply for a specific user does not necessarily coincide with the one of other users connected to the same feeder. Nevertheless, the operational criteria of the feeder are determined both by the individual user's demand and by the simultaneous demands of other network users. As previously mentioned, since the demand of every user

and the degree of coincidence between them constantly varies, so does the operation of the feeder [5].

The above argument demonstrates that although user-specific SM data are primordial for creating reliable network models, there is another challenge that needs to be addressed. The latter lies in the fact that residential (or small-usage) end-users follow, volume-wise (kWh) or capacity-wise (kW), an almost stable daily pattern and that this pattern can be shifted, in time, from one end-user to the other one. In long-term decision making, profiles should be based on the recorded ones considering all possible deviations. Those deviations could be inserted either as random statistical errors or by making random possible combinations of the recorded values or by combining both approaches. **Consequently, reliable models that use user-specific SM readings and take into account load/PV time- and user-variability are necessary for applying a less conservative and more cost-effective network analysis.**

Although the rolling out of SM devices is now a trend in Europe, the total number of LV networks that are actually monitored, as far as nodal energy, power exchange and/or voltage are concerned, remains very sparse. Hence, it is necessary to develop methodologies able to use the currently available SM data for modeling, in an optimized and accurate manner, the current situation in LV networks. Such simple and reduced methodologies will allow a fast optimized elaboration of data, even when big SM datasets will be available, for facilitating the long-term techno-economic evaluation of the distribution system.

Given the natural evolution of LV networks currently including uncontrollable consumption loads, DG sources with time varying generation profiles, multiple stakeholders with diverse random needs and controllable loads or storage elements (in the near future), modeling tools should be based on a multidimensional approach. Security margins, renewable energy gains, power quality and energy losses need to be simultaneously accounted for keeping the pace with latest developments and for fairly allocating network use costs to the whole range of users. The big modeling challenge is to find a way for representing the ever-growing and varying objectives and perspectives of different grid-tied end-users. Given that the real network should be resilient, secure and efficient in balancing the trade-offs of the different end-users and have the flexibility to evolve with the varying resources, the same requirement applies for the long-term network models.

Chapter conclusions

Chapter 1 presents the technical impact of distributed renewable energy sources on the operation of LV networks. The principal challenges that need to be encountered for increasing the PV hosting capacity of LV networks are also discussed.

The analysis concludes that, for increasing the PV hosting capacity of LV networks, policy and regulation bodies should investigate the impact of distributed PV units in an overall manner. The objective includes managing a fair allocation of costs while ensuring benefits and revenue opportunities to the multiple involved stakeholders, given that the reliability and quality of energy supply towards all end-users of the distribution network is not compromised in any manner.

For facilitating the above multidimensional and challenging task, reliable modeling tools are required. Such models should consider the constant variability of the LV network state, caused by the volatility of residential loads and of distributed PV generation. To this end, probabilistic methods, tailored for the LV network, are highly recommended.

The upcoming large deployment of SM devices will increase the reliability of such modeling methodologies. The development and application of reliable models that use user-specific SM readings and take into account load/PV time- and user-variability can lead to a less conservative and more cost-effective LV network analysis.

Chapter references

[1] EWEA, “Wind in power; 2015 European statistics,” 2016.

[2] EPIA, “Connecting the Sun. Solar Photovoltaics on the Road to Large-Scale Grid Integration,” September, 2012.

[3] D. Maillard, “Energy transition Series – The issue of power grids,” *Paristech Review*, 2014. [Online]. Available: http://www.paristechreview.com/2014/05/31/energy-transition-power-grids/.

[4] EN50160, “Voltage characteristics of electricity supplied by public electricity networks,” 2012.

[5] M. B.-P. Antoni Klajn, “Application Note Standard EN50160 Voltage Characteristics of Electricity Supplied by Public Electricity Networks,” European Copper Institute, March, 2013.

[6] B. Bakhshideh Zad, H. Hasanvand, J. Lobry, and F. Vallee, “Optimal reactive power control of DGs for voltage regulation of MV distribution systems using sensitivity analysis method and PSO algorithm,” *Int. J. Electr. Power Energy Syst.*, vol. 68, pp. 52–60, 2015.

[7] SYNERGRID, “Prescriptions techniques spécifiques de raccordementd’installations de production décentralisée fonctionnant en parallèle surle réseau de distribution C10/11,” 2012.

[8] Bollen M.H.J. and F. Hassan, *Integration of Distributed Generation in the Power System*, IEEE Press. Wiley, 2011.

[9] M. K. C.Dierckxsens, A.Woyte, B.Bletterie, A.Zegers, W.Deprez, A.Dexters, K.Van Roey, J.Lemmens, R.Poosen, J.Lowette, K.Nulens, Y.T.Fawzy, B.Blazic, B.Uljanic, “Cost-effective integration of photovoltaics in existing distribution grids,” 2012.

[10] E. De Jaeger, A. Du Bois, and B. Martin, “Hosting capacity of LV distribution grids for small distributed generation units , referring to voltage level and unbalance” in *CIRED*, no. 1303, pp. 10–13, 2013.

[11] L. Degroote, B. Renders, B. Meersman, and L. Vandevelde, “Neutral-point shifting and voltage unbalance due to single-phase DG units in low voltage distribution networks,” in *2009 IEEE Bucharest PowerTech Innov. Ideas Towar. Electr. Grid Futur.*, pp. 1–8, 2009.

[12] B. N. Gafford, W. C. Duesterhoeft, and C. C. Mosher, "Heating of Induction Motors on Unbalanced Voltages," *Trans. Am. Inst. Electr. Eng. Part III Power Appar. Syst.*, vol. 78, no. 3, pp. 282–286, 1959.

[13] J.E. Williams, "Operation of 3-Phase Induction Motors Voltages," *AIEE Trans. pt. III-A, Power Appar. Syst. 73 125–133*, vol. 73, pp. 125–133, 1954.

[14] C.-Y. Lee, B.-K. Chen, W.-J. Lee, and Y.-F. Hsu, "Effects of various unbalanced voltages on the operation performance of an induction motor under the same voltage unbalance factor condition," *Electr. Power Syst. Res.*, vol. 47, no. 3, pp. 153–163, Nov. 1998.

[15] A. Von Jouanne and B. Banerjee, "Assessment of voltage unbalance," *IEEE Trans. Power Deliv.*, vol. 16, no. 4, pp. 782–790, 2001.

[16] Y. J. Wang, "Analysis of effects of three-phase voltage unbalance on induction motors with emphasis on the angle of the complex voltage unbalance factor," *IEEE Trans. Energy Convers.*, vol. 16, no. 3, pp. 270–275, 2001.

[17] EPRI, "Voltage Unbalance: Power Quality Issues , Related Standards and Mitigation Techniques Effect of Unbalanced Voltage on End Use Equipment Performance," 2000.

[18] N. K. Roy and H. R. Pota, "Current Status and Issues of Concern for the Integration of Distributed Generation Into Electricity Networks," *IEEE Systems Journal*, vol. 9, no. 3, pp. 933-944, 2014.

[19] Z. Ziadi, S. Taira, M. Oshiro, and T. Funabashi, "Optimal power scheduling for smart grids considering controllable loads and high penetration of photovoltaic generation," *IEEE Trans. Smart Grid*, vol. 5, no. 5, pp. 2350–2359, 2014.

[20] CWaPE, "ACTE PREPARATOIRE CD-15g15-," 2015.

[21] CIGRE JWG C4.07/CIRED, "Final WG Report: Power Quality Indices and Objectives," 2004.

[22] IEC, "IEC TR 61000-3-13:2008," 2008.

[23] M. H. J. Bollen, "Definitions of voltage unbalance," *IEEE Power Eng. Rev.*, vol. 22, no. 11, pp. 49–50, 2002.

[24] P. Pillay and M. Manyage, "Definitions of voltage unbalance," *IEEE Power Eng. Rev.*, vol. 22, no. 11, pp. 49–50, 2001.

[25] EDSO for Smart Grids, "European Distribution System Operators for Smart Grids Response to the European Commission ' s public consultation on a new energy market design," 2015.

[26] IEC, "IEC, 60364-5-52 Table A5210." .

[27] A. J.Rodolakis, "A comparison of north american (ANSI) and european (IEC) fault calculation guidelines," *IEEE Trans. Ind. Appl.*, vol. 29, no. 3, pp. 515–521, 1993.

[28] M. Abdel-salam, H. Ziedan, R. M. Kamel, and K. Sayed, "Effect of Micro-Grid Renewable Micro-sources on Short Circuit Capacity of Hosting Distribution Networks," in *INTELEC*, 2013, no. October, pp. 458–463.

[29] T. N. Boutsika and S. A. Papathanassiou, "Short-circuit calculations in networks with distributed generation," *Electr. Power Syst. Res.*, vol. 78, no. 7, pp. 1181–1191, 2008.

[30] I. D. A. gómez-expósito, Catalina Gómez Quiles, "State Estimation in Two Time Scales for Smart Distribution Systems," *IEEE Trans. Smart Grid*, vol. 6, no. 1, pp. 421–430, 2015.

[31] A. Abur and A. Gómez Exposito, Power System State Estimation: Theory and Implementation. CRC Press, 2004.

[32] M. Glavic and T. Van Cutsem, "Reconstructing and tracking network state from a limited number of synchrophasor measurements," *IEEE Trans. Power Syst.*, vol. 28, no. 2, pp. 1921–1929, 2013.

[33] M. Pignati, M. Popovic, S. Barreto, R. Cherkaoui, G. Dario Flores, J. Y. Le Boudec, M. Mohiuddin, M. Paolone, P. Romano, S. Sarri, T. Tesfay, D. C. Tomozei, and L. Zanni, "Real-time state estimation of the EPFL-campus medium-voltage grid by using PMUs," *2015 IEEE Power Energy Soc. Innov. Smart Grid Technol. Conf. ISGT 2015*, 2015.

[34] EDSO for Smart Grids, "European Distribution System Operators for Smart Grids Adapting distribution network tariffs to a decentralised energy future," September, 2015.

[35] J. Britton, P. Brown, J. Moseley, and M. Bunda, "Optimizing operations with CIM," IEEE Power *and Energy Magazine*, vol. 14, no. 1, pp. 49–57, 2016.

[36] S. Conti, S. Raiti, G. Tina, and U. Vagliasindi, “Integration of multiple PV units in urban power distribution systems,” Sol. Energy, vol. 75, no. 2, pp. 87–94, 2003.

Chapter 2 Need for Probabilistic Analysis of Low Voltage Networks

Highlights

- *Probabilistic models are widely suggested for accounting for the uncertainties in the operation of LV networks.*
- *This study focuses on models that deploy probabilistic analysis regarding the volatility of the network state which results from the volatility of power exchanges between the end-users and the network.*
- *In this framework, several probabilistic models exist, some of them deploying long-term observability analytics of the network and others focused on real-time or short-term state estimation. The outputs of long-term probabilistic analysis models are useful in both cases.*
- *The cost-effective management of LV networks requires long-term observability methods and historic SM measurements.*
- *The existing probabilistic models focus on one or few operation indices, usually on voltage magnitude or voltage unbalance rise, and they do not treat in a comprehensive manner all parameters that affect the operation of LV networks.*
- *They are not designed for using network- and user-specific long-term measurements for studying a specific network.*
- *They do not integrate evaluation models for distributed control schemes that are very important for the further integration of renewables and for the upcoming automation of the distribution network*

2.1 Current Modeling Methodologies

A large variety of commercial and non-commercial algorithms are nowadays available for the long-term analysis of LV networks. The vast majority of them analyze LV distribution networks with a deterministic approach. The software user models the network by deterministically defining the parameters that influence its operation, considering most of the times worst-case scenarios. The purpose is to ensure 100% security of the system. For example, the steady-state analysis for determining the voltage profile of a LV feeder usually considers that each PV unit injects power equal to its rated power and each supply point consumes its lowest expected load. Based on such extreme cases, voltage magnitudes near PV nodes result to be very high compared to situations that usually occur. As a result, the DSO estimates the PV hosting capacity in a very restrictive manner since the maximum acceptable PV power that a feeder can host heavily depends on its voltage margin.

This design strategy leaves a question mark over the probability of occurrence of such worst-case scenarios. In many cases, the probability is so small that focusing network design on such an extreme hypothesis, instead of more usual conditions, results in over restrictive decisions or oversized costly technical solutions. This argument is very well described by authors in [1]: yesterday's power grid was overbuilt to achieve reliability whereas tomorrow's grid will depend on automation to operate at tighter margins and under a wider range of supply and demand patterns, with network analysis being the cornerstone of this transition. Indeed, since very recently, more and more critical processes have been relying on network analysis for operating more closely to the system limits.

However, if one leaves behind deterministic worst-case approach, a new challenge appears. Is there a reliable and accurate way for simulating the most usual operating conditions in LV networks? How can one choose which network states to focus on?

Given the high volatility of DG and consumption loads and the lack of long-term historic measurements, new planning tools are required for modeling the constant variability of the LV distribution network [2], [3], [4], [5].

The present study investigates whether these questions can be sufficiently answered by applying probabilistic analysis methods while taking advantage of the currently available historic SM measurements. For examining this hypothesis, a careful literature review was initially deployed. Existing contributions regarding the probabilistic analysis of distribution networks and the role of SM measurements are presented in the following sections.

2.2 Existing probabilistic analysis methods for Low Voltage distribution networks

The notion of probabilistic analysis of power systems can be traced back to the 1960s [6]–[11]. Some thirty years later, probabilistic models specifically tailored to the distribution network were introduced [12], [13]. Since then, many research institutes worldwide have presented related contributions and few of the existing commercial tools have been adapted to integrate probabilistic analysis. A big percentage of the developed models deploy stochastic scenario analysis regarding the number, the size and the position of loads or DG units while each network state is still analyzed by deterministically defining power injection and consumption values. Such contributions are out of the scope of the present study. **The following literature review addresses probabilistic methodologies that simulate the uncertainty in the steady operation of distribution networks due to volatility and uncontrollability of nodal power injections and consumptions.**

Prompted by such considerations, probabilistic methodologies both for long-term observability analytics and for real-time state estimation have been proposed, specifically tailored for the distribution network. State estimation of the power system is a data fitting problem whose analysis barely relies on real-time measurements of system's operation indices [14], [15], [16]. However, as previously highlighted, real-time measurements are not deployed in the vast majority of distribution networks nowadays. Practically, an operational system that provides low-latency real-time state estimation for distribution networks by using real-time monitoring data (PMU data) specifically adapted for the MV network, has been very recently presented in [17]. Considering this fact, the massively dispersed nature of LV networks and the significantly uncertain nature of residential single-phase loads and DG, compared to loads in the MV network, one can assume that the development of state estimation techniques adapted for the LV network will not be implemented for the foreseeable future.

The large deployment of bus-level measurements, recorded by SM at intervals ranging from 15 minutes to 24 hours, is considered to be the next milestone in LV distribution. However, the current lack of real-time measurements has motivated the development of heuristic methods combining load flow calculations, machine learning functions or pattern-based load allocation with ad hoc state estimation techniques [14]. Such hybrid schemes deploy a preprocessing phase in which "delayed" SM data or daily load patterns are exploited, in different ways, to generate pseudo-measurements and characterize the operation of LV networks providing useful information for the state estimation phase of the MV level. In this context, several probabilistic methodologies, specially tailored for characterizing LV network's operation indices, have appeared in recent years. Their objec-

tive is to reliably simulate the uncertainty of the LV network state which is significant due to the stochasticity of residential loads and the volatility of distributed PV injection [18], [19]–[23]. The following sections outline the existing contributions regarding the probabilistic analysis of distribution networks, both on a long-term and on a real-time principle.

2.2.1 *Long-term observability probabilistic methods*

Several contributions deploying long-term analysis and evaluation of the distribution network use probabilistic methods, based on analytical or numerical approach. In this context, paper [24] highlights the increased amount of information that can be obtained by applying (analytical) probabilistic load flow analysis in a distribution feeder with wind turbines versus a deterministic type of analysis. In a similar vein, a planning tool developed in a Quasi-Chronological Monte Carlo (MC) environment (numerical method) was proposed in contribution [25]. In that paper, a deterministic approach based on mean hourly generation and consumption values was compared with another one that considered the random behavior of both load and PV generation during each hour of the Quasi-Chronological MC simulation process. The use of a deterministic approach led to an overestimation of the maximum PV peak power that can be installed according to the evaluation performed by the probabilistic approach. However, this paper only considered entire correlation scenarios between load and PV generation, which may not apply in the majority of cases. Papers [26]–[31] evaluate different scenarios of spatial correlation for PV generation and load. Reference [29] introduces an analytical method that combines the cumulants method with the Cornish–Fisher expansion to solve the voltage regulation problem in radial distribution networks. Similarly, the same authors examine in [30] another analytical technique combining the method of cumulants with the Gram-Charlier expansion to solve radial distribution networks with PV generators. In that paper, both analytical approaches are compared with a traditional MC method and they are proved to have better performances in terms of convergence times and computational cost. Paper [32] applies a Quasi-Sequential MC algorithm to perform a reliability analysis of a distribution network with active management system. The repeated iterations involved in MC methods usually cause long execution times before estimations of network states are obtained. Nevertheless, they are often preferred in latest studies because of their implementation simplicity and their flexibility regarding the number of random variables that can be considered [33].

All previously mentioned methodologies aim to analyze the impact of time-varying loading parameters mainly focusing on voltage and current magnitudes. As a matter of fact, a large number of probabilistic models for LV networks can be found in literature. However, only few of them present three-phase power flow (PF) analysis and voltage unbalance consideration. Paper [21] presents a MC algorithm which assesses voltage unbalance at the secondary output of a LV

transformer using correlated Gaussian random variables to represent active and reactive power. This approach uses three-phase power data recorded at the MV/LV transformer and, consequently, does not take into account the random loading parameters at every node of the feeder. Moreover, the time-varying influence of PV injection on voltage unbalance is not studied since distributed PV units are not considered in that model. A stochastic assessment of voltage unbalance due to the single-phase connection of EVs in Germany is presented in [20]. Nevertheless, this paper does not study the effect of numerous distributed PV sources and residential loads connected to the LV network. Paper [23] links a probabilistic analysis method to a three-phase power flow method which simulates PV injection based on meteorological data of solar irradiation. Similarly, reference [18] presents a probabilistic methodology for estimating voltage unbalance in MV distribution networks when monitoring data are not available and [16] presents a methodology using both real-time and pseudo-measurements to statistically estimate voltage unbalance in distribution networks.

The over mentioned contributions study the impact of load variability, on certain operation indices, with a long-term statistical approach. Regarding long-term network analysis and development, long-term probabilistic models are used to obtain refined techno-economic evaluations of possible technical solutions. Technical decisions are adapted to the most usual network conditions driven by cost-effectiveness objectives. Regarding real-time state estimation techniques, the outputs of such long-term probabilistic models can be used for characterizing LV network operation indices, by defining boundary values and by constructing statistical distributions at a higher bus level. As far as real-time state estimation of distribution networks is concerned, several studies have appeared based on probabilistic models that efficiently incorporate uncertainties [34], [35]–[38].

Nowadays, automation of the LV network is not commonly applied. However, several reports published by national or international authority bodies and several research institutions clearly state that the integration of such services will be promoted in the near future [4], [39], [40]. The large deployment of real-time measurements (with PMUs) and SM devices will be the milestone for taking this decisive step. Although real-time state estimation of LV network is out of the scope of the current study, the following paragraph outlines some basic contributions for highlighting that probabilistic techniques are required in order to improve the observability of the distribution network.

2.2.2 *Real-time estimation probabilistic methods*

Regarding this matter, paper [41] presents a probabilistic algorithm for deploying state estimation of the distribution network by using a limited number of telemetered variables as solution constraints. Reference [37] presents a distribution network system estimator containing traditional weighted least square prob-

abilistic algorithms and fuzzy sets for simulating the uncertainty of load and generation given a very restricted number of long-term measurements. Paper [36] develops a probabilistic approach of real-time state estimation requiring real-time measurements of active and reactive power at the transformer and power, voltage and current magnitudes from key locations of the system. Power flows at nodes without metering devices are modeled based on Gaussian distributions of solar irradiance and loads. Similarly, paper [35] introduces an algorithm for probabilistic coordination of energy resources in a microgrid. All mentioned contributions present solid mathematical models for real-time estimation of distribution networks accounting for uncertainties and considering a restricted number of telemetered data.

Recently, the EU funded SINGULAR project [42] presented a complete framework of real-time and short-term scheduling tools for distribution networks with high DER integration, using real-time and long-term historic measurements. These tools apply probabilistic algorithms in order to generate scenarios for the modeling of random system parameters (loads, generation, storage, DR actions, etc.). Scenario reduction techniques are used to minimize the computation effort and appropriate techniques for modeling the cross-correlation of the involved stochastic processes are also incorporated. Some of the developed algorithms have been published in [43]–[48].

2.2.3 *Summary*

Based on the previous findings, the large number of probabilistic models that simulate load and generation uncertainties in the distribution network can be roughly divided into two categories. The first category consists of methodologies that treat the distribution network with a long-term observability scope, most of the times focusing on one specific operation index, without elaborating feeder- and user-specific injection and consumption data. The second category consists of real-time state estimation probabilistic algorithms, using both data fitting probabilistic methods (to address the limited availability of telemetered data) and long-term historic nodal measurements.

Between these categories, the present study addresses the long-term analytics approach specifically tailored for LV networks. As pointed out in [49], the long-term observability approach opposed to the purely passive one (consisting of managing problems in the operational phase or in short-term time frames) would allow for interaction between the distribution network's different timeframes. Real-time analysis is insufficient for the long-term observability of the LV network and for the evaluation of certain technical decisions and solutions with a long-term strategic view. As a matter of fact, averaged measurements or simulation outputs over longer periods are more representative of the network's behavior in steady-state conditions. Consequently, the present study focuses on devel-

oping tools that will directly address the first timeframe of Figure 2.1 [50], namely the planning and network development block.

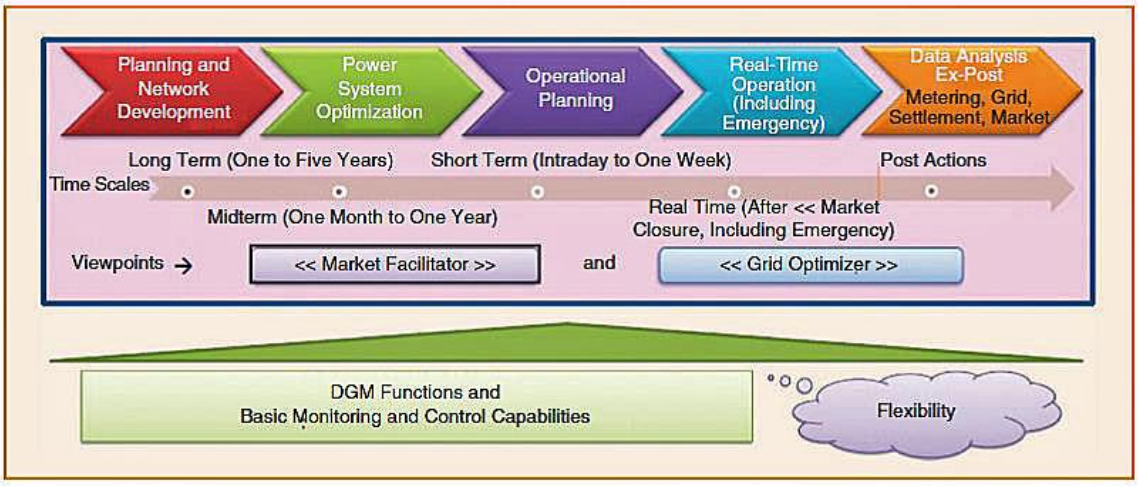

Figure 2.1: The distribution network's different timeframes, necessary for the transition from passive to active scheme [50]

2.3 Monte Carlo techniques for long-term observability of Low Voltage networks

2.3.1 *Theoretical description*

Aiming at developing models for the long-term observability of LV networks, the present work focuses on the steady operation of the system. Consequently, the applied analysis method aims to develop reliable models for the system's variables that mainly affect operation under normal conditions and load flow computation. In this context, **the probabilistic approach models the uncertainty of each system's variable as a random variable that follows a certain statistical distribution. The statistical distribution or the Probability Density Function (PDF) practically models the values that the variable can take with a mathematical expression, in function of its probability of occurrence.**

Regarding load flow computation, uncertainties are hidden in nodal power injection and generation. These nodal variables are represented in terms of PDFs or Cumulative Distribution Functions (CDFs). State of the art methods to get Probabilistic Load Flow (PLF) results include analytical and numerical approaches. Monte Carlo (MC) methods are typical numerical approaches, able to achieve great accuracy at the expense of heavy computational burden. Analytical methods can accelerate the calculation procedure at the expense of precision due to simplifications and approximations introduced in the process [51], [52]. The present study will focus on the MC approach based on four major reasons:

I. *Flexibility of the number of random variables*: LV feeders are subject to many changes, in terms of topology (lines' expansion), new users' connection (increase of the number of nodal random variables), new DG units connection (increase of the number of nodal random variables) or simply modification of users' types or energy use profiles due to proprietor/ renting changes. MC models are standard tools for the analysis of multidimensional complex systems and they can easily be adapted to the modification of the number and the type of variables while analytic approaches would require a bigger modeling effort.

II. *Topology of LV distribution networks*: LV distribution networks usually comprise radial feeders supplying a restricted number of end-users. On the one hand, this means that the number and the mutual dependencies of random variables are limited compared to larger and more complex systems. Therefore, the flexibility and the accuracy of MC techniques (compared to complex analytical approaches that require simplifications) can be exploited without requiring long computational time.

III. *Availability of users' power injection and consumption ¼-hourly historic measurements:* A main driver for the present work is the availability of long-term historic SM measurements of energy flow of end-users connected to the LV network, thanks to a research fellowship between ORES (one of the DSOs in Wallonia, Belgium) and the University of Mons. These data can be easily elaborated for constructing numerical distributions of probability for all the variables with less computational effort and less necessary simplifications compared to analytical computation of PDFs. Therefore, the computation time of the entire probabilistic analysis, which is the main drawback of the MC simulation compared to analytical approach [52], can be significantly reduced.

IV. *Research group's expertise in MC techniques:* The developments of the present work take advantage of the expertise that our research group has developed in MC simulation thanks to previous works addressing uncertainties in HV networks due to offshore wind power integration [53].

The objective of the MC simulation is to obtain the response of a system in function of sampled input values representing the random variables. The sampling process is repeated until the simulation outputs converge. Therefore the solution converges as the number of samplings n increases to $\rightarrow\infty$ and the statistical error $1/2n$ tends to zero [52], [54]. Figure 2.2 graphically presents the inputs/outputs transition in the MC process.

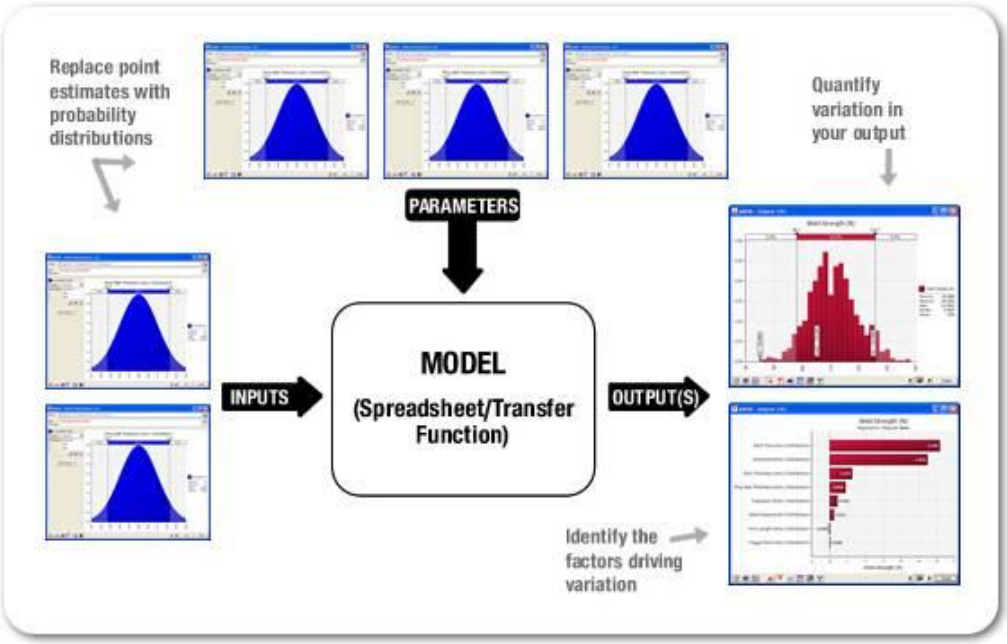

Figure 2.2: The inputs/outputs transition in the MC process [45]

2.3.2 *State transition in MC techniques*

Regarding the chronological aspect of the simulation, MC techniques are classified into three categories: the Non-Sequential methods, the Quasi-Sequential methods and the Sequential methods. A brief description of the three versions follows:

I. *Non-Sequential methods (NSMC):* In Non-Sequential MC simulation, the system states are extracted and evaluated without any chronological dependency determining the system's response to a set of events whose order have no influence or significance. In this way, a sufficient number of samplings are generated from a defined space of states for estimating the required parameters. This method is better adapted for systems in which the mutual dependence of variables does not significantly affect the computation so that it can be ignored resulting in minor errors [52], [55].

II. *Sequential methods (SMC):* Sequential MC models simulate the systems operation by generating an artificial history of events in time sequences that can reproduce all chronological aspects. This feature is fundamental when complex time correlations have to be taken into account which is usually the case when analyzing flexibility or storage integration solutions in the power system. As a drawback, it requires a significant increase of the computational burden [52], [55], [56]. Most of the times the incorporation of scenario reduction techniques such as *important sampling* or similar filters is anyway required for rendering the computation time- and memory-effective .

Some variations of the previous two MC simulation techniques have been proposed trying to preserve their advantages and overcome their drawbacks.

III. *Quasi-Sequential methods (QSMC):* A promising variation of the previous methods is the Pseudo-(or Quasi-) Sequential Monte Carlo simulation which was proposed for the first time by Leite da Silva in 1994 [57]. In this paper, the faster non-sequential sampling of system states is combined with the sequential analysis of the neighboring states only when the extracted initial state satisfies certain defined conditions. Another example is the Quasi-Sequential MC method that is proposed in [58] for general nonlinear dynamic systems. Not being a pure sequential simulation, the quasi-sequential models cannot provide all the detailed results of the sequential approach. However, the chronological description of the system behavior and the capability to represent complex operating procedures can be maintained up to a certain extent. The Quasi-Sequential MC simulation is therefore based on a

compromise that is made between complexity and computational effort reduction.

The three approaches are graphically illustrated in Figure 2.3 [59]. Roughly explained, in the NSM simulation all system states are sampled from a common space not considering any chronological classification of states, in the SMC simulation chronological dependency of system states is fully modeled and in the QSMC simulation the sampling of system states is based on a chronological classification which does not simulate the time-dependency of system states with a mathematical approach.

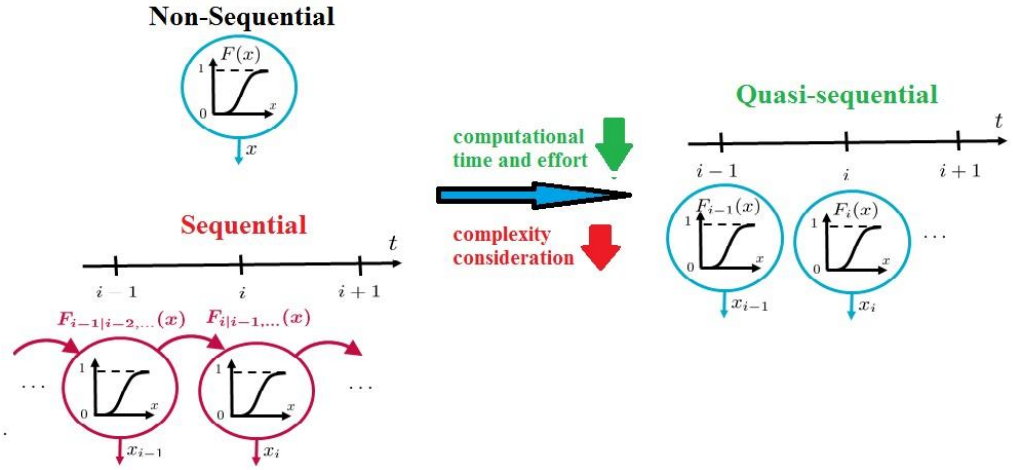

Figure 2.3: Transition between successive system states in the three MC approaches.

The SMC approach is the most faithful one to the real operation of the studied system. Regarding the operation of the LV network, this approach is highly recommended for simulations in which the time-dependency of system states is primordial or in which the time step for the analyzed system states is variable in function of certain parameters. The first case could for example refer to simulations of storage or flexibility services in the LV network like the recent one presented in [60]. The second case mostly refers to real-time or short-term state estimation methods of the network like the ones presented in [43]–[48]. In certain cases, as pointed out in [59], some random variables of the system, such as the load of a single residential user cannot be reliably represented with a sequential model. For reducing such sequentiality constraints while rendering SMC simulation time- and effort-effective, appropriate scenario reduction algorithms and time-dependency functions need to be developed.

The main scope of this study is to provide long-term observability algorithms for the analysis of the LV network (in steady operation mode) and the evaluation of technical solutions with a long-term strategic view. In order to do so, one of the main assets to be deployed, are the available ¼-

hourly SM datasets of energy flow recorded at LV network end-users. Given that the main focus is set on strategies in which the time-dependency of system states is not primordial, such as the reactive power control or the P/V droop control, the QSMC simulation is selected for the presented developments. Indeed, the development of reliable time-dependency functions and scenario reduction techniques for maintaining the required complexity of a SMC simulation, compared to a QSMC or a NSMC one, is out of the scope of the present study. Later on, it will be explained in which way the available SM datasets are exploited such that the compromise between complexity and computational effort reduction has a reduced impact on the output indices. At the end of this work, the developments which turn out to be affected by the QSMC simulation choice will be identified and the need for going forward SMC analysis will be pointed out.

2.4 The Role of Metering Data

As previously highlighted, the large deployment of long-term measurements will drastically enlarge the potential of cost-effective operation, analysis and design of LV networks. First of all, real-time measurements will enable the integration of automation in LV distribution feeders. Secondly, measurements deployed at several locations over a long period will be exploited for a reliable and information-rich observability of the network. If this new influx of data can be readily accessed and mined, long-term studies and analytics will provide a wealth of information that can be used by many different systems across distribution utilities [61].

Unlike transmission systems, where real-time telemetry provides sufficient redundancy to ensure network observability, distribution feeders have so far lacked the required infrastructure (sensors and telecommunication) allowing real-time state estimation. In the upcoming smart grid paradigm, distribution systems will have to cope with a heterogeneous set of information sources that can be roughly classified into the following categories [14]:

a) Remote terminal unit (RTU) measurements captured by the SCADA system at the substation, at rates ranging from few seconds to about a minute [62].

b) Feeder automation devices, including remotely-operated intermediate switching points for fault management.

c) Distributed generation (DG) monitoring, at different rates depending on the specific regulation and rated power and ranging from day-ahead hourly forecasting to real telemetry periodically submitted to the distribution management system (DMS).

d) Data base of historic load patterns/ profiles. This information originates in several sources including load forecasting, load allocation techniques in combination with feeder head measurements, characteristic power factor values of aggregated loads and systematic metering campaigns performed at specific locations. Such information can be used as pseudo-measurements to extend the observable area.

e) The latest and eventually most important addition to the list of information sources at the feeder level comes from the automatic meter reading/advanced metering infrastructure (AMR/AMI) (typically SM concentrators). Nowadays this information is collected in MV feeders and few LV feeders once a day but, depending on bandwidth availability, snapshot latencies of up to 15 min have been reported.

For the purpose of this study, all sources of information summarized above can be grouped in two broad classes of different nature, each one with different accuracy and latency [14].

A. Telemetered data provided by RTUs (items (a), (b), and in some cases, (c)). This comprises quite accurate snapshots captured with latencies ranging from few seconds to about a minute. The set of measurements is insufficient for assuring network observability.
B. (Pseudo-) measurements (items (c), (d), and (e)). Updated at intervals ranging from 15 min to 24 h, these bus-level data are barely critical for observability purposes.

The present study investigates up to which extent the long-term probabilistic analysis of LV networks is more reliable, cost-effective and information-rich versus the currently applied deterministic approach. **Most contributions mentioned in Section 2.2 demonstrated that an increased amount of information can be obtained thanks to the probabilistic approach, which can lead to much less conservative decisions. However, none of these contributions examined the hypothesis of applying long-term probabilistic estimation of LV feeders that addresses, in an overall manner, all operation indices (bus voltage magnitudes and unbalance, current values, captured renewable energy, line losses etc.) by taking advantage of user-specific long-term SM measurements.** So far, the hypothesis that distribution utilities have an interest to leave behind deterministic approach has not investigated the great opportunities appearing with the large deployment of SM measurements at bus level, in the LV network. For examining this hypothesis and the potential advantages, meter readings of the previously mentioned category (B) should be exploited. Such information is the basis and the necessary input for the development of streamlined methodologies that will offer reliable long-term observability analytics of the LV network.

2.5 Probabilistic Modeling of Technical Strategies in Low Voltage Feeders

Currently, the power that distributed PV units inject in the network only depends on the Maximum Power Point Tracking (MPPT) of the panels and does not consider the current state of the network. This passive operation of PV units combined with the trend to integrate more and more distributed generation, often leads DSOs to the necessity of upgrading their network. However, reinforcement of the network by replacing existing lines does not longer appear to be a viable and sustainable solution because it is very expensive [2]. For this reason, passing from grid-following DG units to DG units that act on the actual state of the network becomes more and more mandatory.

Hard curtailment is the traditional approach for coping with overvoltages caused by the high penetration of DGs in LV networks [3], [63], leading to on-off control of the DG units as soon as voltage violation occurs. This approach deteriorates the delivered power quality, due to significant voltage and current transients, and accelerates the degradation of the inverters. Of course, it also leads to an important loss of generated energy which affects the expected income of the PV producer. Hence, a more adequate voltage support by the PV inverters is required in LV networks.

Practically, conventional large power plants are equipped with reactive power/terminal voltage (Q/V) droop controllers when it comes to voltage regulation in transmission grids. In LV grids, the grid-connected DG units can be equipped with analogous Q/V droop functions. However, voltage support through reactive power is generally inefficient in LV network as the cable voltage is linked with the active power (and not the reactive one) due to the high R/X-value of the network connections [64], [65]. Hence, large amounts of reactive power are required to influence the voltage. This observation is not valid for distribution systems with overhead lines, in which R/X-value is adequate for an efficient voltage control by means of reactive power. Nevertheless, reactive power control leads to increased losses in the distribution network [66] that are not acceptable for the DSO. P/V droop controllers are more efficient and straightforward to provide voltage support in a LV network [66]–[78], whereas inter-unit communication for the control support should be avoided because of the large number of small PV units.

In that way, in case of overvoltage, changing the injected active power of a PV unit in function of the local voltage would be preferable rather than imposing its total cut-off during a period of time. This fact is justified by various arguments, which are thoroughly explained in [79]. The on-off control could be effective and sustainable in case of low PV penetration with a small impact on the voltage profile of the feeder. Besides, each cut-off of the PV unit means a loss of

renewable energy, during the specified cut-off period, and thus a loss of income for the PV producer. Finally, decreasing the delivered power of PV units, instead of cutting it off, is also sustainable for increasing the network PV hosting capacity. For the above reasons, locally applied P/V droop control could be adopted and regulated as a profitable (for the PV owner) ancillary service towards the LV network.

Voltage unbalance between phases is another issue that could be mitigated by means of specialized distributed control schemes. Although single-phase PV units are not always the principal source of voltage unbalance, the DSO often imposes conservative limits as for the maximal acceptable power of such units for preventing from further unbalance rise. The lack of monitoring in LV networks restricts the visibility on its operation and may lead to restrictive decisions. In reality, PV units can even contribute in decreasing the existing voltage unbalance. This can be achieved by means of unbalance mitigation controls integrated in three-phase inverters. Such systems have been thoroughly studied in existing literature [80], [81], [82]–[87].

Up to now, distributed local control strategies have only been analyzed with a deterministic worst-case approach. The control parameters tuning has been done in a rigorous manner by using estimations, restricted network configurations and bulk data [66], [67], [71], [73], [75]–[79]. The issue that has always been raised is that the design and parameter tuning of such configurations is not realistic and hence, one should be careful with drawing conclusions based on such analysis [66], [74]. Although the worst-case approach is safe for protection of the electrical system, it often discards multiple intermediate network states that may also lead to overvoltage events and frequent PV units cut-offs. The intermediate states also result in the degradation of network components along with significant PV power loss. Taking these states into account will refine the design of distributed controls, in terms of efficiency and investment cost. For the above reasons, a doubt concerning the sufficiency of the deterministic models in evaluating voltage control strategies has lately arisen in literature. Besides, the lack of real SM data restricted, up to now, the accuracy of existing probabilistic methods.

The contributions that are mentioned in the previous sections of this chapter analyze the LV network by considering the uncertainty of PV generation and loads. All these models present a different approach for simulating the time-variability of the network state, focusing on one or multiple operation indices. Nevertheless, none of these methodologies integrate the action of voltage control schemes or other technical strategies that focus on constraint management in the LV network. Up to now, such schemes have only been studied with models that consider a restricted number of network states. However, the volatility of DG and residential loads and the lack of time-coincidence of end-users' load patterns should also be considered when evaluating the performance of such strategies.

For this reason, **the present work has as a second objective to develop probabilistic models that can reliably simulate and evaluate the performance of several time-varying control schemes considering the constant variability of the LV network. These models will be developed and further discussed in chapters 7 and 8.**

2.6 Problem formulation; principal questions and hypothesis

Considering the currently evolving scheme in LV distribution and the findings of the literature review (sections 2.1-2.5), the present study attempts to answer the following questions:

1 ***Which means to deploy for simulating and analyzing the volatility of renewable generation and loads in LV networks? Considering this volatility, how to evaluate technical and economic indices that regard the long-term design of LV networks?***

2 ***Given that DER integration should further go on, is it possible to achieve a more cost-effective and less restrictive design approach than the one currently applied?***

3 ***How to focus network design on the most "probable" operation states? How to identify those most "probable" states?***

4 ***What to do with and how to exploit effectively the currently available and future SM datasets for improving the long-term observability of the LV network and the cost-effectiveness of technical solutions set to increase DG hosting capacity?***

By attempting to answer these questions, the following arguments could be demonstrated:

I. Better long-term observability of the LV network can be achieved by developing probabilistic models that exploit long-term network- and user-specific measurements.

II. The probabilistic simulation of LV networks can lead to less restrictive decisions regarding further DER integration.

III. The use of SM measurements can yield more reliable and accurate network analysis and design.

IV. Probabilistic models can faithfully simulate the variability of LV network operation.

V. Models that address all together the most important reliability indices result in more information-rich analysis and design.

VI. The benefit of different control schemes and other technical strategies will be more direct and refined if they are also evaluated and designed with a probabilistic approach.

Chapter conclusions

Chapter 2 presents a literature review about existing and currently applied methodologies for the simulation of LV networks. The findings of this review are used in order to formulate the problem that will be treated by the present study.

Most distribution utilities currently analyze and design LV networks based on deterministic worst-case approach which, in many cases, results in over restrictive decisions or oversized costly technical solutions. Prompted by this consideration, several probabilistic methodologies have been proposed in the related literature, both for long-term observability analytics and for real-time state estimation of the distribution network. The present study focuses on the long-term analytics approach, which is applied for network design and development. Most existing contributions (mentioned in Section 2.2) demonstrated that an increased amount of information can be obtained thanks to the probabilistic approach, which can lead to much less conservative decisions. However, none of these contributions examined the hypothesis of applying long-term probabilistic estimation of LV feeders that addresses, in an overall manner, all operation indices (bus voltage magnitudes and unbalance, current values, captured renewable energy, line losses etc.) by taking advantage of user-specific long-term SM measurements.

For the above reason, the present study investigates whether probabilistic analysis methods that take advantage of the currently available historic SM measurements can be reliable and accurate for simulating the most usual operating conditions in LV networks. The main scope is to provide long-term observability algorithms for the analysis of the LV network (in steady operation mode) and the evaluation of technical solutions with a long-term strategic view. In order to do so, one of the main assets to be deployed, are the available ¼-hourly SM datasets of energy flow recorded at LV network end-users. The second objective is to develop probabilistic models that can reliably simulate and evaluate the performance of several time-varying control schemes considering the constant variability of the LV network.

Chapter 2 presents and explains some important decisions that are taken for the development of the present study. Consequently, section 2.3.1 explains the choice of MC techniques for the development of the long-term probabilistic algorithm based on four principal reasons. These reasons include the flexibility of MC techniques regarding the number of random variables, the radial topology of LV feeders, the availability of SM measurements at the end-user lever and the expertise of the research group on MC techniques. Finally, section 2.3.2 explains the choice of the Pseudo-Sequential MC algorithm based on the fact that the main focus of the study is set on strategies in which the time-dependency of system states is not primordial.

Chapter references

[1] J. Britton, P. Brown, J. Moseley, and M. Bunda, "Optimizing operations with CIM," IEEE Power and Energy Magazine, pp. 49–57, 2016.

[2] M. B.-P. Antoni Klajn, "Application Note Standard EN50160 Voltage Characteristics of Electricity Supplied by Public Electricity Networks," European Copper Institute, March, 2013.

[3] S. Conti, S. Raiti, G. Tina, and U. Vagliasindi, "Integration of multiple PV units in urban power distribution systems," Sol. Energy, vol. 75, no. 2, pp. 87–94, 2003.

[4] Epia, "Connecting the Sun. Solar Photovoltaics on the Road to Large-Scale Grid Integration," no. September, p. 24, 2012.

[5] EDSO for Smart Grids, "European Distribution System Operators for Smart Grids Response to the European Commission ' s public consultation on a new energy market design," 2015.

[6] R. Billinton and K. E. Bollinger, "Transmission System Reliability Evaluation Using Markov Processes," IEEE Trans. Power Appar. Syst., vol. PAS-87, no. 2, pp. 538–547, 1968.

[7] X. Wang, "Equivalent energy function approach to power system probabilistic modeling," Trans. Power Syst., vol. 3, no. 3, pp. 823–829, 1988.

[8] EPRI, "Probabilistic Load Flow v4.0." 2006.

[9] EPRI, "Advanced Planning Method for Integrating Large-Scale Variable Generation," 2009.

[10] M. Eliassi, A. K. Dashtaki, H. Seifi, M. R. Haghifam, and C. Singh, "Application of Bayesian networks in composite power system reliability assessment and reliability-based analysis," Gener. Transm. Distrib. IEE Proc., vol. 9, no. 13, pp. 1755–1764, 2011.

[11] EPRI, "Advanced Planning Tools to Study Impact of Variable Generation," 2014.

[12] R. H.; Stillman, "Probabilistic derivation of overstress for overhead distribution in-line structures," IEEE Trans. Reliab., vol. 43, no. 3, 1994.

[13] Y. V. Makarov and N. S. Moharari, "A generalized power system reliability and security index," PowerTech Budapest 99. Abstr. Rec. (Cat. No.99EX376), p. 136, 1999.

[14] I. D. A. gómez-expósito, Catalina Gómez Quiles, "State Estimation in Two Time Scales for Smart Distribution Systems," IEEE Trans. Smart Grid, vol. 6, no. 1, pp. 421–430, 2015.

[15] A. Abdel-Majeed and M. Braun, "Low voltage system state estimation using smart meters," Univ. Power Eng. Conf. (UPEC), 2012 47th Int., pp. 1–6, 2012.

[16] N. C. Woolley and J. V. Milanović, "Estimating the voltage unbalance factor using distribution system state estimation," in IEEE PES Innovative Smart Grid Technologies Conference Europe, ISGT Europe, 2010.

[17] M. Pignati, M. Popovic, S. Barreto, R. Cherkaoui, G. Dario Flores, J. Y. Le Boudec, M. Mohiuddin, M. Paolone, P. Romano, S. Sarri, T. Tesfay, D. C. Tomozei, and L. Zanni, "Real-time state estimation of the EPFL-campus medium-voltage grid by using PMUs," 2015 IEEE Power Energy Soc. Innov. Smart Grid Technol. Conf. ISGT 2015, 2015.

[18] EPRI, Voltage Unbalance : Power Quality Issues, Related Standards and Mitigation Techniques Effect of Unbalanced Voltage on End Use Equipment Performance. 2000.

[19] Z. Liu and J. V. Milanovic, "Probabilistic Estimation of Voltage Unbalance in MV Distribution Networks With Unbalanced Load," IEEE Trans. Power Deliv., vol. 30, no. 2, pp. 693–703, Apr. 2015.

[20] J. Meyer, S. Hähle, P. Schegner, and C. Wald, "Impact of electrical car charging on unbalance in public low voltage grids," in Proceeding of the International Conference on Electrical Power Quality and Utilisation, EPQU, 2011, pp. 635–640.

[21] L. Pierrat, "A method integrating deterministic and stochastic approaches for the simulation of voltage unbalance in electric power distribution systems," IEEE Trans. Power Syst., vol. 16, no. 2, pp. 241–246, 2001.

[22] L. Pierrat and R. E. Morrison, "Probabilistic modeling of voltage asymmetry," IEEE Trans. Power Deliv., vol. 10, no. 3, pp. 1614–1620, 1995.

[23] F. J. Ruiz-Rodriguez, J. C. Hernández, and F. Jurado, "Voltage unbalance assessment in secondary radial distribution networks with single-phase photovoltaic systems," Int. J. Electr. Power Energy Syst., vol. 64, pp. 646–654, 2015.

[24] N. D. Hatziargyriou, T. S. Karakatsanis, and E. P. Division, "In wind," IEEE Trans. Power Syst., vol. 8, no. 1, pp. 159–165, 1993.

[25] S. Conti and S. Raiti, "Probabilistic load flow using Monte Carlo techniques for distribution networks with photovoltaic generators," Sol. Energy, vol. 81, no. 12, pp. 1473–1481, 2007.

[26] R. Billinton and Bagen, "Generating capacity adequacy evaluation of small stand-alone power systems containing solar energy," Reliab. Eng. Syst. Saf., vol. 91, no. 4, pp. 438–443, 2006.

[27] R. Billinton and R. Karki, "Reliability/cost implications of utilizing photovoltaics in small isolated power systems," Reliab. Eng. Syst. Saf., vol. 79, no. 1, pp. 11–16, 2003.

[28] J. C. Hernandez, F. J. Ruiz-Rodriguez, and F. Jurado, "Technical impact of photovoltaic-distributed generation on radial distribution systems: Stochastic simulations for a feeder in Spain," Int. J. Electr. Power Energy Syst., vol. 50, no. 1, pp. 25–32, 2013.

[29] F. J. Ruiz-Rodriguez, J. C. Hernández, and F. Jurado, "Probabilistic load flow for photovoltaic distributed generation using the Cornish-Fisher expansion," Electr. Power Syst. Res., vol. 89, pp. 129–138, 2012.

[30] F. J. Ruiz-Rodriguez, J. C. Hernández, and F. Jurado, "Probabilistic load flow for radial distribution networks with photovoltaic generators," in International Conference on Power Engineering, Energy and Electrical Drives, 2011.

[31] P. Zhang, W. Li, S. Li, Y. Wang, and W. Xiao, "Reliability assessment of photovoltaic power systems: Review of current status and future perspectives," Applied Energy, vol. 104. pp. 822–833, 2013.

[32] G. Celli, E. Ghiani, G. G. Soma, and F. Pilo, "Active distribution network reliability assessment with a pseudo sequential Monte Carlo method," 2011 IEEE Trondheim PowerTech, pp. 1–8, 2011.

[33] J. E. Gentle, Random Number Generation and Monte Carlo Methods. 2003.

[34] W. Alharbi and K. Raahemifar, “Probabilistic coordination of microgrid energy resources operation considering uncertainties,” Electr. Power Syst. Res., vol. 128, pp. 1–10, 2015.

[35] M. Glavic and T. Van Cutsem, “Reconstructing and tracking network state from a limited number of synchrophasor measurements,” IEEE Trans. Power Syst., vol. 28, no. 2, pp. 1921–1929, 2013.

[36] Y. Hu, A. Kuh, A. Kavcic, and D. Nakafuji, “Real-time state estimation on micro-grids,” in Proceedings of the International Joint Conference on Neural Networks, 2011, pp. 1378–1385.

[37] J. Pereira, “A State Estimation Approach for Distribution Networks Considering Uncertainties and Switching,” 2001.

[38] “Impact of Distributed Generation Units on Short- Circuit Capacity (SCC) Calculations,” no. February, 2016.

[39] NYS Department of Public Service, “Reforming the Energy Vision,” p. 85, 2014.

[40] Smart Grid Task Force, “2015 Regulatory Recommendations for the Deployment of Flexibility - EG3 REPORT,” no. January, 2015.

[41] a. K. Ghosh, D. L. Lubkeman, M. J. Downey, and R. H. Jones, “Distribution circuit state estimation using a probabilistic approach,” IEEE Trans. Power Syst., vol. 12, no. 1, pp. 45–51, 1997.

[42] SINGULAR FP7 EU Project, “www.singular-fp7.eu.” .

[43] A. Bakirtzis, P. Biskas, C. Simoglou, E. Bakirtzis, D. Chatzigiannis, A. Domaris, E. Kardakos, S. Vagropoulos, B. Santos, C. Monteiro, J. Contreras, V. Guerrero, J. Lujano, G. Osório, N. Paterakis, J. Catalão, and A. Mavridis, “Report on the state-of-the-art on scheduling tools and the mathematical formulation of the proposed scheduling models,” 2012.

[44] E. a. Bakirtzis, P. N. Biskas, D. P. Labridis, and A. G. Bakirtzis, “Multiple time resolution unit commitment for short-term operations scheduling under high renewable penetration,” IEEE Trans. Power Syst., vol. 29, no. 1, pp. 149–159, 2014.

[45] C. K. Simoglou, E. G. Kardakos, E. a. Bakirtzis, D. I. Chatzigiannis, S. I. Vagropoulos, A. V. Ntomaris, P. N. Biskas, A. Gigantidou, E. J. Thalassinakis,

A. G. Bakirtzis, and J. P. S. Catalão, "An advanced model for the efficient and reliable short-term operation of insular electricity networks with high renewable energy sources penetration," Renew. Sustain. Energy Rev., vol. 38, pp. 415–427, 2014.

[46] R. Napoli, I. A. Sajjad, and G. Chicco, "Probabilistic generation of time-coupled aggregate residential demand patterns," IET Gener. Transm. Distrib., vol. 9, pp. 789–797, 2015.

[47] N. Neyestani, M. Yazdani-Damavandi, M. Shafie-Khah, G. Chicco, and J. P. S. Catalão, "Stochastic Modeling of Multienergy Carriers Dependencies in Smart Local Networks with Distributed Energy Resources," IEEE Trans. Smart Grid, vol. 6, no. 4, pp. 1748–1762, 2015.

[48] S. I. Vagropoulos, E. G. Kardakos, C. K. Simoglou, A. G. Bakirtzis, and J. P. S. Catalão, "ANN-based scenario generation methodology for stochastic variables of electric power systems," Electr. Power Syst. Res., vol. 134, pp. 9–18, 2016.

[49] Eurelectric, "Active Distribution System Management: A key tool for the smooth integration of distributed generation," no. February, pp. 1–53, 2013.

[50] B. M. Mcgranaghan, D. Houseman, L. Schmitt, F. Cleveland, and E. Lambert, "Enabling the Integrated Grid," IEEE power & magazine, no. December 2015, 2016.

[51] RWTH, "A New Method for Probalistic Load Flow Analysis." [Online]. Available: http://www.acs.eonerc.rwth-aachen.de/cms/E-ON-ERC-ACS/Forschung/Projekte/~fbhh/Eine-neue-Methode-fuer-probalistische-La/lidx/1/.

[52] W. C. Briceño Vicente, "Modélisation des réseaux de distribution sous incertitudes," 2012.

[53] F. Vallée, "Modélisation et simulation de la production d'électricité d'origine éolienne pour l'analyse technico-économique des réseaux de transport électrique modernes," 2009.

[54] D. Ellard and P. Ellard, S-Q Course Book. 2003.

[55] G. Celli, E. Ghiani, F. Pilo, and G. G. Soma, "Reliability assessment in smart distribution networks," Electr. Power Syst. Res., vol. 104, pp. 164–175, Nov. 2013.

[56] C. L. T. Borges and D. M. Falcao, "Power System Reliability by Sequential Monte Carlo Simulation on Multicomputer Platforms," in Lecture Notes in Computer Science , Springer, 2001, pp. 242–253.

[57] J. C. O. Mello, M. V. F. Pereira, and a. M. Leite da Silva, "Evaluation of reliability worth in composite systems based on Pseudo-Sequential Monte Carlo simulation," IEEE Trans. Power Syst., vol. 9, no. 3, pp. 1318–1326, 1994.

[58] D. Guo and X. Wang, "Quasi-Monte Carlo filtering in nonlinear dynamic systems," IEEE Trans. Signal Process., vol. 54, no. 6 I, pp. 2087–2098, 2006.

[59] F. Vallée and Z. De Grève, "Utilisation des méthodes probabilistes dans les réseaux électriques modernes," in Journée d'étude SRBE/KBVE, 2016.

[60] R. Torquato, Q. Shi, W. Xu, and W. Freitas, "A Monte Carlo simulation platform for studying low voltage residential networks," IEEE Trans. Smart Grid, vol. 5, no. 6, pp. 2766–2776, 2014.

[61] S. Neumann, F. Wilhoit, M. Goodrich, and V. M. Balijepalli, "Everything's Talking to Each other," IEEE Power and Energy Magazine, pp. 40–47, 2016.

[62] P. Kansal and A. Bose, "Bandwidth and latency requirements for smart transmission grid applications," IEEE Trans. Smart Grid, vol. 3, no. 3, pp. 1344–1352, 2012.

[63] EN50160, "Voltage characteristics of electricity supplied by public electricity networks," 2012.

[64] W. D. B.Blazic, B.Uljanic, B.Bletterie, K.De Brabandere, C.Dierckxsens, T.Fawzy, "Active and Autonomous Operation of Networks with High PV Penetration; MetaPV FP7 project," 2011.

[65] W. D. C.Dierckxsens, K.De Brabandere, "Economic Evaluation of Grid Support with Photovoltaics; MetaPV FP7 project," 2012.

[66] M. K. C.Dierckxsens, A.Woyte, B.Bletterie, A.Zegers, W.Deprez, A.Dexters, K.Van Roey, J.Lemmens, R.Poosen, J.Lowette, K.Nulens, Y.T.Fawzy, B.Blazic, B.Uljanic, "Cost-effective integration of photovoltaics in existing distribution grids," 2012.

[67] M. Au-yeung, G. M. a Vanalme, J. M. a Myrzik, P. Karaliolios, M. Bongaerts, J. Bozelie, and W. L. Kling, "Development of a Voltage and Frequency Control Strategy for an Autonomous LV Network with Distributed

Generators," Univ. Power Eng. Conf. UPEC 2009 Proc. 44th Int., no. May 2009, pp. 0–4, 2009.

[68] a. Engler and N. Soultanis, "Droop control in LV-grids," 2005 Int. Conf. Futur. Power Syst., pp. 2–4, 2005.

[69] A. Engler, O. Osika, M. Barnes, and N. D. Hatziargyriou, "DB2 Evaluation of the local controller strategies," 2005.

[70] J. M. Guerrero, J. Matas, L. G. De Vicuña, M. Castilla, and J. Miret, "Wireless-control strategy for parallel operation of distributed-generation inverters," IEEE Trans. Ind. Electron., vol. 53, no. 5, pp. 1461–1470, 2006.

[71] F. Katiraei and M. R. Iravani, "Power management strategies for a microgrid with multiple distributed generation units," IEEE Trans. Power Syst., vol. 21, no. 4, pp. 1821–1831, 2006.

[72] H. Laaksonen, P. Saari, and R. Komulainen, "Voltage and frequency control of inverter based weak LV network microgrid," 2005 Int. Conf. Futur. Power Syst., p. 6 pp.–6, 2005.

[73] R. H. Lasseter and P. Paigi, "Microgrid: A conceptual solution," in PESC Record - IEEE Annual Power Electronics Specialists Conference, 2004, vol. 6, pp. 4285–4290.

[74] Y. W. Li and C. N. Kao, "An accurate power control strategy for power-electronics-interfaced distributed generation units operating in a low-voltage multibus microgrid," IEEE Trans. Power Electron., vol. 24, no. 12, pp. 2977–2988, 2009.

[75] D. E. Olivares, A. Mehrizi-Sani, A. H. Etemadi, C. A. Ca??izares, R. Iravani, M. Kazerani, A. H. Hajimiragha, O. Gomis-Bellmunt, M. Saeedifard, R. Palma-Behnke, G. A. Jimenez-Este vez, and N. D. Hatziargyriou, "Trends in microgrid control," IEEE Trans. Smart Grid, vol. 5, no. 4, pp. 1905–1919, 2014.

[76] C. K. Sao and P. W. Lehn, "Intentional islanded operation of converter fed microgrids," in 2006 IEEE Power Engineering Society General Meeting, 2006, p. 6 pp.

[77] C. K. Sao and P. W. Lehn, "Control and power management of converter fed microgrids," IEEE Trans. Power Syst., vol. 23, no. 3, pp. 1088–1098, 2008.

[78] T. L. Vandoorn, B. Meersman, L. Degroote, B. Renders, and L. Vandevelde, "A control strategy for islanded microgrids with DC-link voltage control," IEEE Trans. Power Deliv., vol. 26, no. 2, pp. 703–713, 2011.

[79] T. L. Vandoorn, B. Renders, L. Degroote, B. Meersman, and L. Vandevelde, "Active load control in islanded microgrids based on the grid voltage," IEEE Trans. Smart Grid, vol. 2, no. 1, pp. 127–139, 2011.

[80] T. L. Vandoorn, J. De Kooning, B. Meersman, and L. Vandevelde, "Voltage-based droop control of renewables to avoid on-off oscillations caused by overvoltages," IEEE Trans. Power Deliv., vol. 28, no. 2, pp. 845–854, 2013.

[81] L. Degroote, B. Renders, B. Meersman, and L. Vandevelde, "Neutral-point shifting and voltage unbalance due to single-phase DG units in low voltage distribution networks," 2009 IEEE Bucharest PowerTech Innov. Ideas Towar. Electr. Grid Futur., pp. 1–8, 2009.

[82] S. Dierkes, F. Bennewitz, M. Maercks, L. Verheggen, and A. Moser, "Impact of Distributed Reactive Power Control of Renewable Energy Sources in Smart Grids on Voltage Stability of the Power System," 2014.

[83] S. I. Gkavanoudis and C. S. Demoulias, "A control strategy for enhancing the Fault Ride-Through capability of a microgrid during balanced and unbalanced grid voltage sags," Sustain. Energy, Grids Networks, vol. 3, pp. 1–11, Sep. 2015.

[84] D. Graovac, V. A. Katić, and A. Rufer, "Power quality problems compensation with universal power quality conditioning system," IEEE Trans. Power Deliv., vol. 22, no. 2, pp. 968–976, 2007.

[85] B. Meersman, B. Renders, L. Degroote, T. Vandoorn, and L. Vandevelde, "Three-phase inverter-connected DG-units and voltage unbalance," Electr. Power Syst. Res., vol. 81, no. 4, pp. 899–906, 2011.

[86] B. Renders, K. De Gussemé, W. R. Ryckaert, and L. Vandevelde, "Converter-connected distributed generation units with integrated harmonic voltage damping and harmonic current compensation function," Electr. Power Syst. Res., vol. 79, no. 1, pp. 65–70, 2009.

[87] M. Savaghebi, A. Jalilian, J. C. Vasquez, and J. M. Guerrero, "Autonomous voltage unbalance compensation in an islanded droop-controlled microgrid," IEEE Trans. Ind. Electron., vol. 60, no. 4, pp. 1390–1402, 2013.

Chapter 3 Extraction and Treatment of Smart Metering Data for Probabilistic Techno-economic Analysis of Low Voltage Networks

Highlights

- *PV energy injection and energy consumption historic measurements, recorded at several LV end-users in Belgium have been initially collected.*
- *Statistical distributions have been created for studying the variability of energy profiles among different end-users and different ¼-hourly time steps in a typical day.*
- *The high volatility of energy flows in the LV network has been confirmed thanks to the statistical analysis of the available datasets*
- *How can these statistical outputs be used for incorporating uncertainty in the long-term analysis of LV networks?*

3.1 Overview of the necessary data

The necessary historic measurements that will be collected, treated and analyzed, in order to develop the probabilistic algorithms of this thesis, are graphically illustrated in Figure 3.1. Three types of nodes are practically identified in the presented configuration. These types include the node at the secondary output of the MV/LV transformer and the end-users' nodes downstream the MV/LV transformer, which can be end-users with or without PV generation. Figure 3.1 illustrates the parameters that will need to be modeled, based on the available historic measurements (input data), as well as the principal parameters (outputs) that will be simulated by the probabilistic algorithms and the use of the available measurements.

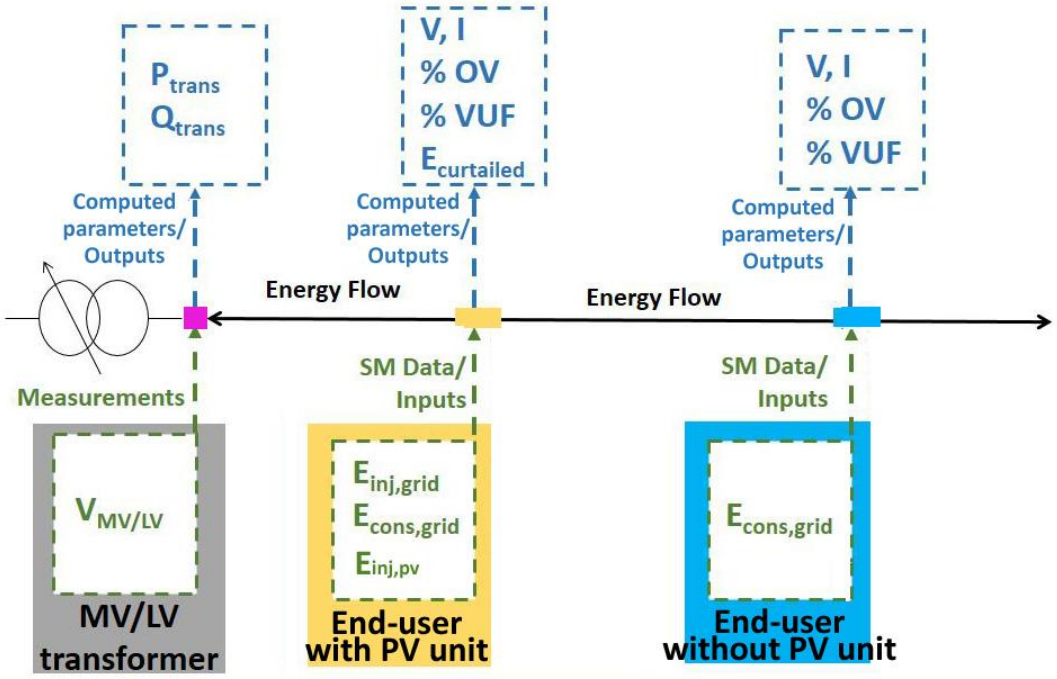

Figure 3.1: The necessary input data for the development of the probabilistic algorithms of this thesis and the principal network operation indices that will be computed

Therefore, as presented in Figure 3.1, the necessary inputs for modeling the variation of the voltage profile at the LV side of the MV/LV transformer are historic measurements (of 10-min or 15-min latencies) of the voltage magnitude ($V_{MV/LV}$) at the respective point of the network.

In order to model the variation of the power exchange at the point of common coupling (PCC) of PV users with the feeder, historic measurements of cumulative consumed ($E_{cons,\ grid}$), injected ($E_{inj,grid}$) and generated ($E_{inj,\ pv}$) PV energy, of 10-min or 15-min latencies, will be necessary. Finally, for modeling the variation of

the power exchange at the point of common coupling (PCC) of end-users without PV generation, historic measurements of cumulative consumed energy ($E_{\text{cons, grid}}$), of 10-min or 15-min latencies, will be necessary. The procedure that is applied for extracting and treating the necessary measurements is thoroughly described in the following sections 3.2 and 3.3.

Figure 3.1 also illustrates the principal indices (outputs) that will be computed, for a given LV feeder, with the probabilistic simulation and the use of the feeder-specific historic measurements. These indices include the variation (with 10-min or 15-min intervals) of the voltage magnitude (V) and unbalance (%VUF) at each node of the feeder, of the current magnitude (I) at each line segment in the feeder and of the total active and reactive power exchange at the MV/LV transformer. Moreover, the overvoltage risk (OV), over a given period, and the total curtailed PV energy, due to temporary cut-offs of PV units, will be computed at each PV node in the feeder. The computation of these indices is thoroughly explained in section 4.1.5.

3.2 Data collection

For supporting the development of the present project, ORES gave to the Electrical Engineering Unit of UMONS online access to long-term historic measurements (of energy flow) of end-users connected to the LV network of the city of Flobecq, in Belgium. The measurements comprise energy consumption, PV injection and PV generation values that are recorded and integrated over ¼-hourly periods by two SM devices (SM1 and SM2). The configuration of the installed devices is illustrated in Figure 3.2.

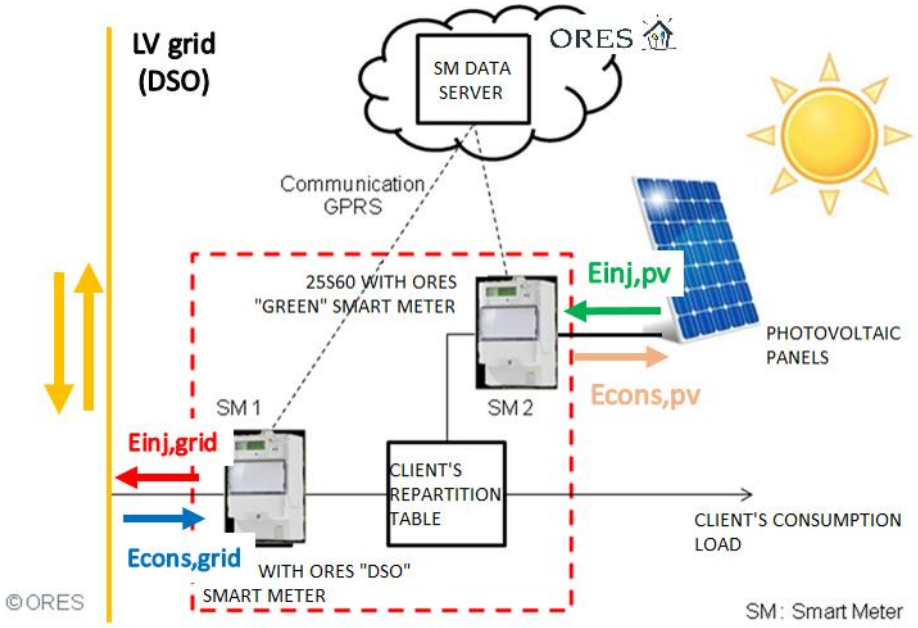

Figure 3.2: Smart metering devices and monitored parameters for residential network users with PV generation, connected to the LV network [1]

The SM1 reads and communicates (locally) two ¼-hourly values, the cumulative consumed $E_{\text{cons, grid}}$ and injected $E_{\text{inj,grid}}$ energy at the PCC of the end-user with the network (in kWh). The SM2 meter reads and communicates the ¼-hourly cumulative generated PV energy $E_{\text{inj, pv}}$ at the respective node (in kWh). In reality only a part of this total ¼-hourly generated energy is finally injected into the grid ($E_{\text{inj,grid}} \leq E_{\text{inj, pv}}$). These recorded values are updated with latencies of 15 minutes and communicated once per day to the database of ORES.

Such readings are available for several end-users with PV generation, connected to LV feeders managed by ORES. The first SM readings have been deployed at few users in 2012. Since then, the installation of SM devices has been going on and the database of ORES has enlarged. These data are a highly precious source for deploying long-term observability analytics of the LV network.

Aiming at providing methodologies and tools for exploiting and evaluating the available datasets, the present study starts with collecting SM1 and SM2 measurements recorded at several end-users over a "long" period (one to three years' time, depending on the SM installation date of the user). Based on the collected data, ¼-hourly total energy consumption, PV generation and PV injection values are extracted. For instance, Figure 3.3 illustrates the total ¼-hourly PV energy injection $E_{\text{inj, grid}}$ and load consumption $E_{\text{cons, grid}}$ values of a given user, recorded by the SM1 over a period of four days in March.

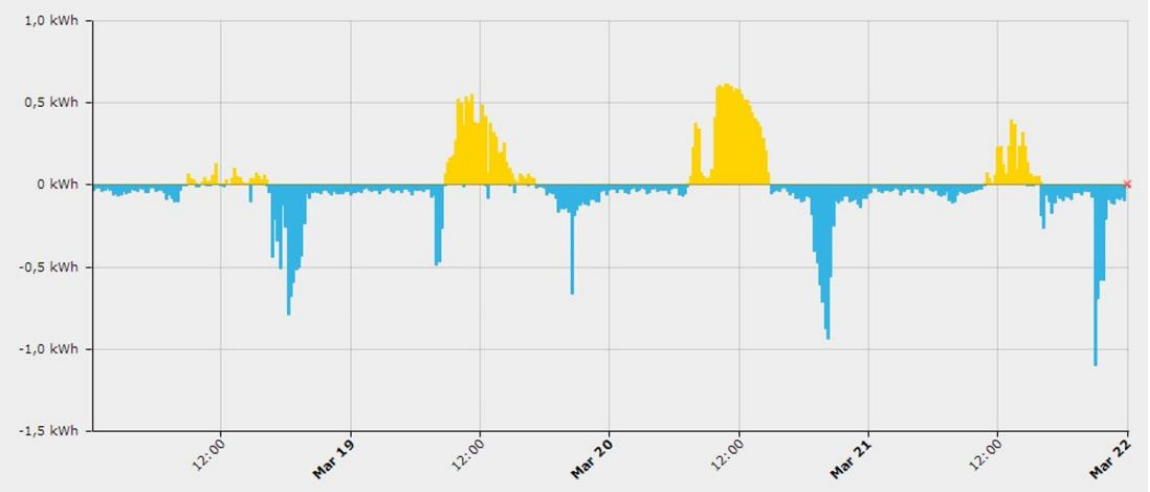

Figure 3.3: Total quarter-hourly injected ($E_{inj, grid}$) and consumed ($E_{cons, grid}$) energy at the PCC of a PV end-user [2]

3.3 Data treatment

The extracted ¼-hourly energy flows have been used to build Typical Day Profiles (TDPs) for each user having a SM installation. The TDPs reflect the variation that each variable parameter ($E_{inj,\ grid}$, $E_{cons,\ grid}$ or $E_{inj,\ pv}$) can take at every individual quarter of an hour of a "typical day". The TDP of energy consumption $E_{cons,\ grid}$, created for the month of April for one of the PV users, is graphically represented in Figure 3.4.

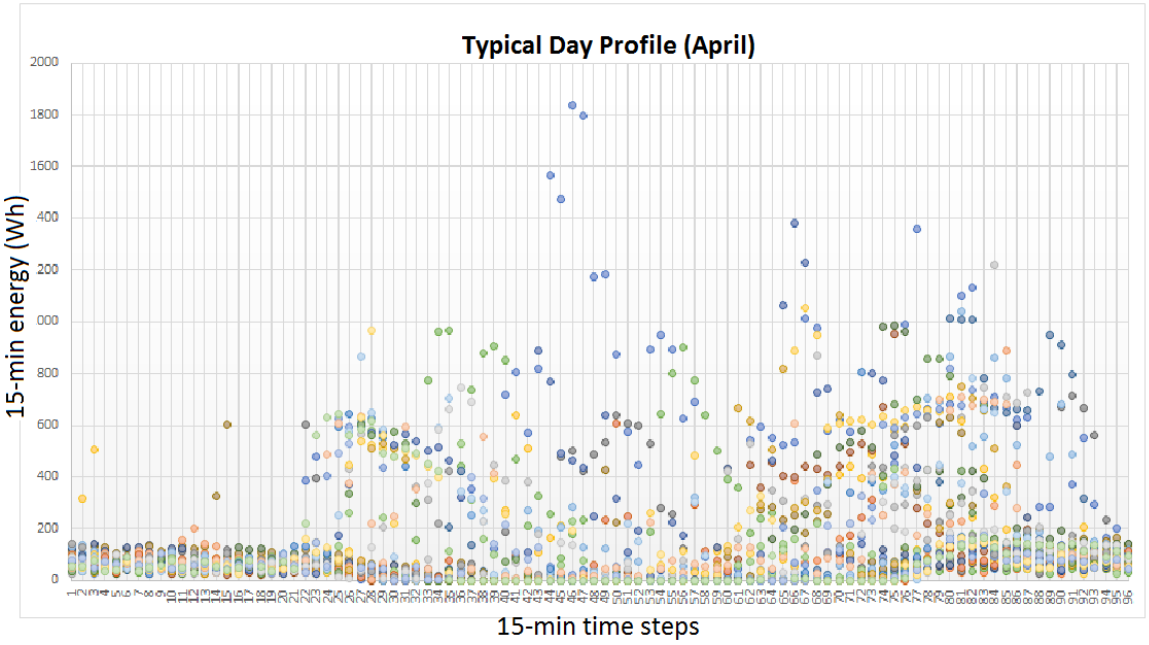

Figure 3.4: Graphical Representation of the Typical Day Profile of energy consumption ($E_{cons,\ grid}$) at the point of common coupling of one PV user, in April. This graph illustrates ¼ hourly-wise the consumed energy values that were recorded day after day.

The "typical day" represents and characterizes a selected period (which can be a month, a season or even a year). Therefore, if one considers nodal $E_{inj,\ grid}$, $E_{cons,\ grid}$ and $E_{inj,\ pv}$ as the random variables that determine each network state, the TDPs are the samples of values that these variables could possibly take on each specific time step. With the use of these samples (TDPs), three Cumulative Distribution Functions (CDFs) of Probability, one for PV generation ($E_{inj,\ pv}$), one for PV injection to the feeder ($E_{inj,\ grid}$) and one for energy consumption ($E_{cons,\ grid}$), can be computed per PV user, per time step q (with q=1:96, where 96 is the number of ¼-hourly periods in a day) (Figure 3.5). For end-users without PV generation, one CDF can be computed, for energy consumption ($E_{cons,\ grid}$) per time step q. Exactly the same methodology is applied to build TDPs for the RMS voltage at the secondary output of the MV/LV transformer, using ¼-hourly data, also rec-

orded by ORES at the MV/LV substation. The methodology that has been applied for this elaboration and the final treatment of the computed CDFs, for their use in the probabilistic algorithms, are described later in paragraph 4.1.2.

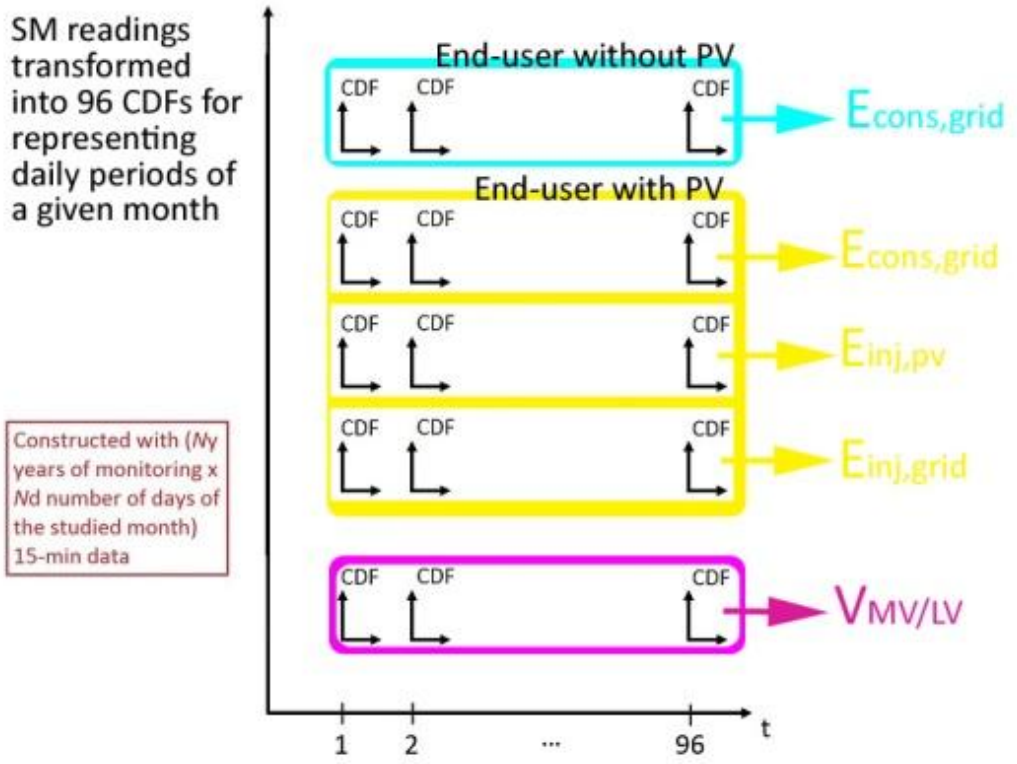

Figure 3.5: Created (PV generation, energy consumption and MV/LV transformer output voltage) quarter-hourly CDFs

Taking a more rigorous view on the computed CDFs of some end-users, one can confirm the high volatility of energy consumption in the LV network. Figure 3.6 shows the CDFs of probability of energy consumption ($E_{cons,\ grid}$) for two end-users, for four ¼ -hourly time steps, based on SM measurements for the month of January (recorded in 2013 and 2014). For example, according to the diagrams of User 1, the energy consumption between 16:30 P.M. and 16.45 P.M. ranges between 0.1kWh and 1.58 kWh while it never exceeds 0.88kWh in the time step between 16:45 P.M. and 17:00 P.M. The amplitude of the range of values remains similar for the period between 17:00 P.M. and 17:15 P.M. while energy consumption can again reach 1.63kWh some time steps later (between 18:00 P.M. and 18:15 P.M.).

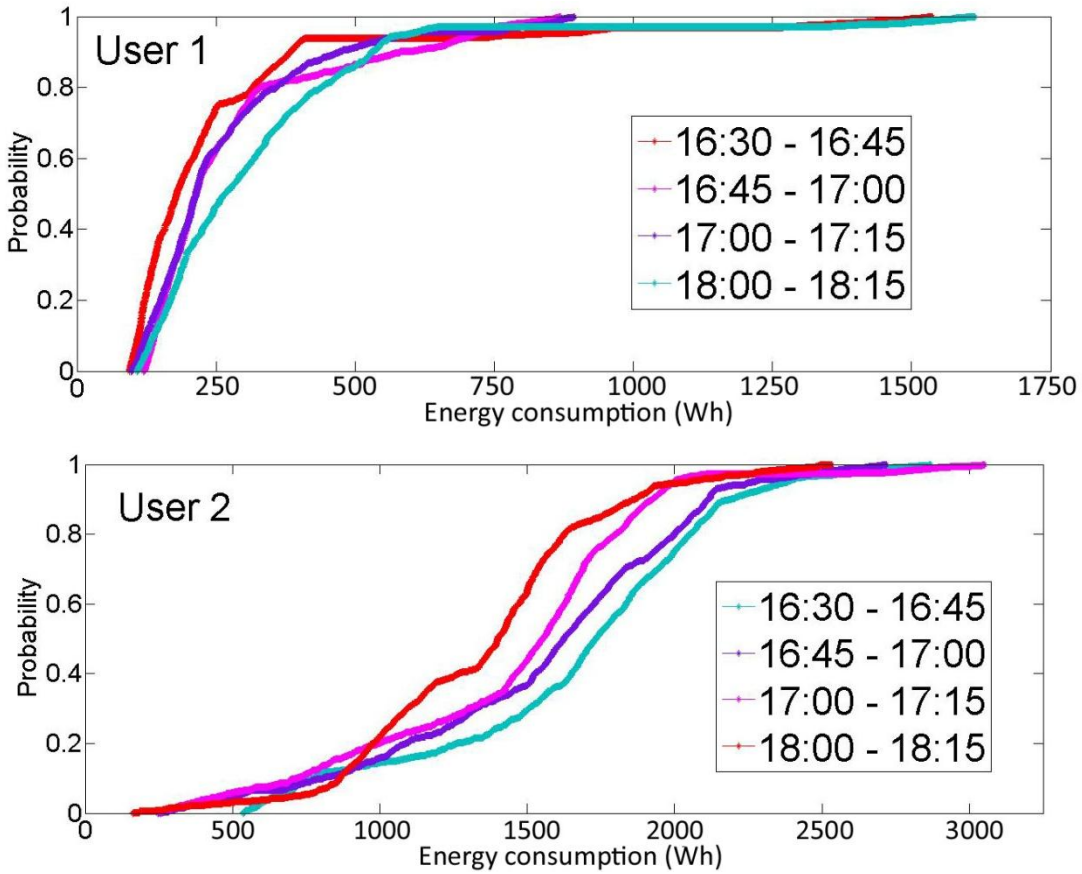

Figure 3.6: CDFs of energy consumption (Wh) for two users connected to the same LV feeder, for 4 ¼ -hourly time steps, based on SM measurements for the month of January.

User 2, who is located very close to User 1, has completely different amplitudes of consumed energy for the same time steps. For example, the energy consumption of User 2 ranges between 0.08kWh and 3kWh in the period between 17:00 P.M. and 17:15 P.M. **Similar differences have been noticed for most of the monitored users. Therefore, high variability applies, not only regarding the energy consumption of the same user over time but also regarding the time-coincidence between the highest or the lowest amount of energy consumed by the different users.** This remark, based on the statistical treatment of available SM datasets, confirmed the high volatility of nodal energy exchanges in LV networks. Chapter 4 presents a methodology for using these datasets in order to incorporate the existing LV network uncertainty in long-term probabilistic analysis models.

Chapter conclusions

Chapter 3 presents the historic measurements that have been collected, treated and analyzed, in order to develop the probabilistic algorithms of this thesis. In this context, the configuration of the SM devices that ORES has installed at the premises of several PV users (connected to the LV network of Flobecq, Belgium) since 2012 is outlined. The procedure that has been implemented, by our research team, for collecting and treating the available SM recordings is also explained step by step. Consequently, the creation of the "typical day" profiles, which are the statistical profiles of the variable parameters that determine the time-varying LV network states, is introduced. This information is primordial for understanding the development of the probabilistic algorithms proposed in the following chapters.

The treatment of the available PV energy injection and consumption historic measurements demonstrated that high variability applies**,** not only regarding the energy consumption of the same user over time, but also regarding the time-coincidence between the highest or the lowest amount of (quarter-hourly) energy consumed by the different end-users. This argument points out the interest of developing LV network modeling methodologies that can simulate the stochasticity of the loading parameters at the end-user level. Chapter 4 presents the probabilistic algorithm that has been developed for this purpose.

Chapter references

[1] ORES, "ORES website," 2012. [Online]. Available: www.ores.be.

[2] ORES, "ORES Smart Metering Platform," 2012. [Online]. Available: https://www.ores-smartmetering.be.

Chapter 4 Probabilistic Framework using Low Voltage Network Metering Data

Highlights

- *A probabilistic framework (methodology and tool) that simulates the time-variability of loading parameters in Low Voltage networks, with the use of user-specific smart metering historic measurements, is presented.*
- *The probabilistic analysis uses a random scenario generation technique that is implemented by means of a Monte Carlo algorithm.*
- *The integrated power flow analysis can either simulate Low Voltage feeders as perfectly balanced systems or consider the existing phase unbalance due to single-phase connections.*
- *Most important Low Voltage network operation indices are computed for an extensive number of possible network states. Boundary values and statistical distributions can be computed for the simulation outputs.*
- *These outputs can be either used in the long-term network analysis, as for example in the evaluation of different technical strategies that can be integrated in the simulation, or for improving network observability in real-time state estimation applied for the Medium Voltage level.*
- *The developed methodology is implemented for a real Low Voltage feeder. Voltage outputs are compared to real measurements and to the outputs of a deterministic approach. Although a great amount of information is missing, the comparison results are quite satisfactory.*
- *A first attempt to address issues like the spatial correlation among end-users, regarding their power flows, and the sparse availability of historic measurements is also presented.*

4.1 Overall Structure

Chapter 4 presents the backbone of this study's developments. The presented structure is a probabilistic framework that has been developed for deploying long-term observability analytics of LV networks. The developed algorithm uses as input measurements that are collected and statistically modeled as presented in Chapter 4.

The main objective of this development is providing the DSO with an analysis methodology and the respective tools that can address, in simulation terms, the volatility of nodal energy flows in the LV network (based on network-specific SM data). By means of this tool, long-term analytics and strategic network design can be based on the evaluation of a whole range of possible system states rather than the least favorable ones, which is the case with the tools currently used by the majority of distribution utilities.

The second utility of the developed methodology and tool is the statistical characterization of operation indices of the LV network, which can importantly improve the observability of the overall network in state estimation techniques currently developed for the MV level. For example, a link between exchanged powers at the MV/LV transformer and the global consumption/generation installed at the LV level could be statistically determined. Other than that, a link between the phase voltages at the MV/LV transformer and the ones at some critical nodes downstream the MV/LV transformer, could also be statistically determined. Similar links could also be determined concerning voltage unbalance. Recently, several contributions discuss the impact of DG units, connected to the LV network, on the operation of the MV distribution or even the transmission network [1]. With the further integration of EVs, this impact will only grow bigger for the foreseeable future.

The probabilistic framework that has been developed for addressing these objectives follows the structure of Figure 4.1. It comprises five principal analysis modules. The first two modules practically apply a deterministic process that uses the topology characteristics and the SM datasets of each studied feeder. The first one models the topology of the network and the parameters of the components of the network while the second one creates the statistical samples that characterize the total consumption and PV injection of end-users' (¼-hourly time steps). The three following modules apply a probabilistic process. In particular, the third module defines, by means of a MC algorithm, the whole range of network states that will be studied in the given network. The fourth module applies the Power Flow (PF) analysis of each individual state and the fifth module implements a statistical analysis and evaluation of the outputs that are computed in the previous PF block. In the next sections, the detailed description and the theoretical background of each computation module are presented.

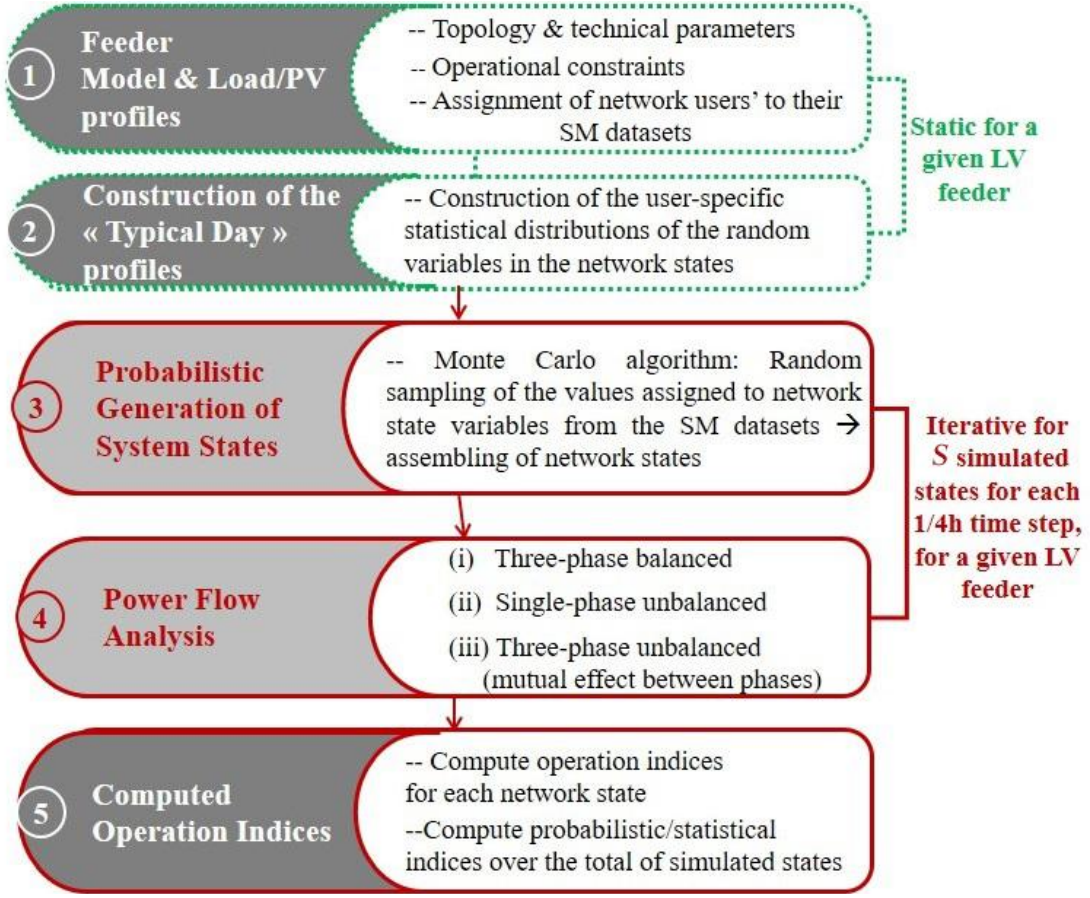

Figure 4.1: Structure of the probabilistic framework

4.1.1 *Feeder model and load/PV profiles*

The first analysis module determines the topology of the studied network, its technical and operational characteristics as well as the loads and PV connections configuration (single-phase, three-phase, etc.). Practically, the position and the type of each node (simple user, PV user, intermediate nodes, lateral root nodes, single-phase or three-phase connection etc.) as well as the network components and lines (physical and electrical parameters) are defined. User nodes are assigned to their respective load/generation statistical profiles and operational constraints with regard to voltage magnitude, unbalance and other operational indices are set. Finally, in this first module, the network configuration (balanced or unbalanced) is selected among the three principal options that are thoroughly described in Section 4.1.4. Therefore, this first module defines the static values which remain exactly the same for the total number of analyzed system states.

4.1.2 *Construction of the "Typical Day" statistical profiles*

The second analysis module creates the statistical samples of values that the random variables can take in each system state. Given the ¼-hourly resolution of

the available SM datasets, the network state is also analyzed with ¼-hourly time intervals. Thus, each ¼-hourly time step q in a day (q=1:96 since the number of ¼-hourly time steps in a day is equal to 96) is linked to a range of S independent network states. This range of independent network states serves for characterizing the operation of the network during the respective time step q, in a statistical manner, as it will be explained in paragraph 4.1.5. The transition between successive quarters of an hour (for example the transition between the simulated states for time step q and the ones sampled for time step q+1) is considered to be independent and not generated by means of a mathematical sequentiality approach. By implementing such a procedure, a Pseudo-Sequential algorithm (cf. section 2.3.2) has been thus developed and will be further commented in paragraph 4.1.3.

As explained in Chapter 3, for each time step q, a large set of $E_{\text{inj,pv}}$ $E_{\text{inj,grid}}$, $E_{\text{cons,grid}}$ values have been recorded at each node i over a long period. Similarly, for each time step q, a set of $V_{\text{MV LV}}$ have been recorded at the LV side of the MV/LV transformer. These recorded values are used to assemble "typical day profiles" (TDP) that will be used for the statistical generation of the network states in the Pseudo-Sequential MC process (described in the following section).

The present simulation module initially groups the recorded values in monthly periods. This means that each month of the year will be characterized by one single set of typical day profiles. The same month can of course be taken into account over several years of measurements. If the generated PV energy of a user is recorded on a ¼-hourly basis over N_{y} years and the studied month has N_{d} days, it comes then that the number of values at our disposal, for creating the TDP of PV generation of the respective user, is equal to N_{tdp}:

$$N_{\text{tdp}} = N_{\text{y}} \cdot N_{\text{d}} \cdot 96 \tag{4.1}$$

Relation (4.1) applies for all the random variables to be sampled. Given that the system is analyzed considering ¼-hourly network states, it means that a given random variable is modeled during a single quarter of an hour thanks to the use of N_{q} values:

$$N_{\text{q}} = N_{\text{y}} \cdot N_{\text{d}} \tag{4.2}$$

For instance, the TDP of Figure 4.2 is based on measurements recorded during the single month of April 2013. Each vertical axis corresponds to an individual quarter of an hour q (¼-hourly sample) and is thus composed of N_{q}=1*30 energy consumption values.

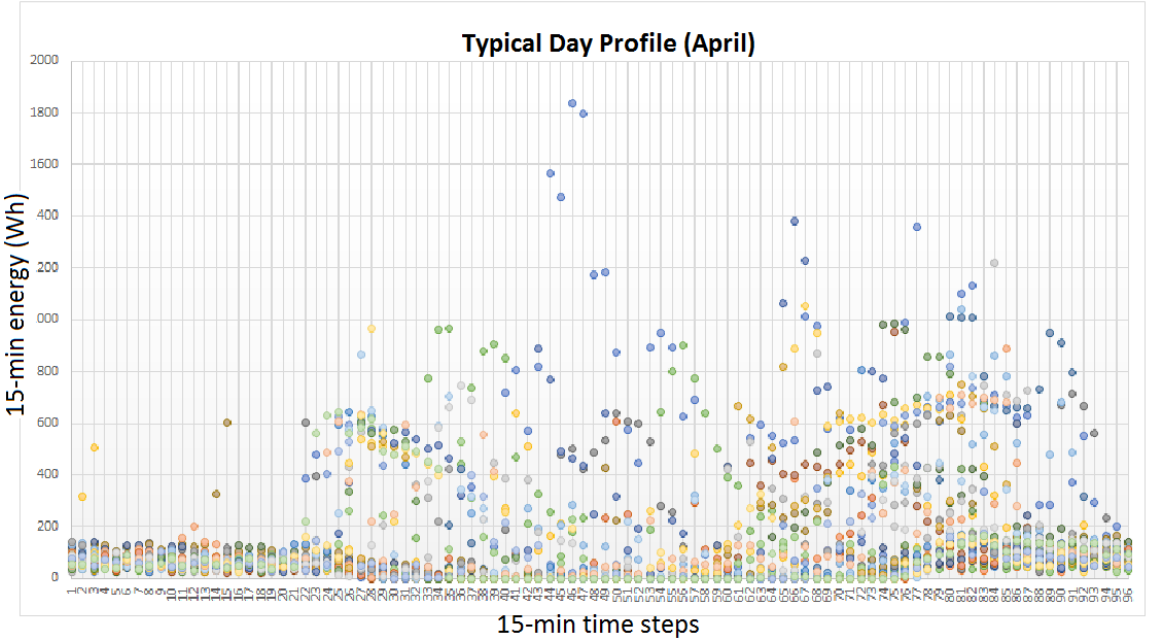

Figure 4.2: Graphical Representation of the Typical Day Profile of energy consumption ($E_{cons,\,grid}$) at the point of common coupling of one PV user, in April. This graph illustrates ¼ hourly-wise the consumed energy values that were recorded day after day.

Practically, each simulated network state will be characterized by a set of random variables. For example, for a given time step q, the population of available (recorded) values $\boldsymbol{E}_{\mathbf{inj,pv,q}}$ in a feeder with N_{pv} nodes (nodes with PV) is given by the following $[N_{\mathrm{pv}}\, x\, N_{\mathrm{q}}]$ matrix:

$$\boldsymbol{E}_{\mathrm{inj,pv,q}} = \begin{matrix} E_{1,1} & \cdots & E_{1,N_{\mathrm{q}}} \\ \vdots & \cdots & \vdots \\ E_{\mathrm{i},1} & E_{\mathrm{i,d}} & E_{\mathrm{i},N_{\mathrm{q}}} \\ \vdots & \cdots & \vdots \\ E_{\mathrm{N_{PV}},1} & E_{\mathrm{N_{PV}},\mathrm{d}} & E_{\mathrm{N_{PV}},N_{\mathrm{q}}} \end{matrix} \tag{4.3}$$

where d stands for the day (d=1: N_{q}) and i stands for the node (i=1: N_{pv}) and $E_{\mathrm{i,d}}$ is the total PV energy generation that was recorded at node i during time step q of day d. Consequently, the data of one line in matrix (4.3) will allow defining one random variable of the global set characterizing network states to be sampled during each quarter of an hour q.

The sampling of the different network states (scenario generation process) will be described in the following section 4.1.3. In each state, three variables ($E_{inj,pv,q,i}$, $E_{load,q,i}$, $V_{MV\ LV,q}$) describe the exchange of power at each end-user node and one variable describes the voltage at the output of the MV/LV transformer (considered as the slack node) as presented in expression (4.4) :

$$E_{inj,pv,q,i} \ , \ E_{load,q,i} \ , \ V_{MV\ LV,q} \ , \quad q = 1{:}\,96 \ and \ i = 1{:}N \quad (4.4)$$

where $E_{inj,pv,q,i}$ is the total PV energy that was generated at node *i* during time step *q*, $E_{load,q,i}$ is the total net energy demand at node *i* during time step *q* and $V_{MV\ LV,q}$ is the voltage at the MV/LV transformer in time step *q*. The net energy demand at node *i* during time step *q* is computed with the relation (4.5):

$$E_{load,q,i} = E_{cons,grid,q,i} + E_{inj,pv,q,i} - E_{inj,grid,q,i} \quad (4.5)$$

where $E_{inj,grid,q,i}$ is the total PV energy that was injected towards the network at node *i* during time step *q*, $E_{inj,pv,q,i}$ is the total PV energy that was generated at node *i* during time step *q* (a part of this energy is locally consumed by the user) and $E_{cons,grid,q,i}$ is the total energy consumption that was absorbed from the network at node *i* during time step *q*. These three values are recorded by the SM devices that are installed at node *i* (see Figure 3.2).

Thus, in a feeder supplying *N* nodes (end-users) in total (with and without DG), the number of random variables used to characterize each network state is equal to RV:

$$RV = 2 \cdot N + 1 \quad (4.6)$$

The operation of the network is therefore emulated at ¼-hourly intervals, considering historic measurements that have been recorded for the respective time interval. The matching of historic measurements and the simulation are performed for statistically characterizing monthly periods although this option can be adapted to the needs of the study. Basically, each system state is determined by a set of values that the random variables can take from their respective distributions. For example, as far as PV energy generation at node *i* during time step *q* is concerned, the sample of values that this variable can take is the vector $E_{\mathrm{inj,pv,q,i}}$:

$$E_{inj,pv,q,i} = E_{\mathrm{i},1} \cdots E_{i,d} \cdots E_{\mathrm{i},N_{\mathrm{q}}} \quad (4.7)$$

The sample of measurements for random bles $E_{inj,pv,q,i}$, $E_{load,q,i}$, $V_{MV\ LV,q}$ is used to construct a probabilistic histogram whose total length is defined by the minimum and the maximum recorded values at the respective time step *q*. Histograms for $E_{inj,pv,q,i}$, $E_{load,q,i}$, $V_{MV\ LV,q}$ are computed separately. The optimal length C_{q} of intervals is obtained with the following formula, proposed by A.H.Sturges in [2] :

$$C_q = \frac{R_q}{1+3.322 \cdot log N_q} \quad (4.8)$$

where R_{q} is the range (absolute difference between the minimum and the maximum recorded value for the respective variable) and N_{q} is the number of the rec-

orded values for the respective time step q. By definition, the probability that a recorded item belongs to a specific energy interval c is equal to:

$$p_c = \frac{k_t}{N_q} \tag{4.9}$$

where k_t is the total number of values (recorded at the respective time step q), that belong to interval c. Once probabilities p_c have been computed for each interval for each variable, Probability Distribution Functions (PDFs) can be established for each time step q. These PDFs are transformed into CDFs of probability. Practically, a set of classes $[x_1, x_2 \ldots x_n]$ is defined and the basic statistical formula (4.10) is applied for transforming the samples of values into CDFs:

$$\text{CDF } X = P(X \leq x) \text{ , where } x = [x_1, x_2 \ldots x_n] \tag{4.10}$$

where X is the variable parameter represented by the respective ¼-hourly statistical profile and x is the boundary of the respective interval of the PDF which is computed with relation (4.8).

Consequently, the CDFs that are finally used for the development of the probabilistic algorithm are the ones graphically illustrated in Figure 4.3. Regarding end-users with PV generation, 2*96 CDFs (96 CDFs for $E_{inj,pv}$ and 96 CDFs for E_{load}) are computed. Regarding end-users without PV generation, 96 CDFs are computed for E_{load}, which in this case is equal to $E_{cons,grid}$ since the part $E_{inj,pv,q,i} - E_{inj,grid,q,i}$ of relation (4.5) is equal to zero for these end-users. Moreover, 96 CDFs are computed for modeling the voltage magnitude $V_{MV/LV}$.

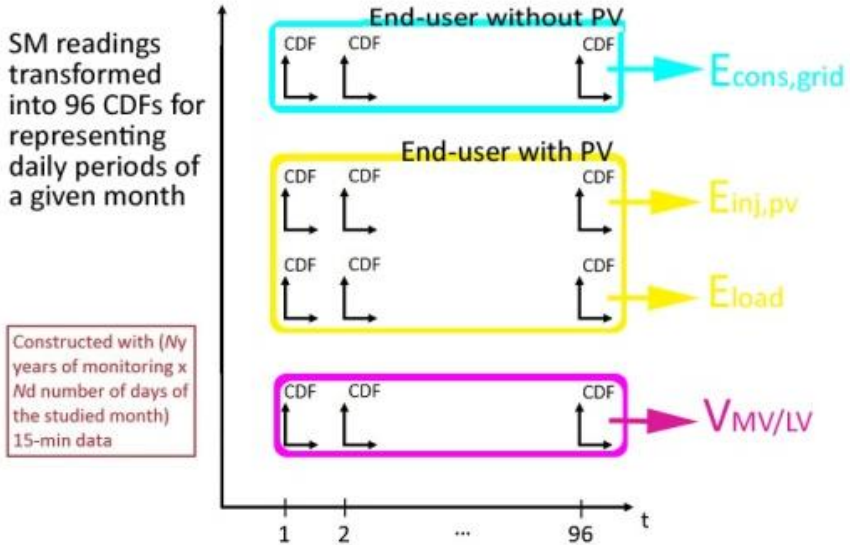

Figure 4.3: Created (PV generation, net energy demand and MV/LV transformer output voltage) quarter-hourly CDFs

For a given time step q, N distributions are created for net energy demand (E_{load}), N distributions are created for PV energy generation $(E_{\text{inj,pv}})$ and one distribution is created for the voltage at the transformer $(V_{\text{MV LV}})$. Given that the constructed CDFs of probability are based on discrete recorded values for each variable, they have to be linearized by means of linear interpolation for applying the MC algorithm (explained in Section 4.1.3).

In conclusion, with the previously described methodology, the bulk data that are recorded for each variable for each time step q (as in Figure 4.2) of a typical day are now represented by 96 statistical distributions as the one of Figure 4.4. This figure represents the CDF of probability of $E_{\text{inj,pv}}$ of one PV user for the time step between 8:45PM and 9:00AM of a typical April day. The created statistical distributions (CDFs of probability) will be used in the MC algorithm as inputs for defining the values of the different variables that characterize each simulated state.

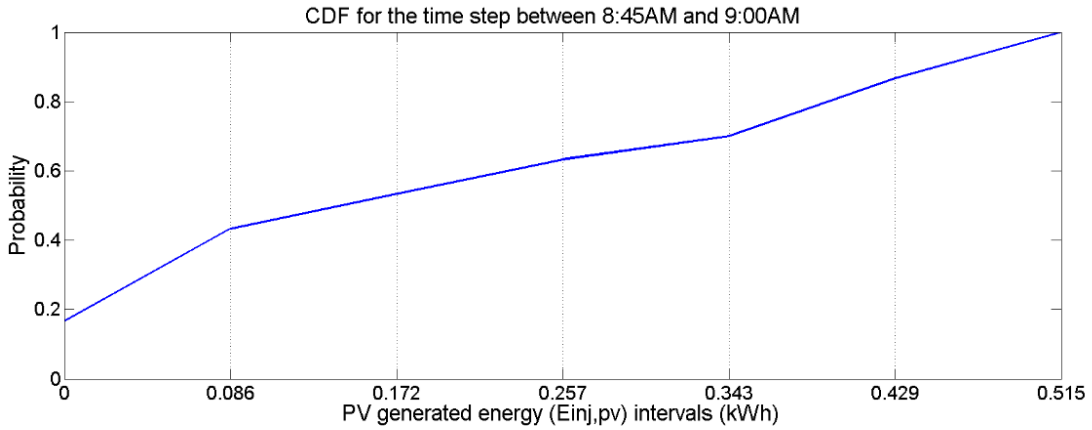

Figure 4.4: CDF of $E_{inj,pv}$ for the ¼-hourly time step between 8:45PM and 9:00AM for one PV user

4.1.3 *Probabilistic generation of system states*

i. *Scenario generation with MC algorithm*

This third computation module practically launches the probabilistic process of the proposed methodology. The determination of the possible system states that should be studied for statistically characterizing the operation of the network is deployed with a probabilistic scenario-generation technique. Basically, a Pseudo-Sequential MC algorithm is used for randomly generating the set of possible system states s for each ¼-hourly time step in a day. The statistical distributions (CDFs of probability) of the previous module are used by the implemented MC algorithm as sampling inputs. Figure 4.5 indicatively illustrates the random variables for which the MC algorithm samples possible values in each simulated

state. Also note that the set of variables varies in function of the node type (PV node, simple node, slack node).

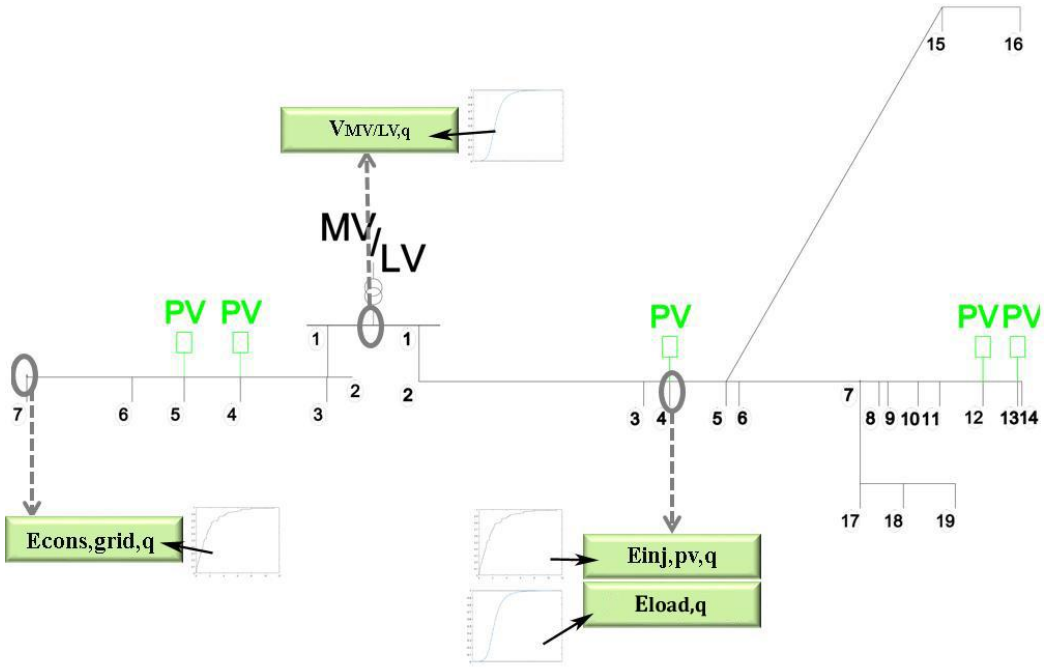

Figure 4.5: Different types of nodes and the respective variables to be sampled for each network state

In detail, for parameterizing each network state, the MC algorithm randomly samples a value $u_{\text{inj,pv,i}}$ from the classical uniform distribution on the interval [0,1] for each PV user *i*. This $u_{\text{inj,pv,i}}$ value is assigned to the CDF of probability for PV generation of PV user *i* and is consequently linked to a PV energy generation $E_{\text{inj,pv,i}}$ value as shown in Figure 4.6. The $E_{\text{inj,pv,i}}$ value is the one considered at node *i* for the respective network state. Independently from the nodal $u_{\text{inj,pv}}$ samplings, the MC algorithm also makes independent samplings of $u_{load,\ wd}$ values for each one of the connected users, in order to determine, similarly as in Figure 4.6, the net energy demand value $E_{\text{load,wd}}$ that corresponds to a week day. In the same way, independently from the previous samplings, an independent sampling of $u_{\text{load, we}}$ value is made per user to obtain the week-end net energy demand $E_{\text{load,we}}$ value.

Finally, the MC algorithm makes a last random sampling of a value *w* on the interval [0,7] in order to determine if the studied network state corresponds to a week (in case $w \in [2,7]$) or a weekend day (in case $w \in [0, 2]$). Based on this last sampling, E_{load} is determined for each user of the studied network state as follows:

$$E_{load} = E_{load,we}\ if\ w \in \ 0,2$$

$$E_{load} = E_{load,wd} \; if \; w \in \quad 2,7 \tag{4.11}$$

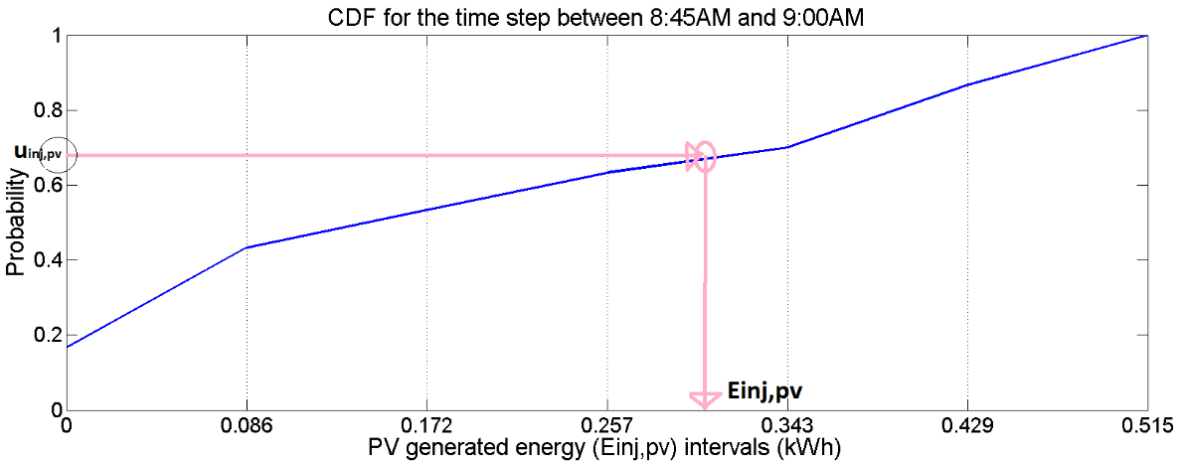

Figure 4.6: Randomly sampled value of $E_{inj,pv}$ of user i for a specific network state by randomly sampling a uniformly distributed $u_{inj,pv}$ value on the interval [0,1]

The overall procedure that is applied with the MC algorithm for sampling the nodal variables is illustrated in the flowchart of Figure 4.7. The PF analysis of the feeder requires considering each system state as a steady-state one. Practically, the sampled energy values need to be transformed into power values ($E_{\text{inj,pv}} \rightarrow P_{\text{inj,pv}}$ and $E_{\text{load}} \rightarrow P_{\text{load}}$). For each node, the power value that represents the power flow at the PCC of each end-user *i* with the feeder is determined as follows:

$$P_{i=} \frac{E_{load_i} - E_{inj,pv_i}}{0.25} \tag{4.12}$$

If P_i is positive the respective user *i* is consuming power from the network whereas if P_i is negative, the user is injecting power into the system during the considered quarter of an hour.

The total number of system states that is generated with the MC algorithm, for the studied period, is equal to *S*96*. Figure 4.7 illustrates the overall scenario generation procedure in which the value of *S* must be initially predefined for the MC simulation. For this reason, an adequate number needs to be set (usually $S \geq 1000$ for a typical radial LV feeder with 10 to 30 nodes) so that the majority of possible assemblings of sampled values (that the random variables can take) can be considered.

The following paragraph 4.13.ii presents an adaptation of this procedure in which the number of simulated days *S* is not predefined but determined during the simulation, in function of the convergence of the most important computed indices. This study shows that a number of 1000 iterations are sufficient to ensure the convergence of those indices. Consequently, in the majority of the simulations presented in the following chapters the procedure that is illustrated in Fig-

ure 4.7 has been applied by setting *S* equal to 1000. The computational time that has been required for the simulations deployed in this thesis, by setting *S* equal to 1000, is considered to be very satisfactory. Table A2 of Appendix A3 presents the computational time for some of the simulations.

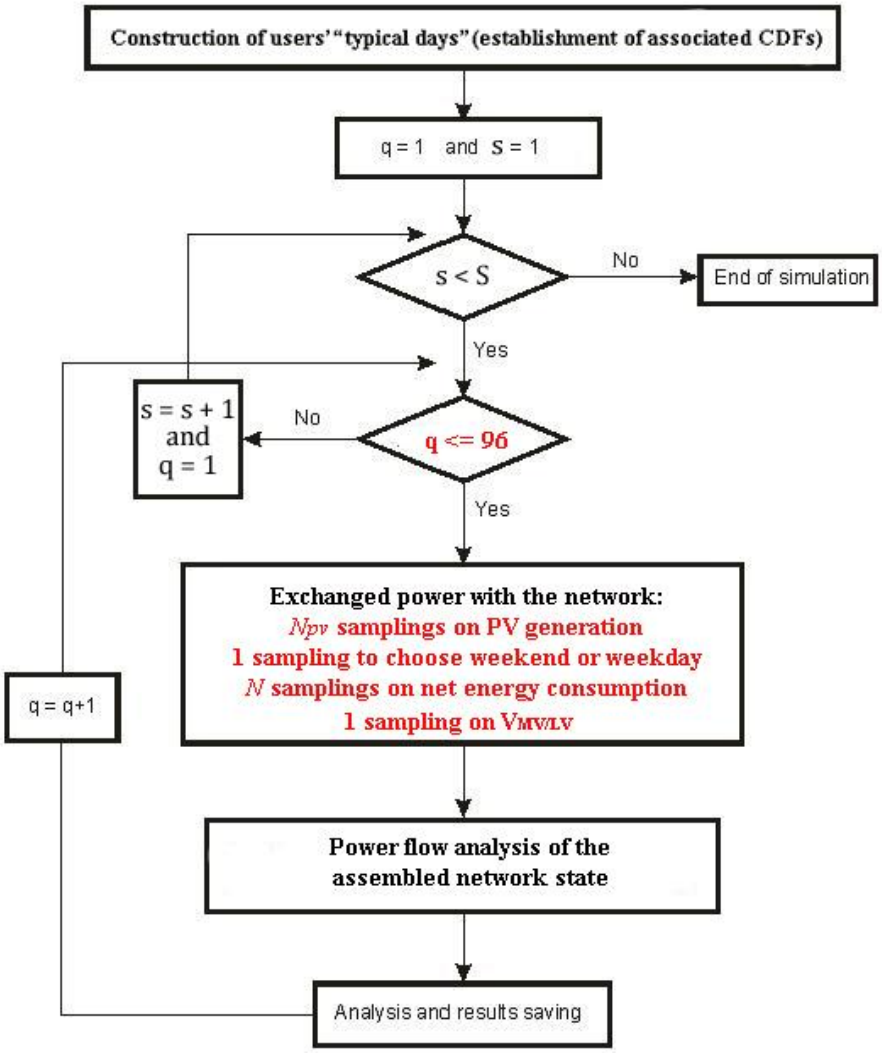

Figure 4.7: The MC algorithm sampling procedure in a feeder with N connected users among which N_{pv} end-users have a PV unit.

ii. *Convergence of the Monte Carlo iterations*

The probabilistic nature of the simulation tool relies on the principle that load/PV generation profiles of users are highly time-varying. The iteration of system states is therefore based on a very large number of random assemblings of the possible values that random variables can take. The procedure described in

the previous paragraph 4.1.3.i is repeated for an extensive number of simulated days *S* (corresponding to *S**96 network states) so that an adequate representation of the studied network is reached. An alternative for achieving this goal, apart from predefining the number of simulated days, is also integrated in the developed algorithm. This alternative procedure is illustrated in Figure 4.8 and applied as follows.

The probabilistic simulation principally focuses on the following electrical parameters (at all nodes and line segments) for each network state:

- Phase voltages $\boldsymbol{V}_{abc}$ (magnitudes and angles)
- Voltage unbalance *VUF*
- Line currents $\boldsymbol{I}_{abc}$ (per phase)
- Line losses S_{loss}

Considering that for each ¼-hourly time step in day, a total number *S* of possible system states is simulated, each individual electrical parameter is thus characterized by a [1xS] matrix (for a given time step *q*). These [1x*S*] matrices allow then statistically representing each of the computed electrical parameters by means of CDFs (one CDF per quarter of an hour).

The value of *S* is determined as the minimum number of evaluated system states for which the obtained CDFs of all the selected indices converge for each ¼-hourly time step. Thus, for a given time step *q*, distributions $\underline{\mathrm{CDF}}_{s-1}^{q}$ and $\underline{\mathrm{CDF}}_{s}^{q}$ converge as soon as relation (4.13) is satisfied for all the defined classes $[x_1, x_2 \ldots x_n]$:

$$\underline{h} < 10^{-2}, \text{where } \underline{h} = \underline{\mathrm{CDF}}_{s-1}^{q} - \underline{\mathrm{CDF}}_{s}^{q} \qquad (4.13)$$

Practically, the convergence of the CDFs is achieved as soon as the difference in the cumulated probability of falling within each one of the defined classes of the CDF, between two consecutive iterations, is smaller than a fixed threshold.

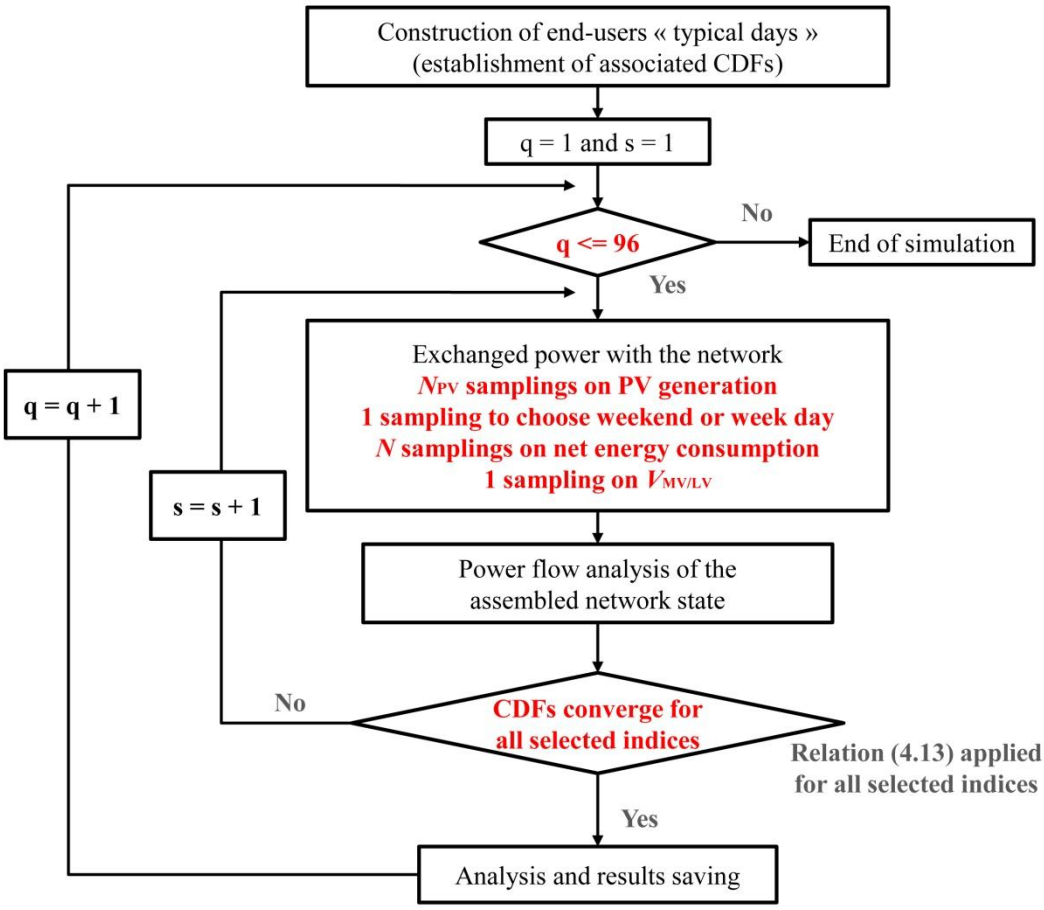

Figure 4.8: The MC algorithm sampling procedure in case the number of simulated days S is not initially predefined but determined, during the simulation, in function of the convergence of important computed indices

For achieving a good level of accuracy, the range of classes [x_1, x_2…x_n] needs to be sufficiently refined in function of the considered parameter. Indicatively, Figure 4.9 illustrates the CDFs created for phase voltage V_a at node 8, for S=500x96, S=950x96 and S=1000x96. One can easily observe that for 950 and 1000 simulated days the computed CDFs for V_a have practically converged. This convergence does not apply between the simulations of 500 and of 950 days. The range of the classes is defined equal to 0.5V in this example. As previously mentioned, in the simulations presented in the following chapters, the focus is principally set on voltage magnitudes and unbalance, which most of the times converge with S=1000 MC iterations (Figure 4.9). For this reason, the algorithm of Figure 4.7 has been applied, in the simulations of this thesis, with S=1000. However, in certain cases, such as networks with a small number of nodes or simulations in which relation (4.13) needs to converge for a restricted number of indices (and not, for example, for phase voltages and unbalance at each node), the algorithm

of Figure 4.8 could require less loops on sampled values and thus require less computational effort.

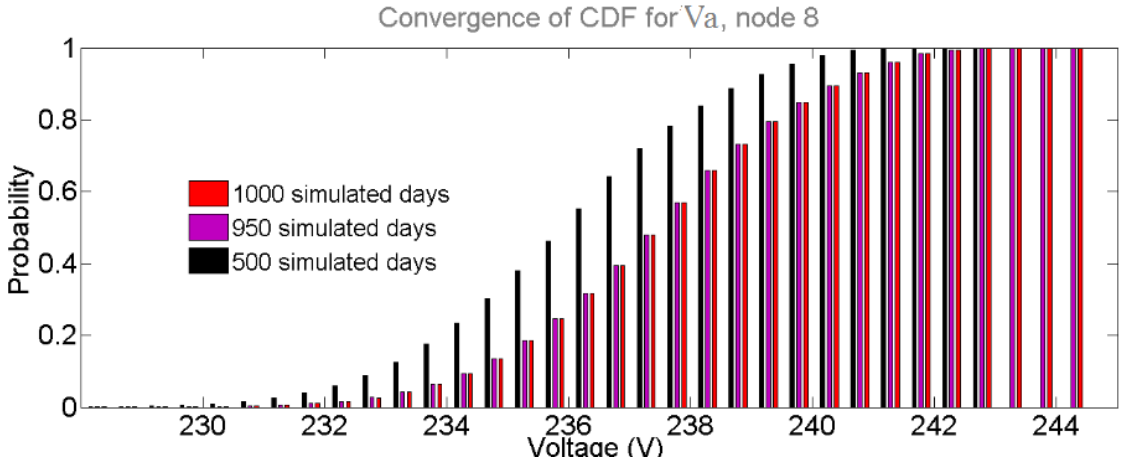

Figure 4.9: CDFs of probability for phase voltage V_a at node 8, for S=500x96, S=950x96 and S=1000x96

The convergence of the computed CDFs (either by predefining the number of simulated days *S* or by applying the procedure illustrated in Figure 4.8) practically demonstrates that once having evaluated an extensive number of possible loading conditions in the feeder, the statistical distributions and the variation of amplitude of the computed magnitudes is realistically estimated. Based on this assumption, operation compliance with the probabilistic criteria of the EN 50160 standard can be verified, the congestion risk can be quantified and statistical distributions can be constructed for line losses.

iii. *Transition between successive system states*

Regarding the transition between successive quarters of an hour (from state q to q+1), the Quasi-Sequential (or Pseudo-Sequential) approach has been selected for the reasons that are outlined in Section 2.3.2. Therefore, the MC algorithm does not require an analytical model for associating the values of the random variables at q+1 with the ones that were sampled at q. The values in each state are sampled independently (in the chronological sense) from the ones of the precedent or the successive state but always from the statistical distributions related to time step q. For example, the values for $E_{inj,pv,q}$ are always sampled from the CDF of probability that is based on values recorded in time step q and the values for $E_{inj,pv,q+1}$ are always sampled from the CDF of probability that is based on values recorded in time step q+1. In this way, the sequentiality of system states is partly respected. Practically a trade-off between computation effort and accuracy is applied. This trade-off might affect studies in which the time-dependency of system states is important (such as the techno-economic evaluation of solutions like storage or DR strategies). However its impact is negligible when the partial

independency of successive system states is not a brake on the studied outputs. Besides, developing scenario reduction algorithms and time-dependency functions is out of the scope of the present study although it is an interesting research subject that deserves thorough investigations. Indeed, this study assumes that statistical analytics and long-term observability studies of the LV network can be deployed, considering this trade-off, without compromising the reliability of the simulation outputs. The use of measurements with a fine resolution (¼-hourly latencies) is one of the main assets for supporting this consideration. The time dependency between system states is also discussed in Chapters 5 to 8 by means of the presented case studies.

4.1.4 *Power flow analysis*

This simulation module uses the previously defined system states as input data for the power flow analysis of the feeder. The network configuration option in the 1st simulation module defines which power flow algorithm will be used to analyze all network states. If the consideration of a perfectly balanced system is selected, then the load flow analysis is done according to case (i). In case of three-phase or two-phase system with unbalanced loads/PV units and with a configuration that allows neglecting mutual coupling effects between phases, the algorithm of case (ii) can be selected. The last and most generic case (iii) covers all other possible configurations of LV radial feeders, including the ones treated with the simplified and faster cases (i) and (ii). The general network configuration that can be treated by case (iii) is shown in Figure 4.10. This last option should be selected in case of an unbalanced three-phase or two-phase main configuration with unbalanced three-phase, two-phase and/or single-phase load/PV connections and eventually unbalanced laterals, where the mutual coupling effect between phases should not be neglected. The three possible configurations are explained in the next subsections:

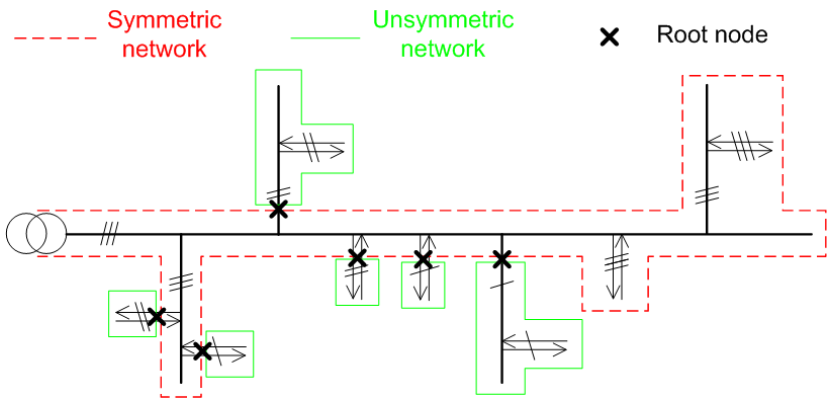

Figure 4.10: General network configuration that can be treated in case (iii)

i. *Three-phase main line with balanced three-phase loads/PV connections*

In this case, the system is analyzed as a three-phase balanced radial system, considering three-phase loads/PV connections as well as three-phase laterals at certain nodes. The applied power flow algorithm is the one used in [3]. This algorithm allows the computation of nodal voltage magnitudes, line power flows and losses, as well as current magnitudes, for every system state. The methodology demonstrates a good computational time, converging after a small number of iterations.

Basically, an iterative procedure is used starting from the last node *N* (Figure 4.11) and estimating the total active and reactive power from expressions (4.14) and (4.15):

$$P_{j+1,N} = \sum_{i=j+1}^{N} P_{load,i} - P_{inj,pv,i} + \sum_{i=j+1}^{N-1} P_{loss,i+1} \quad (4.14)$$

$$Q_{j+1,N} = \sum_{i=j+1}^{N} Q_{load,i} + Q_{inj,pv,i} + \sum_{i=j+1}^{N-1} Q_{loss,i+1} \quad (4.15)$$

where, the active power $P_{j+1,N}$ (Figure 4.11) includes all the active loads $P_{load,i}$ and PV power injections $P_{inj,pv,i}$ computed (by dividing the respective sampled values for $E_{load,i}$ and $E_{inj,pv,i}$ with 0.25, as in relation (4.12)) between node *j+1* and node *N* and $P_{loss,i+1}$ is the active losses in the branch connected between nodes *i* and *i+1* (*i=i+1,…,N-1)*. In the same way, $Q_{j+1,N}$ (Figure 4.11) is the sum of all the reactive loads that are defined considering constant values for $cos\varphi_{cons,i}$ and $cos\varphi_{inj,i}$ in each network state ($Q_{inj,pv,i}$ is positive if the PV node consumes reactive power and negative if it generates reactive power) and $Q_{loss,i+1}$ is the reactive power losses in the branches connected between nodes *j+1* and *N*.

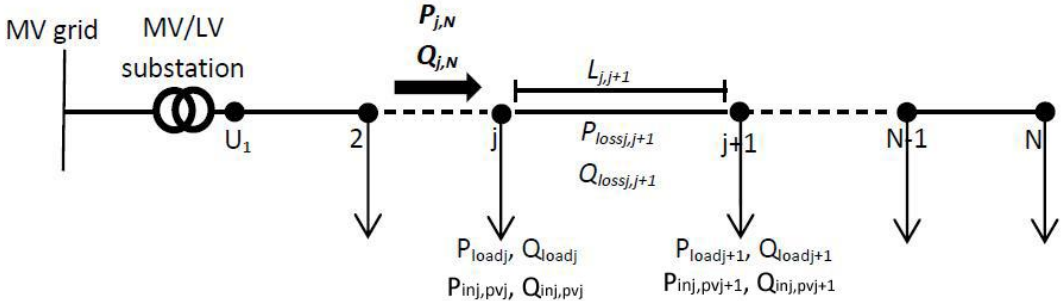

Figure 4.11 Illustration of the load low computation process for radial networks [3

Practically, the active and reactive power absorbed in node *N* can be expressed as:

$$P_{N-1,N} = P_{load,N} - P_{inj,pv,N} \quad (4.16)$$

$$Q_{N-1,N} = Q_{load,N} + Q_{inj,pv,N} \quad (4.17)$$

Moreover, the active and reactive losses between two nodes *j* and *j+1* are obtained by:

$$P_{lossj,j+1} = R' * L_{j,j+1} * I_{j,j+1}^2 \quad (4.18)$$

$$Q_{lossj,j+1} = X' * L_{j,j+1} * I_{j,j+1}^2 \quad (4.19)$$

where, *R*' and *X*' are respectively the resistance and the reactance per kilometer of the branch. $L_{j,j+1}$ is the length of the line between nodes *j* and *j+1*. $I_{j,j+1}$ is the current flowing on this same line.

Based on expressions (4.14) to (4.19) and using the assumption validated in [3] for the computation of $I_{j,j+1}$ in LV networks with PV generation, it is possible to easily solve the active and reactive power flowing ((4.14) and (4.15)) in each branch of the considered feeder. Using those determined power values, the voltage drop $\Delta U_{j,j+1}$ in each branch can finally be computed thanks to expression (4.20):

$$\Delta U_{j,j+1} = L_{j,j+1} * \frac{P_{j+1,N}}{U_j} * R' + X' * \frac{Q_{j+1,N}}{P_{j+1,N}} \quad (4.20)$$

with U_j being the initially fixed or computed (in the previous iteration) voltage at node *j*. It is worth mentioning that, in the initial version of this algorithm [3], authors used the value U_1 instead of U_j in formula (4.20) for simplicity reasons. This approach therefore assumes a balanced three-phase system with the connection of symmetrical three-phase PV generation along the feeder and supposes that the voltage will continuously rise starting from the LV output of the substation. Consequently, the division by U_1 instead of U_j in (4.20) was justified as it was leading to conservative estimation of the expected voltage rise. In this work, both voltage rise and voltage drop could potentially occur and thus justify the adaptation made in relation (4.20).

ii. *Single-phase main lines with unbalanced single-phase loads/PV connections and unbalanced single-phase laterals*

In this case, the distance between phases allows neglecting their mutual coupling effects. Each phase is thus considered independently as a single-phase line with its respective single-phase loads/PV connections and single-phase laterals. This configuration takes into account the loading unbalance between phases but only an independent power flow analysis of each single phase line is deployed, with the same methodology as in (i). Of course, the cases that are treated by this option (and by option (i)) could also be analyzed with the complete three-phase algorithm of case (iii). However, in case of a LV feeder with many nodes in which mutual coupling effects between phases can be neglected, the single-phase algorithm of (i) appears to be slightly faster.

iii. *Three-phase main line with unbalanced single, two- or three- phase loads/PV connections, and unbalanced single, two- or three- phase laterals*

For considering the existing unbalance in power flow computations, various studies have been conducted [4]–[10]. In several cases, the LV network consists of a main three-phase line with different two-phase or single-phase loads and also unbalanced laterals per phase. Papers [4], [5] present a power flow method that allows solving the main three-phase network based on the decoupled positive-, negative- and zero-sequence networks. The unbalanced laterals are solved using the forward/backward method in phase components. The advantage of this power flow algorithm is that it can be easily adapted to cover multiple configurations of LV networks, with multiple three-phase, two-phase and/or single-phase loads and laterals, without requiring long elapsed time. Moreover, depending on the studied case, it can be particularized to independent single-phase lines or to balanced three-phase networks. Finally, the algorithm is structured in a way that it allows modeling voltage control schemes, which are time-varying and distributed over several nodes. This is a great advantage for performing long-term evaluation of such local network state-aware technical strategies which can be very effective for further DER integration.

This integrated power flow algorithm has been more than once presented in the related literature [4], [5], [11], with minor adaptations, but none of these studies linked it with a probabilistic analysis that considers all nodal power flows and voltage at the MV/LV transformer as random variables. This thesis integrates the discussed power flow algorithm in a probabilistic framework.

Thus, this last generic case (iii) considers all existing unbalances due to load/PV connections and laterals, as well as mutual coupling effects between phases. As previously mentioned both previous cases (i) and (ii) can also be treated with the proposed algorithm, by adequately factorizing the sequence components impedance matrix. The methodology can also be adapted to radial networks with single-phase or two-phase main line, or with multiple single-phase, two-phase main lines and/or three-phase loads and laterals (like the general network configuration illustrated in Figure 4.10). This can be done by adapting the phase and sequence components impedance matrix as well as the load/PV connections' matrix. In case three-phase laterals also exist, they are modeled as part of a main three-phase line. In the following explanation, the system is analyzed as a three-phase main line with unbalanced single-phase loads/PV connections and unbalanced single-phase laterals (Figure 4.12). Therefore the case of unbalanced two-phase laterals is not explained in detail although it can also be treated with the proposed algorithm.

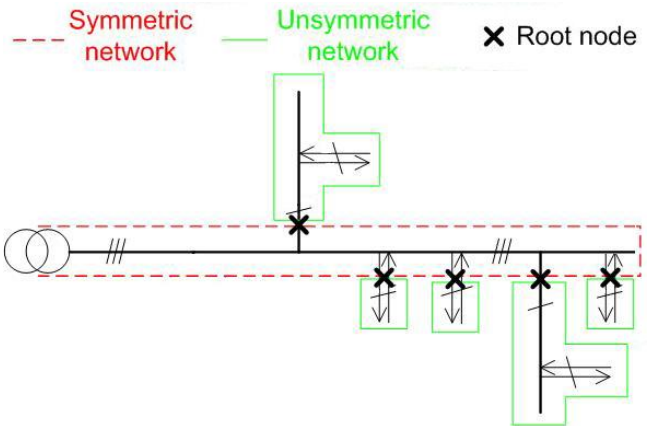

Figure 4.12: Network configuration considered in the presentation of the power flow analysis of case (iii))

The process starts by constructing the sequence admittance matrix for the main line (flowchart in Figure 4.13). In the case of a transposed main line, this matrix is in phase variables full and symmetrical. Therefore, the line can be modeled by three uncoupled sequence circuits as presented by the following relation [5]:

$$Y_{012}^{Z} = \begin{matrix} y_0^z & 0 & 0 \\ 0 & y_1^z & 0 \\ 0 & 0 & y_2^z \end{matrix}, \tag{4.21}$$

where *0, 1, 2* represent respectively the zero, positive and negative sequences, whereas the superscript ^{Z} stands for series admittance. The shunt admittance matrix $[Y_{012}^{S}]$ is not taken into account in this study (due to the short length of the overhead lines, in LV feeders, the capacitance effects can be neglected). Let's remember that the probabilistic framework presented in section 4.1.3 samples the voltage value at the slack node (secondary output of the MV/LV transformer) and the (active and reactive) powers at the other load nodes of the LV system, which are the random variables in each generated state. Then the forward/backward load flow process performs the first forward step considering the slack node voltage as fixed for the three phases:

$$\begin{aligned} \boldsymbol{V}_{\mathrm{a}}^{\text{slack node}} &= V_{nom} \angle 0° \\ \boldsymbol{V}_{\mathrm{b}}^{\text{slack node}} &= V_{nom} \angle 120° \\ \boldsymbol{V}_{\mathrm{c}}^{\text{slack node}} &= V_{nom} \angle 240 \end{aligned} \tag{4.22}$$

where V_{nom} is the sampled voltage at the LV output of the transformer and the bold type stands for complex numbers. Imposing this value at the slack node is necessary for the convergence of the forward/backward method. During this first forward step, the nodal phase voltages $\underline{\boldsymbol{V}}_{\text{initial,abc}}$ are initialized to the slack node phase voltages (where the under bar stands for vectors).

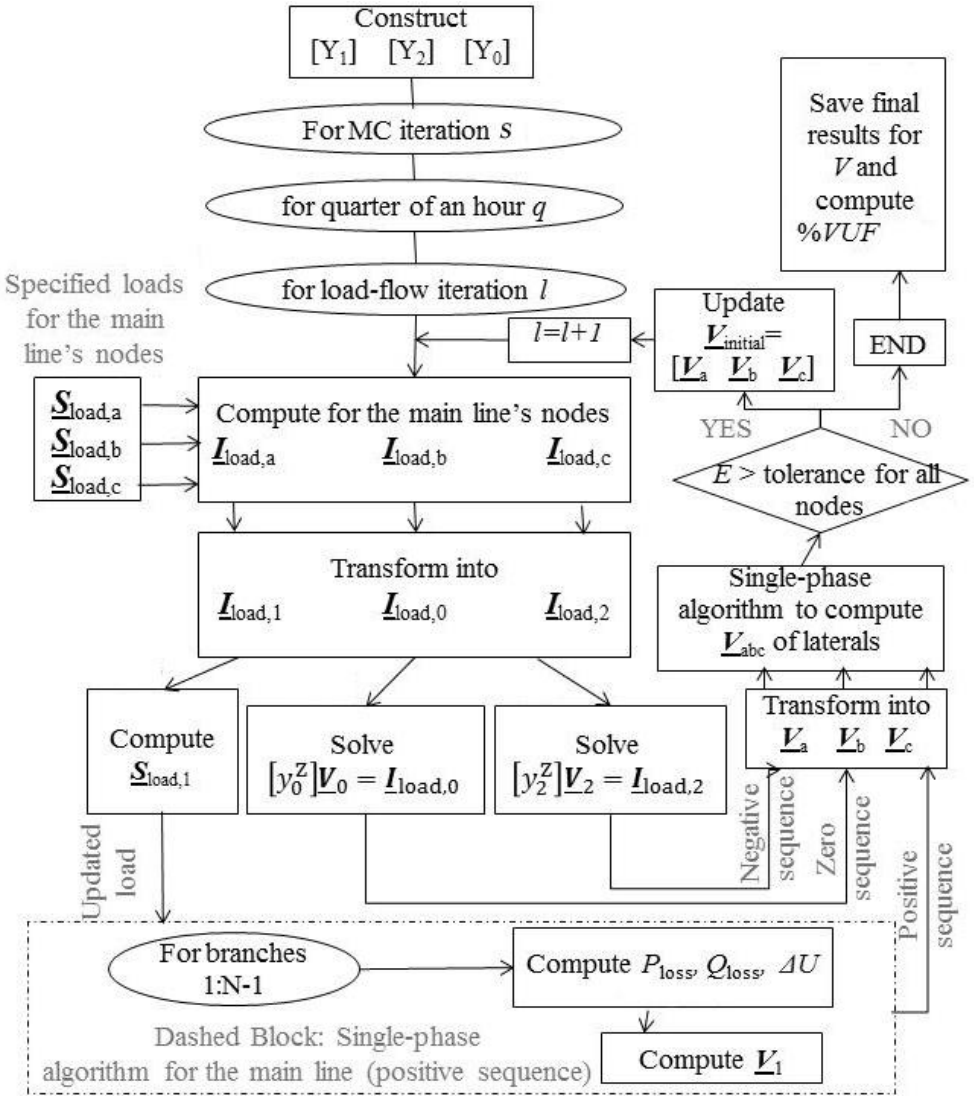

Figure 4.13: Power flow algorithm implemented in case (iii)

In sequence components, this reads [5]:

$$\begin{aligned} \underline{V}_{\text{initial},0} &= 0 \angle 0° \\ \underline{V}_{\text{initial},1} &= V_{\text{nom}} \angle 0° \\ \underline{V}_{\text{initial},2} &= 0 \angle 0° \end{aligned} \tag{4.23}$$

Practically, the analysis of the main line requires the computation of the existing unbalanced (in this case single-phase) laterals. Given that they usually represent small and simple radial networks, a simplified forward/backward method in phase components can be efficiently applied to solve them. This method requires that the voltage at the root node of each lateral is fixed, so that the for-

ward/backward procedure can converge. However, this value cannot be fixed a priori because it depends on the solution of the main line. For this reason, the main line and all the unbalanced laterals take part in an iterative forward/backward method, named the *hybrid power flow method* in [4].

The unbalanced laterals are solved with a forward/backward procedure in phase components. The first forward/backward step of the *hybrid method* gives the power injections $\boldsymbol{S}_{\text{lateral}}$ per phase at each lateral's root node, which is the total flown power on the respective lateral. In the described case the unbalanced laterals are single-phase lines. Therefore $\boldsymbol{S}_{\text{lateral}}$ is computed per phase by a single-phase algorithm. The computed $\boldsymbol{S}_{\text{lateral}}$ takes then the place of each unbalanced lateral at its root node in the main line. During the backward step of the *hybrid method*, the phase currents due to the nodal loads are computed for each node *i* of the main three-phase line (Figure 4.12) as in [4.24]:

$$\boldsymbol{I}_{load,x,i} = \left(\frac{\boldsymbol{S}_{load,x,i}}{\boldsymbol{V}_{initial,x,i}}\right)^{*} \quad (x=a,\ b \text{ or } c \text{ phase}) \tag{4.24}$$

where the superscript * stands for the complex conjugate and $\boldsymbol{S}_{load,x,i}$ is calculated for simple nodes with (4.25) and for lateral root nodes with (4.26):

$$\boldsymbol{S}_{load,x,i} = P_{x,i} + \mathrm{j}\ Q_{x,i} \tag{4.25}$$

$$\boldsymbol{S}_{load,x,i} = P_{x,i} + \mathrm{j}\ Q_{x,i} + \boldsymbol{S}_{\text{lateral,x,i}} \tag{4.26}$$

Active power values $P_{x,i}$ are defined per node and per phase with relation (4.12) whereas reactive values $Q_{x,i}$ are defined considering constant values for $cos\varphi_{\text{cons,x,i}}$ and $cos\varphi_{\text{inj,x,i}}$ in each network state (or in the whole simulation if no reactive power control scheme is applied). Once the $\boldsymbol{I}_{\text{load,abc}}$ *(*phase components) matrix is constructed, it is transformed by means of the Fortescue transformation into the respective $\boldsymbol{I}_{\text{load,012}}$ (sequence components) matrix. The specified nodal loads for the positive-sequence $\boldsymbol{S}_{load,1}$ are computed with (4.27):

$$\underline{\boldsymbol{S}}_{load,1} = \underline{\boldsymbol{V}}_{initial,1} \cdot \left(\underline{\boldsymbol{I}}_{load,1}\right)^{*} \tag{4.27}$$

At this point, the positive-sequence nodal voltages $\boldsymbol{V}_1$ are computed by applying the single-phase load flow algorithm of case (i), by considering $\boldsymbol{S}_{\text{load,1}}$ at all unbalanced (main three-phase line) nodes. The negative- and zero-sequence voltages are then computed by solving the linear systems:

$$\begin{aligned} y_0^{\mathrm{Z}}\ \underline{\boldsymbol{V}}_0 &= \underline{\boldsymbol{I}}_{\text{load,0}} \\ y_2^{\mathrm{Z}}\ \underline{\boldsymbol{V}}_2 &= \underline{\boldsymbol{I}}_{\text{load,2}} \end{aligned} \tag{4.28}$$

Once the $\boldsymbol{V}_{012}$ *(*sequence components) matrix is constructed, it is transformed into the respective $\boldsymbol{V}_{\text{abc}}$ (phase components) matrix for the main line. The values of $\boldsymbol{V}_{\text{i}}$ *(*i=a, b or c*)* at the root nodes of the laterals are fixed and the single-phase algorithm is once again applied to compute the final nodal voltages of the lat-

erals' nodes. At this point, the first forward/backward step of the *hybrid power flow method* is completed and the nodal voltages of the whole network (main line and laterals) are updated with the new values:

$$\underline{\boldsymbol{V}}_{\text{initial,x}} = \underline{\boldsymbol{V}}_{\text{x}} \qquad (x=a,\ b\ or\ c \text{ phase}) \tag{4.29}$$

After each iteration (l) of the power flow algorithm, the convergence error E is calculated for phase x at node i as follows:

$$E_{\text{i,n}} = V_{x,i}^{(\text{l})} - V_{x,i}^{(\text{l}-1)}\ , \quad x = a,b,c \ \text{ and } i = 1\text{: N} \tag{4.30}$$

where N is the number of nodes of the whole feeder. As soon as the error E_{i} becomes smaller than a given tolerance for each phase at each node, the algorithm stops and the last calculated $\boldsymbol{V}_{\text{abc}}$ can be compared to the operational limits in order to compute operation indices of interest (probability of overvoltage, probability of unbalance…). As previously mentioned, the overall structure of the *hybrid load flow algorithm* adapted for this study is presented in Figure 4.13.

4.1.5 *Operation Indices*

In this last section, indices of network operation are computed. This computation uses the power flow results obtained in the previous part. The choice of the long-term observability indices can be easily adapted to the simulation objectives. They are computed separately for each network state while the output datasets are used to construct distributions that represent the long-term statistical behavior of the feeder. Operation indices can be determined for each node or each line segment for the entire feeder. If for each ¼-hourly time step a total number of S states is analyzed, then the obtained outputs are structured in $3xS$ sized matrices as far as phase voltages and phase currents are concerned and in $1xS$ matrices as far as the rest of indices are concerned (see Table 4.1):

Table 4.1: Computed indices for ¼-hourly periods

Voltage	$3xS$
Current	$3xS$
%VUF	$1xS$
Power withdrawal	$1xS$
Flexible load	$1xS$
Line losses	$1xS$
Energy cost savings	$1xS$

The obtained matrices are elaborated as statistical realizations of the observed parameters. They are used to compute statistical distributions that characterize the possible variation of each parameter at each ¼-hourly period or for longer time periods (daily periods, peak hours period etc.). As previously mentioned, the computed statistical distributions are based on the use of SM data as inputs corre-

sponding to a specific month of the year. Compliance with local or national standards is verified afterwards as explained in the following paragraphs.

i. *Voltage profile (magnitude and unbalance)*

The phase voltage magnitudes are computed at each node for all the simulated network states. An extensive number of possible loading conditions are therefore examined such that the variation amplitude of the computed magnitudes is realistically estimated. For the total amount of simulated states, operation compliance with the probabilistic criteria of the EN 50160 standard (mathematically expressed by relations (4.31)) is verified for each node *i* and phase *x*:

$$\begin{gathered} P_{overvoltage}\ V_{i,x} > 1.10 \cdot V_{nom}\ < 0.05 \\ P_{undervoltage}\ V_{i,x} < 0.90 \cdot V_{nom}\ < 0.05 \\ P_{unbalance}\ VUF_i > 2\%\ < 0.05 \\ \textit{for } i\textit{=1:}\ \text{N } \textit{and } x\text{=a, b or c } \textit{phase} \end{gathered} \tag{4.31}$$

where $V_{i,x}$ is the voltage magnitude of phase *x* at node *i*, VUF_i is the Voltage Unbalance Factor at node *i* and *N* is the number of nodes in the feeder. Practically, if *S* iterations are made during the Monte Carlo process, the probability of exceeding the upper limit of the EN50160 standard for voltage magnitude *(%OV Risk*) and unbalance *(%VU Risk*) can be computed for node *i* as follows:

$$\%\ OV\ Risk_i = 100 \cdot \frac{1}{96 \cdot S} \sum_{m=1}^{S} \sum_{i=1}^{96} \text{Network States with } V_{i,x} > 1.10 V_{nom} \tag{4.32}$$

$$\%VU\ Risk_i = 100 \cdot \frac{1}{96 \cdot S} \sum_{m=1}^{S} \sum_{i=1}^{96} \text{Network States with } \%VUF_i > 2\% \tag{4.33}$$

where *S* is, as already mentioned, the number of simulated system states for each ¼-hourly time step. The percentage voltage unbalance factor (%VUF) is computed at each node *i* by applying the IEEE definition which is also used in the EN 50160 standard:

$$\%VUF_i = \frac{V_n}{V_p} \cdot 100 \tag{4.34}$$

subject to:

$$V\text{p} = \frac{V_{ab} + \alpha \cdot V_{bc} + \alpha^2 \cdot V_{ca}}{3} \tag{4.35}$$

$$V\text{n} = \frac{V_{ab} + \alpha^2 \cdot V_{bc} + \alpha \cdot V_{ca}}{3} \tag{4.36}$$

$$\alpha = 1 \angle 120^\circ \text{ and } \alpha^2 = 1 \angle 240^\circ$$

where V_{ab}, V_{bc}, V_{ca} are the line-to-line voltages at node *i.*

Although most international documents and regional or national standards address unbalance in the LV network in function of the negative-sequence components, the reason for this consideration is not thoroughly explained. IEC TR

61000-3-13:2008 standard [12], which assesses the emission limits for the connection of unbalanced installations to MV, HV and EHV power systems, mentions that "*Problems related to unbalance fall into two basic categories. - Unbalanced installations that draw negative-sequence currents which produce negative-sequence voltages on the supply system. ... Negative-sequence voltage superimposed onto the terminal voltage of rotating machines can produce additional heat losses. Negative-sequence voltage can also cause non-characteristic harmonics (typically positive-sequence 3rd harmonic) to be produced by power converters. - Unbalanced installations connected line-to-neutral can also draw zero-sequence currents which can be transferred or not into the supply system depending on the type of connection of the coupling transformer. ... This is not normally controlled by setting emission limits, but rather by system design and maintenance. Ungrounded-neutral systems and phase-to-phase connected installations are not, however, affected by this kind of voltage unbalance. This report gives guidance only for the coordination of the negative-sequence type of voltage unbalance between different voltage levels in order to meet the compatibility levels at the point of utilization. No compatibility levels are defined for zero-sequence type of voltage unbalance as this is often considered as being less relevant to the coordination of unbalance levels compared to the first type of voltage unbalance. However, for situations where a non-zero impedance exists between neutral and earth with the system still being effectively grounded (i.e., where the ratio between zero-sequence, X0 and positive-sequence reactance X1 is 0 < X0/X1 = 3), this type of voltage unbalance can be of concern especially when the type of connection of the coupling transformer allows zero-sequence path to flow from MV to LV and vice-versa.*" The Final WG report on "Power Quality Indices and Objectives" [13] only mentions that "The unbalance is a condition in a polyphase system in which the RMS values of the line voltages (fundamental component), and/or the phase angles between consecutive line voltages, are not all equal. For a three phase system, the degree of the inequality should be expressed as the ratios of the negative (NPS) and zero-sequence components to the positive-sequence (PPS) components. Only the negative-sequence component is addressed here because it is often of more concern."

Based on these considerations, relations (4.34)-(4.36) are applied for computing %VUF in each simulated state, as recommended by the EN 50160 standard.

ii. *Current magnitudes, line losses and other indices*

The maximum current capacity of the lines can be determined considering values suggested by the distribution utility or standard tables like the one established in reference [14]. Practically, compliance with the upper limits that are set by the standards (or the distribution utility) must be verified in all simulated system states. The line segments with the highest current magnitudes can be identified thanks to the probabilistic process. The statistical distribution of total energy

losses in the feeder can also be constructed characterizing daily, monthly or even yearly periods, depending on the objective of the simulation.

The cost of line losses can be monetized as energy consumption that is not directly included in the network use tariff. In most EU countries, the DSO has a clear economic interest in reducing line losses, especially in countries that have adopted a "*Revenue cap*" methodology framework for the use of the distribution network. In a similar way, statistical distributions for captured or curtailed renewable energy can be constructed, per node or for the entire feeder. Moreover, the amount of reverse flows can also be determined in a statistical manner, thanks to our developed tool.

4.2 Validation of the developed probabilistic framework

4.2.1 *Validation of the three-phase power flow algorithm*

The three-phase power flow algorithm of [4], [5], before its integration in the probabilistic framework, has been validated in a very simple example. Let's consider the simple three-phase network of Figure 4.14, with two loads, both equal to $Z_{L,}$, connected to node 3, in phases a and b.

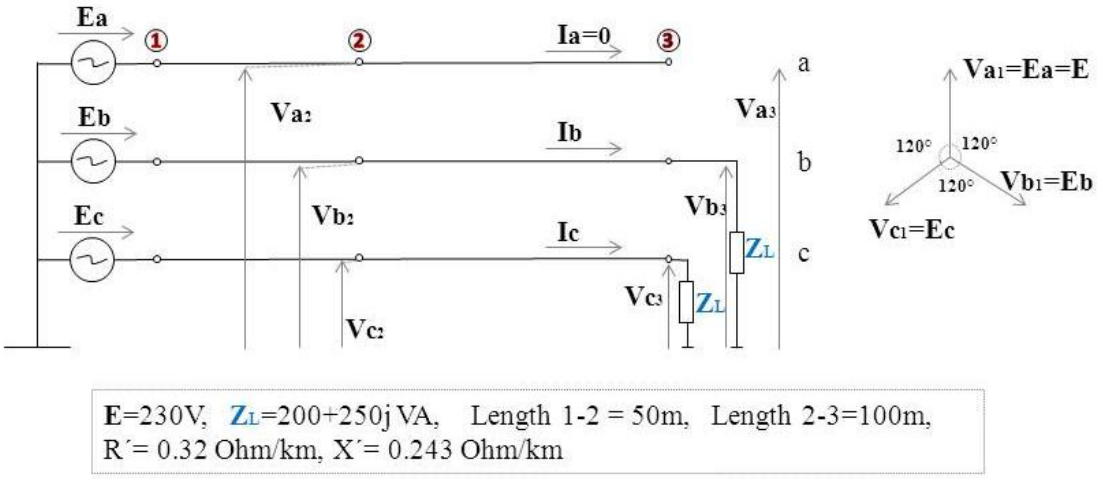

Figure 4.14: Three-phase network with unbalanced loads

By applying the Fortescue transformation (method of symmetrical components), the network of Figure 4.14 is equivalent to the interconnection of the positive-, negative- and zero-sequence networks shown in Figure 4.15.

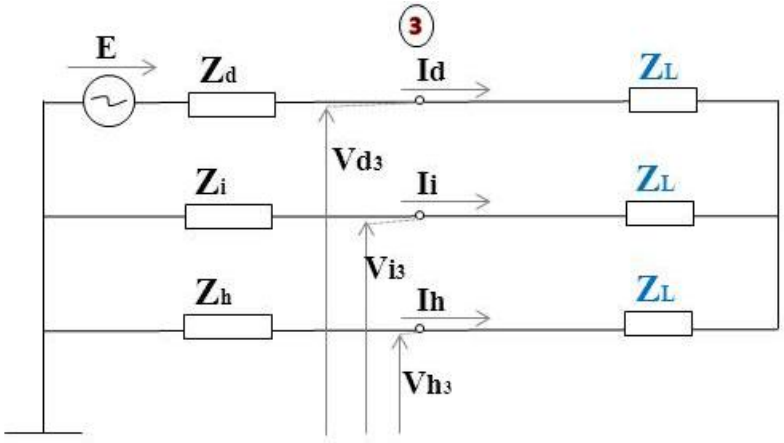

Figure 4.15: Equivalent scheme of the positive, negative and zero symmetrical components (of the network in Figure 4.14)

In the symmetrical components scheme of Figure 4.15, equations (4.37) apply:

$$\begin{aligned} \boldsymbol{Z_1} &= \boldsymbol{Z_{1_{12}}} + \boldsymbol{Z_{1_{23}}} \\ \boldsymbol{Z_2} &= \boldsymbol{Z_{2_{12}}} + \boldsymbol{Z_{2_{23}}} \\ \boldsymbol{Z_0} &= \boldsymbol{Z_{0_{12}}} + \boldsymbol{Z_{0_{23}}} \end{aligned} \tag{4.37}$$

where:

$$\begin{aligned} \boldsymbol{Z_{1_{12}}} &= (Length\ 1-2)\cdot(R' + jX') \\ \boldsymbol{Z_{1_{23}}} &= (Length\ 2-3)\cdot(R' + jX') \end{aligned} \tag{4.38}$$

with *R*' and *X*' respectively the resistance and the reactance per kilometer of the lines. Based on a commonly used ratio, $\boldsymbol{Z_{0_{12}}}$ and $\boldsymbol{Z_{0_{23}}}$ are considered as follows:

$$\begin{aligned} \boldsymbol{Z_{0_{12}}} &= 3\cdot\boldsymbol{Z_{1_{12}}} \\ \boldsymbol{Z_{0_{23}}} &= 3\cdot\boldsymbol{Z_{1_{23}}} \end{aligned} \tag{4.39}$$

while $\boldsymbol{Z_{2_{12}}}$ and $\boldsymbol{Z_{2_{23}}}$ are respectively equal to $Z_{1_{12}}$ and$Z_{1_{23}}$.

With the application of the Thevenin's Theorem and the use of the Fortescue transformation, the currents $\boldsymbol{I}_0$, $\boldsymbol{I}_1$ and $\boldsymbol{I}_2$ of the three symmetrical components and the three phase currents $\boldsymbol{I}_a$, $\boldsymbol{I}_b$ and $\boldsymbol{I}_c$ are computed with relations (4.40) and (4.41) respectively:

$$\boldsymbol{I_1} = \frac{E}{\boldsymbol{Z_1} + \boldsymbol{Z_L} + \dfrac{\boldsymbol{Z_2} + \boldsymbol{Z_L}\ \cdot\ \boldsymbol{Z_0} + \boldsymbol{Z_L}}{\boldsymbol{Z_2} + \boldsymbol{Z_0} + \boldsymbol{2}\cdot\boldsymbol{Z_L}}}$$

$$\boldsymbol{I_2} = -\frac{\boldsymbol{Z_0} + \boldsymbol{Z_L}}{\boldsymbol{Z_2} + \boldsymbol{Z_0} + \boldsymbol{2}\cdot\boldsymbol{Z_L}}\cdot\boldsymbol{I_1} \tag{4.40}$$

$$\boldsymbol{I_0} = -\frac{\boldsymbol{Z_2} + \boldsymbol{Z_L}}{\boldsymbol{Z_2} + \boldsymbol{Z_0} + \boldsymbol{2}\cdot\boldsymbol{Z_L}}\cdot\boldsymbol{I_1} = -\boldsymbol{I_1} - \boldsymbol{I_2}$$

and

$$\begin{aligned} \boldsymbol{I_a} &= 0 \\ \boldsymbol{I_b} &= \boldsymbol{I_0} + \alpha^2\cdot\boldsymbol{I_1} + \alpha\cdot\boldsymbol{I_2} \\ \boldsymbol{I_c} &= \boldsymbol{I_0} + \alpha\cdot\boldsymbol{I_1} + \alpha^2\cdot\boldsymbol{I_2} \end{aligned} \tag{4.41}$$

where $\alpha = e^{j\cdot 2\pi}{}_3$

The voltages $\boldsymbol{V}_0$, $\boldsymbol{V}_1$ and $\boldsymbol{V}_2$ of the three symmetrical components at node 3 and the three phase voltages $\boldsymbol{V}_a$, $\boldsymbol{V}_b$ and $\boldsymbol{V}_c$ at node 3 are computed with relations (4.42) and (4.43) respectively:

$$\begin{aligned} \boldsymbol{V_{0_3}} &= -\boldsymbol{Z_0} \cdot \boldsymbol{I_0} \\ \boldsymbol{V_{1_3}} &= E - \boldsymbol{Z_1} \cdot \boldsymbol{I_1} \\ \boldsymbol{V_{2_3}} &= -\boldsymbol{Z_2} \cdot \boldsymbol{I_2} \end{aligned} \tag{4.42}$$

and

$$\begin{aligned} \boldsymbol{V_{a_3}} &= \boldsymbol{V_{0_3}} + \boldsymbol{V_{1_3}} + \boldsymbol{V_{2_3}} \\ \boldsymbol{V_{b_3}} &= \boldsymbol{V_{0_3}} + \alpha^2 \cdot \boldsymbol{V_{1_3}} + \alpha \cdot \boldsymbol{V_{2_3}} \\ \boldsymbol{V_{c_3}} &= \boldsymbol{V_{0_3}} + \alpha \cdot \boldsymbol{V_{1_3}} + \alpha^2 \cdot \boldsymbol{V_{2_3}} \end{aligned} \tag{4.43}$$

The above methodology has been in programmed in Matlab® (algorithm presented in Appendix A2), for the network of Figure 4.14 and the obtained voltages $\boldsymbol{V_{a_3}}, \boldsymbol{V_{b_3}}, \boldsymbol{V_{c_3}}$ at node 3 are presented in Table 4.2.

The same network has been solved with the *hybrid power flow method* (described in paragraph 4.1.4.iii) and the obtained voltages $\boldsymbol{V_{a_3}}, \boldsymbol{V_{b_3}}, \boldsymbol{V_{c_3}}$ at node 3 are also presented in Table 4.2. The difference between the obtained results, from the two analysis methods, is negligible. Based on the analysis of the above simple example of a three-phase network, we have validated the accuracy of the *hybrid power flow method.*

Table 4.2: Phase voltages at node 3

	Analytical computation	Hybrid Power Flow
$\boldsymbol{V_{a_3}}$	229.999-j0.0029 (V)	229.998 - j0.003 (V)
$\boldsymbol{V_{b_3}}$	-114.96-j199.23 (V)	-114.97-j199.11 (V)
$\boldsymbol{V_{c_3}}$	-115.04+j199.14 (V)	-114.99+j199.22 (V)

4.2.2 *Comparison of probabilistic and deterministic simulation outputs with real voltage measurements*

This section describes the simulation of the Aulnoit LV feeder "towards Ghou", in Belgium, with SM measurements recorded at three out of the four PV end-users that are connected to the feeder. The available SM datasets comprise total ¼-hourly $E_{\text{inj,grid}}$, $E_{\text{inj,pv}}$ and $E_{\text{cons,grid}}$ measurements as well as phase voltages recorded every 15 minutes. **The purpose of this simulation is to compare the voltage outputs from the probabilistic simulation and from a real-case situation with phase voltage measurements at two PV nodes (users 4 and 14)**

during one winter and one summer month in 2014. The tested feeder is illustrated in Figure 4.16. The months of December and of July have been chosen for this comparative analysis.

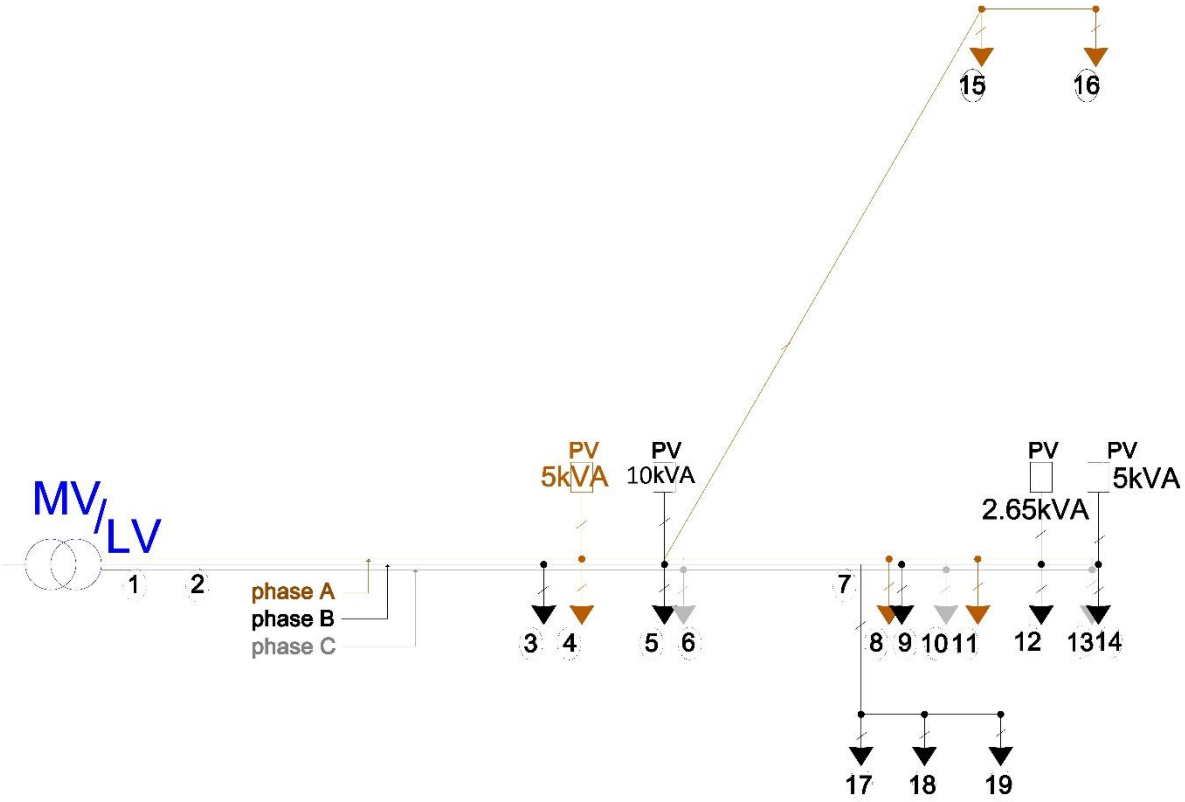

Figure 4.16: The simulated LV feeder

As highlighted in Chapter 1, nowadays, the biggest share of LV networks is not monitored. **Given this fact, the availability of SM datasets for three end-users connected to the simulated feeder allows a higher level of visibility, compared to the vast majority of such feeders. However, still in this case, an important amount of information is missing, including topology, technical parameters and power flow indices of the feeder.** Unfortunately, this fact reduces to an important extent the accuracy of the comparative analysis. As a result, the presented outputs should only be considered on an "order of magnitude" principle. The missing information which reduces the numerical precision of both the probabilistic and the deterministic evaluation is outlined in the following points:

a) Loads and PV units are all connected in single-phase mode. However their real repartition over the three phases is not known.

b) For simulating the voltage magnitude at the MV/LV transformer (slack node), real ¼-hourly voltage measurements are used. However such

measurements are not available for the simulated months of December and July 2014. Instead, measurements recorded in January and in July 2013 are used.

c) The real values of direct, inverse and homopolaire ($Z1$, $Z2$, $Z0$) impedance are not known. Typical LV network values are considered in the computation to model these parameters.

d) User-specific energy flow measurements are only available for 3 out of the 16 connected users and voltage measurements are only available for 2 out of the 16 users. To address this lack of measurements, a statistical methodology that creates reference models for the users without SM device, using SM feeder-specific measurements, is applied [15]. This methodology is outlined in a following section 4.4.

e) The PV unit of 10kVA has been connected to the feeder (at node 5) later than the other three PV units. However, it is not known whether the available voltage measurements at nodes 4 and 14 were recorded formerly. Given that SM measurements are not currently available for this unit, it has been modeled in the probabilistic simulation by using the PV generation profile of the 5kVA unit at node 4, multiplied by 2 in each network state. Clearly, the integration of a 10kVA PV unit significantly affects the voltage profile in the feeder and so does its consideration in the computation. Thus, this lack of information possibly results in an important gap between the simulation outputs and the available measurements.

f) A worst-case scenario (in terms of overvoltage risk) has also been applied, considering the available SM datasets. This means that each PV unit was modeled with the highest PV generation ¼-hourly value ($E_{\mathrm{inj,pv}}$) recorded in the respective simulated month. The consumption of each PV owner was modeled with the lowest ¼-hourly net energy demand value $E_{load,}$ based on the respective SM dataset for the simulated month. Network users without SM measurements were modeled with the lowest consumption value that has been recorded in the feeder at the PCC of the end-users that are equipped with a SM device. This approach has been considered more realistic than the commonly used Synthetic Load Profiles (SLP) which represents energy consumption considering values on a national level and not adapted to the specific geographical location of the users. Of course, this assumption can lead to an under- or over-estimation of the worst-case outputs (compared to the real measurements) and to make less evident the comparison of the probabilistic and the worst-case approach. However, as previously explained, the purpose in this case was to apply an approach that is

faithful to the common distribution utility's practice in case feeder-specific measurements are available.

The comparative analysis concluded that the worst-case computation results for phase voltage values are higher than 80-90% of the values recorded with the SM devices at the respective nodes, both for July and for December. The fact that a share of 10-20% recorded values are still higher than the worst-case approach outputs proves that modeling users without SM device considering data recorded for other users in the feeder can lead to an underestimation of the voltage rise. In Figure 4.17, it can be seen that in certain cases phase voltages were recorded to be very close to the upper limit of the EN 50160 standard. This risk could have been identified with the worst-case computation in case a better (monitored) visibility had been present in the feeder. **On another hand, the fact that the vast majority of the recorded values are much lower than the ones obtained with the worst-case approach highlight that the latter can lead to conservative decisions regarding voltage margin and PV hosting capacity in a similar LV feeder.**

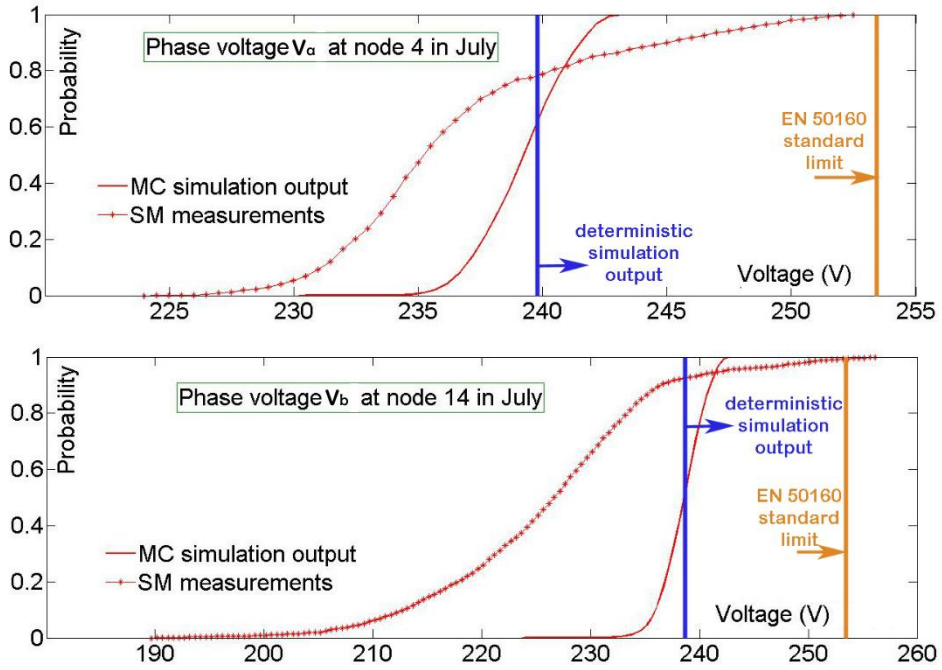

Figure 4.17: CDFs for phase voltage V_a at node 4 and for phase voltage V_c at node 14 (in July), constructed with the recorded datasets (dotted line), the probabilistic framework outputs (continuous red line) and the deterministic worst-case analysis (blue line).

Comparing with the probabilistic framework outputs for the respective nodes, the deterministic worst-case approach still results in higher values compared to around 50-60% of the probabilistically computed voltage values. **For achieving higher precision in both approaches, the monitored visibility needs to in-**

crease or reliable methodologies should be developed for addressing the availability of sparse measurements (see section 4.4).

Comparing the probabilistic framework outputs with the recorded values, the two datasets are quite similar in certain cases (Figure 4.18, node 4, July) while in other cases they are quite different (Figure 4.18, node 14, December). As illustrated with the CDFs of probability in Figure 4.17, in both approaches, the biggest share of obtained values fall within the same range of values (230V-244V). Some recorded values are quite lower than 210V or higher than 250V which is not the case with the values computed with the probabilistic simulation. However, these cases are very rare and they do not represent more than 1-2% of the recorded values.

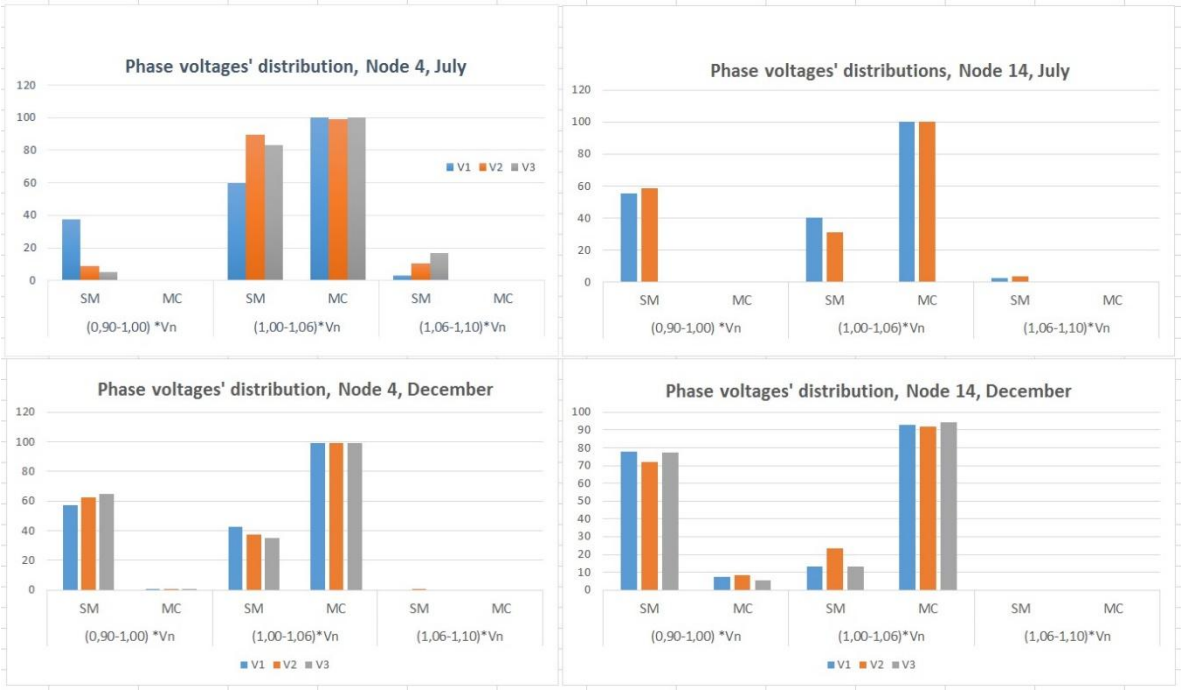

Figure 4.18: Phase voltages' distributions created with SM measurements and with the MC simulation outputs

Indeed, measurements of voltages higher than $1.10*V_{nom}$ were recorded in July at node 14, in phases *a* and *c*, with a frequency of 7.68% and 14.04% respectively. Similarly, measurements of voltages lower than $0.90*V_{nom}$ were recorded at node 14 in December, in phase *a*, with a frequency of 8.84%. In all these cases the EN 50160 voltage 95-percentile limits were instantaneously violated. However, based on the available instantaneous voltage measurements (snapshots), recorded every 15 minutes, it is not possible to know whether these violations took place during more than 10 minutes resulting in temporary PV unit cut-offs. On another hand, the probabilistic simulation based on total ¼-hourly energy flow measurements and power exchange values averaged over ¼-hourly periods,

did not identify the probability of these instantaneous voltage violations. The use of power exchange values that are averaged over ¼-hourly periods leads to computed voltage values that are also averaged over the ¼-hourly interval.

Consequently, considering that the statistical distribution of voltage values, obtained with the probabilistic framework and with the SM readings, have a similar outline and are of the same order of magnitude (Figure 4.17), we assume that the difference of outputs is caused by the lack of information explained in points (a) to (f). In this case, the important contribution of the probabilistic simulation that uses the available SM measurements mostly lies in the identification of critical nodes, in terms of voltage rise or drop, and in the statistical estimation of the possible range of values that voltages can take at each node. **For obtaining reliable long-term observability analytics, it is important either to develop methodologies that can reliably model random variables for which measurements are not available or to increase the visibility in LV feeders by deploying more monitoring devices.**

In the following paragraphs, the feeder of Figure 4.16 is modeled in different situations, considering different phase connections of loads and distributed generation, depending on the objectives of each simulation. In these situations, we assume that certain technical parameters of the network are known although they might be different from the real ones. This assumption does not affect the precision and the reliability of the results, since the comparative evaluations are always done by analyzing the same feeder (conserving the same initial hypotheses that were made on the technical parameters).

4.3 Clustering of Metering Data

Given that PV generation is totally dependent on solar irradiation, the energy generation of PV units in close proximity is undoubtedly correlated at the considered time scale (mean PV injection values on a quarter of an hour basis). In small sized LV feeders, this consideration would mean that during periods of high solar irradiation, most of the connected PV units would generate and potentially inject in the network a similar amount of PV energy, always in function of their installed power. Taking this assumption into account can accelerate the computation time and possibly lead to more realistic results. Besides, residential network users located in the same area often have similar energy consumption patterns, since an important amount of their energy use covers heating or cooling needs that also depend on their location.

For the above reasons, a study exploring the potential correlation of PV generation and energy consumption of PV users located in a close geographical area has been deployed [16]. The aim of this study was, first of all, to implement a clustering technique that groups PV users of Flobecq for every quarter of an hour in function of their PV generation and energy consumption. This study has, of course, been based on the available SM datasets that are described in paragraph 3.2. The three following scenarios were investigated for 19 PV users located in the area of Flobecq:

I. Correlation of users concerning their PV generation $E_{\text{inj, pv}}$

II. Correlation of users with PV generation concerning their net energy demand E_{load} (as defined in relation (4.5))

III. Correlation between PV generation $E_{\text{inj, pv}}$ and net energy demand E_{load} of each individual user with PV generation

The potential correlation of every pair of studied parameters X and Y has been investigated by means of the Pearson coefficient for every "useful" ¼-hourly time step:

$$r = \frac{\operatorname{cov}(X,Y)}{\sigma_X \cdot \sigma_Y} = \frac{\sum_i (x_i - \bar{x}) \cdot (y_i - \bar{y})}{\sqrt{\sum_i (x_i - \bar{x})^2} \cdot \sqrt{\sum_i (y_i - \bar{y})^2}} \tag{4.44}$$

where X and Y are the studied parameters, x_i and y_i represent the set of recorded values for X and Y during the considered quarter of an hour and x and y are their respective mean values. Also note that, by the term "useful", we mean the quar-

ters of an hour during which all PV users generate (at least one day of the studied period) PV energy.

When studying the first two correlation scenarios (correlations I and II), users are clustered by use of a fast incremental algorithm [16]. The fast incremental algorithm is a non-iterative algorithm. With this kind of approach, data are treated and classified one by one. The different steps of the algorithm are the following ones:

- *Step 1:* Initialization: an initial arbitrary order of the data is selected and the number *n*c of clusters is set to 1;

- *Step 2:* Treatment of the other data: the data are considered one by one and are put in each of the *n*c existing clusters in view of deciding which one is the most convenient for the considered data. For performing this operation, an objective function must be defined. For each data, there are thus *n*c values of the objective function to be calculated;

- *Step 3:* Increase of the number of clusters: if, for a given data, the *n*c values of the objective function are beyond a given threshold, it is concluded that the data does not belong to any of the *n*c clusters. Consequently, a new cluster is created, containing this data, and the number of clusters is incremented to *n*c +1.

The incremental algorithm is fast since each data is considered only once and the clusters do not have to be changed after the classification of each data. This advantage is very interesting when the number of data is huge [17]. On the opposite, a drawback of the incremental algorithm comes from the fact that the creation of clusters depends on the value assigned to a threshold. As a consequence, the more demanding the threshold, the greater the number *n*c of defined clusters. An appropriate value of the threshold has thus to be found in agreement with the investigated clustering problem. Finally, the main inconvenient of the fast incremental algorithm is that the clustering solution depends on the order in which the data are treated. Therefore, when using such an algorithm, it will be imperative to launch it a sufficiently high number of times so as to avoid being trapped in a local extremum.

In this study, two correlation matrices (generation between users, consumption between users) are defined for each quarter of an hour. Practically, for each correlation level, the Pearson correlation threshold is fixed to be equal to 0.5 which is a value traditionally accepted to represent high positive correlation between random variables [18]. Therefore, for example, when studying the correlation between the ¼-hourly generations of PV units, users grouped into the same cluster can be supposed to be strongly correlated from their generation point of view. Therefore, concerning PV generation, the obtained results are illustrated in Figures 4.19 and 4.20. Figure 4.19 shows the correlation matrix (Pearson coefficients for each pair of users) for all the considered 19 users during the period be-

tween 11:30AM and 11:45AM of a typical day in January. Figure 4.20 shows the average correlation between PV users for every "useful" quarter of an hour for all the 12 months of a year. Clearly, it can be concluded that all PV users are strongly correlated as far as their PV generation is concerned since the majority of *r* values is close to 1 for all months. Consequently, one can assume that these PV users are entirely correlated and that they all belong to a single cluster. This result can be justified by the geographical proximity between all PV users (the longest distance between two users, is indeed, 6km long in the tested case). Moreover, it implies that the shadow effect due to clouds has no significant impact on the quarter of an hour time scale.

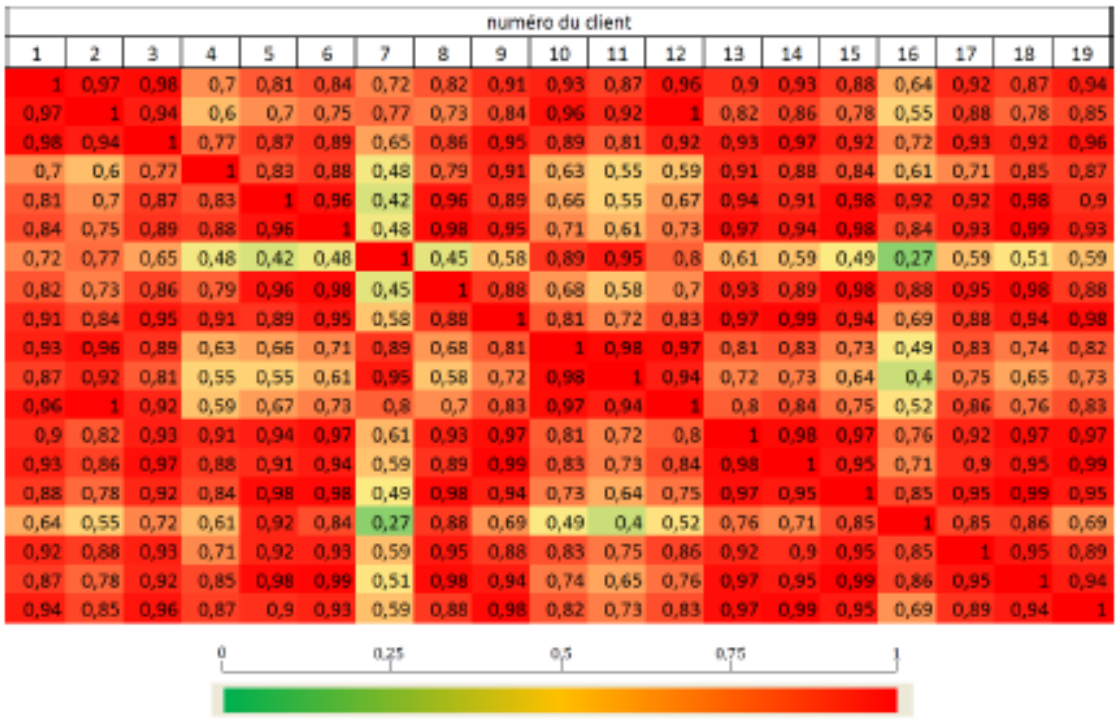

Figure 4.19: Correlation matrix between all customers for the period between 11:30AM and 11:45AM of a typical day in January.

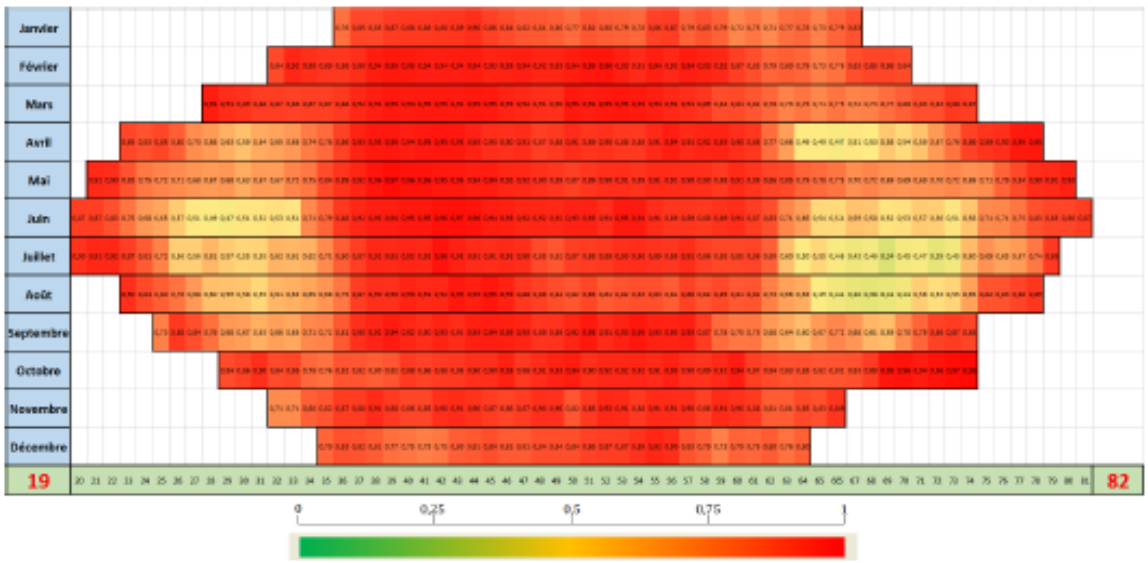

Figure 4.20: Average correlation between PV end-users for every "useful" time step for the 12 months of the year

The respective results for E_{load} demonstrated that the average correlation values are quite low for the 12 months of the year. Given that the analysis is done on a quarter of an hour basis, this result is quite logical. Indeed, although the profile of net energy demand of these residential users might be very similar on a daily basis (Figure 4.21), one does not expect that this similarity is also valid at a quarter of an hour time scale. In conclusion of the previous analysis, it can be therefore assumed that, practically, PV users are correlated as far as their net energy use is concerned but mostly on a daily basis rather than on a ¼-hourly one.

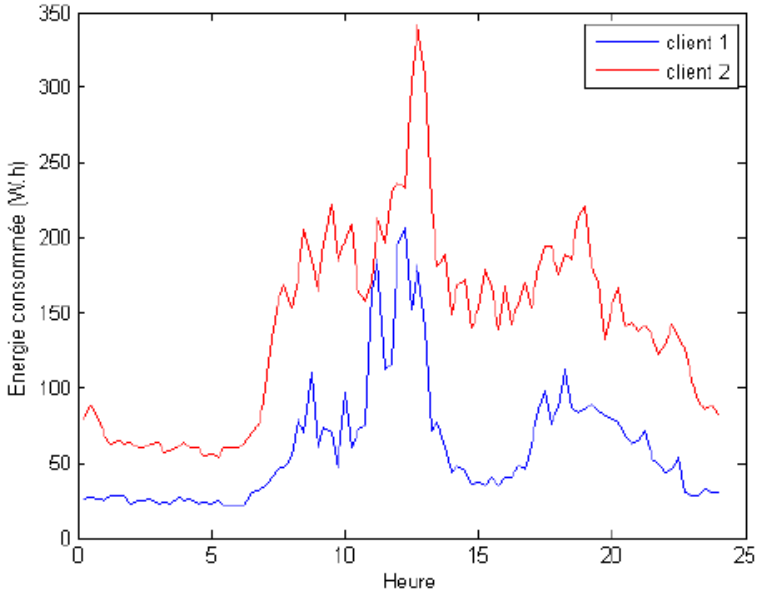

Figure 4.21: Time variation of average net energy consumption of two customers for the month of January

Based on the previous assumption, in order to make a deeper correlation analysis, the net energy use dataset (E_{load}) was divided into two groups: the "week" dataset and the "weekend" dataset. The respective correlation matrices have been computed for each one of the two groups. As far as week days are concerned, the correlation coefficients for energy use resulted to be very low so that these users can be considered as entirely independent. On the opposite, the results for week-end days demonstrated that users could eventually be grouped into some clusters. In this purpose, an Incremental Clustering algorithm [19] has been implemented and the clusters of Figure 4.22 were created on basis of their correlation level (still with the correlation threshold fixed at 0.5):

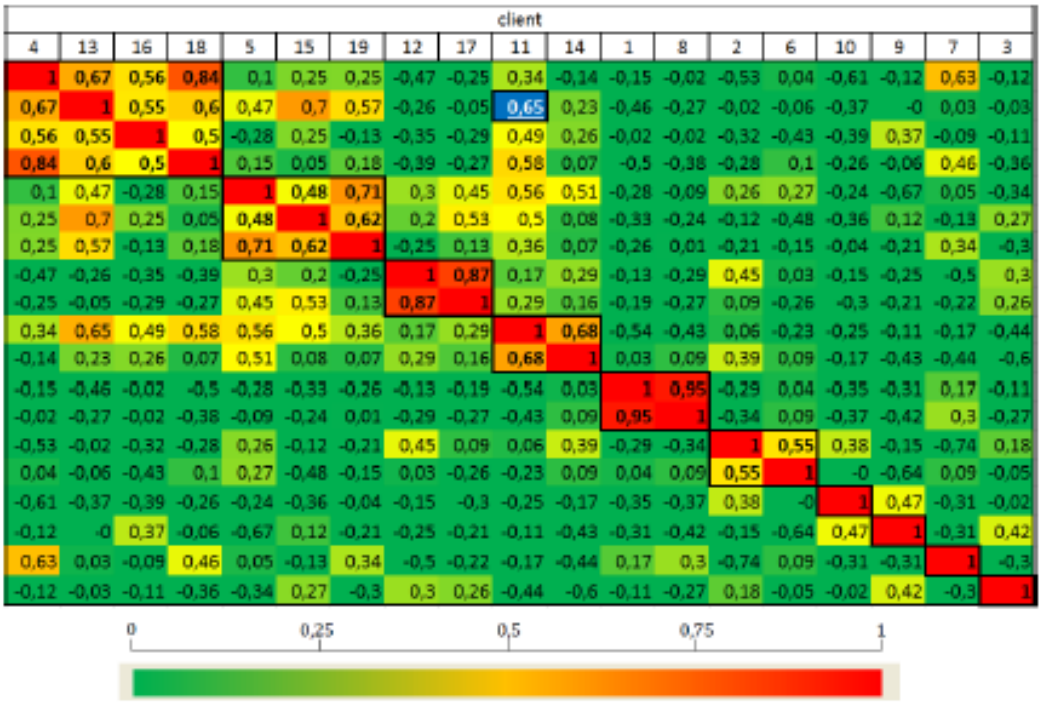

Figure 4.22: Clusters that were created for grouping PV customers in function of their net energy use on week-end days

Finally, the computation of correlation coefficients between ¼-hourly PV generation and ¼-hourly net energy demand of the same user (scenario III) proved that these parameters had to be considered as entirely uncorrelated and, therefore, independent. The overall results of the correlation study between the 19 considered users are presented in Table 4.3:

Table 4.3: Correlation of 19 end-users in Flobecq

	Week day	Week-end day
PV generation	Entirely correlated	Entirely correlated
Net energy demand	Independent	6 clusters

The presented results address a specific group of network users who are not in reality connected to the same feeder, although they are located in proximity (LV network of Flobecq). Nevertheless, the scope of this section is to present a methodology that can be applied in any LV feeder with user-specific SM measurements, for accounting for the spatial correlation of PV generation and energy demand of closely located users. In the simulations that are presented in the following chapters, end-users connected to the same feeder are considered entirely correlated regarding their PV generation and independent regarding their energy demand while no correlation is considered between the PV generation and energy demand of the same user.

4.4 Availability of Sparse Metering Data

An undoubtful value lies in creating reliable models for representing the random variables of the LV network. Such models can increase the reliability of the long-term LV network analytics while they can also be valorized in real-time state estimation techniques applied for the MV network. Nowadays, when modeling energy systems in Europe, the consumption pattern of households is often characterized with purely deterministic consumption profiles, referred to as Standard Load Profiles (SLPs), e.g., the H0 profile of the German Association of Energy and Water Industries (BDEW), or the 4 different SLPs used in the Belgian power market for modeling distribution end-users. These SLPs consist of aggregated profiles at the country level and do not account for specificities related to the studied area (e.g. the difference in the consumption pattern between a city apartment and a villa in the countryside [20]).

In order to overcome limitations inherent to this ageing approach, the present section introduces a statistical modeling methodology that uses available feeder-specific ¼-hourly SM datasets to create statistically representative consumption and generation patterns for users that are also connected to the considered feeder but without having a SM device [21]. This load profile modeling approach presents several assets. Firstly, the accuracy of the models is increasing with the number of available SM data, particularly for what concerns the capture of extreme scenarios with low probability of occurrence. Then, the principle of assigning the same dispersion model to clients of the same type is valuable even if all LV nodes are equipped with measurement recording devices. Indeed, in the context of large-scale system simulations, this would permit to considerably decrease the problem size since using tailored models for each client requires too many resources and is far from optimal. Then, the proposed technique can also be used for state estimation in MV distribution systems, whose development is a growing need in supporting active network management. In this respect, an adequate load modeling could avoid relying on classical pseudo-measurements and, as a result, accelerate the implementation of efficient state estimators.

The global methodology can be decomposed into three complementary steps that are summarized in Figure 4.23 [22]. The available data are initially categorized into several components (e.g. residential load, tertiary sector, PV generation, etc.). Thus, the proposed formulation assumes that the total active power in a distribution network can be divided into c different LV components. It is also based upon the hypothesis that all users belonging to the same type of component are evolving similarly. Therefore, a strong dependence among loads and distributed generators of the same type, within the same area, is assumed. The statistical behavior of each user of a particular component can thus be inferred from the en-

ergy flows coming from the other users of the same type. As a second step, reference CDFs are constructed with the respective available SM datasets for each category and they are used to represent end-users without SM devices that belong to the same category. Finally the models are included in the probabilistic algorithm presented in section 4.1 in order to perform the desired studies.

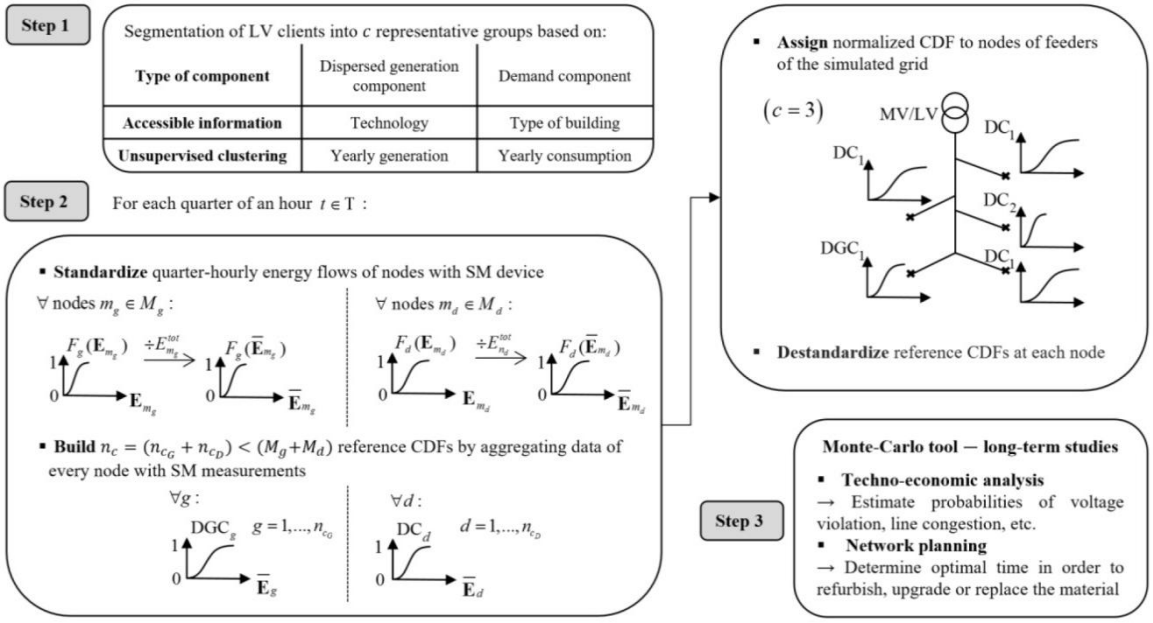

Figure 4.23: *General principle of the Pseudo-Sequential load and generation modeling.*

A. *Step 1- Demand and dispersed generation classification*

In order to establish the optimal number of models, efficiently capturing the statistical behavior of its constitutive elements, a prior classification of loads into components is required. In this way, the whole active power consumed at LV level is split into c_D *demand components*, one for each defined type of load, e.g. residential, farm, administrative building, shop, etc. Similarly, the whole active power generated at LV level is partitioned into c_G *dispersed generation components* based on the technology (i.e. PV panels, small wind turbine, etc.). In this study, c_G=**1** since only PV units are present. Note that c=c_D+c_G and that the same bus can belong to more than one component, for instance when a domestic end-user is equipped with PV panels.

Then, for each type of component, an appropriate filter should be used for grouping typical pattern into the same cluster, thanks to easily accessible exogenous variables. The classification of loads can be improved by knowing the type of heating system of the building, its size and energy efficiency, the number of occupants, their employment status as well as net income, lifestyle and activities. But the knowledge of such information by the DSO raises privacy questions and

this, in this study, it is assumed to be inaccessible. However, a deeper segmentation can be realized thanks to the total energy consumed annually by a particular end-user since such a yearly metering is carried out for billing purposes. In some countries, such as Belgium, this electricity reading encompasses contributions of both total consumption and generation. In that case, the annual consumption is derived by firstly estimating the energy generated by the installation based on its installed power and location.

B. *Step 2-Construction of statistical profiles*

Let us consider a particular quarter of an hour (although the time-dependence is omitted in the following notations, for clarity) and define:

$E_{n_g}^{tot}$: Annual consumed energy for node $n_g \in N_g$, with N_g the set of nodes assigned to cluster $g = 1, \dots, n_{c_G}$

$E_{n_d}^{tot}$: Annual generated energy for node $n_d \in N_d$, with N_d the set of nodes assigned to cluster $d = 1, \dots, n_{c_D}$

E_{m_g}: Vector of ¼-hourly consumed energy flows for node $m_g \in M_g \subseteq N_g$ equipped with SM device

E_{m_d}: Vector of ¼-hourly generated energy flows for node $m_d \in M_d \subseteq N_d$ equipped with SM device

Since the clients pertaining to the same LV component can be of different sizes, the principle is to create a standardized distribution of reference CDF_{ref}, based on all the measurements collected by smart meters. The E_{m_g} and E_{m_d} values are respectively standardized with the yearly generation and the yearly electricity meter reading (i.e. the total energy consumed annually by a particular client) according to:

$$E_{m_g} = \frac{E_{m_g}}{E_{n_g}^{tot}},\ E_{m_d} = \frac{E_{m_d}}{E_{n_d}^{tot}},\ \ g = 1, \dots, n_{c_G},\ \ d = 1, \dots, n_{c_D} \qquad (4.45)$$

The values E_{m_g} and E_{m_d} are considered to be realizations of random variables $E_{m_g}$and E_{m_d} $d$that characterizes the dispersion of individual end-users of the g-th and d-th component respectively. The CDFs of the variables can then be built from the collected values.

The CDFs of reference are in this way sequentially constructed for each quarter of an hour and are assigned to the right LV nodes (though a PV user is characterized by two CDF_{ref}, one for its consumption and the other for the generation). To that end, the average annual consumption of end-users is compared to the centroid of each cluster thanks to an Euclidean distance and each client is consequently allocated to the closest cluster. It should be noted that for an exhaustively monitored LV system, the clustering can be carried out with a purely mathemati-

cal approach, directly based on the real SM measurements. Indeed, in this situation, the clusters do not need to have any explicit physical meaning since there is no unmonitored client to assign to its most appropriate group.

C. *Step 3 – Monte Carlo simulation*

The objective of the third step is to use destandardized CDFs of reference in the probabilistic algorithm presented in section 4.1, in order to perform long-term network studies. It is worth noting that the SM database is segmented in order to account for the different seasonality patterns. The data are thus divided into a monthly basis with an additional subdivision between week and weekend days.

The proposed methodology has been applied in a real feeder presented in Figure 4.24 [22]. The feeder encompasses 1 small shop as well as 20 residential end-users, among which 4 are equipped with rooftop PV installation, typically between 3 and 5 kVA. Hence, $\boldsymbol{c}_{\mathrm{D}} = 2$ and $\boldsymbol{c}_{\boldsymbol{G}} = 1$.

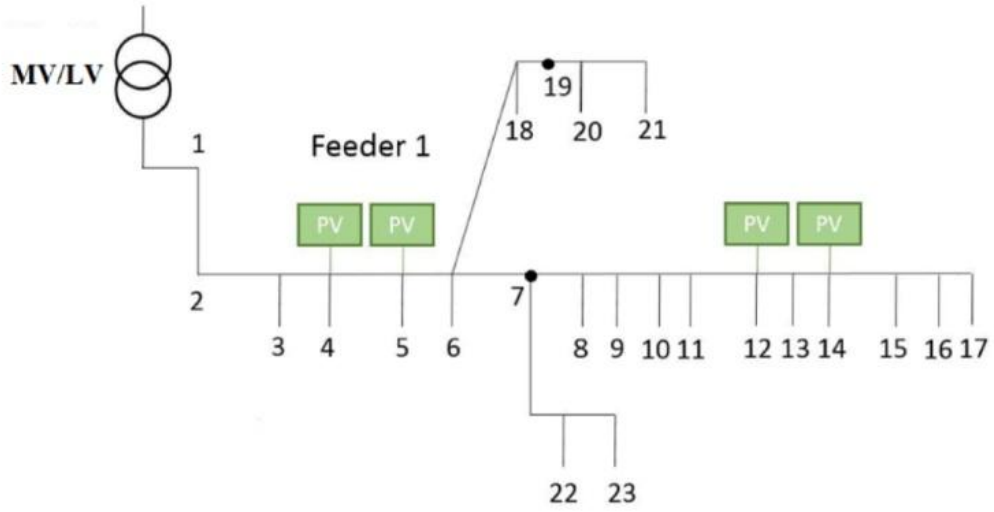

Figure 4.24: Single-line diagram of the studied LV network.

A. *Classification of loads*

At first, a pre-analysis for dividing the LV load based on the end-users' characteristics is carried out. Two groups are defined, one for residential end-users and the other for the small shop. Concerning residential end-users, a subdivision using one-dimensional clustering based on total annual consumption of residential end-users is performed. This clustering is obtained thanks to a *k*-means algorithm, which consists in an unsupervised classification of data aiming at minimizing the variance within the *k* clusters (where the parameter *k* is fixed by the experimenter).

A sensitivity analysis on the parameter *k* (i.e. on the way of splitting the total active power of domestic loads) is realized for obtaining the optimal number of

clusters. This analysis allows assessing the best trade-off between quality of models and amount of data to embed and process in the MC algorithm.

In this work, values of k = 1, 2 and 3 are tested. For the sake of example, the classification of residential loads for k = 3 is illustrated in Table 4.4. In such a case, $n_{c_D} = k + 1 = 4$ whereas $n_{c_G} = 1$.

Table 4.4: Ranges in the energy consumption of domestic end-users

	# of end-users	Yearly consumed energy (KWh)	
Cluster 1	11	701	4504
Cluster 2	4	5165	6730
Cluster 3	4	10095	18428

The clustering algorithm has grouped the majority of the residential end-users into the same cluster, which typically stands for traditional small families. Then, the second group, consisting of larger consumers, probably represents bigger houses with a higher number of inhabitants. Finally, the last cluster logically includes end-users with electrical heating system.

The quality of models, obtained with SLP as well as with CDF_{ref} for different values of k, is evaluated thanks to a validation set. This set consists of end-users with SM devices whose data are not used for constructing the load profile of reference. A statistical distance is then used to evaluate the divergence between real SM measurements and the distribution obtained with the investigated methodologies. Numerous distances are developed in the statistics literature [23]. However, for the simple task of quantifying the dissimilarities between two empirical distributions of different sizes, the chi-squared χ^2 distance leads itself to the task. In order to compute this distance, a preliminary grouping of the observations into n specified ranges, referred to as bins, is required. The optimal number of bins is determined using the Freedman-Diaconis rule [24], which is more robust and accurate than conventional Sturges' rule for large dataset. The χ^2 distance between random variables p and q is then computed as follows:

$$D_{\chi^2}\ p||q \ = \ \sum_{i=1}^{n} \frac{p_i - q_1}{p_i + q_1} \tag{4.46}$$

The χ^2 distance is computed for the 96 quarters of an hour in a typical day (week and weekend days aggregated) of a winter month (January) and of a summer month (July). In Tables 4.5 and 4.6, the averaged results are illustrated and put into perspective with those obtained using current Synthetic Load Profiles (SLPs) used by Belgian DSOs.

Table 4.5: Statistical distance between distributions of reference and real measurements for the month of January

	Mean χ^2 for different classifications			
	Cluster 1	Cluster 2	Cluster 3	Cluster 4
SLP	1.33	n/a	n/a	n/a
k=1	0.89	n/a	n/a	n/a
k=2	0.61	0.37	n/a	n/a
k=3	0.43	0.17	0.38	n/a
k=4	0.42	0.39	0.23	0.29

Table 4.6: Statistical distance between distributions of reference and real measurements for the month of July

	Mean χ^2 for different classifications			
	Cluster 1	Cluster 2	Cluster 3	Cluster 4
SLP	1.25	n/a	n/a	n/a
k=1	0.87	n/a	n/a	n/a
k=2	0.42	0.51	n/a	n/a
k=3	0.38	0.34	0.22	n/a
k=4	0.36	0.32	0.32	0.30

Firstly, the model computed with a single CDF of reference, representative of dispersion of all residential end-users, shows higher accuracy than traditional SLPs, with an improvement of around 40 % in terms of statistical similarities with real load profiles. This constitutes a promising result in the context of load modeling in the absence of large-scale energy recordings at the end-user level. Secondly, the quality of models is also significantly improved with a further classification within the domestic load cluster. In this way, this total number of clusters has to be adequately chosen. Indeed, when the size of the considered area increases, a compromise between the number of clusters and the impact on network studies has to be found. In this work, a clustering with $k = 3$ is used for the following analyzes.

B. *Performance of the method*

In order to assess the performance of the implemented approach with regard to traditional SLPs, a method based on the knowledge of real quarter-hourly

measurements at the MV/LV substation (recorded during a 1-year period) is applied. The MC algorithm presented in section 4.1 is used for computing the distribution function of active power flows at the substation with both SLP profiles and CDFs of reference techniques. The results are compared by a visual comparison of the distributions as well as their associated boxplot, using the R environment for statistics. The outcomes are illustrated in Figure 4.25 and 4.26 for the months of January and July respectively.

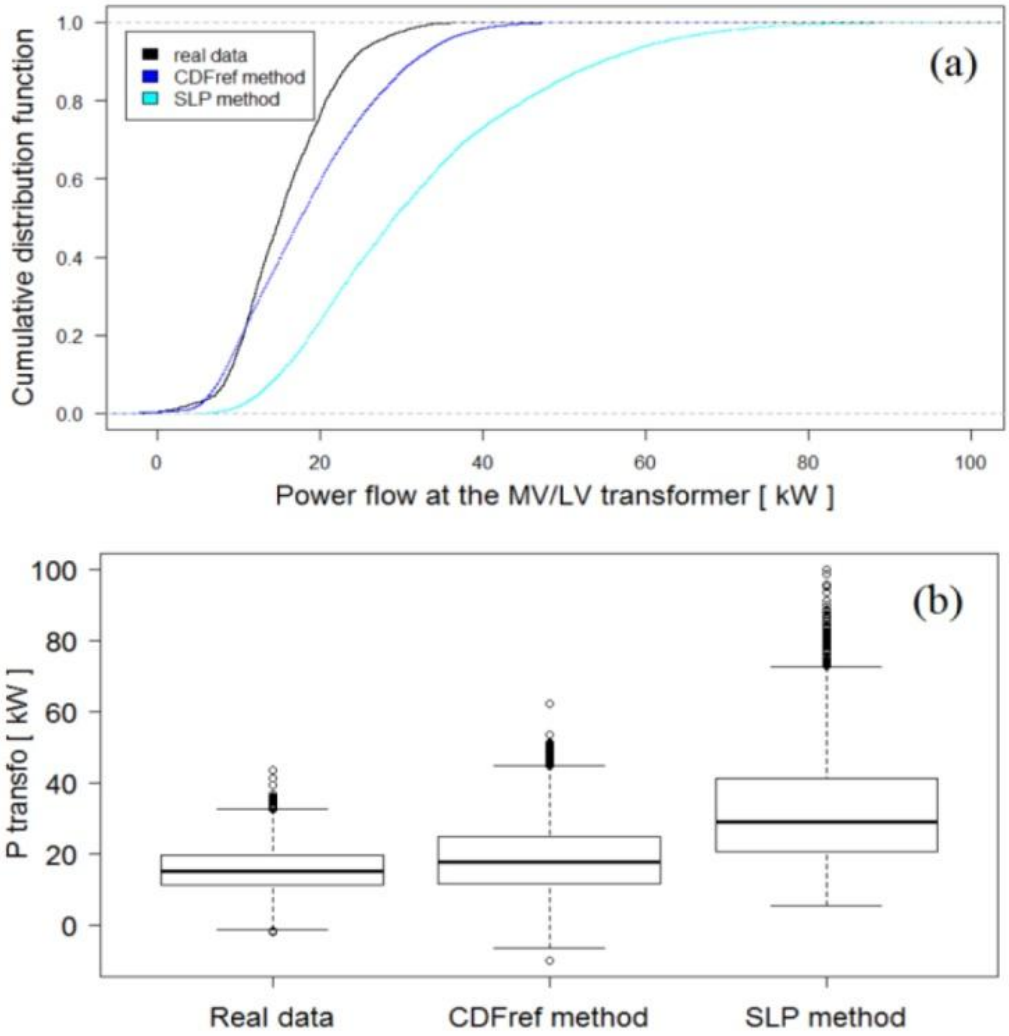

Figure 4.25: Comparison of both CDF_{ref} and SLP methods with regard to the real measured data for the month of January.

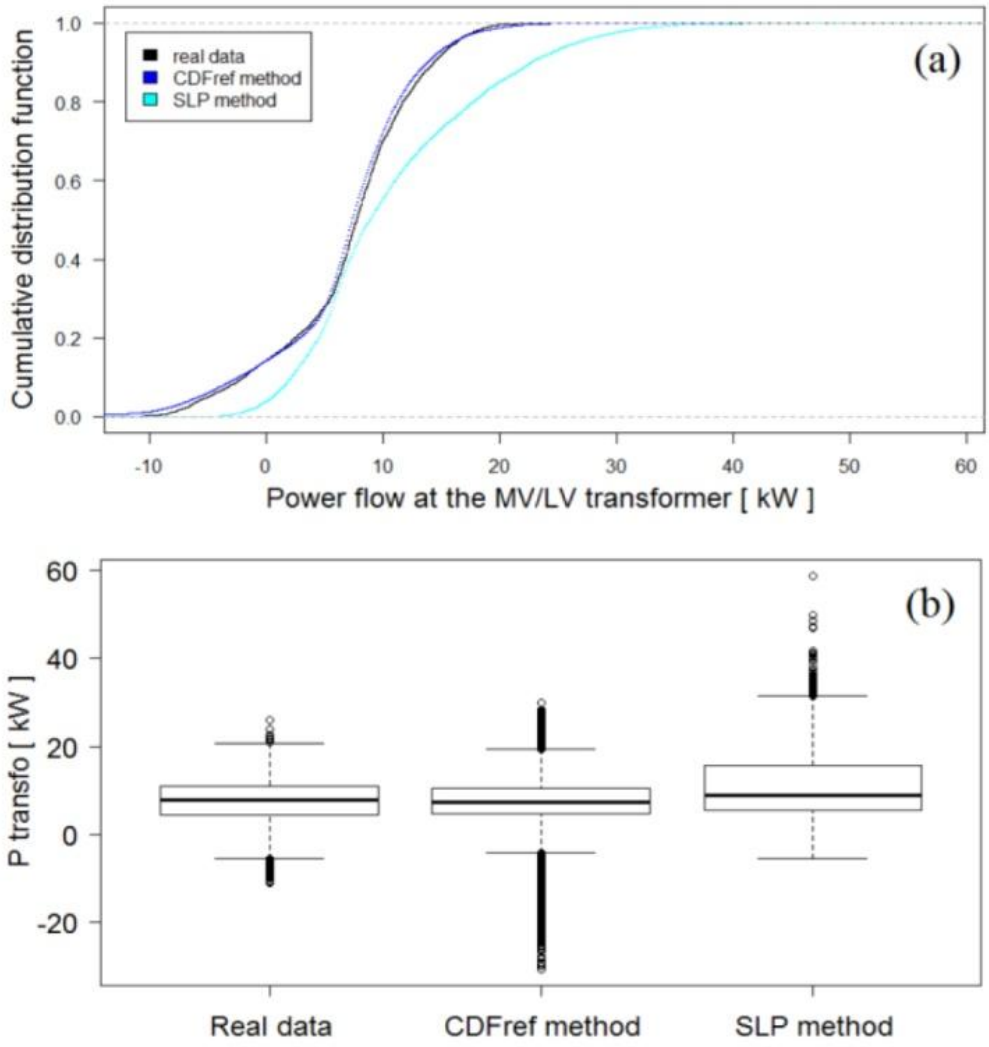

Figure 4.26: Comparison of both CDF_{ref} and SLP methods with regard to the real measured data for the month of January.

A significant improvement of the results is observed with our proposed method compared to the classical load profiles. However, these results are aggregated and it is interesting to investigate the accuracy of the method for quarter-hourly time steps. To that end, the analysis focuses on the month of July and the boxplots for four representative quarters of an hour are shown in Figure 4.27.

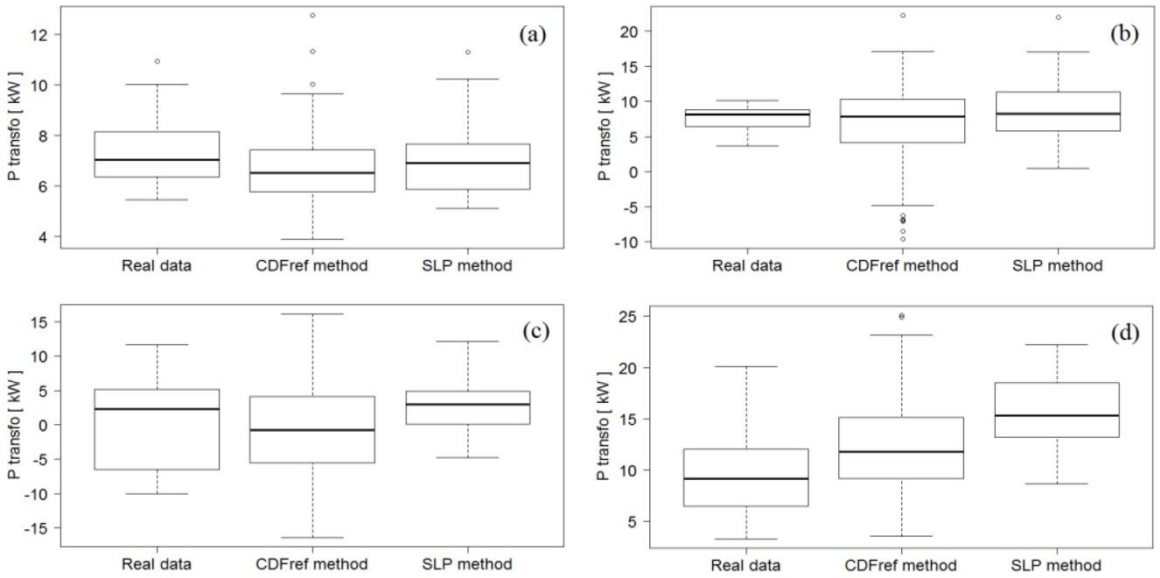

Figure 4.27: Comparison of CDF_{ref} and SLP methods with regard to the real measured data for the four representative quarters of an hour, namely 03:00-03:15 (a), 07:00-07:15 (b), 14:00-14:15 (c) and 19:00-19:15 (d) for the month of July.

Overall, the power flows at the MV/LV interface obtained with the CDF_{ref} approach are characterized by a greater variability than those observed in reality. This can be explained by the presence of a single year of measurement data at the substation that allows covering only few extreme events. Such extreme scenarios are however simulated in the probabilistic algorithm thanks to the representative power profile of end-users. The variability generated by the SLP method is less marked due to the deterministic nature of the approach. For these reasons, the described methodology has been applied for creating the CDFs for energy consumption and generation of users without a SM device in the analysis of section 4.2.2.

Chapter conclusions and further developments

Chapter 4 presented the basic structure of the probabilistic algorithm that has been developed for deploying long-term observability analysis of the LV network with the use of historic SM measurements. The presented developments are an attempt to answer to the first and to the third question of section 2.6. Indeed, Chapter 4 presented a methodology and the respective algorithm for modeling LV network uncertainty and redirecting long-term network design towards the most frequent network states rather than the extreme ones.

The simulation of a real LV feeder, with some available SM measurements, is also presented. The purpose is to compare the voltage outputs from the probabilistic simulation with real-case phase voltage measurements at two PV nodes, during one winter and one summer month. The comparison demonstrated that the studied datasets (probabilistic simulation outputs and real measurements) are quite similar in certain cases (Figure 4.18, node 4, July) while in other cases they are quite different (Figure 4.18, node 14, December). Regarding the worst-case (deterministic) computation, phase voltage values are higher than 80-90% of the values recorded with the SM devices.

The above findings underlined that the worst-case approach can lead to conservative decisions regarding voltage margin and PV hosting capacity of a LV feeder. It was also concluded that for achieving higher precision in both approaches (probabilistic and worst-case), the monitored visibility needs to increase or reliable methodologies should be developed for addressing the availability of sparse measurements.

Chapter 4 also presented a study exploring the potential correlation of PV generation and energy consumption of PV users located in a close geographical area. It has been demonstrated that the energy generation of all PV users is entirely correlated while no spatial correlation can be considered for their energy consumption on week days. Finally, Chapter 4 proposed a method for LV load and generation modeling for systems with little or no metering devices. This method uses the available information of end-users located in a nearby area. The methodology was incorporated in the probabilistic algorithm, proposed by this thesis, and the results have highlighted the added value of this approach compared to current approaches, such as SLP.

Consequently, Chapter 4 presented the developments that are the backbone of the present thesis work. The following Chapters 5 to 8 will demonstrate the utility of these developments for analyzing the operation of LV networks and for evaluating, in the long term, different technical solutions that can increase the PV hosting capacity of such networks.

In this way, Chapter 5 presents the application of the developed framework for the analysis of an existing three-phase LV feeder in Belgium. The analyzed feeder is the one studied in section 4.2.2 but in Chapter 5, an extensive analysis, addressing all important operation indices for a yearly period, is presented. Consequently, the current situation of the feeder is studied based on the available SM datasets and on a set of assumptions regarding the modeling of the unknown parameters (also listed in paragraph 4.2.2). The objective of this chapter is to give an example on how the developed methodology can be applied for computing the most important operation indices in a LV feeder with distributed PV units and SM deployment.

The following Chapters 6 to 8 present further developments and extensions of the algorithm's basic structure developed for addressing problems currently met in LV networks (overvoltage, voltage unbalance …). Different technical solutions dedicated to such problems are integrated in the algorithm so that their potential performance can be evaluated with a long-term approach. The use of the available SM datasets and the probabilistic analysis yield an information-rich and more reliable evaluation compared to deterministic analysis, because the volatility of loading parameters is considered. Thus, the principal objective of Chapters 6 to 8 is to answer to the second and to the fourth question of section 2.6 by presenting examples in which the probabilistic approach indeed led to more information-rich analysis and to less restrictive or costly technical decisions.

In this context, Chapter 6 presents a probabilistic methodology for estimating the PV hosting capacity of a given LV feeder based on user-specific SM historic datasets. Chapter 7 presents the modeling and simulation of a set of distributed control schemes with time-varying action, designed for mitigating voltage rise and voltage unbalance in LV feeders with DG units. Chapter 8 presents the modeling and the probabilistic simulation of a demand side management (DSM) strategy and of two different implementations of EVs. Depending on the needs and objectives of each simulation, the considered node connections and phase configurations might vary. However the topology of the feeder will remain the same throughout the simulations (similar to the one presented in Chapter 5).

Chapter publications

The developments of Chapter 4 have been published in:

[1] F. Vallee, V. Klonari, T. Lisiecki, O. Durieux, F. Moiny, and J. Lobry, "Development of a probabilistic tool using Monte Carlo simulation and smart meters measurements for the long term analysis of low voltage distribution grids with photovoltaic generation," Int. J. Electr. Power Energy Syst., vol. 53, pp. 468–477, 2013.

[2] V. Klonari, J.-F. Toubeau, Z. De Grève, O. Durieux, J. Lobry, and F. Vallée, "Probabilistic simulation framework for balanced and unbalanced low voltage networks," Int. J. Electr. Power Energy Syst., vol. 82, pp. 439–451, Nov. 2016.

[3] F. Vallee, F. Moutier, V. Klonari, J.-F. Toubeau, F. Lecron, Z. De Greve, and J. Lobry, "On The Correlation between Prosumers in Probabilistic Analysis of Low Voltage Distribution Systems," Int. Rev. Electr. Eng., 2016.

[4] J. L. V.Klonari, F.Vallee, O.Durieux, "Probabilistic tool based on smart meters data to evaluate the impact of distributed photovoltaic generation on voltage profiles in low voltage grids," in Proc. 3rd SIW, 2013.

[5] F. Vallée, V. Klonari, J. Lobry, and O. Durieux, "Study of the combined impact of auto-consumption behaviour and correlation level between prosumers on overvoltage probabilities in low voltage distribution grids," in IEEE PES T&D Conference and Exposition, 2014.

[6] V. Klonari, F. Vallée, O. Durieux, Z. De Grève, and J. Lobry, "Probabilistic Modeling of Short Term Fluctuations of Photovoltaic Power Injection for the Evaluation of Overvoltage Risk in Low Voltage Grids," in Energycon, 2014.

[7] V. Klonari, J.-F. Toubeau, Z. De Grève, O. Durieux, J. Lobry, and F. Vallée, "Probabilistic Analysis Tool of the Voltage Profile in Low Voltage Grids," in 23rd CIRED, 2015.

[8] V. Klonari, J.-F. Toubeau, Z. De Greve, J. Lobry, and F. Vallée, "Probabilistic Analysis of Low Voltage Networks with Distributed Photovoltaic Generation Sources: Case study in Belgium," in MedICT, 2015.

[9] J.-F. Toubeau, V. Klonari, Z. De Grève, J. Lobry, and F. Vallée, "Probabilistic Study of the Impact on the Network Equipment of Changing Load Profiles in Modern Low Voltage Grids," in ICREPQ'14, 2015.

[10] F. Vallée, F. Moutier, V. Klonari, J. Toubeau, and J. Lobry, "Clustering of Photovoltaic Generation for the Consideration of Time Changing Geographical Correlation in Probabilistic Analysis of Low Voltage Distribution Systems," in 5th Solar Integration Workshop, 2015.

[11] J.-F. Toubeau, M. Hupez, V. Klonari, Z. De Greve, and Vallée, "Statistical Load and Generation Modelling for Long Term Studies of Low Voltage Networks in Presence of Sparse Smart Metering Data," in IECON, 2016.

[12] J.-F. Toubeau, V. Klonari, J. Lobry, Z. De Greve, and F. Vallée, "Planning tools for the integration of renewable energy sources in low and medium voltage distribution grids.," in Renewable Energy - Utilisation and System Integration, Intech Open Access Publisher, 2016.

Chapter references

[1] J. Von Appen, M. Braun, T. Stetz, K. Diwold, and D. Geibel, "Time in the Sun," IEEE Power Energy Mag., February, pp. 55–64, 2013.

[2] H. A. . Sturges, "The Choice of a Class Interval: Reviewed work," J. Am. Stat. Assoc., vol. 21, no. 153, pp. 65–66, 2012.

[3] I. T. Papaioannou, A. Purvins, and E. Tzimas, "Demand shifting analysis at high penetration of distributed generation in low voltage grids," Int. J. Electr. Power Energy Syst., vol. 44, no. 1, pp. 540–546, 2013.

[4] M. Abdel Akher, K. M. Nor, and a. H. a Rashid, "Improved three-phase power-flow methods using sequence components," IEEE Trans. Power Syst., vol. 20, no. 3, pp. 1389–1397, 2005.

[5] M. Abdel-Akher, K. M. Nor, and A. H. Abdul-Rashid, "Development of unbalanced three-phase distribution power flow analysis using sequence and phase components," in 2008 12th International Middle East Power System Conference, MEPCON 2008, 2008, pp. 406–411.

[6] L. R. de Araujo, D. R. R. Penido, and F. de A. Vieira, "A multiphase optimal power flow algorithm for unbalanced distribution systems," Int. J. Electr. Power Energy Syst., vol. 53, pp. 632–642, Dec. 2013.

[7] A. R. Baran and T. S. P. Fernandes, "A three-phase optimal power flow applied to the planning of unbalanced distribution networks," Int. J. Electr. Power Energy Syst., vol. 74, pp. 301–309, Jan. 2016.

[8] T. H. Chen and N. C. Yang, "Three-phase power-flow by direct Z(BR) method for unbalanced radial distribution systems," Iet Gener. Transm. Distrib., vol. 3, no. 10, pp. 903–910, 2009.

[9] C. S. Cheng and D. Shirmohammadi, "A three-phase power flow method for real-time distribution system analysis," IEEE Trans. Power Syst., vol. 10, no. 2, pp. 671–679, 1995.

[10] D. Thukaram, H. M. Wijekoon Banda, and J. Jerome, "A robust three phase power flow algorithm for radial distribution systems," Electr. Power Syst. Res., vol. 50, no. 3, pp. 227–236, 1999.

[11] K. L. Lo and C. Zhang, “Decomposed three-phase power flow solution using the sequence component frame,” in Generation, Transmission and Distribution, IEE Proceedings C, 1993, vol. 140, no. 3, pp. 181–188.

[12] IEC, “IEC TR 61000-3-13:2008,” 2008.

[13] CIGRE JWG C4.07/CIRED, “Final WG Report: Power Quality Indices and Objectives,” 2004.

[14] IEC, “IEC, 60364-5-52 Table A5210.” .

[15] S. Lefebvre, “Contribution à l’utilisation d’un outil d’analyse technico-économique de réseaux de distribution Basse Tension en l’absence de compteurs électriques intelligents,” 2015.

[16] F. Vallee, F. Moutier, V. Klonari, J.-F. Toubeau, F. Lecron, Z. De Greve, and J. Lobry, “On The Correlation between Prosumers in Probabilistic Analysis of Low Voltage Distribution Systems,” Int. Rev. Electr. Eng., 2016.

[17] I. H. Witten, E. Frank, and M. a Hall, Data Mining: Practical Machine Learning Tools and Techniques (Google eBook). 2011.

[18] Gingrich. P, Introductory Statistics for the Social Sciences. 2015.

[19] W. J. G. Guojun, M. Chaoqun, “Center-based Clustering Algorithms,” in Data Clustering. Theory, Algorithms and Applications. ASA-SIAM Series on Statistics and Applied Probability, 2007, p. 488.

[20] M. Hayn, V. Bertsch, and W. Fichtner, “Electricity load profiles in Europe: The importance of household segmentation,” Energy Res. Soc. Sci., vol. 3, pp. 30–45, Sep. 2014.

[21] J.-F. Toubeau, M. Hupez, V. Klonari, Z. De Greve, and Vallée, “Statistical Load and Generation Modelling for Long Term Studies of Low Voltage Networks in Presence of Sparse Smart Metering Data,” in IECON, 2016.

Chapter 5 Simulation of an Existing Three-phase Low Voltage Feeder

Highlights

- *The developed probabilistic framework is deployed for simulating an existing three-phase Low Voltage feeder with 16 end-users including 4 photovoltaic units.*
- *The variations in voltage magnitude and the voltage unbalance factor are computed, with the probabilistic approach, at several nodes of the feeder, for each month of a year.*
- *The range of variation of voltage magnitudes results to be larger in the colder months of the year. The highest voltage magnitudes are obtained during the sunnier months of the year. However, important voltage rise sometimes also occurs in the colder months.*
- *Voltage unbalance results to be higher during the colder months of the year. This parameter seems to be mostly affected by single-phase unbalanced loads rather than by single-phase unbalanced photovoltaic injection.*
- *The congestion risk results to be quite high (for the simulated phase configurations) during evening peak hours while reverse power flows occur in almost 60% of the simulated network states of summer months (long sunny period, photovoltaic injection all day long)*
- *The consideration of loading unbalance and mutual coupling effect between phases has been proved essential for not over- or underestimating the impact of single-phase loads and generation units on the computed operation indices.*
- *A simulation that did not consider the spatial correlation among end-users (regarding photovoltaic generation) let to an underestimation of the computed overvoltage risk.*

Chapter 5 presents the implementation of the basic algorithm structure, developed in Chapter 4, for the probabilistic analysis of an existing LV feeder in Belgium. The description of the simulation and the obtained outputs are presented in the following paragraphs.

5.1 Description of the simulated feeder

The topology and the technical parameters of the simulated feeder are presented in Figure 5.1 and table A1 of Appendix A1. As explained in subsection 4.2.2, since the phase connections of loads and PV units in the feeder are not known, the simulation assumes the ones presented in Figure 5.1. Similarly, the values for the direct, inverse and homopolaire impedances are assumed based on commonly used values. The purpose of the current simulation is not to compare outputs with real measurements but to set a base scenario for testing whether the developed probabilistic algorithm can indeed allow a more information-rich and refined network analysis, compared to common deterministic approaches. For this reason, certain parameters are set differently than the ones used in subsection 4.2.2. so that the computation of the principal operation indices becomes clearer. For example, the repartition of loads and PV units over the three phases is less balanced than the one assumed in subsection 4.2.2 so that the impact of unbalanced single-phase connections on the voltage profile can be highlighted.

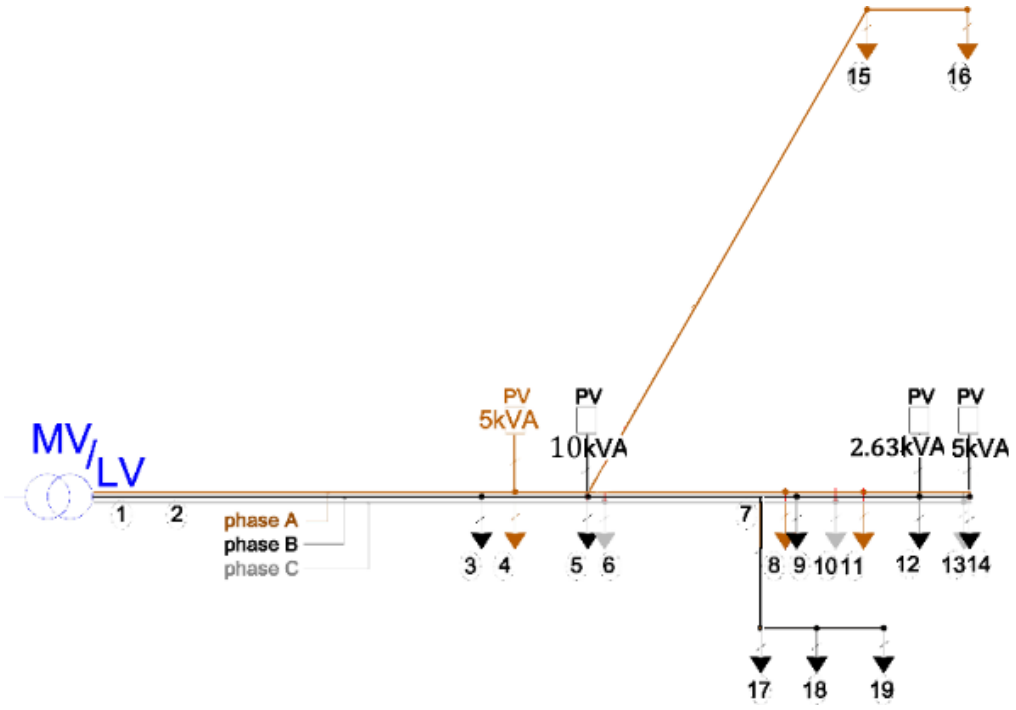

Figure 5.1: Topology of the simulated three-phase LV feeder

Concerning the consideration of spatial correlation between end-users (in terms of PV generation and energy consumption), the findings of section 4.3 have been considered in the simulations. Consequently, the end-users connected to the feeder of Figure 5.1 are considered entirely correlated regarding their PV generation and independent regarding their net energy demand while no correlation is considered between the PV generation and energy demand of the same end-user.

5.2 Voltage profile

The analysis of the feeder for a yearly period, using SM measurements recorded between 2012 and 2014, demonstrated that the range of values of possible voltage magnitudes varies with the studied month (see Figure 5.2). For the period between November and February the obtained variation of voltage is much larger than the one obtained for the period between March and October. In colder months, the simultaneous load demand for heating needs, during evening peak hours, can result in an important drop of the voltage profile while high PV injection during morning or noon hours (even in cold winter days), combined with low load demand, can lead to important voltage rise. In warmer months, load demand for heating needs is not important while PV injection in morning hours can also lead to important voltage rise. It is worth mentioning that the upper computed values for phase voltages do not vary significantly in function of the considered month while the lower obtained values are much lower in colder months compared to the ones obtained during summer months.

Another interesting remark is that the range of voltage magnitudes at node 5 has a much narrower variation of amplitude than the ones of nodes 13 and 14. Although a big PV unit is connected to node 5 (10kVA) and local voltage values generally result to be high compared to nearby nodes, the local voltage profile is not significantly affected by the variation of loads and generation in the entire feeder. This is not the case for nodes 13 and 14 which are located at the end of the line. A 5kVA unit is connected to node 14 while node 13 has no generation. However, the variation of both nodes' voltage profiles is much more vulnerable to the constant variability of loading parameters in the entire feeder compared to the one at node 5. The EN 50160 standard's 95-percentile voltage limits were not exceeded during none of the simulated months.

Similar observations can be made regarding voltage unbalance. Nevertheless, concerning this parameter, the upper acceptable limit is locally violated at some nodes in the period between September and April. For example, the %VUF at nodes 13 and 14 is computed higher than 2%, at least once during the mentioned period (Figure 5.3). The simulation of a yearly period highlighted that voltage unbalance is mostly affected by single-phase loads rather than by single-phase

PV units, in particular for nodes located at the end of the feeder (see Figure 5.3). Indeed, in the period between May and August the upper computed values for %VUF are quite low compared to the rest of the year. Figure 5.4 shows the ¼-hourly variation of %VUF at node 14 during two simulated January days. During PV injection hours %VUF rises but during evening peak hours its increase is clearly more significant.

Thanks to the probabilistic analysis of a given network, not only extreme values can be computed in a more refined and accurate manner but also the risk of exceeding the standard's limits can be more realistically approximated, since an extensive range of possible loading conditions is evaluated. Consequently, compliance with the EN 50160 standard (relations 4.31) can be quantified in a less conservative manner compared to deterministic worst-case analysis.

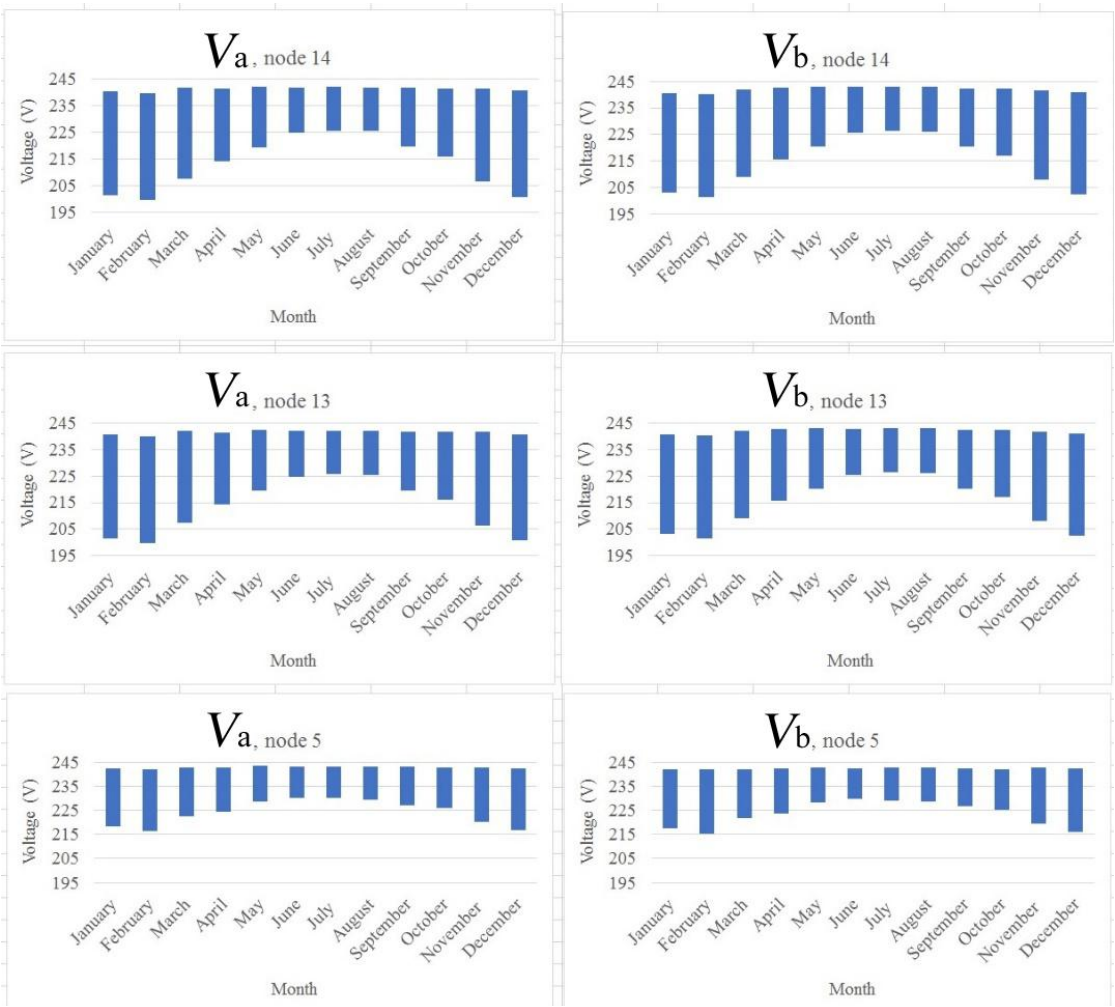

Figure 5.2: Range of variation of phase voltage (V_a and V_b) magnitudes computed with a yearly simulation of the feeder

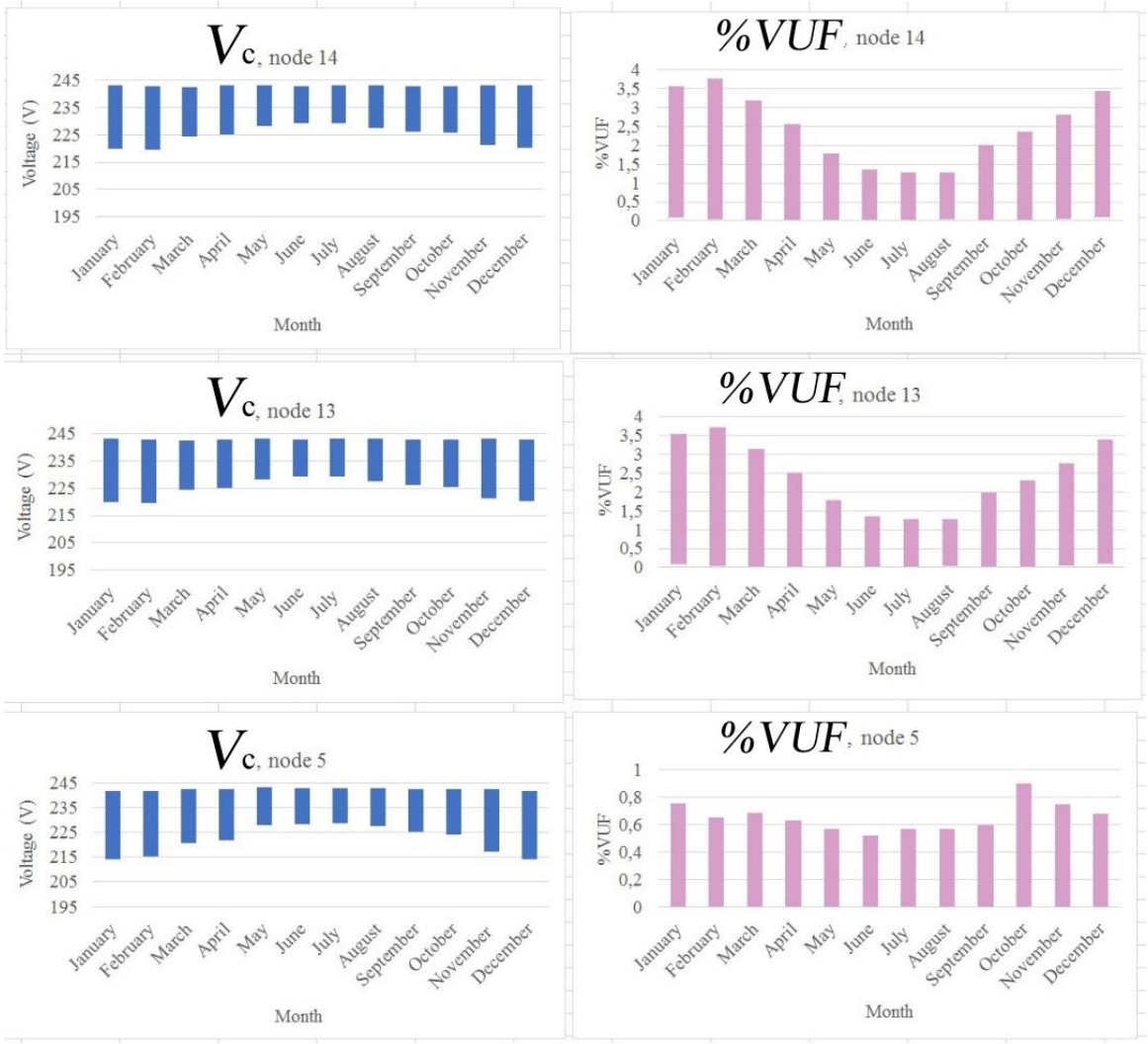

Figure 5.3: Range of variation of phase voltage (V_c) magnitude and of voltage unbalance (%VUF) computed with a yearly simulation of the feeder

Regarding voltage magnitudes, although no limits' violation occurs in the studied feeder, the probabilistic analysis gives a much more information-rich overview of the statistical distribution of voltage magnitudes per month. In this way, the behavior of the feeder is evaluated focusing on the most possible cases rather than the extreme ones (highest and lowest computed values). For example, Figure 5.5 presents the CDFs for phase voltage V_a at node 14 for the months of July and December. Although the upper computed values for these two months are very similar, the created CDFs demonstrate that V_a takes values in the range of 233-241V in more than 90% of the simulated network states for July while in December, V_a resulted to be lower than 233V in around 60% of the simulated network states. Such refined information is very useful for improving the long-

term observability of the network's operation and for designing technical solutions in order to circumvent local voltage rise and unbalance problems.

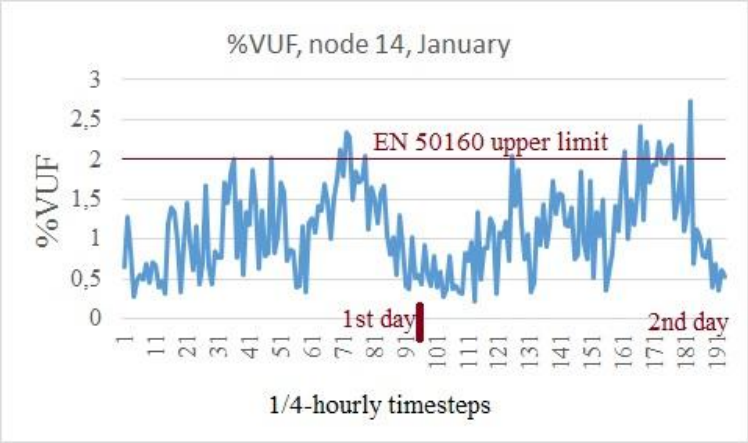

Figure 5.4: ¼-hourly variation of %VUF at node 14 over two daily periods in January

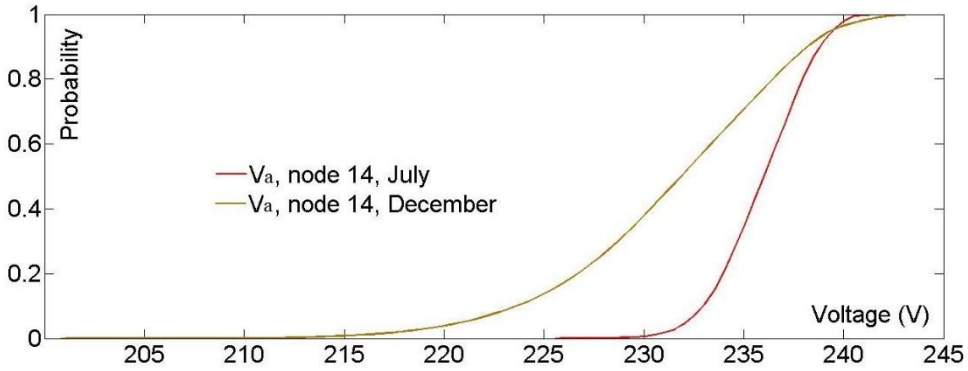

Figure 5.5: CDFs for V_a at node 14 for July and December

5.3 Line current, reverse power flows and losses

The analysis of a yearly period demonstrated that the maximal capacity of the lines can be easily exceeded during evening peak hours in winter months. Given the assumed unbalanced connection of single-phase loads in the feeder (all single-phase loads connected to phase c), this conclusion was expected. Table 5.1 lists the maximal current magnitudes that have been computed in each monthly simulation of line segment 1-2 (first segment at the head of the feeder). The maximal current capacity of the line is determined based on reference [1]. In reality, the repartition of single-phase loads and generation units among phases is more balanced (compared to the simulated configuration of Figure 5.1) and the resulting current flows in segment 1-2 do not exceed the maximum line capacity.

Table 5.1: Computed maximal phase current magnitudes in line segment 1-2

Month	Line Segment: Current capacity (A)	Phase current magnitude (A)
January	Segment 1-2: 270A	330,50 (phase c)
February	Segment 1-2: 270A	306,90 (phase c)
March	Segment 1-2: 270A	267,07 (phase c)
April	Segment 1-2: 270A	196,05 (phase c)
May	Segment 1-2: 270A	179,85 (phase c)
June	Segment 1-2: 270A	131,11 (phase c)
July	Segment 1-2: 270A	116,04 (phase c)
August	Segment 1-2: 270A	144,27 (phase c)
September	Segment 1-2: 270A	161,98 (phase c)
October	Segment 1-2: 270A	200,69 (phase c)
November	Segment 1-2: 270A	258,40 (phase c)
December	Segment 1-2: 270A	331,28 (phase c)

Apart from current magnitudes, the analysis of an extensive range of possible network states gives a better insight on the probability of occurrence of reverse flows in the feeder. Table 5.2 presents the maximum reverse current magnitudes that were computed in the first line segment 1-2, at the head of the feeder, for each monthly simulation. The highest magnitude of reverse flows does not vary significantly from month to month. Practically, all along the yearly period, there are many power exchange scenarios that result in reverse flows without necessarily corresponding to extreme cases of PV injection. This argument highlights the importance of simulating the operation of the network not only in extreme worst-case conditions but also in more common power exchange scenarios. Such

scenarios can also lead to power quality problems especially if one considers the upcoming integration of flexibility services and EVs in LV feeders. All operation parameters need to be carefully studied considering the constant variability of the LV network.

Table 5.2: Maximum computed reverse (phase) current magnitudes at the MV/LV transformer

Month	Phase current magnitude (A)
January	-45,96
February	-48,27
March	-56,29
April	-52,95
May	-56,18
June	-54,82
July	-50,41
August	-50,26
September	-51,7
October	-37,08
November	-29,37
December	-45,96

Table 5.2 basically presents the highest possible values that reverse flows can take in segment 1-2. A certain interest can also be found in studying the frequency of such reverse flows and the period of the day in which they occur. This information is useful for evaluating their impact on line losses and also for studying, with a long-term statistical approach, the local storage potential of network-injected energy while taking into account the time-variability of loading parameters. Indeed, high values of reverse power flows in the feeder result from high local energy excess, due to simultaneous PV injection, which would possibly justify the integration of local storage technologies.

Figures 5.6 and 5.7 illustrate the statistical distributions of current flows in line segment 1-2 during the simulated months of July and of December. In July, reverse power flows occur in 60% of the simulated network states while in December they occur in 10% of the simulated network states. Practically, this means that during 90% of the time in December the injected PV energy is absorbed in order to cover the load demand of end-users while the injected energy in July is only fully absorbed during 40% of the time. Figure 5.8 presents the mean value and the range of values (minimum and maximum values) that phase currents can

take, based on the probabilistic analysis, during every ¼-hourly time step of a typical December day.

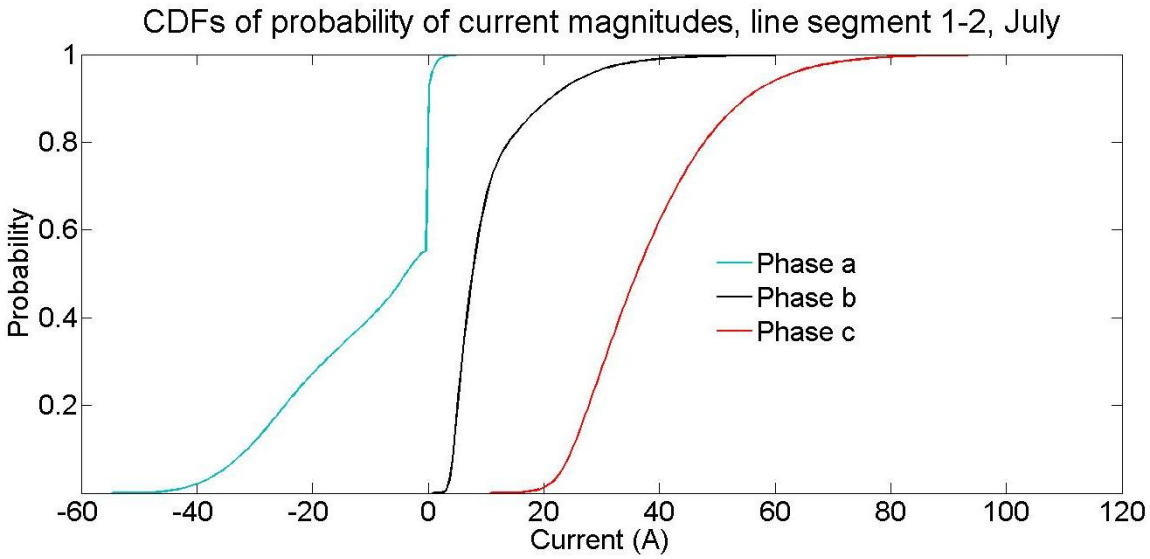

Figure 5.6: CDFs of probability of simulated reverse current magnitudes of line segment 1-2 in July

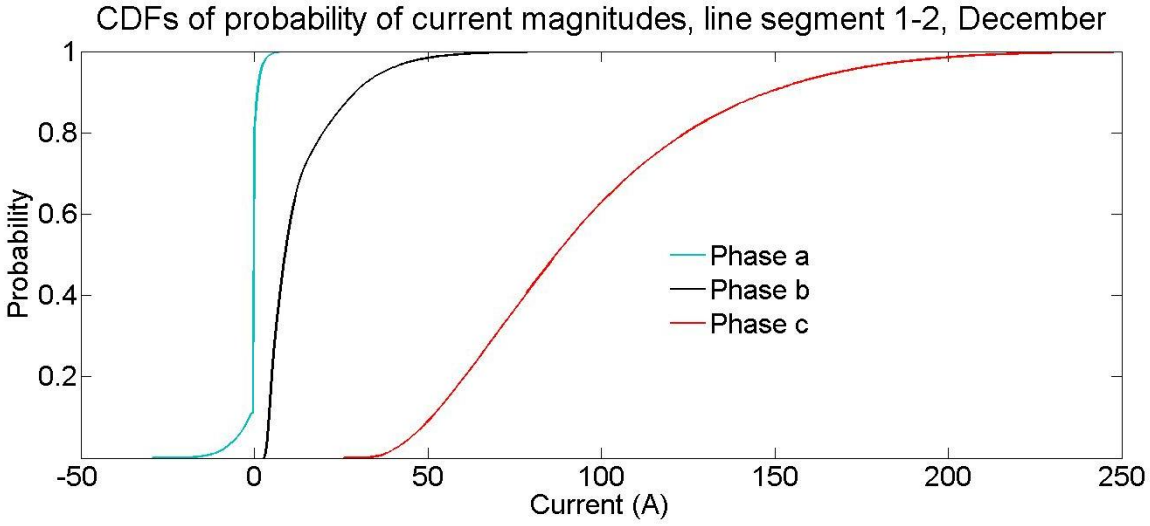

Figure 5.7: CDFs of probability of simulated reverse current magnitudes of line segment 1-2 in December

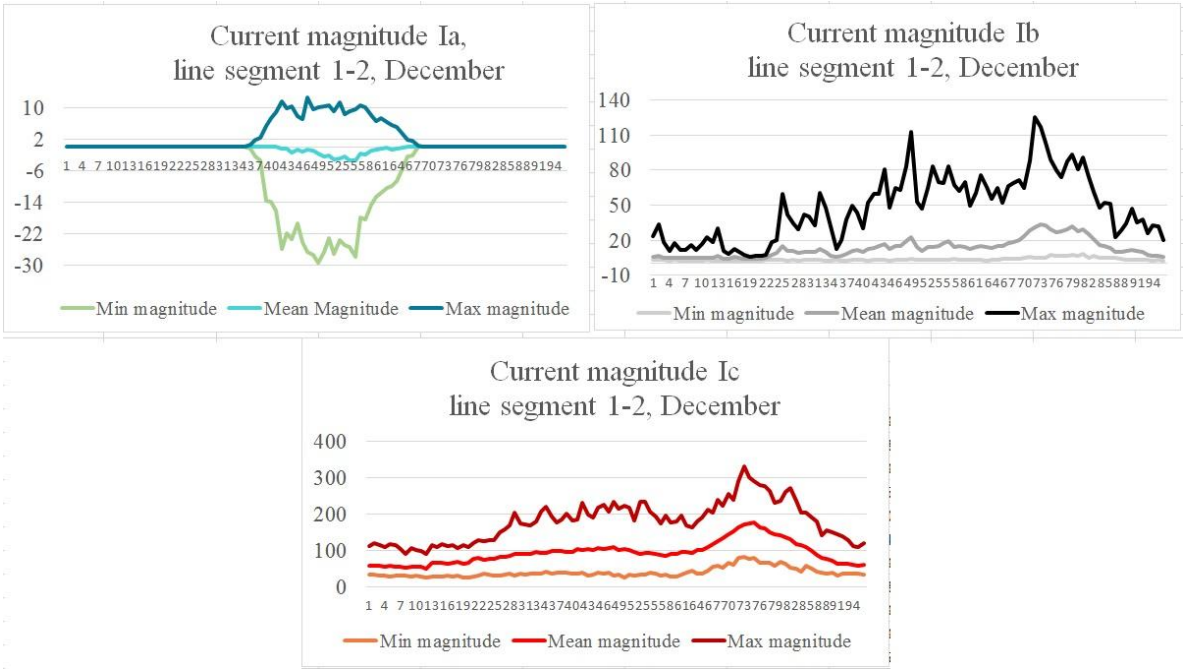

Figure 5.8: Min, max and mean values of current magnitudes I_a, I_b and I_c for every individual ¼-hourly time step of a typical December day

Regarding energy losses in the feeder, the yearly simulation demonstrated that they are much more important during winter months. Figure 5.9 illustrates the possible range of values that total energy line losses (in the entire feeder) can take over daily periods and their respective mean values. Similar outputs are available separately for each line segment.

Energy losses in each line segment and in the entire feeder are computed as follows. For a given time step *q*, the magnitude of active power losses $P_{loss,x_{i,i+1}}$ in the line segment between nodes *i* and *i+1* are computed separately in each phase *x* with relation (5.1):

$$P_{loss,x_{i,i+1}} = R' * L_{i,i+1} * \boldsymbol{I}^2_{x_{i,i+1}}, \text{ with } x\text{= a, b or c phase} \qquad (5.1)$$

where $\boldsymbol{I}_{x_{i,i+1}}$ is the current flowing in the same line segment (and phase), computed (for time step *q*) with the *hybrid power flow method* described in paragraph 4.1.4.iii.

Total energy line losses in a LV feeder can be considered as a lost amount of energy over a given period (energy that is not supplied to end-users). Assuming that $P_{loss,x_{i,i+1}}$ is stable during the ¼-hourly time step, the total (averaged) energy loss during this period, in the line segment between nodes *i* and *i+1*, in phase *x*, is computed with relation (5.2):

$$E_{loss,q,x_{i,i+1}} = 0.25 \cdot P_{loss,q,x_{i,i+1}} \quad (5.2)$$

and the total energy loss in all three phases is computed as follows:

$$E_{loss,q_{i,i+1}} = E_{loss,q,a_{i,i+1}} + E_{loss,q,b_{i,i+1}} + E_{loss,q,c_{i,i+1}} \quad (5.3)$$

The energy loss in the entire feeder (with *N* nodes), during time step *q*, is the sum of ¼-hourly energy losses $E_{loss,_{i,i+1}}$ in each line segment of the feeder, as expressed in relation (5.6):

$$E_{loss,feeder,q} = \sum_{i=1}^{N-1} E_{loss,q_{i,i+1}} \quad (5.4)$$

Consequently, the total daily energy losses in the feeder for one simulated day *s* can be computed with the following expression

$$E_{loss,feeder,s} = \sum_{q=1}^{96} E_{loss,feeder,q} \quad (5.5)$$

As previously mentioned, Figure 5.9 presents the mean values and the range of values that total daily energy losses $E_{loss,feeder,s}$ can take in the studied feeder for the months of April, July, September and December.

Figure 5.9: Range and mean values of simulated total daily losses (in the entire feeder) for April, July, September and December

5.4 Assuming a perfectly balanced network

The objective of this paragraph is to evaluate whether and up to which extent the consideration of phase unbalance and coupling effect between phases affects the computed voltage profile in a LV feeder. To this end, the same feeder is analyzed considering configurations (i) and (ii) (Section 4.1.4) and the computed voltage magnitudes at some nodes are compared to the ones computed considering configuration (iii).

Figure 5.10 presents the CDFs for voltage magnitudes at node 14 in July, computed with configurations (i) and (iii). Given the importantly unbalanced configuration of the studied feeder (Figure 5.1), it results that, if the feeder is analyzed as a perfectly balanced system, without considering the single-phase connections of loads and PV units, the obtained voltage profile will be underestimated. Indeed, Figure 5.10 shows that although configurations (i) and (iii) result in equal possible worst-case values (highest voltage magnitudes≈243V in both cases)), configuration (i) results in voltage magnitudes around 5V lower compared to configuration (iii) in around 99% of the simulated states. This difference in the obtained results is very important and it highlights the fact that, when a feeder is heavily unbalanced, it is necessary to consider the existing loading unbalance between phases in long-term analysis.

Figure 5.11 presents the CDFs of probability for phase voltages at node 14 in July, computed with configurations (ii) and (iii). The fact that configuration (ii) does not consider mutual coupling effects between phases leads to much higher phase voltage magnitudes V_a, compared to configuration (iii), since all PV units are connected to phase *a*. Indeed, in this case, the voltage rise due to PV injection only affects phase *a* (it is not distributed over the three phases). Configuration (ii) computes some violations of the EN 50160 standard limits which are not the case with configuration (iii). Similarly, configuration (ii) leads to much lower phase voltage magnitudes V_c since all single-phase loads are connected to phase *c* and they only affect the voltage profile of this phase. These findings highlight the importance of deploying detailed three-phase analysis of heavily unbalanced feeders (like the studied one) because not considering phase loading unbalance or coupling effects between phases can lead to overestimation or underestimation of important operation indices. Such inaccuracies can eventually affect long-term planning decisions such as further integration of DER in a given network.

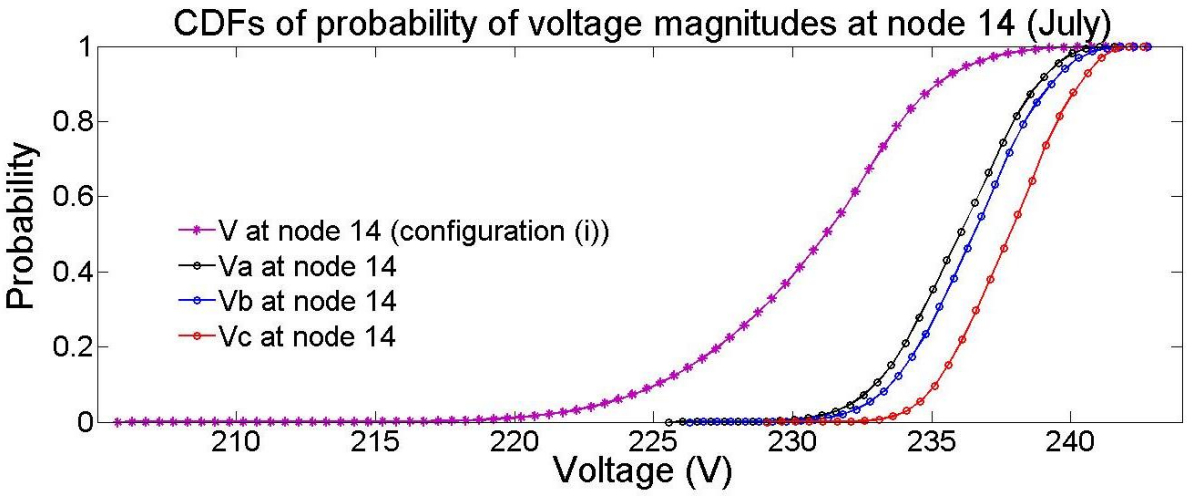

Figure 5.10: The effect of considering loading unbalance between phases on the computed voltage profiles at node 14 (configuration (i) and (iii))

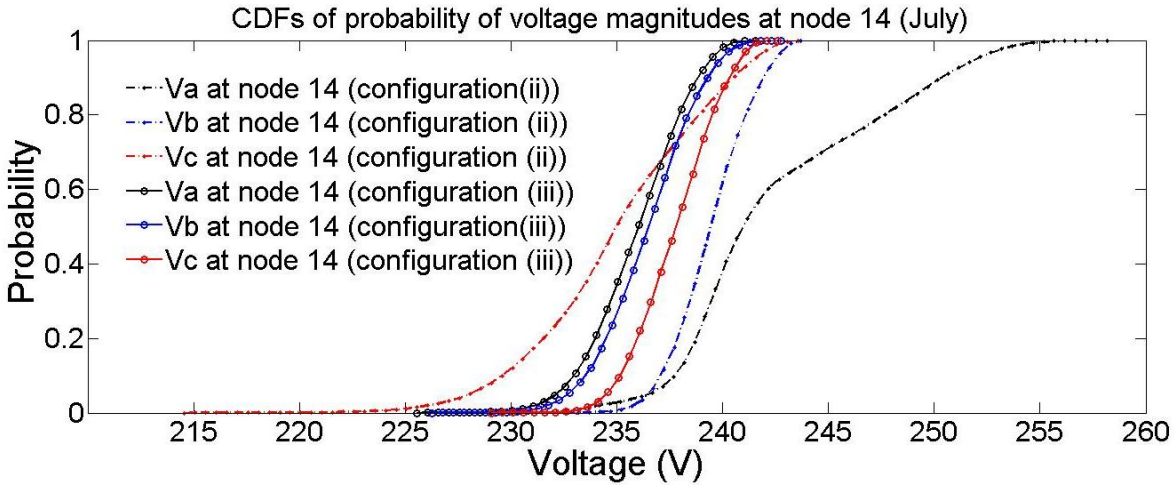

Figure 5.11: The effect of considering mutual coupling effects between phases on the computed voltage profiles in the three-phase unbalanced LV feeder (node 14)

5.5 Consideration of spatial correlation

In order to investigate how the consideration of the spatial correlation among end-users (in terms of power exchange with the network) affected the computed operation indices in the previous simulations, two scenarios have been investigated. The 19 end-users that were studied in section 4.3 have been assigned to the 19 nodes of the feeder depicted in Figure 5.1. The PV installations of the considered users are presented in Table 5.3.

Table 1.3: 19 end-users with PV units (see Section 4.3) assigned to the nodes of the simulated LV feeder

Nodes	1	2	3	4	5	6	7	8	9	10	11	12	13	14	15	16	17	18	19
PV (kVA)	2,63	2,65	2,65	2,65	2,65	2,8	3,4	3,47	3,5	3,47	4,1	4	4,6	4,2	5	5	5	5	5

The first simulated scenario considered the findings of section 4.3 regarding the spatial correlation of the 19 end-users (in terms of PV generation and energy consumption). In this way, the computed clusters concerning weekend load demand, full dependency between their PV generations and entire independency between their week day load demands have been considered. The second case considered them as entirely independent. The consideration of spatial correlation between PV units resulted in a higher overvoltage risk at all nodes of the feeder (Figure 5.12). This observation can be explained by the fact that, when full correlation is considered between all the PV units, a power injection increase is simultaneously generated all over the network. As load demand is not correlated with this PV injection (see the results of Table 4.3), local overvoltage situations can be observed all over the nodes of the system.

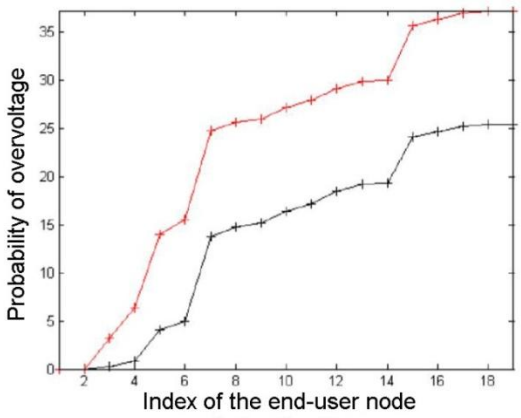

Figure 5.12: Simulated overvoltage risk for fully correlated (red) and the independent (black) cases concerning nodal PV power injections.

Chapter conclusions

Chapter 5 presented the implementation of the basic structure of the probabilistic methodology, developed in Chapter 4, for simulating the operation of a three-phase LV feeder located in Flobecq (Belgium). The implementation of a probabilistic approach gave a detailed statistical analysis of the values that the various operation indices can take. In this way, extreme worst-case values were computed and probability functions were constructed for each studied time step at each node. Critical nodes have been identified and statistically characterized in terms of technical constraints' violation.

For the studied feeder, it has been demonstrated that high voltage values can easily occur, even during months with lower solar irradiation, during periods of low load demand and high PV injection. Nevertheless, the highest voltage rise has been computed in the summer months. Regarding voltage unbalance, it has been shown that single-phase loads have a bigger impact compared to single-phase generation units. The important time-variation and the variability among different locations in the feeder have been proved both for voltage magnitudes and voltage unbalance.

It has been demonstrated that, during summer months, an important amount of injected PV power is not locally absorbed by end-users' loads which leads to frequent reverse power flows towards the head of the feeder. This fact increases line losses and gives an indication on the usefulness of integrating local storage technologies during such situations.

The analysis of a three-phase feeder (with several unbalanced single-phase connections of loads and PV units), assuming a perfectly balanced system and no coupling effects between phases, highlighted the importance of deploying detailed three-phase analysis of such feeders. It was demonstrated that not considering phase loading unbalance or coupling effects between phases can lead to overestimation or underestimation of important operation indices. Finally, it was demonstrated that the overvoltage risk in a LV feeder with several PV users results higher when the correlation of their PV generation is taken into account. Consequently, assuming that PV users, located in proximity, are independent concerning their PV generation might lead to an underestimation of the voltage rise in the feeder.

Chapter references

[1] IEC, “IEC, 60364-5-52 Table A5210.” .

Chapter 6 Probabilistic Estimation of Photovoltaic Hosting Capacity using Smart Metering Measurements

Highlights

- *A probabilistic photovoltaic hosting capacity methodology (and tool), using the basic algorithm of Chapter 4, is presented and tested in the studied Low Voltage feeder.*
- *The probabilistic computation of maximum acceptable photovoltaic hosting capacity leads to much less restrictive results, in the studied feeder, compared to the deterministic analysis, if one considers voltage and voltage unbalance margins that are treated in a statistical manner in the EN 50160 standard.*
- *Probabilistic and deterministic analyses lead to the same maximum hosting capacity if congestion risk is considered. However, the probabilistic approach gives a more refined information-rich overview such that congestion problems can be locally treated for not restricting the further increase of photovoltaic integration.*
- *The integration of a control scheme (three-phase damping control) for mitigating local unbalance problems and improving voltage profiles, in an overall manner, leads to considerably higher maximum acceptable hosting capacity.*

In many regions worldwide, DER integration is hampered due to slow or over rigid hosting capacity review processes. As a result, end-users who want to invest and play an active role in managing their energy usage are increasingly unable, in expediency and cost-efficiency terms, to do so. In this context, a stream-lined approach together with the expansion of allowable DER integration approvals seem to be a necessity [1]. However, the expansion of allowable approvals depends heavily on DER admissible penetration levels, which are determined by local distribution utilities. In order to increase penetration levels while facilitating the application review process, DSOs should incorporate automated DER hosting capacity analyses. An example process flowchart for incorporating such analysis into the DER integration review process is proposed in Figure 6.1.

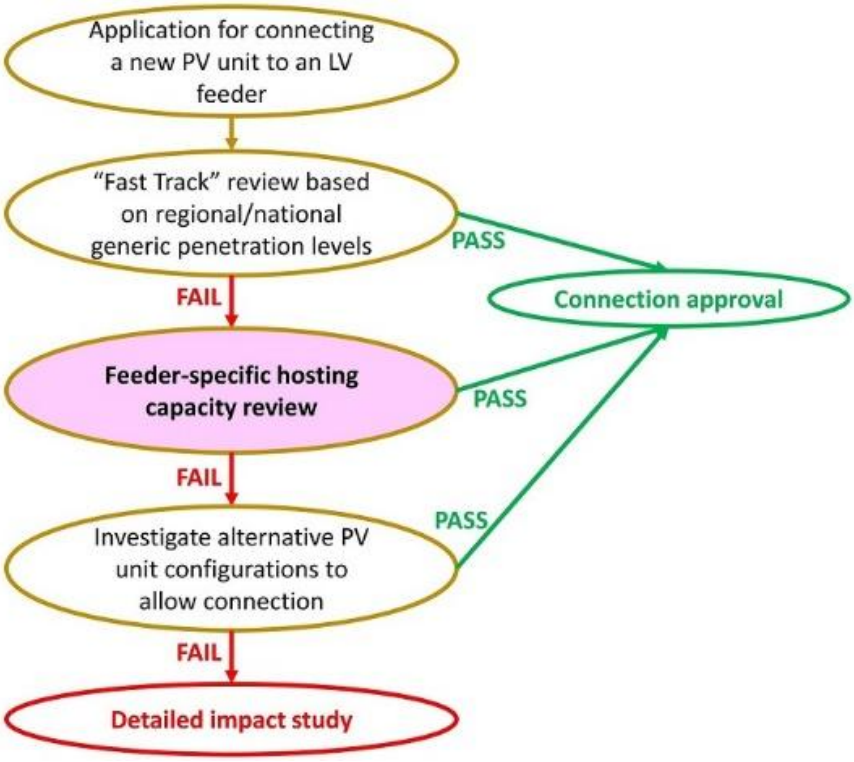

Figure 6.1: Process flowchart for incorporating hosting capacity analysis into the DER integration process.

Currently, many energy utilities are adapting their DER hosting capacity review so as to remove or update restrictive maximum allowable limits [2]. To this end, the Electric Power Research Institute (EPRI) presents a set of models that could be used by DSOs or electric utilities [3], [4]. These feeder-based methodologies are very solid computation examples that take account of all steady-state operational criteria.

Focusing on PV hosting capacity, the EPRI report presents stochastic analysis as a highly appropriate tool for determining feeder hosting capacity for distributed PV units. The stochastic deployment concerns the position and size of

future PV units while the steady-state estimation of the feeder is done with a deterministic approach. Indeed, the analyzed state estimation scenarios are based on four worst-case load/ PV generation profiles. Practically, it is to be noted that most of the existing probabilistic methodologies for determining PV hosting capacity of a network deploy the stochastic analysis regarding the size and position of PV units and not the load/generation profiles of customers. However, the ongoing integration of SM devices in LV networks enlarges the potential of using feeder-specific or even customer-specific data for modeling energy flows.

Considering these facts, the EPRI report [4] estimates PV hosting capacity using feeder-specific data to create either absolute worst-case scenarios (maximum recorded generation-minimum recorded load) or load/PV time-of-day coincident worst-case scenarios. Therefore feeder-specific data are used. However, the steady-state estimation of the feeder is still done with a deterministic approach. Consequently, this approach does not consider the fact that the time-of-day in which worst-case values apply for a specific customer does not necessarily coincide with the one of other customers connected to the same feeder. Nevertheless, the operational criteria of the feeder are determined both by the individual user's demand and by the simultaneous demand of other network users. Since the demand of every user and the degree of coincidence between them constantly varies, so does the operation of the feeder [5].

The above argument demonstrates that, although user-specific SM data are primordial for creating reliable network models, there is another challenge that needs to be addressed. The latter lies in the fact that end-users follow, volume-wise (kWh) or capacity-wise (kW), an almost stable daily pattern. However, this pattern does not necessarily remain the same on the time axis. In long-term decision making, profiles should be based on the recorded ones considering all possible deviations. Those deviations could be inserted either as random statistical errors or by making random possible combinations of the recorded values or even by combining both approaches.

Consequently, reliable models that use user-specific real SM readings and take into account load/PV time- and user-variability are necessary for applying a less conservative and more cost-effective hosting capacity analysis. Probabilistic and particularly MC algorithms are very suitable to address this modeling challenge.

6.1 The PV Hosting Capacity Computation Tool

Hosting capacity is defined as the maximum amount of PV that can be accommodated in the feeder without impacting system operation (reliability, power quality, etc.) under existing control and infrastructure configurations [6]. This chapter proposes a methodology that aims at addressing the central block of Figure 6.1 ("Feeder-specific hosting capacity review") by providing a detailed location- and user-specific DER hosting capacity analysis. The analysis takes into account the EN 50160 standard operational criteria. In particular, the focus is on voltage magnitude and unbalance which are the primary technical concerns in LV feeders with distributed PV generation. The maximum line capacity is also taken into account so as to address important reverse power flows due to high PV injection and simultaneous low consumption.

Although the EN 50160 standard sets the same voltage limits in all EU countries (except from cases where stricter limits are locally imposed), the maximum line capacity heavily depends on the respective distribution utilities. In certain countries, line sections are chosen based on a long-term strategy that aims at minimizing voltage and congestion risk even if loads and generation increase importantly in the future. However, such approach leads to higher initial investment which is not necessarily cost-effective. In other cases, line sections are chosen based on actual conditions or short term future scenarios so that customized solutions are applied as soon as problems arise.

Apart from steady-state constraint management, there are other considerations that could be accounted for, such as transformer aging factor, line losses, etc. Such criteria are usually considered in an overall cost-benefit analysis (CBA) but nowadays they are not addressed by the EN 50160 standard. Depending on the country and the applied DSO tariff methodology ("cost-plus", "revenue cap", etc.), DSOs are incentivized to reduce certain operation costs that can (or cannot) be integrated in their tariffs. Thus, the impact of such criteria on decision making varies in function of the distribution utility. For this reason, this chapter computes PV hosting capacity focusing on commonly adopted EN 50160 standard criteria and line capacity issues. Line losses in the feeder, during PV injection hours, are also addressed. However, their rise is not imposed as a constraint to the further increase of admissible PV hosting capacity.

6.1.1 *Overview of the simulation tool*

This section presents an algorithm for determining the PV hosting capacity of a given LV feeder by elaborating feeder-specific SM measurements. The developed algorithm uses the basic MC structure that is presented in Chapter 5. The flowchart in Figure 6.2 illustrates the developed PV hosting capacity computation algorithm. The network state scenarios are randomly sampled by the basic MC

algorithm and the power flow analysis is performed with the three-phase algorithm, both of them presented in Chapter 4.

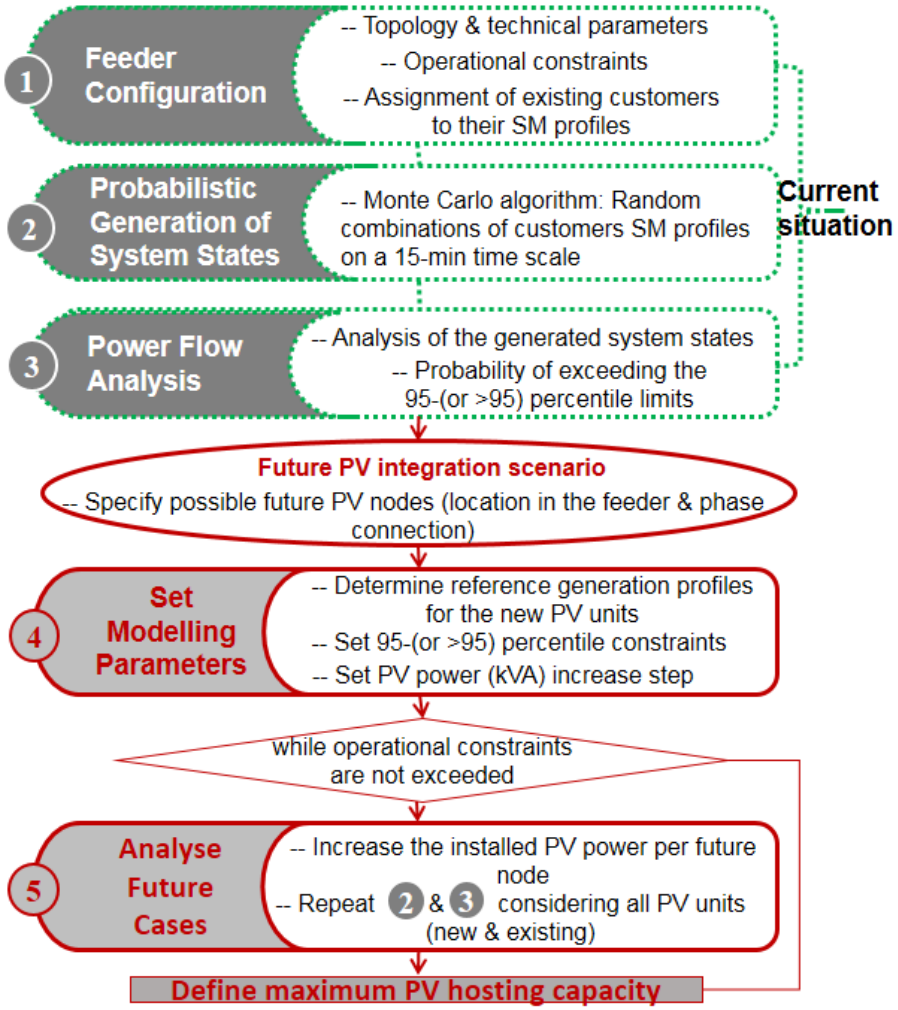

Figure 6.2: Flowchart of the PV hosting capacity computation tool

Regarding the PV hosting capacity computation, the possible future locations of PV units have to be specified in the feeder model. This analysis is not based on stochastic random distribution of PV units along the feeder. A set of scenarios regarding the positions of future PV nodes is specified and each one of them is studied separately so as to focus on its specific impact on the feeder (which is feasible thanks to the availability of the user-specific SM datasets).

The technical constraints that must be respected for the current situation and for future scenarios are the ones specified in local, regional or national directives. In the EU framework, the steady-state 95-percentile limits of the EN 50160 standard are considered. Besides, the simulation tool verifies that the following criteria apply for the whole system (in current and future installed PV power scenarios):

$$\begin{aligned} P_{overvoltage}\ V_{i,x} > 1.10 \cdot V_{nom}\ &< 0.05 \\ P_{undervoltage}\ V_{i,x} < 0.90 \cdot V_{nom}\ &< 0.05 \\ P_{unbalance}\ VUF_i > 2\%\ &< 0.05 \end{aligned} \quad (6.1)$$

where $P_{overvoltage}$, $P_{undervoltage}$ and $P_{unbalance}$ represent respectively the probabilities of overvoltage, undervoltage or exceeding the phase voltage unbalance limit at node *i* (phase *x*) over a number *S* of simulated network states. In $V_{i,x}$, *i* stands for nodes 1 to *N* (total number of nodes in the feeder) and *x* stands for phase *a, b* or *c*. VUF_i stands for the Voltage Unbalance Factor at node *i*.

The thermal limits of the cables are also considered in the computation. The current carrying capacities of the lines should not exceed the utility's requirements or the recommended values in technical standards such as [7].

6.1.2 *Future PV nodes generation statistical profiles*

Regarding end-users' energy consumption and existing PV nodes generation, the energy exchange profiles are constructed as explained in Chapter 4. Concerning future PV nodes, a key component in accurately assessing their impact on the feeder is reliably representing their generation profiles. Based on the findings of Table 4.3 (section 4.3), geographically close customers are entirely correlated (on a quarter of an hour time scale) as far as their PV generation profiles are concerned [8]. For this reason, this study considers that the generation profiles of future PV units will be very similar, along the time axis, to the ones of the existing PV units.

As previously explained, the load/PV generation profiles of end-users with SM devices are made of 96 Cumulative Distribution Functions (CDFs) of probability built with the ¼-hourly recorded datasets. Concerning PV generation, such CDFs are not available for the future PV units. For this reason, the available SM datasets are used in this case to create a reference CDF_{ref}, based on the ¼-hourly generation SM datasets of the existing PV owners, with the methodology presented in section 4.4 [9]. This reference CDF is used to simulate the time-variability of PV generation at the future PV nodes.

Practically, end-users connected to the same LV feeder can have different PV units' sizes. Assuming an equivalent statistical distribution of their PV power profiles due to geographical proximity, the principle is to create a standardized reference CDF_{ref} for PV generation in the specific feeder, based on the measurements of the available SM devices. Based on the methodology of section 4.4 (and relation (4.45)), the CDF for the ¼-hourly PV energy generation $E_{inj,pv,j,q}$ of each existing PV node *j* is normalized by applying the following relation, for each time step *q*:

$$\overline{E_{inj,pv,j,q}} = \frac{E_{inj,pv,j,q}}{E_j^{tot}}\text{,, for } j = 1{:}N_{\text{SM}} \tag{6.2}$$

where N_{SM} is the number of PV users in the feeder that are equipped with a SM device, $\overline{E_{inj,pv,j,q}}$ values are the normalized ¼-hourly energy generation values of end-user j during time step q, $E_{inj,pv,j,q}$ values are the recorded ¼-hourly energy generation values of end-user j during time step q and E_j^{tot} is the total yearly PV energy generation of end-user j.

Once this operation is done, the ¼-hourly CDFs of every user are aggregated, as graphically outlined in Figure 4.23, in order to create a reference CDF_{ref} that can represent all the PV nodes in the specific feeder. For creating the CDF of each particular future PV node, CDF_{ref} should be denormalised in function of its annual PV generation (based on equation 6.2). For existing PV nodes, such information is usually available to the distribution utility even if the end-user is not monitored by a SM device. In case of future PV nodes, such information is not available since no PV unit was connected before. Consequently, CDF_{ref} is denormalised with the annual PV generation of an existing PV unit (in the feeder or in close proximity to the feeder) multiplied by a reference factor f, as explained in the following section.

6.1.3 *PV hosting capacity computation*

Practically, the algorithm starts with the probabilistic analysis of the current situation (existing PV units), by simulating a large number S of possible system states. It is important to note that although system states are based on ¼-hourly resolution data, each one of them is considered as a possible instantaneous state of the system. Thus, the accuracy and reliability of the computation increases with the number of treated system states.

The probabilities $P_{overvoltage}$, $P_{undervoltage}$ and $P_{unbalance}$ are computed at every node, based on the analysis results. Compliance with the conditions set by (7.1) is verified for the whole feeder. Moreover, compliance with the maximum current capacity is verified in the entire feeder for all the studied system states. In case both conditions are respected, the algorithm increases the installed PV power at the future (specified by the user) PV nodes by the defined increase step. Therefore, let us consider a LV feeder that is simulated with a total number N_{PV} of PV nodes. Some of the simulated N_{PV} nodes may be currently existing PV nodes while the rest of them are considered as future PV nodes. If the total number of future PV nodes is equal to K ($K \leq N_{\text{PV}}$), the new installed power at each future PV node i is computed as follows:

$$P_{rated,l,i} = P_{rated,l-1,i} + P_{step,i}\ , i = 1{:}K \text{ nodes} \tag{6.3}$$

where $P_{rated,l,i}$ is the new installed PV power at node *i* in the current configuration *l* of the system to be analyzed by the algorithm, $P_{rated,l-1,i}$ is the installed PV power at node *i* that was analyzed in configuration *l*-1 of the system and $P_{step,i}$ is the increase step (defined by the user for the respective node). A small P_{step} value (≈ 0.5-1kVA for residential or small commercial end-users) is recommended so as to make an accurate computation. Note that, in several countries, concerning residential and small-business customers, the maximum admissible installed power per distributed single-phase PV unit, in the LV network, is equal to 5kVA. In such cases, the condition $P_{rated,l,i} \leq 5\text{kVA}$ should be integrated in step 5 of the proposed algorithm.

Once relation (6.3) is applied, the new installed PV power $P_{rated,l,i}$ is defined at every new PV node before the algorithm performs the next "hosting capacity review" iteration. However, CDF_{ref} that represents the time-variability of generation at the new PV nodes needs to be scaled in function of $P_{rated,l}$ at each node. To do so, CDF_{ref} has to be denormalised in function of the annual PV generation of the PV unit. Unfortunately, such information is not available since there are currently no PV units at the specified nodes. Consequently, CDF_{ref} is denormalised with the annual PV generation of an existing PV unit (in the feeder or at proximity). Then, a reference factor *f* is introduced for scaling the normalised CDF_{ref} in function of $P_{rated,l}$. This factor f_{i} is computed as follows:

$$f_i = \frac{P_{rated,l,i}}{P_{rated,ref}} \text{ , i=1: K} \tag{6.4}$$

where $P_{\text{rated,ref}}$ is the installed PV power of the existing PV unit that has been used to denormalize CDF_{ref} for the new PV unit *i*.

Once the generation profiles have been set up for the future PV nodes, the algorithm repeats steps 2 and 3 for analyzing the current configuration *l*. At this point, it is important to clarify that each "hosting capacity review" iteration *l* practically performs the power flow analysis of configuration *l* by applying a full MC simulation, similar to the one of step 2. This means that each "hosting capacity review" iteration *l* runs the same large number of MC iterations *S* that were analyzed in step 2. Thus, in every iteration *l*, a very large number of system states is analyzed (=*S*·96) so that the values of $P_{overvoltage}, P_{undervoltage}$ and $P_{unbalance}$ can converge. Thanks to this procedure, the verification of compliance with equations (6.1) for each configuration *l* is assumed to be reliable. If the analysis of *S* system states, in configuration *l*, demonstrates that the operational constraints are not violated, the installed PV power is again increased at each future node. Then, the algorithm passes again to steps 4 and 5.

The described iterations stop as soon as the operational constraints are for the first time exceeded at least at one of the LV system nodes. The PV size of some units could probably increase even more, given that the operational constraints at their PCC are not violated. However, this study treats the LV feeder as a whole since the violation of limits at one node is always affected by the energy flows at all nodes. $P_{rated,l,i}$ values that are applied in the last iteration *l* (which led to a violation of acceptable limits) are the ones considered as the maximum admissible hosting capacity per node.

The aggregated PV hosting capacity of the feeder is computed by adding $P_{rated,l,i}$ (existing and new) along the feeder:

$$P_{rated,tot} = \sum_{i=1}^{N_{pv}} P_{rated,l,i} \quad (6.5)$$

In order to make a more detailed computation, different increase steps could be applied per node in function of its position in the feeder. The voltage limits are, indeed, usually more easily violated at the end of the line. Consequently, the PV power steps could be bigger for the nodes at the head of the line. However, this strategy could eventually result in an earlier (in terms of installed PV capacity per node) violation of the limits at the last nodes, which would not permit to ensure a common welfare among end-users.

6.2 CASE STUDY: A LV feeder in Belgium

6.2.1 *Description of the simulation*

This section describes the application of the previously described analysis tool for computing the PV hosting capacity of the LV feeder that is analyzed in Chapter 5. A set of different scenarios have been simulated regarding the position and phase connection of future PV units as well as the action of voltage control schemes. The analyzed scenarios are listed in Table 6.1.

Table 2.1: The simulated PV hosting capacity scenarios

No	Description
A	12 new PV units at nodes 2, 3, 6, 7, 8, 10, 11, 13, 15, 17, 18, 19. The PV units at nodes 8, 11, 17, 18, 19 are connected to phase *a*, the PV unit at node 3 is connected to phase *b* and the PV units at nodes 2, 6, 7, 10, 13, 15 are connected to phase *c*.
B	Similarly to scenario A but all new PV units connected to phase B, except from PV unit at node 15 that is connected to phase *a*.

C	3 new PV units connected to nodes 13, 18 and 19 (end of the line). All three new units connected to phase *b*.
D	1 new PV unit connected to node 13 (phase *b*).
E	Similarly to scenario A but considering 100-percentile and not 95-percentile operational limits. Practically the PV hosting capacity is not more increased as soon as voltage and VUF limits are exceeded at least once in the feeder.
F	Similarly to scenario A but considering the action of three-phase damping control integrated in the new PV inverters. In this case, the new PV units need to be connected by means of three-phase PV inverters.
G	Similarly to scenario A but considering the action of a reactive power control scheme

Concerning scenarios A-D, only the on-off control scheme is considered, which is currently implemented by most DSOs in Europe. This control scheme enables a total cut-off of the PV unit (in most cases during, at least, 3 minutes) as soon as the voltage limit has been locally exceeded for a period longer than 10 minutes.

The control scheme applied in scenario F is the three-phase damping control scheme which behaves resistively towards the negative- and zero-sequence voltage component, without modifying the injected power, so as to eliminate phase voltage unbalance [10]. This control scheme requires a three-phase PV inverter and it is very promising in terms of voltage magnitude and unbalance mitigation. The scheme will be further evaluated and discussed in the following Chapter 7. It is actually implemented in a EU pilot program [11].

The control scheme applied in scenario G is reactive power control in the way it is implemented in the Italian distribution system [12] concerning new small PV units (<6kVA) connected to the LV network. This strategy modifies the PV unit power factor $cos\varphi_{inj}$ in function of the instantaneously injected active power and of the instantaneous network voltage, according to a predefined graph [12] . In such a way, when the network voltage exceeds a certain value (usually $1.05V_{nom}$) the PV inverter absorbs an amount of reactive power such that the voltage rise is mitigated. The control schemes that are applied in scenarios G and F will be thoroughly explained in the following section 7.2.

6.2.2 *Comparing with a deterministic approach*

One of the main purposes of this chapter is to investigate, up to which extent a probabilistic method based on feeder-specific SM readings leads to a less re-

strictive computation of PV hosting capacity, compared to a deterministic approach. For this purpose, a deterministic approach has been implemented simulating worst-case energy flow profiles. The load profiles of all end-users and the PV generation profiles of existing PV units have been also based on SM recorded data. The deterministic steady-state analysis has been deployed for scenarios A-D, F, G. Scenario E is not mentioned because, although SM readings are used, only 100-percentile limits are considered which means that probabilities are not accounted for in the computation of hosting capacity. Thus, this scenario is, by nature, a deterministic one.

The following load/ PV generation profiles have been considered in the deterministic approach:

1. Maximum PV power per node (installed PV power) – Minimum recorded load per node; absolute values, irrespective of time coincidence between end-users.

2. Maximum PV power recorded in the feeder – Coincident PV generation/load values for the other nodes.

3. Minimum recorded load in the feeder during PV injection hours – Coincident PV generation/load values for the other nodes.

6.2.3 *Results and discussion*

The probabilistic hosting capacity review results are illustrated in Figure 6.3 and analytically listed in Table 6.2. The aggregated maximum admissible PV hosting capacity in the feeder is presented for each individual scenario, considering separately the EN 50160 standard voltage limits and the maximum current capacity of the lines. This separate presentation has been chosen because voltage limits are treated with a probabilistic approach in the EN 50160 standard while congestion risk is treated by each DSO with a different approach. Most of them apply a deterministic approach that considers an upper (100-percentile) current limit. The violation which forbade further increase of the PV hosting capacity is also presented and quantified for each scenario. The aggregated PV hosting capacity obtained with deterministic analysis is presented in Figure 6.4 and Table 6.3 for all treated scenarios.

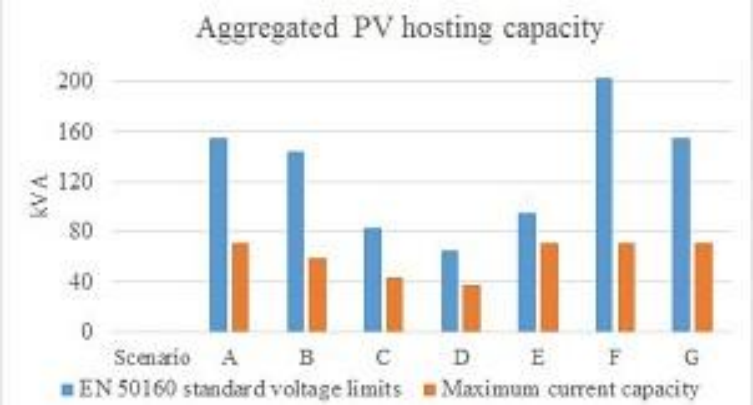

Figure 6.3: The computed aggregated PV hosting capacity of the feeder for scenarios A-G. The number of new PV units is also indicated.

Table 6.2: Aggregated maximum PV hosting capacity and violated parameter for each simulated scenario (Probabilistic Simulation Tool)

No	**EN 50160 standard voltage limits' consideration**		**Maximum current capacity and voltage limits' consideration**	
	Aggregated PV hosting capacity (kVA)	*Violation*	*Aggregated PV hosting capacity (kVA)*	*Violation*
A	154.63kVA (11kVA/ per new PV node + existing PV units)	-- Povervoltage at nodes 18 and 19 (phase (B)) resulted 5.7% and 6.4% respectively	70.63kVA (4kVA/ per new PV node + existing PV units)	Imax of line 6-7: 13% deviation (13% higher than the maximum current capacity of the lines)
B	144.63kVA (10kVA/ per new PV node + existing PV units)	-- Povervoltage at nodes 13,14,15 (phase (C), resulted 5.4%, 6.16% and 6.18% respectively	58.63kVA (3kVA/ per new PV node + existing PV units)	Imax of line 6-7: 50% deviation (50% higher than the maximum current capacity of the lines)

C	82.63kVA (20kVA/ per new PV node + existing PV units)	-- Povervoltage at node 19 (phase (B)) resulted 6.3%	43.63kVA (7kVA/ per new PV node + existing PV units)	Imax of line 6-7: 10.5% deviation (10.5% higher than the max-
D	65.63kVA (43kVA/ per new PV node + existing PV units)	-- Povervoltage at node 19 (phase (B)) resulted 5.15%	37.63kVA (15kVA/ per new PV node + existing PV units)	Imax of line 6-7: 6.2% deviation (6.2% higher than the max-
E	94.63kVA (6kVA/ per new PV node + existing PV units)	-- Povervoltage at nodes 13,14, (phase (C)), resulted 0.0001% in both cases (> 0%, which is the condition in scenario E)	70.63kVA (4kVA/ per new PV node + existing PV units)	Imax of line 6-7: 13% deviation (13% higher than the maximum current capacity of the lines)
F	202.63kVA (15kVA/ per new PV node + existing PV units)	-- Povervoltage at nodes 2-19 (at all three phases) resulted from 5.5% to 28% -- Punbalance at nodes 2-19 resulted from 10% to 32%	70.63kVA (4kVA/ per new PV node + existing PV units)	Imax of line 6-7: 11% deviation (11% higher than the maximum current capacity of the lines)
G	154.63kVA (11kVA/ per new PV node + existing PV units)	-- Povervoltage at node 19 (phase (B)) resulted 5.17%	70.63kVA (4kVA/ per new PV node + existing PV units)	Imax of line 6-7: 11% deviation (11% higher than the maximum current capacity of the lines)

Table 6.3: Aggregated maximum PV hosting capacity for each simulated scenario (Deterministic Approach)

No	**Aggregated PV Hosting Capacity (kVA) (considering EN 50160 standard voltage limits)**			
	Profile (I)	*Profile (II)*	*Profile (III)*	*Violation*
A	70.63kVA (4kVA/ per new PV node + existing PV units)	82.63kVA (5kVA/ per new PV node + existing PV units)	82.63kVA (5kVA/ per new PV node + existing PV units)	Overvoltage at all new PV nodes
B	58.63kVA (3kVA/ new PV node + existing PV units)	58.63kVA (3kVA/ new PV node + existing PV units)	58.63kVA (3kVA/ new PV node + existing PV units)	Overvoltage at all new PV nodes
C	43.63kVA (7kVA/ new PV node + existing PV units)	43.63kVA (7kVA/ new PV node + existing PV units)	43.63kVA (7kVA/ new PV node + existing PV units)	Overvoltage at all new PV nodes
D	37.63kVA (15kVA/ new PV node + existing PV units)	37.63kVA (15kVA/ new PV node + existing PV units)	37.63kVA (15kVA/ new PV node + existing PV units)	Overvoltage at all new PV nodes

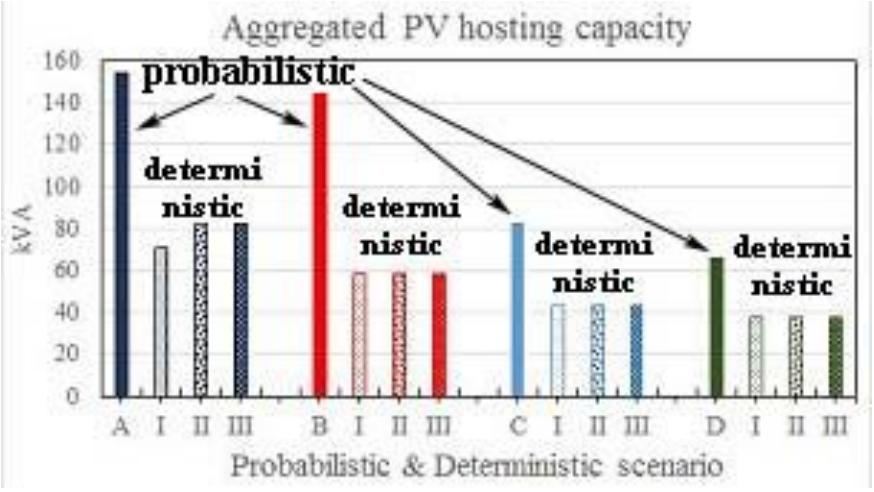

Figure 6.4: The computed aggregated PV hosting capacity of the feeder for scenarios A-D with the probabilistic and deterministic approaches.

Firstly, one should note that the results considering the maximum current capacity coincide for the probabilistic and the deterministic computations since this metric is not addressed with probabilistic terms. In case the maximum value is exceeded at one point of the feeder during just one of the simulated states, the PV hosting capacity is no further increased in the respective simulation. Also, the result of scenario E (applying 100-percentile limits) is similar to the ones of the deterministic scenarios A.I, A.II and A.III that analyze the same topology as scenario E but with a deterministic approach. Based on these remarks, one can reasonably assume that the probabilistic computation covers (samples and analyses) almost the whole range of possible system states, including the most restrictive ones.

Accounting only for voltage violation and applying the probabilistic approach, the restrictive condition of scenario E based on which voltage limits must never be exceeded (in none of the simulated states), results in a quite lower admissible PV hosting capacity compared to scenario A. Basically, in scenario E, PV hosting capacity could not further increase because the computed $P_{\text{overvoltage}}$ resulted to be different than zero. Therefore, if the admissible PV hosting capacity does not exceed 94.63kVA, the operational limits will never be violated in the feeder, based on the elaboration of the available historic data. Otherwise, if the admissible PV hosting capacity increases up to 154.63kVA, as in scenario A, violation of voltage limits will only take place in less than 5% of the time. Therefore, even with such an increase of the aggregated PV hosting capacity, the temporary cut-offs of the PV units due to overvoltage will be very rare. This result clearly demonstrates that scenario A takes advantage of the probabilistic character of EN 50160 standard (limits violation allowed during 5% of the time), which is not the case in scenario E or in deterministic approaches.

Figure 6.5 demonstrates how the probabilistic consideration of overvoltage risk affects the computation. This figure shows the evolution of the CDF of phase voltage V_b at node 19 while the total installed PV power increases in scenario A. Based on the probabilistic analysis of the feeder, when total installed PV power increases by 144kVA (12kVA per new PV unit), V_b at node 19 respects the defined limits in 94.6% of the simulated states. However, EN 50160 defines that the limits should be respected in at least 95% of cases. Thus, the maximum PV power that can be added to the feeder, considering this configuration, is 132kVA (11kVA per new PV unit).

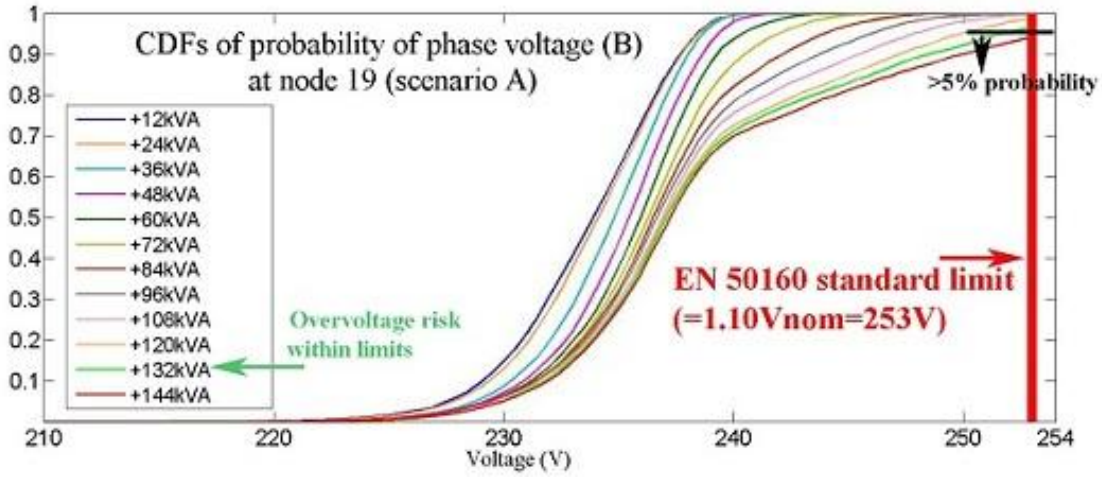

Figure 6.5: CDFs for V_b at node 19, for each step increase of installed PV power in the feeder (scenario A).

The above arguments should be considered in a cost-benefit analysis (CBA) that compares costs for exceeding operational limits to losses due to an eventual penalty for low DER integration or loss of potential revenue for customers and energy utilities. Such considerations may allow a much more cost-effective PV integration strategy which also respects the applied standard criteria. At the same time, the identification of critical points regarding congestion risk should also be considered. Both arguments highlight the usefulness of considering SM historic datasets in similar studies so that critical points and probabilities are carefully mapped and quantified.

In order to point out the cost-effectiveness of deploying long-term measurements in the LV network and analyzing it with a probabilistic approach, a more detailed computation of energy line losses in the feeder was performed for scenario A. Assuming that the computed maximum admissible PV power is installed (=154,63kVA if one considers only the voltage limits), the study focuses on the total energy losses along the lines of the feeder during hours of high PV injection in a typical day. Based on the available historic data for the feeder, this period is

between 12:00AM and 18:30PM on a typical July day. The sum of energy losses has been computed along the feeder for the considered period, for each simulated day, by applying relation (5.5), but only for the period between 12:00AM and 18:30PM (q=48:74) :

$$E_{loss,feeder,s} = \sum_{q=48}^{74} E_{loss,feeder,q} \quad (6.6)$$

where $E_{loss,feeder,q}$ for each time step q is computed with relations (5.1)-(5.7). Figure 6.6 illustrates the statistical distribution (CDF) of the computed total daily losses $E_{loss,feeder,s}$ in the feeder.

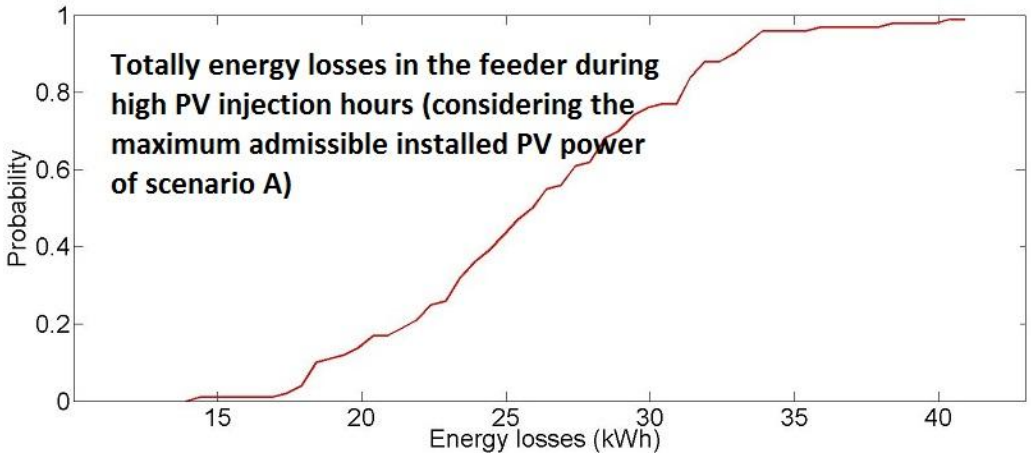

Figure 6.6: CDF of total energy losses in the feeder during high PV injection hours on a typical July day

The probabilistic approach and the consideration of the SM measurements demonstrated that total energy losses in the feeder vary significantly, depending on the system state. Consequently, in 95% of the simulated days, total energy losses during high PV injection hours (12:00AM to 18:30PM) do not exceed 35kWh in a day. In the deterministic approach which assumes the worst-case scenario taking place all along the high PV injection period, the respective energy losses result to be equal to 148kWh. This important difference is due to the fact that the probabilistic approach considers the extremely low frequency of worst-case scenarios to take place simultaneously for all feeder users. Considering such probabilities, the DSO could manage a less conservative and more cost-effective long-term strategy.

Undoubtedly, the computed PV hosting capacity values depend on the load profiles of the end-users that are located in the feeder. However, the results clearly indicate in relative terms, that smaller distributed PV units have a much smoother impact than bigger ones concentrated in one small area of the feeder. This fact is demonstrated by the comparison of scenario A with scenarios C and

D. Moreover, in several cases, the maximum admissible installed power per PV unit, connected to the LV network in single-phase mode, is equal to 5kVA. In case of three-phase connection, it is not recommended, for residential PV units, to exceed an installed power of 10kVA, due to the high required operational cost of bigger units. In such cases, scenarios C and D might not be appropriate based on the probabilistic simulation results. Indeed, the admissible total installed power would have to limit to 32.63kVA (for scenario D) although the network would be able to support 37.63kVA. Generally, bigger PV units, connected to three-phase LV feeders are mostly destined for industrial users. Finally, in scenarios C and D, the difference between the PV hosting capacity computed with the probabilistic and the deterministic approaches (considering only voltage limits) is not as big as for scenarios A and B. Indeed, in scenarios A and B, the volatile character and the extremely rare coincidence of worst-case values for 12 units cannot be reliably represented by a deterministic model.

Regarding the distribution of units among phases, the comparison of scenarios A and B shows that the existing phase unbalance affected the computation. Indeed, the violated parameter in this case is the voltage magnitude of phase *c* although all new PV units are connected to phase *b*. Therefore, the unfair distribution of new PV units among phases did not directly affect $P_{\text{unbalance}}$ but it had an impact on the voltage magnitude of phase *c*. Considering voltage limits, the aggregated PV hosting capacity for scenario B resulted to be equal to 144.63kVA if one considers the probabilistic character of EN 50160 standard voltage limits. However, the connection of the majority of new PV units at phase *b* resulted in very high current values so that the maximum current capacity was exceeded by 50%.

Scenario F demonstrated that the connection of new PV units by means of three-phase inverters integrating three-phase damping control can increase the aggregated hosting capacity by 36%, if the probabilistic character of EN 50160 standard voltage limits is considered. Thanks to the resistive behavior of this control scheme towards the zero- and negative-sequence voltage component, the deviation of voltage magnitude and unbalance becomes much smoother compared to the currently applied on-off control. Thus, the risk of exceeding the defined limits is reduced and a bigger share of PV generation can be integrated.

Based on the results of scenario G, reactive power control does not result in higher PV hosting capacity compared to scenario A (on-off control). Voltage profile in the feeder is, however, improved compared to scenario A. As a matter of fact, voltage limits are not violated in scenario G whereas the maximum current capacity limit is exceeded for the same amount of PV integration compared to scenario A.

In the first two cases (scenarios A and B), comparing the probabilistic simulation results to the respective ones obtained with the deterministic approach, an

important difference in the aggregated admissible hosting capacity is observed. At this point, it is important to mention that the violated parameter in the deterministic approaches is mainly the voltage magnitude and secondly the maximum current capacity of the lines. Practically, the deterministic approach led to between 74 and 146% lower aggregated PV hosting capacity.

When it comes to scenarios C and D, one can note that if less but bigger size PV units are connected, the results of the probabilistic and the deterministic approach do not differ significantly. This result proves that in case of many distributed PV units, an approach that considers all worst-case customers' profiles coinciding in time is mostly extreme. Deterministic approach cannot accurately simulate the volatile character of PV generation and the random loading parameters of residential and small commercial customers.

A general remark would concern the design strategy of distribution feeders like the studied one. The studied feeder currently hosts 22.63kVA of distributed PV generation and supplies 19 residential customers. The analysis of the current conditions demonstrated that both voltage violation risk and congestion risk are very low. Moreover, the above probabilistic load-flow analysis demonstrated that, in scenario A, congestion and voltage problems would only appear if 48kVA of distributed PV generation, that is the difference between the computed maximum hosting capacity when both congestion and voltage problems are considered (22,63kVA) and the total existing PV generation (70.63kVA), are further integrated in the feeder This remark highlights the cost-efficiency of designing distribution networks based on the most frequent system states or on well-studied future scenarios. This approach can lead to customized solutions and help to avoid over-dimensioning and costly initial investments for the DSO.

Based on the above analysis, certain renewable integration scenarios could increase to an important extent the self-sufficiency of feeders like the studied one. As a result, their dependency on big conventional power plants, connected at the transmission level, could be efficiently reduced. However, big conventional plants are important for maintaining grid stability. In a high DER integration scenario, without large and reactive storage facilities and/or flexibility services, the amount of RES should be carefully reviewed. To this end, costs induced by the use of grid services, including insurance against periods when it is not possible to consume own generated electricity, should be considered and reflected in the bill of generator owners [13]. Reliable feasibility studies and comprehensive CBAs are necessary for evaluating various strategies in the decision making process.

6.2.4 *The role of feeder-specific SM data in PV hosting capacity reviews in LV networks*

The above analysis is based on the use of feeder-specific SM energy flow readings. Various maximum PV hosting capacity scenarios have been analyzed

by applying a probabilistic steady-state analysis of the feeder on a ¼-hourly time scale, sampling from models established on basis of the available SM data. In this way, the real probability of worst-case scenarios has been accounted for and as a result, a probabilistic view of several technical metrics has been enabled (voltage and current magnitudes, voltage phase unbalance, line losses). Even if DSO long-term planning is based on deterministic approaches, the use of SM datasets to establish the stochastic models can lead to a validation of the considered worst-case scenarios. Besides, the use of SM measurements, instead of solar irradiation data, for simulating PV generation, is more reliable, given that the latter do not consider the efficiency of the PV cells. Moreover, solar irradiation measurements are not easily available to distribution utilities, for many different locations. Finally, the wide deployment of SM devices can offer other possibilities such as better coordination and control of technical parameters of the LV network as well as better visibility and adaptability to actual load and generation profiles of LV customers. The long-term planning of LV networks can become more customized to local conditions and therefore more cost effective.

Chapter conclusions

Chapter 6 presented a probabilistic methodology for estimating the PV hosting capacity of a given feeder, considering a set of predefined PV location scenarios, with the use of models based on feeder-specific SM measurements. The outputs of the methodology are compared to the ones of a typical deterministic approach that also uses feeder-specific historic measurements.

The application of a probabilistic methodology for estimating the PV hosting capacity of LV feeders allows the consideration of the statistical constraints of the EN 50160 standard (for overvoltage, undervoltage risks and voltage unbalance violation), when assessing the voltage margin of a given feeder. Regarding line congestion, the probabilistic approach gives a more detailed mapping and quantification of the risk along the feeder so that local reinforcements can be considered instead of generalized ones.

For the studied feeder, the probabilistic methodology led to much higher hosting capacities compared to the deterministically computed ones regarding voltage margin. Thus, the second argument (II) of section 2.6 has been confirmed since the probabilistic hosting capacity review led to less restrictive results. Concerning the impact of congestion risk on the hosting capacity, the probabilistic approach allowed identifying which would be the line segment to reinforce while the deterministic approach resulted in very high current magnitudes in all line segments. Therefore, the fifth and sixth arguments (V and VI) of section 2.6 have been validated since the critical segments with a high congestion risk have been identified.

The reliability of the probabilistic hosting capacity review has been demonstrated since the consideration of 100-percentile limits for voltage constraints led to outputs very similar to the ones of the deterministic approach. Finally, the probabilistic simulation demonstrated that the integration of several distributed PV units evenly distributed over the three phases led to much higher PV hosting capacities compared to the integration of less but bigger PV units.

Chapter publications

The developments of Chapter 6 have been published in:

[1] V. Klonari, J.-F. Toubeau, J. Lobry, and Vall, “PV integration in smart city power distribution A probabilistic PV hosting capacity assessment based on smart metering data,” "*Best student paper"* award in SMARTGREENS, 2016.

[2] V. Klonari, J.-F. Toubeau, J. Lobry, and F. Vallée, “Estimating the Photovoltaic Hosting Capacity of a Low Voltage Feeder Using Smart Meters’

Measurements," in Smart Metering Technology and Services - Inspirations for Energy Utilities, InTech Open Access Publisher, 2016.

Chapter references

[1] Solar City Grid Engineering, “Integrated Distribution Planning: A holistic approach to meeting grid needs and expanding customer choice by unlocking the benefits of distributed energy resources,” 2015.

[2] B. (Australian P. A. Noone, “PV Integration on Australian distribution networks: Literature review,” 2013.

[3] J. Smith, “Alternatives to the 15% Rule: Modeling and Hosting Capacity Analysis of 16 Feeders,” 2015.

[4] Electric Power Research Institute, “Stochastic Analysis to Determine Feeder Hosting Capacity for Distributed Solar PV 1026640,” 2012.

[5] M. B.-P. Antoni Klajn, “Application Note Standard EN50160 Voltage Characteristics of Electricity Supplied by Public Electricity Networks,” European Copper Institute, March, 2013.

[6] Bollen M.H.J. and F. Hassan, Integration of Distributed Generation in the Power System, IEEE Press. Wiley, 2011.

[7] IEC, “IEC, 60364-5-52 Table A5210.” .

[8] F. Vallee, F. Moutier, V. Klonari, J.-F. Toubeau, F. Lecron, Z. De Greve, and J. Lobry, “On The Correlation between Prosumers in Probabilistic Analysis of Low Voltage Distribution Systems,” Int. Rev. Electr. Eng., 2016.

[9] J.-F. Toubeau, M. Hupez, V. Klonari, Z. De Greve, and Vallée, “Statistical Load and Generation Modelling for Long Term Studies of Low Voltage Networks in Presence of Sparse Smart Metering Data,” in IECON, 2016.

[10] B. Meersman, B. Renders, L. Degroote, T. Vandoorn, and L. Vandevelde, “Three-phase inverter-connected DG-units and voltage unbalance,” Electr. Power Syst. Res., vol. 81, no. 4, pp. 899–906, 2011.

[11] FP7 INCREASE Project, “http://www.project-increase.eu/.” .

[12] C. E. I. CEI, “Reference technical rules for the connection of active and passive users to the LV electrical utilities,” 2012.

[13] EDSO, “European Distribution System Operators for Smart Grids Adapting distribution network tariffs to a decentralised energy future,” 2015.

Chapter 7 Probabilistic Modeling of Distributed Control Schemes in Low Voltage Networks

Highlights

- *The basic probabilistic algorithm is restructured in order to integrate the models of different time-varying control schemes.*
- *The performance of four control schemes, mitigating voltage rise and voltage unbalance, is evaluated with a long-term probabilistic approach.*
- *The currently applied hard curtailment (on-off control), in case of overvoltage, results to be less efficient for the improvement of voltage profile and for the overall capture of photovoltaic energy in the feeder, compared to the other simulated control schemes.*
- *The probabilistic simulation of the different control schemes, with the use of the feeder-specific smart metering data, can be useful for an accurate and less conservative tuning of the control schemes settings.*

Chapter 7 presents the adaptation of the basic version of the probabilistic algorithm, presented in Chapter 4. The goal is to integrate the action of time-varying control schemes in the power flow computation. The modeled control schemes include common currently applied strategies such as the on-off and reactive power controls as well as recently developed schemes, especially tailored for LV feeders, in the purpose of achieving a LV customized mitigation of voltage rise and unbalance. Such schemes are the power/voltage-based (P/V) droop control [1] and the three-phase damping (3ph-DPC) control [2], developed by the Department of Electrical Energy, Systems and Automation (EELAB) of the University of Ghent (Belgium). Those schemes are simulated, as a case study, in the feeder that is analyzed in Chapter 5 so that their effect can be evaluated with a long-term techno-economic view. The developments that are presented in Chapter 7 have resulted from the collaboration of our research team with the EELAB of the University of Ghent.

7.1 Voltage rise mitigation

As previously explained in section 2.5, in case of overvoltage, changing the injected active power of a PV unit in function of the local voltage would be preferable rather than imposing its total cut-off during a period of time. For this purpose, locally applied P/V droop control could be adopted and regulated as a profitable (for the PV owner) ancillary service towards the LV network.

7.1.1 *Droop Control Configuration*

The authors in [1] developed a soft curtailment methodology which involves a fast-acting primary control scheme based on voltage droops, without requiring communication infrastructure. The use of communication among PV units and centralized control [1], [3], [4] is not advisable for primary control schemes. Centralized control can lead to single point failure and inter-unit communication can harm the robustness and the rapid responsiveness of local droop control.

Reference [1] shows that P/V droop control is efficient in avoiding frequent power modifications while maintaining the voltage profile within the required limits. Along with this advantage, it achieves a higher capture of renewable energy, compared to hard curtailment, while avoiding on-off oscillations. Moreover, it is highly flexible so that it can be applied in LV feeders with various kinds of DG sources as well as for the control of storage elements. This strategy was initially designed for islanded microgrids but it can also be implemented in network-connected PV units in order to modify their delivered active power in function of the network state. In this primary control scheme, the P/ V droop controller modifies *P* according to the local voltage change, as shown in Figure 7.1 [1].

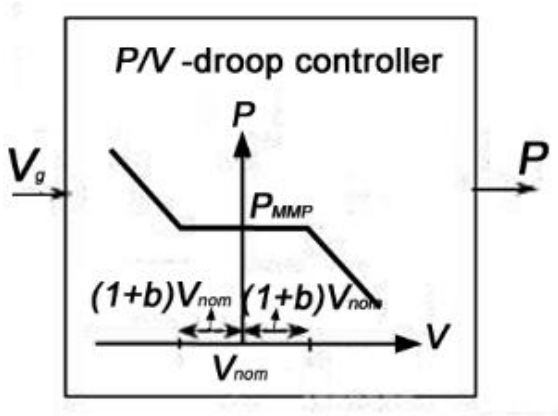

Figure 7.1: P/V droop control [1]

7.1.2 *Need for Probabilistic Evaluation of P/V Droop Control*

Up to now, P/V droop control has only been analyzed with a deterministic approach. Consequently, its benefit was only proved for a restricted number of network states which are poorly representative of the time-varying operation of real networks. Focusing on the most possible network states will practically ensure a refined design of the P/V control, in terms of efficiency and investment cost.

As previously mentioned, the deterministic approach considers neither the time-variance of PV energy injection nor the randomness of consumption loads in LV systems. These uncertain parameters undeniably influence the time-dependent behavior and quality of the distributed power and thus the implementation of the control. For the above reasons, a doubt concerning the sufficiency of the deterministic models in evaluating network state-aware voltage control strategies has lately arisen in literature and a set of probabilistic methods was presented [5], [6]. However, the lack of real SM data restricted up to now the results of these probabilistic methods. **Consequently, the first objective of this chapter is to evaluate the effect of P/V droop control, in an extensive range of possible network states, by integrating it in the probabilistic simulation.**

In the literature, the control parameters tuning has been done in a rigorous manner by using estimations, a restricted set of network configurations and bulk data [7], [8], [9]–[17]. The issue that has always been raised is that parameter tuning for such configurations is not realistic and hence, one should be careful with drawing conclusions based on such analysis [17]. In this scope, the restructured probabilistic framework has been used in this chapter for parameter tuning of droop control in the LV feeder that is analyzed in Chapter 5. The results of this evaluation are compared to the ones obtained considering the base scenario, namely no application of P/V droop control. The second objective of this chapter is to present how the basic structure of the probabilistic algorithm could be

adapted in order to include time-based control strategies (in this case the P/V droop control) in the long-term simulation of LV networks.

7.1.3 *Integration of the Droop Control within the Probabilistic Framework*

i. *Network state loop*

The integration of P/V droop control has been treated in this chapter assuming a balanced three-phased system (case (i) of section 4.1.4) with the connection of symmetrical three-phase DG generation units and, therefore, it does not take into account an eventual voltage drop along the neutral.

ii. *Droop control loop*

The P/V droop control strategy is implemented by means of a control algorithm, with its operation depending on the RMS voltage V at the coupling point of the PV unit with the network. As it is presented in [1], if the voltage at the coupling point of the PV unit exceeds the reference band, a P/V droop controller is turned on in order to change the P_{MPP} of the unit, which is the injected PV power without the action of the droop control. Changing P_{MPP} can be achieved with various strategies as for instance storage charging, deviation from the Maximum Power Point (MPP) for lowering the generated power, load increasing or dump loads. The method of modifying the active power delivered via the dc-link does not affect the control method. In this study, the focus is on overvoltage due to PV power injection. It is therefore considered that each time the RMS voltage exceeds the defined voltage reference value and therefore, an overvoltage event could be expected, the injected power is adapted following expressions (7.1) and (7.2) [1]**:**

$$P = P_{MPP} - k \cdot \left(V - V_{up} \right) \tag{7.1}$$

$$V_{up} = V_{nom} \cdot \left(1 + b \right), \qquad b < 0.1 \tag{7.2}$$

where the droop coefficient k is generally determined according to the ratings of the PV units connected to the network, P_{MPP} is the instantaneous MPP at the respective node during the respective ¼-hourly network state (it is considered to be the value of the injected power just before the action of droop control), V_{up} is the upper adjustment grid voltage, namely the reference voltage for enabling the P/V control and V is the calculated RMS voltage at the respective node for the considered network state. The use of an upper adjustment voltage ($V_{up} = V_{nom} \cdot \left(1 + b \right)$) enables a dead-band thanks to which P/V droop control is not active at the specific node in case its voltage is lower than this upper value. The value of b is determined based on the specific needs and the background history of the feeder. Consequently, P/V droop control strategy changes the power P_{MPP} delivered by the PV panel to a different value P, under the following conditions:

- power is injected into the grid (P_{MPP}>0),
- $V_{up}=V_{nom}\cdot(1+b) < V < V_{nom}\cdot(1+0,1)$, with b <0.1

Let's remember that, according to the EN 50160 standard (section 1.2) [18], in case only conventional on-off control of PV inverters is available in a feeder (and no droop control is implemented) and the mean RMS voltage at a node remains higher than $1.10V_{nom}$ during ten minutes, the PV unit at this node turns off for the next ten minutes. If this RMS voltage instantaneously exceeds $1.15V_{nom}$, the PV unit is instantaneously disconnected for the next ten minutes. With the implemented droop control, as soon as $V>1.10V_{nom}$, the PV unit instantaneously turns off but only for some seconds or a set of minutes until the value of V is again stabilized at a value lower than $1.10V_{nom}$ and the unit can step by step re-inject its initial P_{MPP}.

iii. *Overall structure of the model*

The merging of the network state loop and the droop control loop is done according to the flowchart of Figure 7.2. Firstly, the probabilistic framework samples a network state, namely a random combination of the variable parameters, as explained in section 4.1.3. In this way, P_{MPP} is determined at every node ($P_{MPP} = Pi\ , \forall P_i < 0$, so that PV power is injected at the respective node and P_i is computed with relation (4.12)) and the power flow computation gives the nodal RMS voltage values V for the current network state. Therefore, V is initially computed at all nodes before droop control is enabled. Up to this point, only the basic algorithm of the probabilistic framework has been used.

Afterwards, the reformed probabilistic framework takes action. Initially a new value of P is calculated, by applying relation (7.1), for each PV node that lies under the conditions for the application of the P/V droop control. In case $V>1.10V_{nom}$ at a certain node, the injected power P of this node is set equal to zero. After these actions are completed for all PV nodes that lie under the respective conditions, a new PF computation is deployed. Therefore, a new V value is computed at each node. A new iteration of the droop control starts at this point and a new value of P is determined at the respective PV nodes, which lie under the conditions for application of the droop control. For the PV units whose P was set equal to zero in the previous iteration, if their new voltage V is, in the current iteration, lower than $1.10V_{nom}$ they are again step by step set to inject their initial P_{MPP} into the network. The reformed probabilistic algorithm performs again the PF computation considering the updated values of P and, therefore, it computes updated values for V. This procedure goes on until the value of P for two consecutive iterations of droop control converges at every node and until no voltage values higher than $1.10V_{nom}$ are computed at the PV nodes of the feeder. Once the P value at each PV node is stabilized, a final PF calculation takes place for the specific ¼-hourly network state.

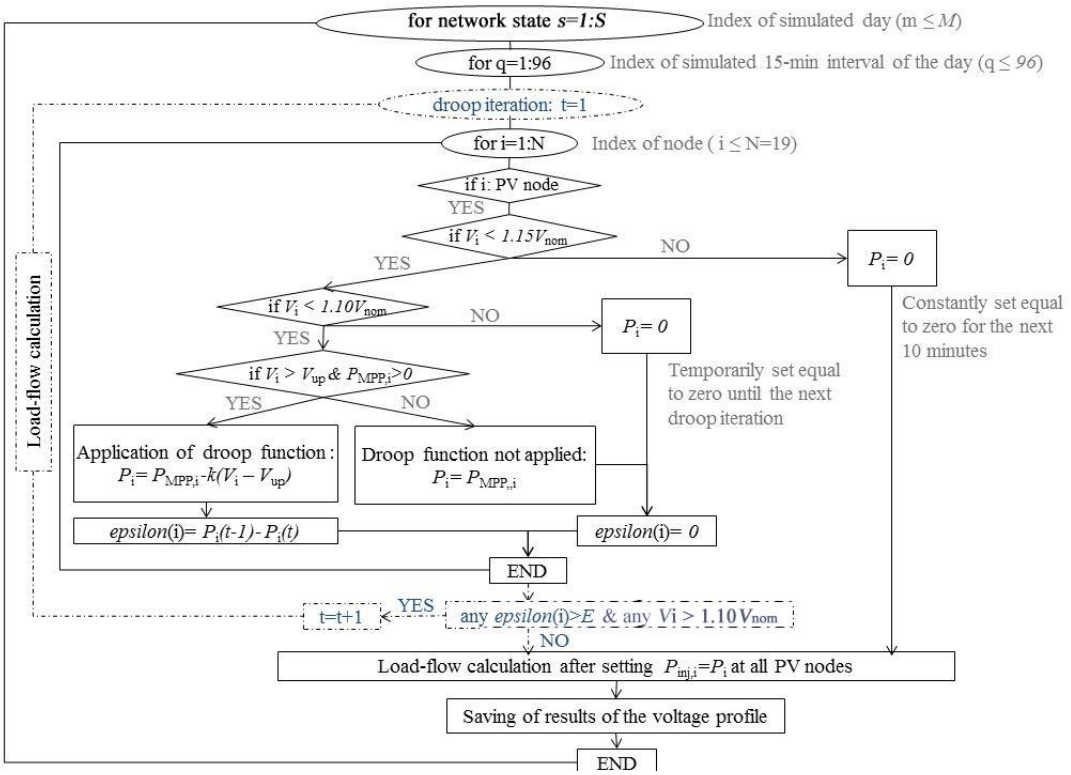

Figure 7.2: Algorithm flowchart with the integration of P/V droop control in the probabilistic framework

iv. *Tuning of droop control parameters*

The coefficients "*k"* and "*b"* can be customized for the simulated network in order to improve the performance of the control. Regarding the slope of the P/V control, namely the droop coefficient "*k*", greater values deliver a more direct decrease of the voltage profile. However, they usually implement a greater curtailment of the injected active power. Concerning the value of *"b"*, lower values ensure a more active and decisive droop control but with a greater active power curtailment. The application of different *"b"* values among the PV nodes can establish an automatic priority allocation for the droop control, allowing the fair distribution of curtailed PV power along the feeder. When higher *"b"* values are applied at nodes towards the end of the feeder where the voltage profile along radial LV feeders with high PV penetration tends to raise more, the unfair distribution of curtailed PV power can be compensated. In such a case, the primary control acts more rapidly for nodes near the transformer than for the ones located at the end of the feeder. This might decrease voltage profile towards the end of the feeder while shifting a part of the curtailed energy towards the nodes close to the substation. The probabilistic model will be applied for the tuning of those control parameters in the following subsections.

7.1.4 *Evaluating the benefit of droop control*

The droop control benefit is evaluated considering three criteria that are: the reduction of overvoltage risk, the general decrease of the voltage profile for increasing the voltage margin (and the resulting hosting capacity) of the network and the amount of captured renewable energy from the PV units. The overvoltage probability per node is computed with relation (4.31). The average daily injected PV energy $E_{\text{tot,mean}}$ (in case no on-off or droop control would be applied) and the average daily curtailed energy $E_{\text{curt,mean}}$ (for both the on-off and the droop control scenario) are computed per node as follows:

$$E_{tot,mean,i} = \frac{1}{S} \sum_{s=1}^{S} \sum_{q=1}^{96} E_{inj,pv,i,s,q} \tag{7.3}$$

$$E_{curt,mean,i} = \frac{1}{S} \cdot \sum_{s=1}^{S} \left(\sum_{q=1}^{96} t \cdot (P_{MPPi,s,q} - P_{i,s,q}) \right) \tag{7.4}$$

where S is the number of simulated days, $E_{inj,pv,s,q}$ is the ¼-hourly amount of energy that is injected by the PV unit (in case no droop control would be applied) at node i in simulated day s during time step q, t is the time repartition factor that will be defined in the following paragraph, $P_{i,s,q}$ is computed as P in relation (7.1) and $P_{MPPi,s,q}$ is equal to Pi , $\forall P_i < 0$ where P_i is computed with relation (4.12)).

Concerning the on-off scenario (the one currently applied by the DSO), in case V exceeds $1.10V_{\text{nom}}$ during ten minutes or $1.15V_{\text{nom}}$ instantaneously, the temporary disconnection period of the PV inverter is considered to be equal to 600 seconds, which is the one applied in most EU countries (EN 50160 standard). This period of time is considered in the computation of the curtailed energy for the base (on-off) scenario. Therefore, in this case, the value of t in relation (7.4) corresponds to a period of 600 seconds (10 minutes → t=0.17h). Also, since a temporary cut-off of the unit takes place, $P_{i,s,q}$ in expression (7.4) is set equal to zero.

Concerning the droop control scenario, in case V instantaneously exceeds $1.10V_{\text{nom}}$, in reality a temporary disconnection of the unit takes place, which lasts some seconds or minutes, until the next droop attempt. In the simulation, this temporary cut-off is considered to last 180 seconds (3 minutes → t=0.05h). This period is used for computing the curtailed energy due to droop control as soon as V>$1.10V_{\text{nom}}$. When V instantaneously exceeds $1.15V_{\text{nom}}$, the PV unit disconnection also lasts 600 seconds for the droop scenario.

7.1.5 *Simulation of the LV feeder*

The LV feeder that is analyzed in Chapter 5 is also studied in this case, considering a perfectly balanced three-phase network. Unbalanced phase connections are therefore not regarded, as shown in Figure 7.3.

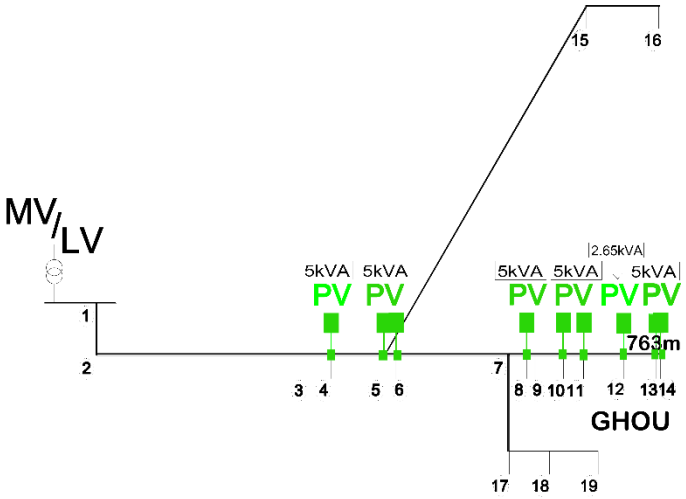

Figure 7.3: Simulated LV network with nine PV users (nodes 4, 5, 6, 8, 10, 11, 12, 13, 14) and seven customers without PV (nodes 3, 9, 15, 16, 17, 18, 19)

In order to highlight the benefits of the droop control in smoothing the feeder voltage profile, nodes 6, 8, 10, 11 and 13 were also simulated as PV nodes with identical SM data as the existing PV user at node 14 (P_{rated}=5kVA). All PV inverters are considered to have P/V control. Droop control has been initially simulated with the "*k*" and "*b"* values that were applied in [1], which means: $k \approx P_{rated}/100$ and $b=0.06$. A step by step study has been done in this section for tuning these control parameters to enhance performance and reduce power curtailment.

(i) (k1, V1)

Initially the droop function has been implemented with the following parameters:

- $k1=P_{rated}/100$ and $b=0.06$, thus $V_{up}=V1=1.06V_{nom}$ (voltage "unsafe" zone in which the P/V controllers are activated*:* $V_{up} < V < 1.1V_{nom}$ and V_{nom}=230V).

The benefit of droop control on eliminating overvoltage (cases with $V>1.10V_{nom}$) is proved since overvoltage probability changes to zero for all nodes. The priority is to eliminate overvoltage risk and consequently temporary disconnections of PV units. Besides, droop control has a beneficial effect on decreasing the voltage profile along the feeder (not only at PV nodes). This fact leads to an increase of the margin of the maximal acceptable PV penetration.

In order to draw interesting conclusions, the cost to pay for this overvoltage elimination should be compared with the one due to on-off control (base scenario) during a defined period. This comparison can be based on generated energy losses, namely the daily average curtailed energy $E_{curt.mean}$ (kWh) due to on-off and droop control actions. The amount of $E_{curt.mean}$ per PV node due to on-off

control and to five different droop control scenarios (explained in the next subsections) is demonstrated for the month of April in Figure 7.4. Given the increased solar irradiation during a long period of the day in April (sunrise at 6:30AM and sunset at 21:00PM), this period of the year is interesting for studying the overvoltage risk. For the initial droop scenario *(i)*, $E_{\text{curt.mean}}$ decreases compared to on-off scenario at all PV nodes. This amount apparently depends on the P_{rated} of each unit, since k is defined in function of P_{rated} (in this case: $k1=P_{\text{rated}}/100$). As P_{rated} at node 12 is lower than the ones at adjacent nodes 11 and 13, a smaller amount of energy is curtailed at this node.

$E_{\text{curt.mean}}$ is not important when compared to average daily PV energy $E_{\text{tot,mean}}$ (kWh) that could be potentially injected if no on-off or no droop control (Table 7.1) was applied. For the studied period, the application of droop control is preferable rather than on-off control since overvoltage risk is eliminated while a smaller of amount of generated energy is curtailed. Moreover, in case of droop control, disconnection and reconnection of PV units is smooth, gradual and controllable until stability along the feeder is achieved.

Table 7.1: Average daily injected PV energy (if no temporary cut-offs due to overvoltage took place)

Nodes	4	5	6	8	10	11	12	13	14
$E_{\text{tot,mean}}$	13,1	13,22	13,09	13,21	13,18	13,24	7,78	10,82	13,23

(ii) (k2, V1)

The results of scenario *(i)* indicate the benefit of droop control in this feeder. However, the performance of the control can be enhanced by tuning its parameters. Indeed, by decreasing the slope of the droop control, namely the value of "k", a more gradual curtailment of PV energy can be achieved. The effect of this tuning is studied in the present scenario *(ii)*. In reality, this modification of "k" is locally done based on the needs or the background history of the specific PV unit. This chapter aims at demonstrating the benefit of fast acting local droop control which requires no communication among units and no overlaying control. This means that the parameters tuning is done offline and not dynamically imposed by a central controller or by distributed controllers in function of the network state. In this scenario, the droop parameters are set as follows:

- $k2= P_{\text{rated}}/500$ and $V_{\text{up}}=V1=1.06V_{\text{nom}}$

The overvoltage risk is also eliminated in this case while $E_{\text{curt.mean}}$ is decreased for all nodes (compared to scenario *(i)*) especially for the ones towards the head of the line (Figure 7.4).

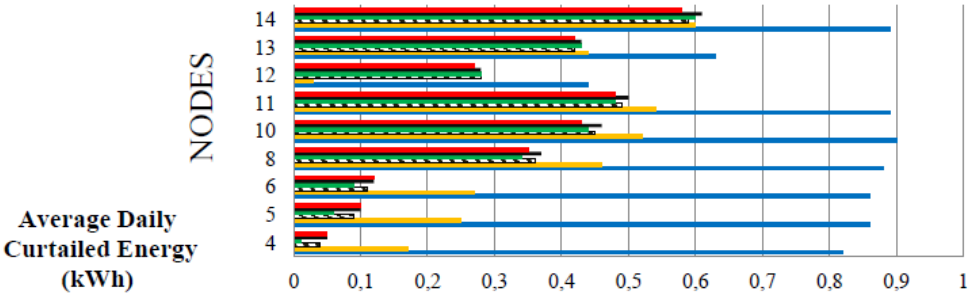

	4	5	6	8	10	11	12	13	14
(v) Vup=1.03->1.09->1.095Vnom (k2)	0,05	0,1	0,12	0,35	0,43	0,48	0,27	0,42	0,58
(iv) Vup=1.06->1.065->1.08Vnom (k2)	0,05	0,1	0,12	0,37	0,46	0,5	0,28	0,43	0,61
(iv) Vup=1.08Vnom (k2)	0,01	0,06	0,09	0,34	0,44	0,48	0,28	0,43	0,6
(ii) Vup=1.06Vnom (k2)	0,04	0,09	0,11	0,36	0,45	0,49	0,28	0,42	0,59
(i) Vup=1.06Vnom (k1)	0,17	0,25	0,27	0,46	0,52	0,54	0,029	0,44	0,6
On/off control	0,82	0,86	0,86	0,88	0,9	0,89	0,44	0,63	0,89

Figure 7.4: Average Daily Curtailed Energy (Ecurt,mean) per PV node for the on-off control and the droop control scenarios for April

The voltage profile of nodes 6 and 12, during ten consecutive time steps of a typical day in July, is presented in Figure 7.5((i) and (ii)) for three scenarios. The first one shows voltage profile in case no control is applied or just before the action of any control scheme (green line). The second one shows the case of on-off control applied in the feeder (yellow line) and the third one the case of P/V droop control applied in the feeder (blue line).

According to this diagram, droop control acted during several time steps of the period between 12:00PM and 14:30PM, at node 6, having as a result a voltage drop (Figure 7.5(i)) and a slight energy curtailment (Figure 7.5(iii)) during the respective time steps (blue line). In these cases, the final voltage value (blue line) at node 6, for the scenario of P/V droop control, is determined by the action of the control at node 6 but also by the action of the control at other nodes in the feeder. The on-off control was not activated at node 6, since the initial voltage value (green line) at this node did not exceed the 95-percentile limit of the EN 50160 standard ($1.10V_{nom}$=253V) in any of the presented time steps. This can be also confirmed by the fact that the ¼-hourly curtailed energy, due to on-off control, is equal to zero during the whole period (Figure 7.5(iii)) at node 6. However, during the time step between 12:15P.M. and 12.30P.M., the on-off control was activated at other nodes, as for example at node 12 (Figure (7.5(ii)), having also as a result a voltage drop at node 6. Consequently, the voltage at node 6 dropped from the initial value of 250V (green line) to the value of 230V (yellow line).

Regarding node 12 (Figure 7.5(ii)), the P/V droop control also acted during several time steps of the presented period. As a result, a voltage drop and a slight energy curtailment took place during the respective time steps. During the time step between 12.15P.M. and 12.30P.M. the initial voltage value (green line) at node 12 exceed $1.10V_{nom}$(=253V) and this fact led to a total cut-off of the injected PV power at this node (Figure 7.5(iv)). In the case of on-off control (yellow line), this power curtailment was applied during ten minutes while in the case of droop control (blue line) this power curtailment was considered to take place until the next droop attempt (in this study we have considered a 180 seconds period, as explained in paragraph 7.1.4). For this reason, the total ¼-hourly curtailed energy in the on-off scenario (yellow line in Figure 7.5(iv)) resulted to be much higher than the respective one in the droop control scenario. During the period of 180 seconds, the action of P/V droop control at nodes where the $1.10V_{nom}$ limit was not exceeded, contributes in recovering the voltage profile all along the feeder. In this way, the temporarily disconnected PV units might start injecting power sooner than in the case of on-off control while several PV units' disconnections, at nodes with a voltage profile near the upper limit might be avoided.

Consequently, in the droop control scenario, if the voltage at a node where a PV cut-off took place, returns at a value lower than $1.10V_{nom,}$, during the next droop iteration, the PV injection at this node turns again on. In the probabilistic simulation, this means that if the next load flow computation gives a voltage value that is lower than $1.10V_{nom,}$ the PV injection of the unit is considered to be equal to the initially sampled one and another load flow computation takes place until all voltage values in the feeder are lower than $1.10V_{nom.}$ For this reason, in Figure 7.5(ii) the final voltage at node 12, during the time step between 12.15P.M. and 12.30P.M., is not as low as the respective one in the on-off scenario. Although the unit at this node has been indeed turned off for some seconds and an important voltage drop took place, as soon as the action of the control along the feeder reduced voltage magnitudes, the PV injection at node 12 turned on after a while and voltage values (blue line in Figure 7.5(ii)) in the final load flow computation for this network state did not result to be as low as the ones in the on-off control scenario (yellow line in Figure 7.5(ii)).

Although droop control is more often activated compared to on-off control, $E_{curt.mean}$ in case of on-off control results to be higher for the studied period (Figure (7.5(iv)). This remark is very favorable for droop control. The challenge is to evaluate the effect of this argument on the income of PV owners (especially in environments with time-varying PV energy rates) and on the operational expenses currently managed by the respective DSO.

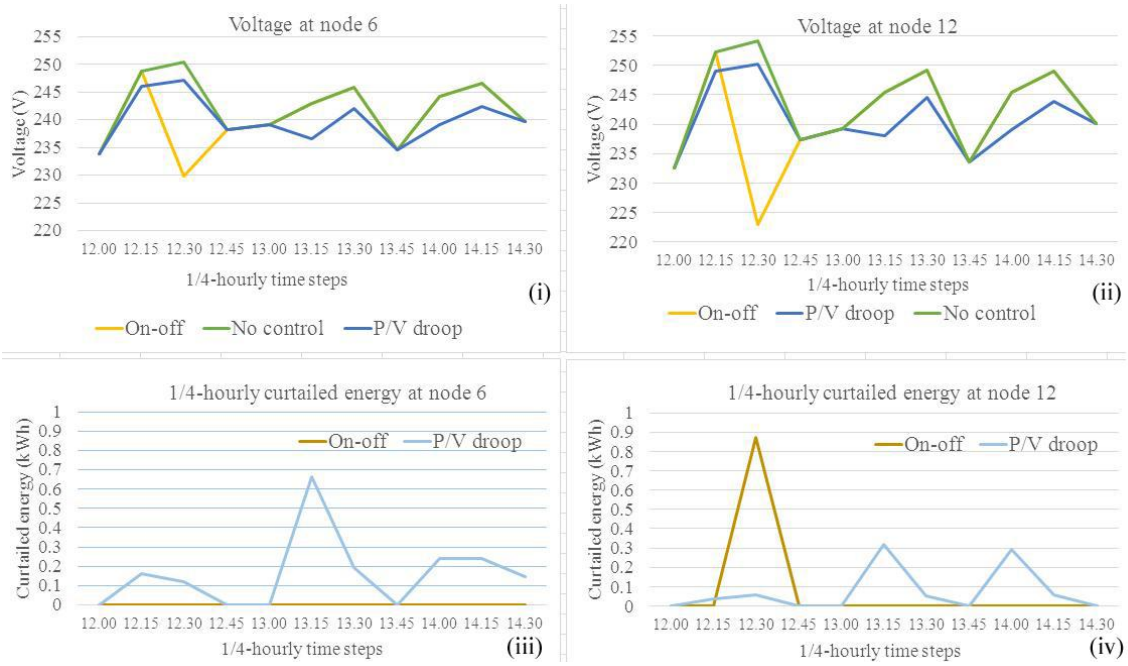

Figure 7.5: ¼-hourly voltage profile (diagram (a)) and ¼-hourly curtailed energy (diagram (b)) at nodes 6 and 12 (no control, on-off control and droop control scenarios)

In Figure 7.6, the ¼-hourly curtailed energy at node 14 is presented for on-off and droop control scenarios *(ii)* for 20 typical days of July, April, October and March. The curtailment of energy in the droop scenario is much more gradual and kept within an almost stable band of values during all these months. This observation is an advantage as far as the end-users' acceptance of compensation measure is concerned (in comparison to on-off control). Moreover, PV curtailment due to on-off control resulted to be quite unpredictable during the whole studied period. Concerning the parameters tuning, the application of value *k2* *(=P_{rated}/500)* allowed a more gradual application of the control and it is, therefore, selected for the next studied scenarios. The simulation of the feeder for other months (November to March) demonstrated that overvoltage is almost equal to zero and, consequently, no droop or on-off control action (due to voltage rise) is needed.

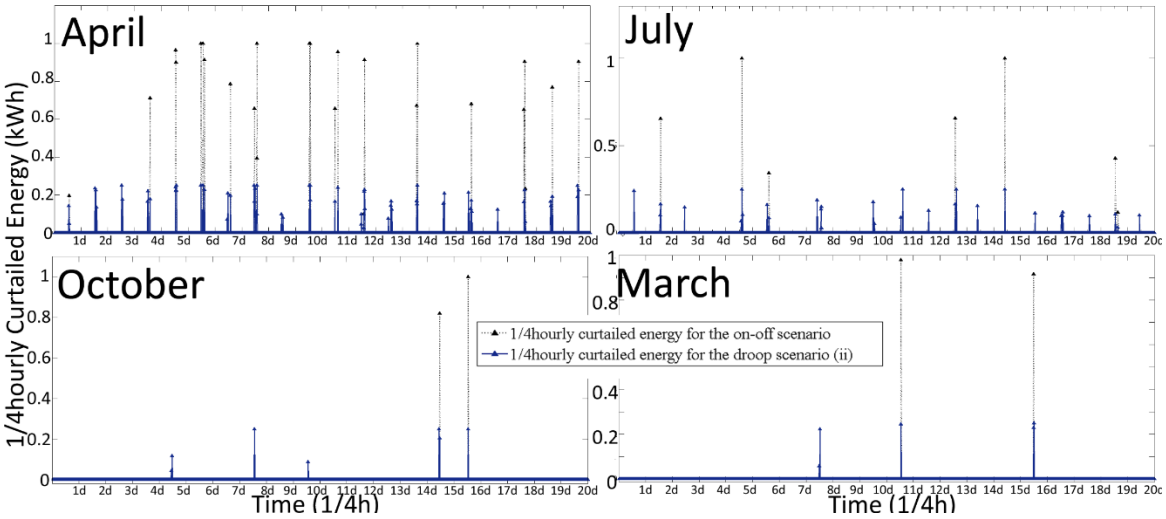

Figure 7.6: ¼-hourly curtailed energy in function of time at node 14 for the on-off control and droop control scenario (ii) for 20 typical days of April, July, October and March.

(iii) (k2, V2)

Another parameter that can be tuned for customizing droop control to the specific needs of the feeder or certain PV units is the reference voltage V_{up}. Practically, P/V control is enabled at every PV node as soon as V_{up} is exceeded. In case a higher value of V_{up} is selected, droop control might still be efficient inducing a smaller amount of curtailed energy. To analyze such a choice, the droop control is simulated in this scenario *(iii)* with the following parameters:

- $k2 = P_{rated}/500$ and $V_{up} = V2 = 1.08 V_{nom}$

The results are presented in Figure 7.4. The overvoltage risk was indeed eliminated. The values of $E_{curt.mean}$ are slightly lower for the first five PV nodes but almost the same for the rest of the network. In order to achieve a more fairly distributed curtailed energy along the feeder, it is interesting to try a further tuning of "*k*" and "*b*" parameters as explained in the following scenarios.

(iv) (k2, V1 for i=4:6, V3 for i= 8, 10:12, V4 for i=13:14)

As shown in Figure 7.4, $E_{curt.mean}$ at nodes close to the end of the feeder is greater than the one computed at nodes near the transformer. To compensate this effect and to establish a more fair distribution of the curtailed energy along the feeder, the value of reference voltage V_{up} can be customized per node or per group of nodes. The probabilistic framework is used to tune this parameter and to indicate the preferable values of V_{up} per PV node for a balanced curtailment of renewable energy along the studied feeder. Based on the analysis of the results of the previous scenarios *(i)*, *(ii)* and *(iii)*, droop control is here simulated with the following parameters:

- $k2=P_{rated}/500$, $V_{up}=V1=1.06V_{nom}$ for i=4:6, $V_{up}=V3=1.065V_{nom}$ for i=8,10:12, $V_{up}=V4=1.08V_{nom}$ for i=13:14

The values of "*b*" parameters per node have been chosen by means of a trial and error procedure, based on the nodal voltage results of the previous simulations. The simulation of this scenario *(iv)* resulted in $E_{curt,mean}$ slightly higher than the one of scenario *(ii)* and *(iii)* (Figure 7.4) while the distribution of curtailed energy along the feeder is almost not affected. Even though the overvoltage is also in this case eliminated, there is an optimization potential to be further studied. This potential concerns a more fair distribution of the curtailed energy along the feeder and this hypothesis led to the simulation of the following case.

(v) (k2, V4 for i=4:6, V5 for i=8,10:12, V6 for i=13:14)

In this case droop control is applied with the next parameters:

- $k2=P_{rated}/500$, $V_{up}=V4=1.03V_{nom}$ for i=4:6, $V_{up}=V5=1.09V_{nom}$ for i= 8,10:12, $V_{up}=V6=1.095V_{nom}$ for i=13:14

Indeed, in this scenario *(v)*, the amount of curtailed energy is slightly more fairly distributed along the feeder. Compared to all previous scenarios, $E_{curt,\,mean}$ is slightly lower for nodes towards the end of the feeder while it logically increases for nodes close to the head of the feeder.

In the previous paragraphs the restructured probabilistic framework (with P/V controllers) has been applied to simulate multiple network states (S=1000) in an existing LV feeder with the use of feeder-specific SM measurements. Such reduced and simple statistical models of the available SM data allow quickly tuning (compromise between curtailed energy and voltage quality) the parameters of the droop control. We can thus assume that the implemented evaluation model is more faithful to the real network behavior compared to previous deterministic studies. In the purpose of fully evaluating the control's performance in a realistic manner, the probabilistic model was applied to tune the control parameters in the specific feeder for the studied period. Indeed, such an evaluation was not feasible with the worst-case approach as it would have led to an over evaluation of those parameters.

The simulation results demonstrated that the implementation of P/V droop control has an important benefit on the voltage profile at all nodes. Practically, it was shown that P/V droop control is efficient in eliminating overvoltage while keeping the amount of daily curtailed energy per PV node very low. Also, it was demonstrated that the control is more beneficial, in terms of efficiency and power curtailment, when the system parameters are locally tuned. As far as the specific LV feeder is concerned, the last scenario (k2, V4 for i=4:6, V5 for i= 8, 10:12, V6 for i=13:14) is the suggested one for the month of April, since it offers a total elimination of overvoltage and a more fair distribution of curtailed energy among the connected PV users. These findings highlight the utility of deploying such

long-term evaluations and refinement of technical strategies aiming at increasing the PV hosting capacity of LV networks.

7.2 Voltage unbalance mitigation

Although single-phase PV units connected to the LV network are not always the principal source of voltage unbalance, distribution utilities often impose the maximal acceptable nominal power of such units in a conservative manner. Their objective is to prevent from further unbalance rise. In most cases, such decisions do not consider the time-variability of single-phase loads and generation. As a result, voltage magnitude and unbalance margin may be misleadingly computed and lead to restrictive decisions about further renewables' integration. However, in certain cases, PV units can even contribute in decreasing the existing voltage unbalance. This can be achieved by means of mitigation control schemes integrated in three-phase inverters. Such systems have been thoroughly studied in the relevant literature [19]–[26].

Reference [2] presents the three-phase damping control strategy (3ph-DPC) which acts resistively towards the zero- and negative-sequence voltage components without modifying the injected PV power. The fact that this control strategy acts locally, based on the instantaneous values of the network phase voltages, makes it effective and easy to implement. The 3ph-DPC scheme was tested and verified by means of an experimental setup [2], [26]. It was then demonstrated that this control significantly improves voltage unbalance and magnitude in LV systems. However, in that case, 3ph-DPC scheme was evaluated in a restricted number of network states, mostly representing the worst-case power exchange scenarios in a feeder. Therefore, its impact on network operation metrics (voltage level, voltage unbalance, congestion risk, line losses) was not regarded with a long-term view such that it can be extensively and reliably compared to currently implemented control strategies.

Driven by these considerations, this section integrates the 3ph-DPC scheme in the probabilistic framework so that its performance is evaluated in an extensive range of possible network states, based on the available SM data. The effect of this control scheme is compared to the one of the traditionally applied on-off control and reactive power control and to another new control scheme, the three-phase symmetrical injection (3ph-SI). The integration of both new control schemes (3ph-DPC and 3ph-SI) in the basic structure and their simulation in the feeder of Chapter 6 are described in the following subsections.

7.2.1 *Power flow analysis integrating control actions*

In order to integrate the action of the considered control schemes in the three-phase power flow forward/backward iterative process presented in section 4.1.4, the computation of the specified nodal loads $\underline{\boldsymbol{S}}_{\text{load,abc}}$ and the resulting nodal currents $\underline{\boldsymbol{I}}_{\text{load,abc}}$ needs to restructured. The necessary modification of this computa-

tion changes in function of the considered control scheme. For this reason, the typology of each scheme and the modification that it brings in the determination of the variable parameters of each network state is explained separately in the following paragraphs. The two first control schemes have been already applied in LV networks in Europe for local voltage magnitude rise mitigation but they do not take any focused action against voltage unbalance. The last two integrated schemes have been designed for mitigating voltage unbalance but at the same time they can also simultaneously act against local voltage rise.

i. *On-off control*

As already mentioned, the on-off control is the strategy that most distribution utilities in Europe currently apply. This control scheme imposes a temporary disconnection (off mode) of the PV unit for the next 600 s, as soon as the 10-min mean RMS voltage at the PCC of a PV user exceeds the value of $1.10V_{\text{nom}}$ during 10 min or the value of $1.15V_{\text{nom}}$ instantaneously. This hard curtailment is the traditional way of coping with overvoltage even though it deteriorates the delivered power quality due to significant voltage and current transients. Moreover, it accelerates the degradation of the inverters and it leads to an important loss of generated renewable energy which affects the expected income of the PV producer.

The on-off control is considered in the probabilistic framework as the base scenario for single-phase PV units. Basically, if this control is selected in the simulation process, the three-phase power flow algorithm then performs, for each simulated system state, an initial analysis of the feeder considering the nodal power exchange values that are defined by the MC sampling. In this way, nodal voltages $\underline{\boldsymbol{V}}_{\text{abc}}$, are computed and their magnitude is compared to the 95-percentile limit of EN 50160 standard ($=1.10V_{nom}$). In case one of the voltage magnitudes $V_{\text{a,i}}$, $V_{\text{b,i}}$ *or* $V_{\text{c,i}}$ at node i exceeds this limit, then $E_{\text{inj,pv,i,q}}$ is considered entirely curtailed and relation (4.12) becomes:

$$P_{i,q} = \frac{E_{load,i,q}}{0.25} \tag{7.5}$$

The algorithm computes again nodal voltages $\underline{\boldsymbol{V}}_{\text{abc}}$ and nodal %VUF (as in section 4.1.4) after having applied relation (7.5) at all nodes i for which voltage limits are locally violated.

ii. *Reactive Power Control*

In some EU countries, distribution utilities allow the connection of new single-phase PV units to the LV network as far as they are equipped with Q/V control functions. Such strategies modify the PV unit power factor $cos\varphi_{\text{inj}}$ in function of the instantaneously injected active power and of the instantaneous network voltage [27], [28]. For example, concerning small PV units (<6kVA) connected to the Italia LV network, the power factor $cos\varphi_{\text{inj,i}}$ should change in function of

the injected active PV power $P_{\text{inj,pv,i}}$ at node *i*, according to the predefined graph of Figure 7.7 (see expressions (7.6-7.8)). In such a way, when the network voltage exceeds a certain value (usually $1.05V_{\text{nom}}$) the PV inverter absorbs an amount of reactive power such that the voltage rise is mitigated. Reactive power control (Q control) has no direct action against voltage unbalance.

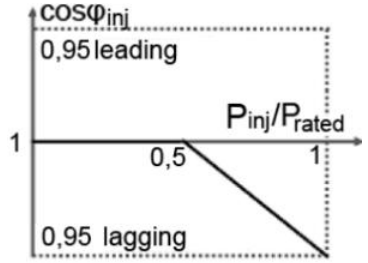

Figure 7.7: The Q/V function of standard CEI 0-21 for new PV units < 6kVA [27]

In case Q control is selected in the simulation process, the following steps are performed. For a given network state, the power flow algorithm performs an initial analysis of the feeder and nodal voltages $\underline{\boldsymbol{V}}_{\text{abc}}$ are computed. In case one of the voltage magnitudes $V_{\text{a,i}}$, $V_{\text{b,i}}$ *or* $V_{\text{c,i}}$ at node *i* exceeds the value $1.05V_{\text{nom}}$, (but not the one of $1.10V_{\text{nom}}$, for which a total cut-off would be required), the power factor of PV injection $cos\varphi_{\text{inj,pv,i}}$ at node *i* is computed with (7.6), as far as the condition of (7.7) is satisfied. In this case, the reactive power $Q_{\text{pv},i}$ that is absorbed by the PV inverter is not anymore equal to zero but is determined with (7.8):

$$cos\varphi_{inj,i} = 1 - \frac{0.05 \cdot \left(\frac{P_{inj,pv,i}}{P_{rated,i}} - 0.5\right)}{0.5} \tag{7.6}$$

$$\text{if} \quad \frac{P_{inj,pv,i}}{P_{rated,i}} - 0.5 > 0 \quad \text{and} \quad cos\varphi_{inj,pv,i} < 0.95 \tag{7.7}$$

$$Q_{pv,i} = P_{inj,pv,i} \cdot tan\varphi_{inj,pv,i} \tag{7.8}$$

In relation (7.7) $P_{\text{rated},i}$ is the nominal active power of the PV unit at node *i* while $P_{\text{inj},i}$ is the PV active power injection at node *i* for the considered system state *s*. Considering the updated $Q_{\text{pv},i}$ value, the specified nodal load at each node *i*, where the control action is applied, is modified and so do the nodal currents $\underline{\boldsymbol{I}}_{\text{load,abc}}$. The power algorithm performs again the analysis of the feeder, considering the updated nodal loads $\underline{\boldsymbol{S}}_{\text{load,abc}}$ and the resulting nodal currents $\underline{\boldsymbol{I}}_{\text{load,abc}}$. Consequently, the nodal voltages $\underline{\boldsymbol{V}}_{\text{abc}}$ are updated. In case there are again nodes with voltage magnitudes higher than the value $1.05V_{\text{nom}}$ (and complying with relation (8.7)), the same process is repeated. This iterative process goes on until all nodal

voltages at PV nodes become smaller than the $1.05V_{\text{nom}}$ value. At this point, the final $Q_{\text{pv},i}$ value is defined at each node *i*, for the considered network state, and the final nodal voltages $\underline{\boldsymbol{V}}_{\text{abc}}$ are computed all along the feeder.

iii. *Three-phase symmetrical injection (3ph-SI)*

In case a new PV inverter is connected to the feeder in a three-phase mode (with a three-phase inverter) and no special action is taken for the repartition of phase currents, then in every network state, the phase with the lowest voltage magnitude will have the lowest PV injection current. Indeed, voltages $\boldsymbol{V}_{\text{a,i}}$, $\boldsymbol{V}_{\text{b,i}}$ *or* $\boldsymbol{V}_{\text{c,i}}$ at the coupling point of the PV node *i* with the feeder will most probably be unbalanced due to other single-phase loads and PV units connected along the feeder. In such cases, it is useful to ensure that the PV injection at the new node *i* will be balanced over the three phases so that local unbalance can be partly mitigated thanks to the new connection. In order to achieve a balanced repartition of PV injection among the three phases, a control action is required. If such a control scheme is applied in the simulation, then phase currents $\underline{\boldsymbol{I}}_{\text{load,abc,i}}$ due to the nodal loads are computed for simple nodes *i* with (7.9) and for lateral root nodes with (7.10):

$$\boldsymbol{I}_{load,x,i} = \left(\frac{P_{load,x,i} - \frac{P_{inj,pv,i}}{3} + j\ Q_{x,i}}{\boldsymbol{V}_{initial,x,i}} \right)^{*} \quad (x=a,\ b\ or\ c \text{ phase}) \qquad (7.9)$$

$$\boldsymbol{I}_{load,x,i} = \left(\frac{P_{load,x,i} - \frac{P_{inj,pv,i}}{3} + j\ Q_{x,i} + \boldsymbol{S}_{\text{lateral,x,i}}}{\boldsymbol{V}_{initial,x,i}} \right)^{*} \quad (x=a,\ b\ or\ c \text{ phase}) \qquad (7.10)$$

where active power values $P_{\text{load},i}$ are defined per node and per phase with relation (7.5) ($P_{\text{i}} = P_{\text{load}}$) and $P_{\text{inj,pv,i}}$ is the total generated active PV power at node *i* for the considered network state *s*.

iv. *Three phase Damping Control (3ph-DPC)*

An alternative for connecting PV units to a three-phase LV feeder is the damping control that acts resistively against zero- and negative-sequence voltage components in order to locally mitigate voltage unbalance. This strategy results in the decrease of the existing voltage unbalance at the PCC of the PV unit by distributing the injected PV current over the three phases in function of the local network voltage. Roughly speaking, if for instance one of the phase voltages is rising, the 3ph-DPC scheme adapts the distribution of the total PV power among phases so as to ensure that a smaller share will be injected in the phase with the highest voltage. This behavior relies on the resistive behavior towards zero- and negative-sequence voltages which is thoroughly explained in [2] and outlined in Figure 7.8.

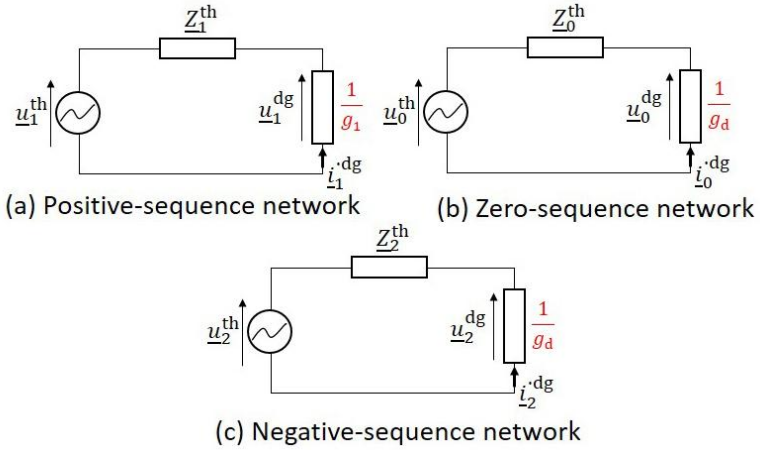

Figure 7.8: Basic principle of the 3ph-DPC [2], [29]

In case the 3ph-DPC strategy is selected in the simulation, the following process is applied. For a given network state, the algorithm starts by analyzing the feeder considering the nodal power exchange values that were initially sampled by the MC algorithm for this state. In this way, nodal phase voltages $\boldsymbol{V}_{a,i}$, $\boldsymbol{V}_{b,i}$ or $\boldsymbol{V}_{c,i}$ are computed before the application of the control. The voltage angles $\theta_{abc,i}$ at each node *i* are computed thanks to relation (7.11):

$$\theta_{x,i} = tan^{-1}\left(\frac{\Im\, \boldsymbol{V}_{x,i}}{\Re\, \boldsymbol{V}_{x,i}}\right), \text{ x=a, b, or c phase} \qquad (7.11)$$

At this point, an iterative process starts. The latter computes the nodal PV injection currents $\underline{\boldsymbol{I}}_{pv,abc,i}$ with relations (7.12), then the nodal currents with relations (7.13) (for simple nodes) or (7.14) (for lateral root nodes) and uses them to deploy a new power flow analysis of the feeder. In each iteration *l*, the voltages magnitudes $V_{abc,i}$ and voltage angles $\theta_{abc,i}$ that were computed in the previous iteration *l-1* are used to determine the new set point for the phase currents.

$$\boldsymbol{I}_{pv,a,i}(l) = \frac{1}{3}\ \boldsymbol{V}_{a,i}(l-1)\ e^{j\theta_{\alpha}(l-1)}\ G_1 + 2G_d + \boldsymbol{V}_{b,i}(l-1)\ e^{j\ \theta_b(\mathrm{l}-1)+\frac{2\pi}{3}} + \boldsymbol{V}_{c,i}(l-1)\ e^{j\ \theta_c(\mathrm{l}-1)-\frac{2\pi}{3}}\ G_1 - G_d$$

$$\boldsymbol{I}_{pv,b,i} = \frac{1}{3}\ \boldsymbol{V}_{b,i}(l-1)\ e^{j\theta_b(l-1)}\ G_1 + 2G_d + \boldsymbol{V}_{a,i}(l-1)\ e^{j\ \theta_a(\mathrm{l}-1)-\frac{2\pi}{3}} + \boldsymbol{V}_{c,i}(l-1)\ e^{j\ \theta_c(\mathrm{l}-1)+\frac{2\pi}{3}}\ G_1 - G_d$$

$$\boldsymbol{I}_{pv,c,i} = \frac{1}{3} \; \boldsymbol{V}_{c,i}(l-1)\; e^{j\theta_c(l-1)}\; G_1 + 2G_d + \boldsymbol{V}_{a,i}(l-1)\; e^{j\;\theta_a(\mathrm{l}-1)+\frac{2\pi}{3}} + \boldsymbol{V}_{b,i}(l-1)\; e^{j\;\theta_b(\mathrm{l}-1)-\frac{2\pi}{3}} \quad G_1 - G_d \tag{7.12}$$

$$\boldsymbol{I}_{load,x,i} = \frac{P_{load,x,i} + j\;Q_{x,i}}{\boldsymbol{V}_{initial,x,i}} - \boldsymbol{I}_{pv,x,i}^{\;*} \quad (x=a,\ b \text{ or } c \text{ phase}) \tag{7.13}$$

$$\boldsymbol{I}_{load,x,i} = \frac{P_{load,x,i} - \frac{P_{inj,pv,i}}{3} + j\;Q_{x,i} + \boldsymbol{S}_{\mathrm{lateral,x,i}}}{\boldsymbol{V}_{initial,x,i}}^{\;*} \quad (x=a,\ b \text{ or } c \text{ phase}) \tag{7.14}$$

where active power values $P_{\mathrm{load},i}$ are defined per node and per phase with relation (7.5) and reactive power values $Q_{x,i}$ are computed as explained in the *hybrid power flow method* in paragraph 4.1.4.iii.

The iterations are repeated until the difference between the values of $P_{\mathrm{inj,pv,i}}$ (relation (7.15)) during two successive iterations is lower than a fixed convergence criterion:

$$P_{inj,pv,i}\;l\; = \Re\; \boldsymbol{V}_{a,i}\;l\; \cdot \boldsymbol{I}_{pv,a,i}\;l\;^{*} + \boldsymbol{V}_{b,i}\;l\; \cdot \boldsymbol{I}_{pv,b,i}\;l\;^{*} + \boldsymbol{V}_{c,i}\;l\; \cdot \boldsymbol{I}_{pv,c,i}\;l\;^{*} \tag{7.15}$$

where conductances G_1 and G_d are computed as explained in [2],[26]. Note that the damping output conductance G_d has the opposite sign of G_1 in DG applications (G_d >0) and that the choice of the value of G_d depends on the rated power $P_{\mathrm{rated},i}$ of each PV inverter [2], [26], [29]. $P_{\mathrm{inj,pv,i}}$ is the PV power that was initially sampled by the MC algorithm. The final computed phase voltages $\boldsymbol{V}_{\mathrm{abc,i}}$ (and the resulting VUF_i) are the ones considered as the outputs of the studied network state. Moreover, it can be shown that no PV power curtailment takes place with the action of the 3ph-DPC scheme (see relation (7.12)). Phase injection currents are re-distributed over the three phases, in function of the local voltages (magnitudes and angles) such that, finally, local unbalance is mitigated as much as possible and current flow in the neutral conductor is decreased. One should note that this control scheme can only be implemented in a 3-phase 4-wire configured feeder. The iterative process that is applied for the integration of the control in the probabilistic algorithm is illustrated in Figure 7.9.

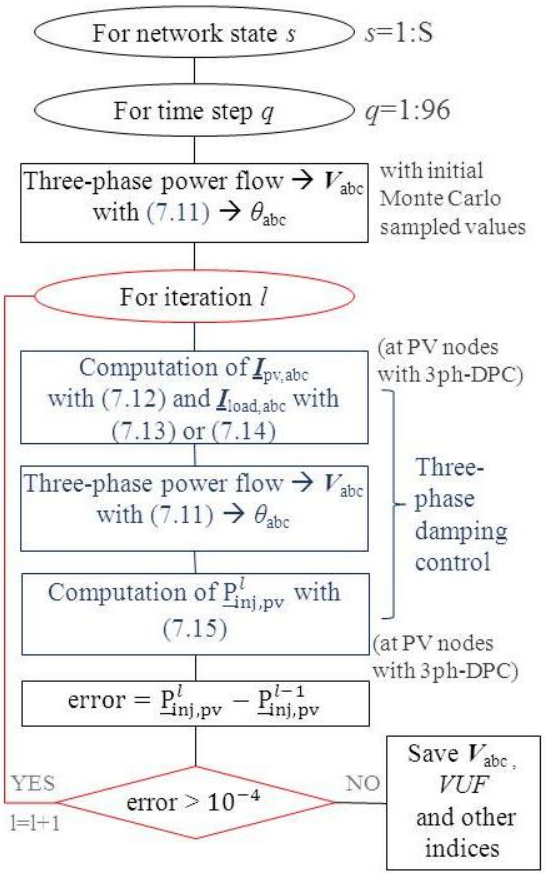

Figure 7.9: Flowchart for the integration of the three-phase damping control scheme in the probabilistic simulation framework

v. *PV inverter sizing*

The common way for sizing grid-tied PV inverters is to consider the total power rating of the PV panels. Based on this principle, the continuous power rating of an inverter (total amount of power that it can support indefinitely) should be approximately equal to the one of the PV installation, once having considered cells efficiency and solar irradiation factors. The power rating of the inverter should not be much higher than the one that it will need to support otherwise its efficiency will drop. Indeed, when the PV panels are not producing close to their full capacity, the inverter will only be operating at partial load which is not economically interesting neither for the PV owner nor for the distribution utility (depending on the legislative and the tariff framework). On another hand, if an inverter is not able to operate in overload conditions, then energy loss will probably occur. Finally, a grid-tied PV inverter should customize its output voltage so that it is not higher than the LV feeder voltage.

Based on these considerations, the outputs of the probabilistic simulation can be used in order to guarantee a more cost-effective sizing of new PV inverters

connected to a LV feeder. To this end, the computed (in each simulated network state) nodal PV power injection*s* S_{i} can be considered for determining the maximum power rating that should be supported by each PV inverter, depending on the applied control scheme. For each new PV node *i*, the maximum power S_{i} that will need to be supported by the inverter is computed with (7.16):

$$S_i = max \quad \boldsymbol{V}_{a,i} \cdot \boldsymbol{I}_{pv,a,i}{}^{*} + \boldsymbol{V}_{b,i} \cdot \boldsymbol{I}_{pv,b,i}{}^{*} + \boldsymbol{V}_{c,i} \cdot \boldsymbol{I}_{pv,c,i}{}^{*} \tag{7.16}$$

where $\boldsymbol{I}_{pv,a,i}$, $\boldsymbol{I}_{pv,b,i}$, $\boldsymbol{I}_{pv,c,i}$ are the nodal PV injection currents computed with relations (7.12).

7.2.2 *Simulation of the three-phase Low Voltage feeder*

The feeder analyzed in Chapter 5 is considered in the present simulation. For simulating a future scenario, nodes 6, 8, 11 and 13 (Figure 7.10) are considered as future PV nodes that should be connected based on a cost-effective approach. All the loads of the main line are connected to phase *c*. Four scenarios have been simulated, corresponding to the control schemes of Section 8.2.1. Practically, the action of the reactive power control, the 3ph-DPC and the 3ph-SI schemes was only considered available at the new PV nodes. The latter are either considered connected in single-phase mode (connected to phase *a*, as all existing PV units) or in three-phase mode (by means of three-phase four-wire inverters). The value of $G_{\mathrm{d,i}}$ in the 3ph-DPC strategy applied by the three phase PV inverter at node *i* is considered to be equal to $10P_{\mathrm{rated,i}}/V_{\mathrm{nom}}$. The nominal voltage V_{nom} is, as usually, equal to 230V.

The future PV nodes are considered to have identical SM data as the already available of other PV users. Specifically, for simulating the PV generation profile at new PV nodes 6, 8, 11 and 12, SM datasets recorded at PV units of 2.8kVA, 3.5kVA, 4kVA and 4.2kVA have respectively been used. Total spatial correlation between their generation powers is considered for all network users.

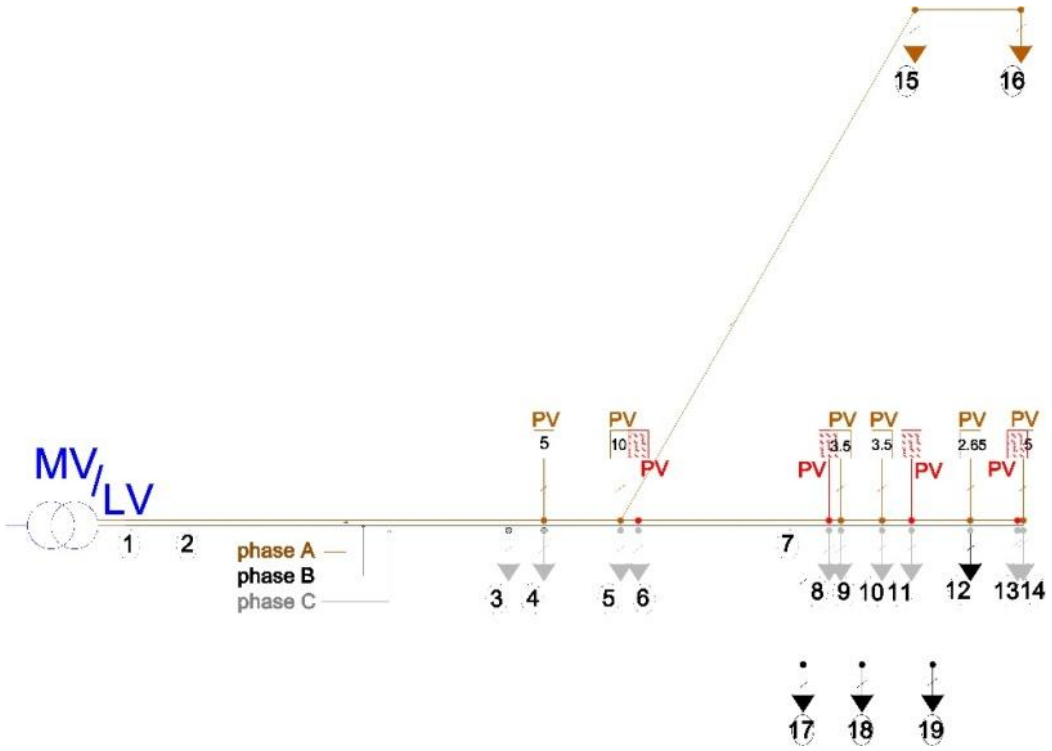

Figure 7.10: Simulated LV feeder (the new PV nodes are illustrated in red colour)

i. *Operation indices*

Looking at the entire feeder, the analysis of a yearly period demonstrated that the application of the 3ph-DPC scheme significantly improved voltage magnitudes of all phases, compared to the traditionally applied on-off control, the reactive power control and the 3ph-SI strategy. Indicatively, Figure 7.11 presents voltage magnitudes and unbalance *(%VUF*) at nodes 13 (new PV node) and 14 (existing PV node) during the same ¼-hourly time step (between 15:30P.M. and 15:45P.M.) on five simulated July days. Although the simulated control schemes are only applied at new PV nodes, their positive effect on voltage magnitudes and unbalance of existing PV nodes is demonstrated.

In the presented simulation snapshots of Figure 7.11, the 95-percentile limit of the EN 50160 standard was not exceeded which means that the on-off control was inactive at both nodes. The reactive power control was activated during 2 of the 5 illustrated days, practically the ones in which the first condition of (8.7) ($P_{inj,pv,i} > 0.5P_{rated,i}$) was satisfied. In the other 3 states, the PV inverter did not inject reactive power to the network and the voltage magnitude at node 13 was not improved compared to its initial value. The 3ph-DPC and the 3ph-SI schemes were activated during all the 5 network states and decreased the voltage profile at node 13. Thanks to their action, the voltage profile at node 14 was also decreased. Similar results were obtained for the variation of the *%VUF* at the same nodes, as illustrated in Figure 7.11.

One can easily notice that the effect of 3ph-DPC scheme on the phase voltages is much more obvious compared to the reactive power control and the 3ph-SI schemes. Indeed, the 3ph-DPC scheme delivered a reduction in the range of 0.5V to 2V (in the illustrated cases and in the overall simulation results) while the effect of the other two schemes remains most of the time lower than 0.5V. Regarding voltage unbalance, the 3ph-DPC and the 3ph-SI schemes had again a much more decisive effect compared to the reactive power control. This result was expected since these two schemes account both for local phase voltage magnitudes and unbalance. It is also to be noted that the 3ph-SI scheme has a slightly more decreasing effect than the 3ph-DPC scheme.

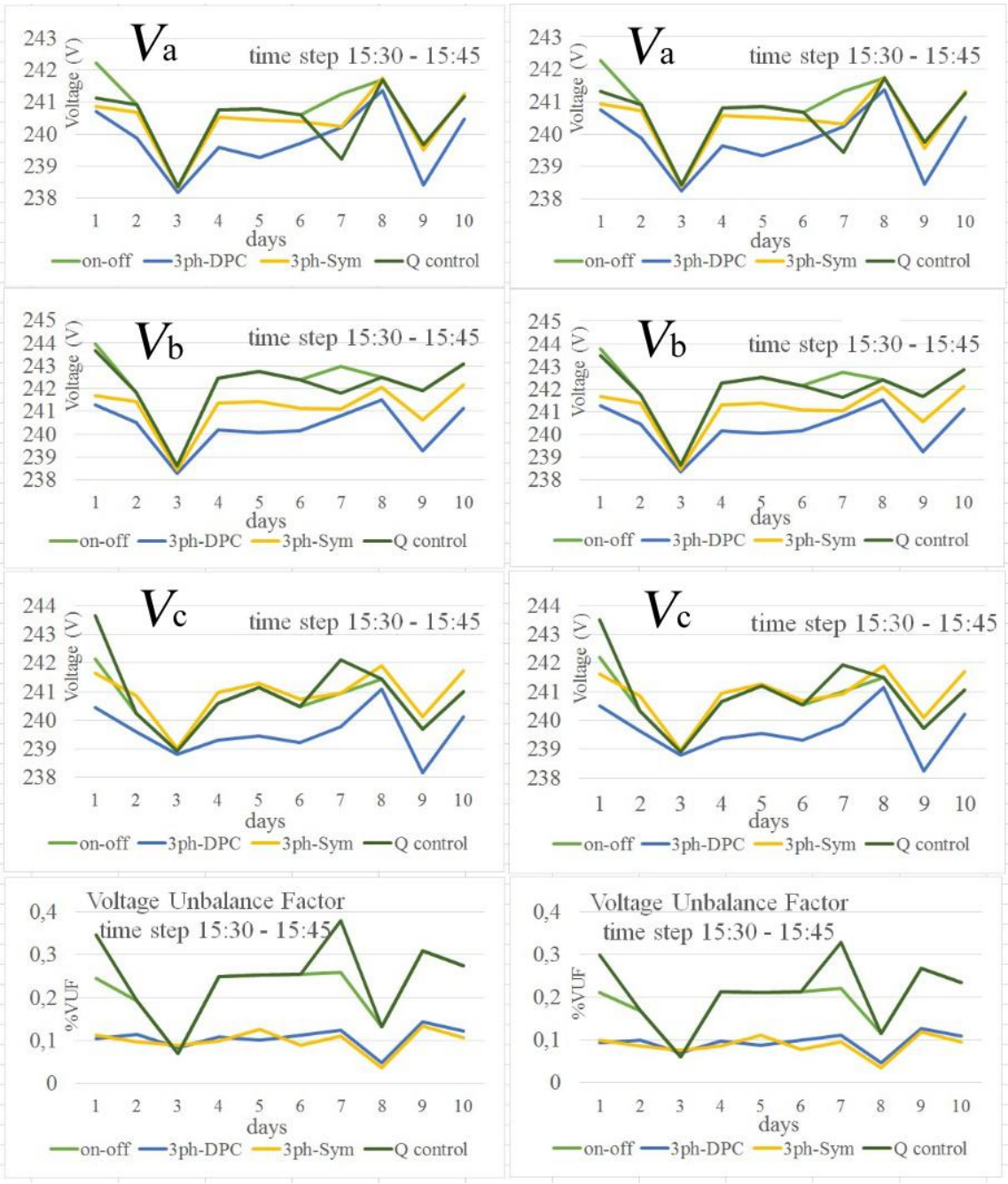

Figure 7.11: Phase voltage magnitudes and unbalance at nodes 13 (new PV node) and 14 (existing PV node) during the same ¼-hourly time step (15:30P.M. to 15:45P.M.) of five simulated July days

Figure 7.12 gives a statistical overview of the effect of the four control schemes on phase voltage V_a at nodes 8, 13 (new PV nodes) and 14 (existing PV node) based on the simulation of the feeder for July. The presented statistical distributions address only the PV injection period. One should also note that all ex-

isting PV units in the feeder are connected to phase *a* and therefore, this is the one directly affected by the variable PV injections.

According to the diagrams, the 95-percentile limit is not exceeded in any of the simulated network states (100% of computed values are lower than $1.10V_{nom}$). Moreover, it is shown that in more than 85% of the simulated states, the 3ph-DPC scheme results in voltage magnitudes 1-2V lower than the ones resulting from the other simulated schemes. For example, according to the diagram for node 8, if the on-off control or the reactive power control is applied at this node, the voltage magnitude will be greater or equal to 240V in 50% of the simulated cases. The respective value for the 3ph-DPC scheme is 238V. This result demonstrates the benefit of the 3ph-DPC action which can be very significant in future scenarios of high PV integration in similar LV feeders.

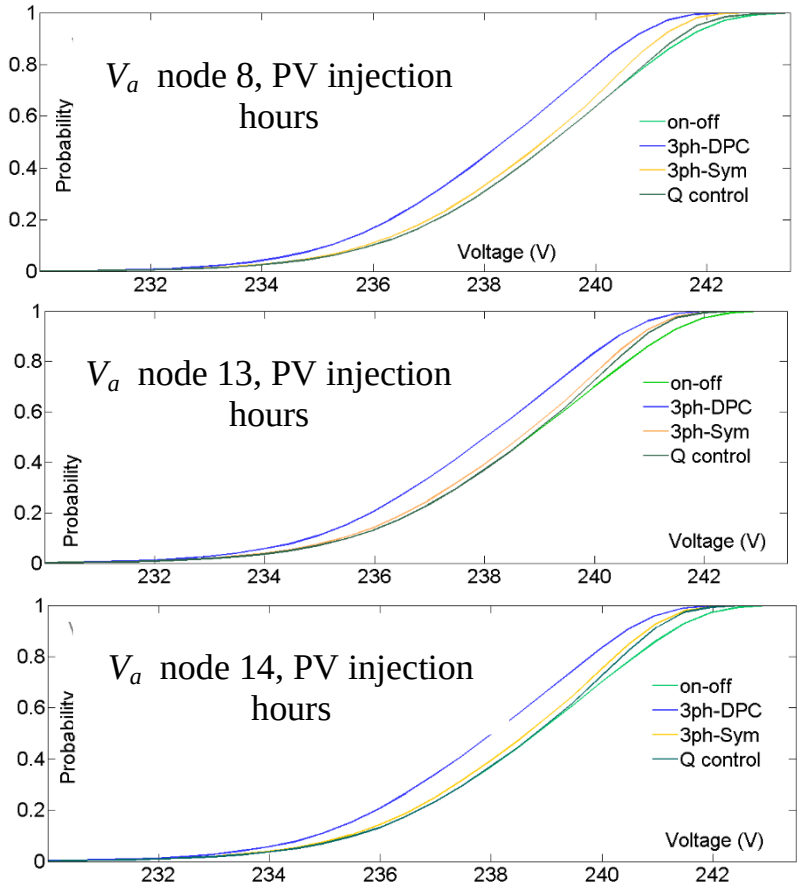

Figure 7.12: CDFs of phase voltages V_a at nodes 8, 13 (new PV nodes) and 14 (existing PV node) for the month of July

Similarly, Figure 7.13 clearly shows that the 3ph-DPC and the 3ph-SI schemes had a much more decisive effect on voltage unbalance compared to the other schemes in 100% of the simulated states for July. In all cases, the action of these two control schemes resulted in 50% reduction of the initial %VUF values.

Although the connections in the feeder are heavily unbalanced (all existing PV units connected to phase *a*, all loads connected to phase *c*), voltage unbalance never exceeded the 95-percentile limit of the EN 50160 standard (=2%). The reason is that both connected single-phase loads and PV units are quite small and do not significantly affect the operation of the feeder. Considering a further integration of PV generation, the %VUF at nodes 13 and 14 might increase and reach the upper acceptable limit. In such cases, the application of control strategies specifically tailored to address local voltage imbalances will be required.

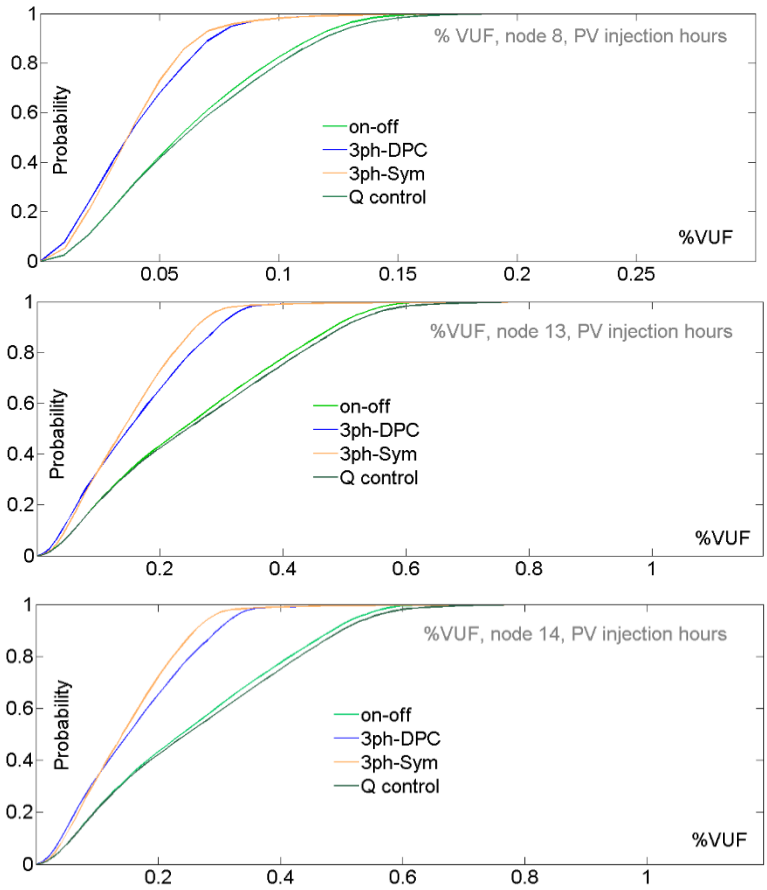

Figure 7.13: CDFs of %VUF at nodes 8, 13 (new PV nodes) and 14 (existing PV node) for the month of July

Regarding current magnitudes, the simulation of the feeder for a yearly period resulted in the same order of magnitude for current values considering all four control schemes. Moreover, the congestion risk was very low in all cases, all along the feeder. Segments 1-2, 4-5 and 6-7 have the highest current magnitudes, according to the probabilistic analysis, but there is no congestion risk. For evaluating the economic performance of the 4 controls, line losses E_{loss} were also computed for each network state. In the current configuration, the choice of the control scheme did not affect the amount of line losses in the feeder. This means that 3ph-DPC scheme can be applied without having any impact on the line losses in

the feeder while it delivers a much improved voltage profile, without modifying the injected PV power.

ii. *PV inverter sizing in the simulated feeder*

Based on the probabilistic simulation and the consideration of the available SM input, the maximum required power that needs to be supported by the new PV inverters was identified for all new PV nodes, considering the four control schemes. Given that the 3ph-DPC and the 3ph-SI schemes do not alter the total magnitude of the injected PV current, they resulted in the same power rating as the one in case the on-off control is applied. The reactive power control resulted in much higher requirements because its principle is based on the absorption of reactive power by the PV inverters. The injection of reactive power practically increases the value S_i that is required for the inverter (relation (8.16)). Table 7.2 gives the required power ratings for the new PV inverters:

Table 7.2: Minimum required power rating of PV inverter (kVA)

Control scheme:	on-off / 3ph-DPC/ 3ph-SI	Q control
node 13	4.54	8.48
node 11	4.11	6.04
node 8	3.62	8.80
node 6	2.85	3.39

Therefore, in an overall manner, the probabilistic analysis of the feeder highlighted the following points:

Advantage: It is techno-economically efficient to consider the connection of new PV units using 3-phase 4-wire inverters that integrate the 3ph-DPC scheme or 3ph-SI. 3ph-DPC has a much more decisive effect on voltage unbalance and magnitude without modifying the injected PV power. Its implementation would require inverters with power ratings similar to the ones required with currently applied on-off control.

Disadvantage: The use of three phase four-wire inverters is not allowed in the Europea LV network based on the current legislation because current flow in the neutral conductor is not allowed. However all existing three-phase LV feeders are unbalanced due to numerous single-phase loads and distributed generation units, necessarily resulting in current flows in the neutral conductor. In reality the action of the 3ph-DPC scheme would reduce the current flow in the neutral conductor. For this reason, based on the results of this simulation, distribution utili-

ties would clearly have an interest in considering this solution for the connection of new PV units in three-phase LV feeders. The voltage profile would be improved without inducing more line losses or requiring bigger power ratings for the inverters that integrate this new control scheme.

Chapter conclusions

Chapter 7 presented the adaptation of the basic probabilistic algorithm of Chapter 4 in such a way that it can simulate the action of different distributed time-varying control schemes against voltage rise and voltage unbalance. Five control schemes have been modeled and compared. Therefore, Chapter 7 presents a reliable long-term assessment of the considered control schemes, which considers an extensive range of possible system states rather than a set of deterministically defined ones. The stochasticity of nodal loads and generation and their interaction with the respective control schemes has been modeled, leading to a more refined design of each control strategy for a given feeder.

For the studied feeder, it was demonstrated that P/V droop control has indeed a decreasing effect on the voltage profile along the feeder while ensuring a gradual and network state aware energy curtailment at every node, which is not the case with the application of the traditionally applied on-off control (hard curtailment for longer periods). The control parameters tuning with the use of the probabilistic framework, demonstrated that customizing the reference voltage (V_{up}) in function of the position of a node in the feeder and applying a small droop slope (k) is efficient in terms of overvoltage mitigation and more conservative in terms of PV energy curtailment. This last argument validates the sixth argument (VI) of section 2.6, namely the argument that the benefit of different control schemes and other technical strategies will be more direct if they are refined based on a probabilistic simulation that uses feeder-specific historic measurements.

The simulation of the reactive power control scheme, the 3ph-DPC scheme and the 3ph-SI scheme demonstrated that distribution utilities would have a clear interest in considering the connection of new PV units in three-phase feeders, with the use of three-phase four-wire inverters integrating the three-phase damping control (3ph-DPC) scheme. The latter can decisively improve voltage magnitudes and unbalance without modifying the injected PV power and without inducing more line losses.

Chapter publications

The developments of Chapter 7 have been published in:

[1] V. Klonari, J.-F. Toubeau, T. L. Vandoorn, B. Meersman, De Grève, Zacharie, J. Lobry, and F. Vallée, “Probabilistic Framework for Evaluating Droop Control of Photovoltaic Inverters,” Electr. Power Syst. Res., vol. 129, pp. 1–9.

[2] V. Klonari, B. Meersman, D. Bozalakov, T. L. Vandoorn, L. Vandevelde, J. Lobry, and F. Vallée, “A Probabilistic Framework for Evaluating Voltage

Unbalance Mitigation by Photovoltaic Inverters," Sustain. Energy, Grids Networks, vol.71.

[3] V. Klonari, J.-F. Toubeau, Z. De Grève, T. L. Vandoorn, B. Meersman, J. Lobry, and F. Vallée, "Probabilistic assessment of P/V droop control of PV inverters," in 23d CIRED, 2015.

[4] V. Klonari, B. Meersman, D. Bozalakov, T. Vandoorn, J. Lobry, and F. Vallée, "Probabilistic Assessment of a Voltage Unbalance Mitigation Scheme implemented by Photovoltaic inverters," in Energycon, 2016.

Chapter references

[1] T. L. Vandoorn, J. De Kooning, B. Meersman, and L. Vandevelde, "Voltage-based droop control of renewables to avoid on-off oscillations caused by overvoltages," IEEE Trans. Power Deliv., vol. 28, no. 2, pp. 845–854, 2013.

[2] B. Meersman, B. Renders, L. Degroote, T. Vandoorn, and L. Vandevelde, "Three-phase inverter-connected DG-units and voltage unbalance," Electr. Power Syst. Res., vol. 81, no. 4, pp. 899–906, 2011.

[3] T. L. Vandoorn, B. Renders, L. Degroote, B. Meersman, and L. Vandevelde, "Active load control in islanded microgrids based on the grid voltage," IEEE Trans. Smart Grid, vol. 2, no. 1, pp. 127–139, 2011.

[4] D. E. Olivares, A. Mehrizi-Sani, A. H. Etemadi, C. A. Caezares, R. Iravani, M. Kazerani, A. H. Hajimiragha, O. Gomis-Bellmunt, M. Saeedifard, R. Palma-Behnke, G. A. Jimenez-Estevez, and N. D. Hatziargyriou, "Trends in microgrid control," IEEE Trans. Smart Grid, vol. 5, no. 4, pp. 1905–1919, 2014.

[5] M. H. J. Bollen and F. Hassan, "Probabilistic Methods for Design of Distribution Feeders, in Integration of Distributed Generation Sources in the Power System," in Integration of Distributed Generation in the Power System, 2011.

[6] F. Ruiz-Rodriguez, J. Hernandez, and F. Jurado, "Probabilistic load flow for radial distribution networks with photovoltaic generators," IET Renew. Power Gener., vol. 6, pp. 110–121, 2012.

[7] M. Au-yeung, G. M. a Vanalme, J. M. a Myrzik, P. Karaliolios, M. Bongaerts, J. Bozelie, and W. L. Kling, "Development of a Voltage and Frequency Control Strategy for an Autonomous LV Network with Distributed Generators," Univ. Power Eng. Conf. UPEC 2009 Proc. 44th Int., no. May 2009, pp. 0–4, 2009.

[8] A. Engler and N. Soultanis, "Droop control in LV-grids," 2005 Int. Conf. Futur. Power Syst., pp. 2–4, 2005.

[9] J. M. Guerrero, J. Matas, L. G. De Vicuña, M. Castilla, and J. Miret, "Wireless-control strategy for parallel operation of distributed-generation inverters," IEEE Trans. Ind. Electron., vol. 53, no. 5, pp. 1461–1470, 2006.

[10] F. Katiraei and M. R. Iravani, “Power management strategies for a microgrid with multiple distributed generation units,” IEEE Trans. Power Syst., vol. 21, no. 4, pp. 1821–1831, 2006.

[11] H. Laaksonen, P. Saari, and R. Komulainen, “Voltage and frequency control of inverter based weak LV network microgrid,” 2005 Int. Conf. Futur. Power Syst., p. 6 pp.–6, 2005.

[12] R. H. Lasseter and P. Paigi, “Microgrid: A conceptual solution,” in PESC Record - IEEE Annual Power Electronics Specialists Conference, 2004, vol. 6, pp. 4285–4290.

[13] Y. W. Li and C. N. Kao, “An accurate power control strategy for power-electronics-interfaced distributed generation units operating in a low-voltage multibus microgrid,” IEEE Trans. Power Electron., vol. 24, no. 12, pp. 2977–2988, 2009.

[14] C. K. Sao and P. W. Lehn, “Intentional islanded operation of converter fed microgrids,” in 2006 IEEE Power Engineering Society General Meeting, 2006, p. 6 pp.

[15] C. K. Sao and P. W. Lehn, “Control and power management of converter fed microgrids,” IEEE Trans. Power Syst., vol. 23, no. 3, pp. 1088–1098, 2008.

[16] T. L. Vandoorn, B. Meersman, L. Degroote, B. Renders, and L. Vandevelde, “A control strategy for islanded microgrids with DC-link voltage control,” IEEE Trans. Power Deliv., vol. 26, no. 2, pp. 703–713, 2011.

[17] M. K. C.Dierckxsens, A.Woyte, B.Bletterie, A.Zegers, W.Deprez, A.Dexters, K.Van Roey, J.Lemmens, R.Poosen, J.Lowette, K.Nulens, Y.T.Fawzy, B.Blazic, B.Uljanic, “Cost-effective integration of photovoltaics in existing distribution grids,” 2012.

[18] EN50160, “Voltage characteristics of electricity supplied by public electricity networks,” 2012.

[19] S. I. Gkavanoudis and C. S. Demoulias, “A control strategy for enhancing the Fault Ride-Through capability of a microgrid during balanced and unbalanced grid voltage sags,” Sustain. Energy, Grids Networks, vol. 3, pp. 1–11, Sep. 2015.

[20] B. Renders, K. De Gussemé, W. R. Ryckaert, and L. Vandevelde, “Converter-connected distributed generation units with integrated harmonic

voltage damping and harmonic current compensation function," Electr. Power Syst. Res., vol. 79, no. 1, pp. 65–70, 2009.

[21] EPRI, Voltage Unbalance: Power Quality Issues , Related Standards and Mitigation Techniques Effect of Unbalanced Voltage on End Use Equipment Performance. 2000.

[22] S. Dierkes, F. Bennewitz, M. Maercks, L. Verheggen, and A. Moser, "Impact of Distributed Reactive Power Control of Renewable Energy Sources in Smart Grids on Voltage Stability of the Power System," 2014.

[23] L. Degroote, B. Renders, B. Meersman, and L. Vandevelde, "Neutral-point shifting and voltage unbalance due to single-phase DG units in low voltage distribution networks," 2009 IEEE Bucharest PowerTech Innov. Ideas Towar. Electr. Grid Futur., pp. 1–8, 2009.

[24] D. Graovac, V. A. Katić, and A. Rufer, "Power quality problems compensation with universal power quality conditioning system," IEEE Trans. Power Deliv., vol. 22, no. 2, pp. 968–976, 2007.

[25] M. Savaghebi, A. Jalilian, J. C. Vasquez, and J. M. Guerrero, "Autonomous voltage unbalance compensation in an islanded droop-controlled microgrid," IEEE Trans. Ind. Electron., vol. 60, no. 4, pp. 1390–1402, 2013.

[26] D. Bozalakov, T. L. Vandoorn, B. Meersman, C. Demoulias, and L. Vandevelde, "Voltage dip mitigation capabilities of three-phase damping control strategy," Electr. Power Syst. Res., vol. 121, pp. 192–199, Apr. 2015.

[27] C. E. I., "Reference technical rules for the connection of active and passive users to the LV electrical utilities," 2012.

[28] L. Handelsman, "Implementing Advanced Grid Codes," in Eilat-Eilot Conference, 2012, no. November.

[29] Bart Meersman, "Regeling van driefasige invertorgekoppelde decentrale generatoren met betrekking tot de verbetering van de netkwaliteit," 2012.

Chapter 8 Statistical Long-term Simulation of Electric Vehicles and Demand Side Management Applications

Highlights

- *The probabilistic algorithm is adapted for simulating three strategies that deploy nodal loads modification (Plug-in Hybrid Vehicles charging station, e-bikes charging stations and Demand Side Management).*
- *The three strategies are simulated in a three-phase Low Voltage feeder and their time-varying effect on network operation indices is assessed based on the analysis of an extensive range of possible system states and the use of feeder-specific smart metering historic measurements.*
- *The simulation gives an information-rich evaluation of the integration of such strategies in Low Voltage feeders. Nevertheless, their simulation in a fully sequential Monte Carlo environment would allow avoiding short-term unrealistic transitions between successive network states.*

Chapter 8 presents the integration of Plug-in Hybrid Vehicles (PHEVs), storage and demand side management (DSM) models in the basic structure of the probabilistic framework. The impact of such strategies on the operation of the network and on end-users energy expenses is again evaluated with a long-term statistical view. Each network state (or each ¼-hourly time step) is analyzed independently from the previous and the following one, considering SM measurements that have been recorded for the respective time step (Pseudo-Sequential configuration). The modeled strategies are simulated in the feeder that was presented in Chapter 5. Note that the latter is slightly adapted to the needs of each simulation. The objective of this assessment is to determine statistical distributions and boundary values for a set of indices (operational and economic) that concern the integration of future appliances in LV feeders like electric vehicles, demand side management tools and other examples.

8.1 Electric Vehicles with coordinated charging

The developments presented in the present section have resulted from the collaboration of our research team with the "Net-Zero Energy Efficiency on City Districts" ERA chair of the Research Institute for Energy (University of Mons). This study examines the effect of several PHEVs fleets (distinct by the number of vehicles) on the electricity demand profile of a University building in Mons (Belgium) under a real-time pricing (RTP) scheme.

Electric vehicles (EVs) including hybrid electric vehicles (HEVs), battery electric vehicles (BEVs) and plug-in hybrid electric vehicles (PHEVs) have been experiencing considerable development in recent years [1], [2] and EVs are now commercially available from a number of car manufacturers worldwide. The benefits of using vehicle energy have urged many researchers to work on modeling several EVs concepts. Special attention has been given to charging and discharging algorithms for gridable vehicles (i.e. BEVs or PHEVs with grid capacity) [3], optimal scheduling for vehicle-to-grid (V2G) operation [4] and the impact of plug-in EVs on power systems [5], [6]. The V2G concept could contribute to the increase of the quality and performance of a distribution network in terms of system efficiency, stability and reliability. EVs can act either as distributed storage devices delivering power to a grid at peak hours or serve as load.

A PHEV, more specifically, is a hybrid vehicle equipped with a larger battery pack. It uses electricity when its battery state of charge (SoC) is high; otherwise its internal combustion engine is used consuming gasoline [7]. The impact on the distribution grid of PHEVs charging is non-negligible. PHEVs consume a large amount of electricity which could lead to high undesirable peaks in the electric consumption. It is estimated that the electrical consumption for charging PHEVs

might take up to 5% of total electricity production in Belgium by 2030 [8]. The two main places to recharge PHEVs batteries are either at home or in a car park, corporate or public. In this study, we focus on the latter.

A V2G system could be used through a demand response (DR) mechanism to reduce peak electricity usage and to incentivize load shedding. Currently, the DR schemes are usually deployed through either incentive-based or time-based rates schemes. While in the incentive-based DR schemes end-users enroll voluntarily in certain rewarding programs, time-based rates schemes rely on dynamic pricing of electricity to regulate electricity consumption. The time-based rates scheme can have many different forms. The most common but not limited to are the time-of-use pricing (TOUP), the critical peak pricing (CPP) and the real-time pricing (RTP) [9]. The power load could be managed by charging the PHEVs when the electricity price received from the utility is lower and discharge the PHEVs batteries to the grid when prices are higher. Shifting load can effectively reduce the impact of the PHEVs fleet on the grid and this task can be achieved by charging and discharging coordination.

As initially mentioned, in this study, we examine the effect of several PHEVs fleets, distinct by the number of vehicles, on the electricity demand profile of a university building in Mons, Belgium under a RTP scheme. Our goal is to optimize the charging-discharging process of the PHEVs so as to minimize the energy demand and thus the electricity cost of the building. Our second goal is to examine the impact of the charging process on the LV distribution network. The probabilistic algorithms developed in this thesis have been used to evaluate the interaction of the PHEVs when they are connected to a LV feeder with distributed PV units.

8.1.1 *Modeling and Assumptions*

A. Load Scenarios and Pricing

We chose two typical daily winter and summer electrical load profiles from an available set of a university building load measurements. The load profile covers 10 hours, from 8 am to 6 pm, and the electrical energy consumption is available on a ¼-hourly time base as shown in Figure 8.1.

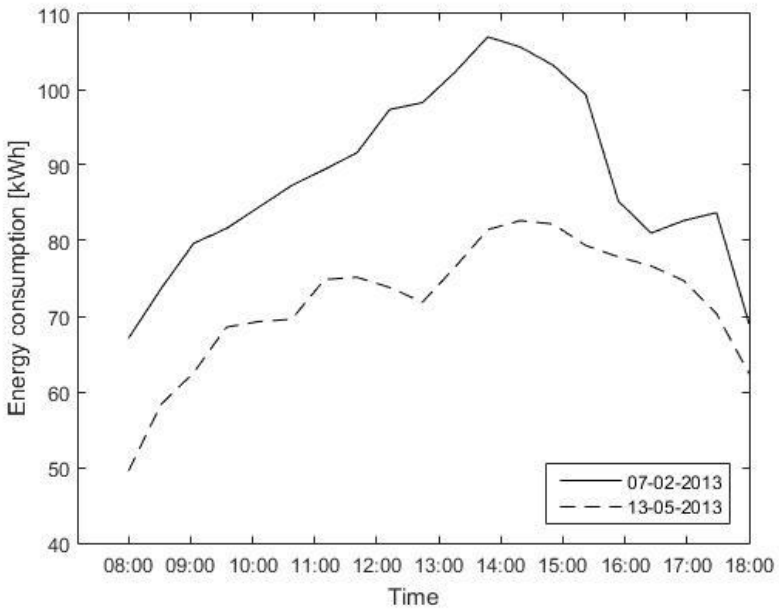

Figure 8.1: University building load during a typical day in February and May 2013

We considered this timetable taking into account the usual working hours at the University. The PHEVs charging-discharging optimization as well as the probabilistic analysis regarding the impact of the PHEVs on the LV network takes place during these hours. Figure 8.2 shows the used pricing data. Electricity cost reaches its peak value between 4 pm and 7 pm.

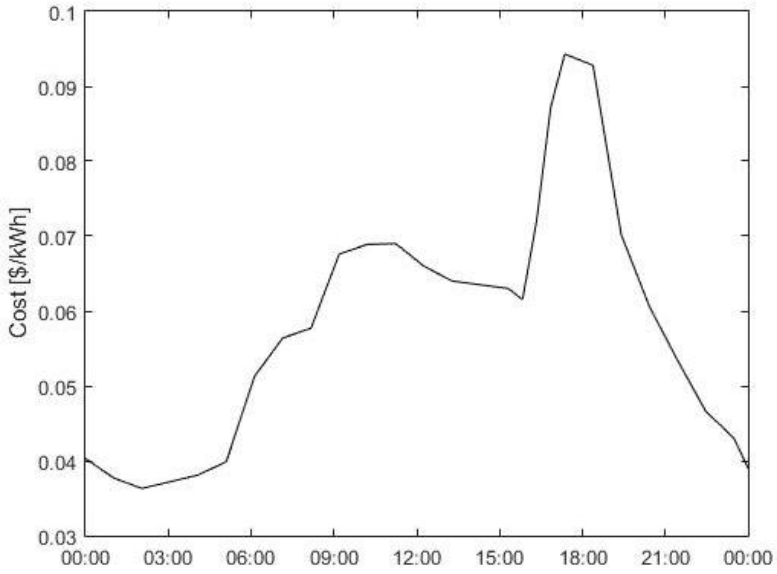

Figure 8.2: Electricity tariff (spot price) [12]

B. PHEVs Specifications

Each PHEVs battery is equipped with a maximum capacity of C_{max}^{PHEV} = 10.15 kWh and is characterized by its all-electric range (AER). AER is the total distance that the PHEVs can cover running on an all-electric mode. Different PHEVs require different amounts of energy based on their type. The energy required to accomplish their AER is called electrical energy per kilometer. In this work, it is selected equal to 0.37 kWh/km [12]. Assuming an energy conversion efficiency η^{PHEV} = 0.88 from the AC energy absorbed from LV to DC energy stored in the battery of the vehicle, a full charge would require 11.53 kWh. Among the different available standards and codes for the EVs charging, we have chosen the SAE J1772. More specifically the AC level-1 has been selected which defines single phase charging at 120V, 16A and 1.92 kW of power. This standard defines a common EV and supply equipment vehicle conductive charging method. Although this standard defines only the charging process (thus, a unidirectional flow of energy), in this study, we have considered a bidirectional energy flow of energy. It has been assumed that the discharging rate is equal to the charging rate. Note that fast charging was not considered as it requires higher voltage levels and a higher short-circuit power which induces extra investments increasing the total implementation costs.

C. PHEVs Arrivals-Departures and Charging-Discharging Period

In this study we have considered that the batteries of all the vehicles have been fully charged when departing from home. It has been also assumed that all PHEVs run on an all-electric mode until they arrive at the university. Assuming that a fully charged PHEV drives s_l kilometers on electricity (which is nothing else that the AER), the SoC of a vehicle driven on a distance of d kilometers when arriving at university is calculated as:

$$\%SoC = \begin{cases} 100\ \frac{s_l - d}{s_l}, & d \le s_l \\ 0, & d > s_l \end{cases} \tag{8.1}$$

In this work, the length of the trip and consequently the SoC of each PHEV upon arrival ($s_{l_i}^0$) is calculated using the normal distribution taking as base case (mean) value d=10 km [13] and standard deviation σ = 3 km. These values have been selected based on the fact that Belgium is a country with high density population and the distances are in general short. In addition, there is an ongoing research in university of Mons for analyzing the commuting behavior of its personnel. Upon its completion we will be able to modify accordingly the used base case and add more scenarios. In this study, three different scenarios of PHEVs fleets have been considered, including 10, 20 and 50 PHEVs. The scheduling horizon is divided into a set of Q_{ev} time slots (having the same duration of 30

minutes). Thus, the duration of a 10 h period is divided into 20 time slots (Q_{ev} =20) for a more realistic and detailed time analysis. It has been also assumed that all the vehicles arrive at the university at the beginning of the time slot n=1 (8 am) and depart at the end of the time slot q= Q_{ev} (6 pm). Upon their arrival the PHEVs are immediately available for charging-discharging or they can remain in standby mode, whatever the considered time slot n.

D. Problem Formulation

The objective is to find the optimum time slots during which the PHEVs should charge/discharge in order to minimize the building's energy demand under the current pricing scheme. A charging-discharging schedule of the PHEVs batteries is therefore to be determined in function of the pricing scheme and the current SoC of the batteries. Regardless the charging-discharging schedule during the day, a constraint is imposed which expresses that the SoC of all the batteries is at least 50% by the time the PHEVs depart (last time slot).

There exist two kinds of loads: fixed and adjustable. In this work, the fixed load is the building load demand and is characterized for each time slot q by the overall energy consumption p_F^q. The deferrable load is the load of the electric vehicles ($i=1, \ldots, I$) and it is the only load that can be rescheduled according to electricity tariff.

In order to model the charging-discharging process of the vehicles, we introduce three sets of variables. First, we consider two sets of binary variables: ξ_i^q and σ_i^q which are defined for every vehicle and every time slot. If the *i-th* PHEV is charging during the time slot q, ξ_i^q is equal to 1, otherwise it is equal to 0. In a similar way, whether the PHEV is discharging or not, σ_i^q is equal to 1 or 0. The charging and discharging rates are constant and they are both worth 1.92 kW according to the SAE J1772. We denote as C^{PHEV} and d^{PHEV} the energy obtained and given from charging and discharging during one time slot respectively. The SoC of the *i-th* PHEV for the time slot q is represented by the continuous non-negative variable $s_{l_i}^q$. Recall that all the vehicles are characterized by their initial SoC ($s_{l_i}^0$). The SoC of each PHEV in a time slot depends on its previous time slot and on the charging/discharging rates. It can be estimated according to the following equations and constraints:

$$s_{l_i}^q = s_{l_i}^0 + \xi_i^q \cdot C^{PHEV} - \sigma_i^q \cdot d^{PHEV} \quad \forall i \in I, q = 1 \tag{8.2}$$

$$s_{l_i}^q = s_{l_i}^{q-1} + \xi_i^q \cdot C^{PHEV} - \sigma_i^q \cdot d^{PHEV} \quad \forall i \in I, q > 1 \tag{8.3}$$

$$\xi_i^q + \sigma_i^q \leq 1 \qquad \forall i \in I, \forall q \in Q_{ev} \tag{8.4}$$

$$s_{l_i}^q \leq C^{PHEV} \quad \forall i \in I, \forall q \in Q_{ev} \tag{8.5}$$

$$s_{l_i}^{q} \geq 50\%\, C^{PHEV} \quad \forall i \in I, q = Q_{ev} \tag{8.6}$$

Constraint (8.4) guarantees that in every time slot, PHEVs can be only in charging, discharging or standby mode. The other constraints ensure that the SoC of the PHEVs cannot exceed the maximum battery capacity (see (8.5)) at any time and that the battery of each PHEV will be charged at least 50% of its total capacity before departure (see (8.6)). The following constraint establishes the energy balance between the input and output electric power of the system in each time slot:

$$y^{q} + \sum_{i \in I} \sigma_i^{q} \cdot d^{PHEV} = p_F^{q} + \frac{1}{\eta^{PHEV}} \sum_{i \in I} \xi_i^{q} \cdot C^{PHEV} \tag{8.7}$$

where y^q is the energy required from the LV network at each time slot to cover the building load demand and the PHEVs charging load. Finally, the objective function to be minimized is:

$$min \sum_{q \in Q_{ev}} e^{q}\, y^{q} \tag{8.8}$$

where e^n is the cost of energy absorbed from the grid according to the current pricing scheme at time slot q. A mixed integer linear programming (MILP) model is run in order to schedule the energy usage plan over the time horizon $q = 1, \ldots, Q_{ev}$.

8.1.2 *Results*

A. Uncoordinated Charging

For the uncoordinated charging scenario, there is no control on the charging process. Uncoordinated charging indicates that the batteries of the PHEVs start charging immediately when plugged in. The vehicles in every case start charging at n=1 (i.e. 8 pm) and continue to charge until the SoC of the battery reaches 100%, regardless the cost of energy at any time slot. The impact of uncoordinated charging on the buildings' energy consumption from the LV network is shown in Figure 8.3 and Figure 8.4.

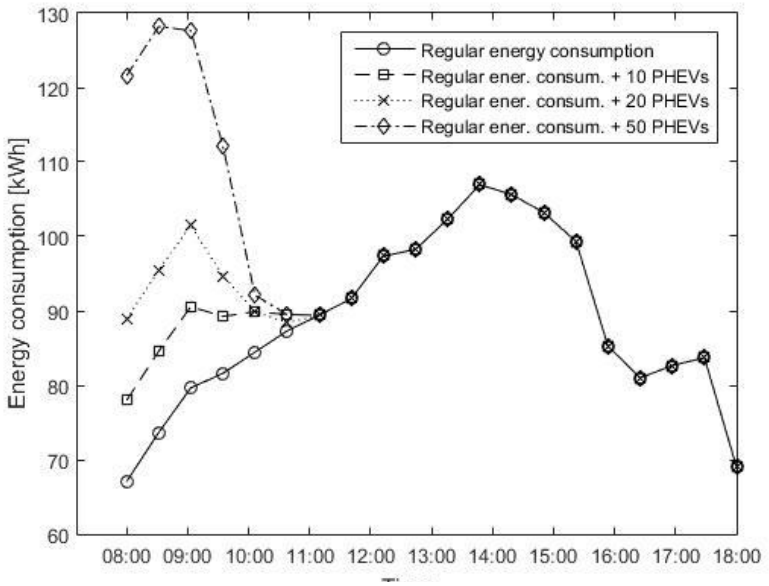

Figure 8.3: Energy consumption of the university building for uncoordinated charging (7th February 2013)

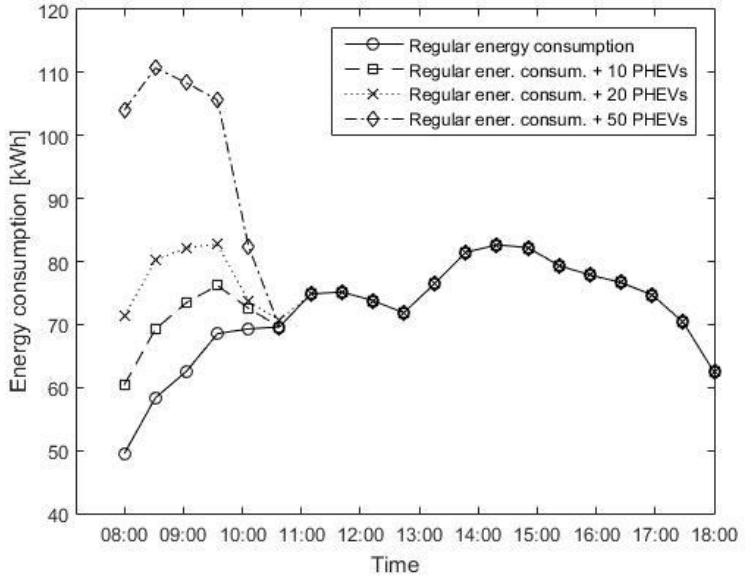

Figure 8.4: Energy consumption of the university building for uncoordinated charging (13th May 2013)

A similar pattern is observed in both Figure 8.3 and Figure 8.4. The total energy consumption includes the regular load demand of the building and the charging of the PHEVs. We can see that in both scenarios, due to the lack of any control in the charging process, all the PHEVs start charging when plugged in and until 11:00 a.m. all the vehicles have already been charged. As a result of this

behavior, the total energy required is substantially increased during the first six time slots. After that, all the PHEVs batteries are fully charged and the energy consumption is normalized again. The increase of the number of PHEVs leads to a significant increase in energy demand. It should be noted that within this scenario, no PHEVs discharging takes place between 8 am and 6 pm and all the PHEVs are fully charged upon departure from university.

B. Coordinated Charging-Discharging

In the previous paragraph the charging process of the PHEVs occurred immediately after plug-in ignoring the pricing scheme. In this paragraph, the idea is to show how the optimal charging-discharging control of the PHEVs leads to the minimization of the energy demand and thus of the electricity cost of the building. The charging-discharging times of the PHEVs are decided by the model along with the required energy to cover the building's load. The impact of the coordinated PHEVs charging-discharging on the building's energy consumption is illustrated in Figure 8.5 and Figure 8.6.

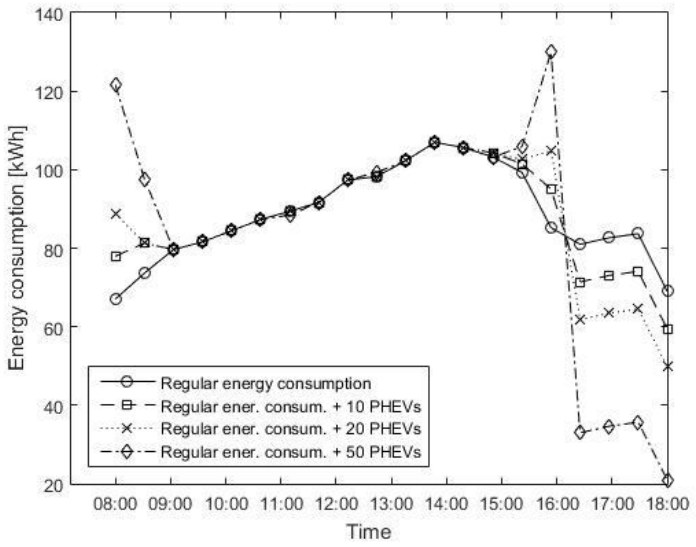

Figure 8.5: Energy consumption of the university building for coordinated charging-discharging (7th February 2013)

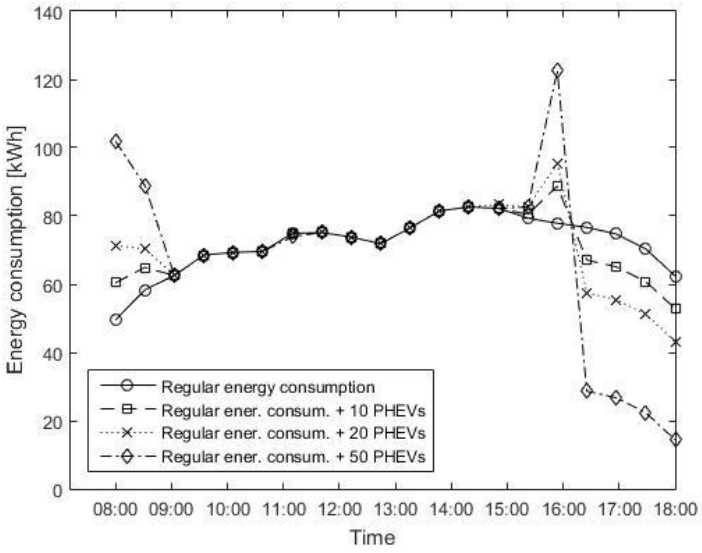

Figure 8.6: Energy consumption of the university building for coordinated charging-discharging (13th May 2013)

The two figures indicate one again similar patterns of the PHEVs charging-discharging process. The optimization algorithm tries to minimize the energy consumption when the electricity prices are high. Consequently, the PHEVs batteries charge mainly during the early hours and in the afternoon during the time-slots just before the electricity price starts to increase. During the electricity price peak hours (4pm – 7pm), the PHEVs mostly discharge resulting in a substantial decrease of the total required energy. The increase of the number of the PHEVs leads to a proportional and significant reduction of the total energy demand. Indicatively, the total energy requirement during the last time slot (5.30 pm – 6.00 pm) for i=50 PHEVs in both scenarios (winter and summer) has been reduced more than 70%.

The peak in load demand (mostly visible in the case of 50 PHEVs) is increased around 4 pm ($q=16$) before starting to decrease due to the constraint imposing that all the PHEVs must be delivered at the end of the time horizon with a minimum SoC=50%. In the coordinated charging-discharging control, the PHEVs are not forced to reach their maximum battery capacity level but only to satisfy the 50% SoC constraint. Thus, the PHEVs are either in stand-by mode (9 am -3 pm) or in charge mode (when the electricity price is the lowest) and in discharge mode (when electricity price is higher, 4.30 pm– 6.00 pm). Table 8.1 shows the total cost of energy per day for the simulated load scenarios under the current pricing.

Table 8.1: Total cost of energy for all scenarios ($)

Month	Reg-ul. load	10 PHEVs		20 PHEVs		50 PHEVs	
		Unco-ordinat-	Coordi-nated	Unco-ordinat-	Coordi-nated	Unco-ordinat-	Coordi-nated
Feb.	121.9	125.1	120.5	127.4	118.5	134.5	113.1
May	99.6	102.4	98.1	104.9	96.3	112.5	90.8

In all cases, the coordinated charging-discharging process results in the lowest cost/day. It is worth mentioning that the cost of the coordinated process (including the additional PHEV charging load cost) is even lower than the cost of the regular load (no PHEVs charging included).

The contribution of EVs in minimizing the electricity cost of the building is undeniable but it brings forward an important aspect. It is very possible that some EV owners will have to leave university with a lower SoC level compared to the one they had when arrived in the morning (the constraint only imposes final SoC $\geq$ 50% of total capacity). In case the EVs are offered from university to its personnel, electricity cost could be minimized without taking into account the EV drivers. But in case that people own the EVs and have to contribute in paying university's electricity bill, some incentives have to be granted to motivate their participation. In private/corporate buildings for instance, companies could offer the EVs charging to be free of charge for the owners in exchange of participating in the scheme. In public buildings, the state could offer other kind of discounts/privileges to the participants such as reduced electricity tariffs for their house electricity bill or further tax reductions. Furthermore, taking into consideration that the participation in such schemes could reduce the vehicles battery lifetime, an additional incentive for the EVs owners could be the financial co-contribution of the beneficiaries for buying new batteries for the vehicles.

8.1.3 *Impact on the LV Network*

The presented problem formulation addresses the optimal time allocation of PHEVs charging so as to minimize the building's energy demand over the concerned period. However, the integration of a PHEVs installation in a LV feeder involves an extra complexity regarding the high volatility of loads and distributed generation over time. Let us consider the previous PHEVs charging schedule as a day-ahead schedule based on a day-ahead forecasting for a day in February and in May. The first goal is to determine the effect of network state uncertainty on the optimized parameters (the energy demand of the building in the presented formulation). The second goal is to investigate how PHEVs integration, with the

proposed charging schedules (coordinated and uncoordinated) would impact the operation indices of the network.

To address these issues, the previously considered university building (paragraphs 8.1.2 and 8.2.2) is considered to be connected to the LV feeder of figure 8.7 while, for the other nodes, residential SM datasets (selected among the ones described in Chapter 3) have been considered. Two different scenarios of PHEVs fleets have been studied; including respectively 10 and 20 PHEVs. The feeder is simulated in steady-state operation with the use of the probabilistic algorithms presented in this thesis. The objective is to simulate the variability of nodal power exchange based on the available datasets. Concerning the university campus, ¼-hourly energy flow datasets are used, recorded in 2013-2014 at the previously considered building. Given the small size, the technical parameters and the voltage level of the network, the scenario of 50 PHEVs cannot be considered because it results in line congestion and important voltage dips. Only the scenarios of 10 and 20 PHEVs are therefore treated.

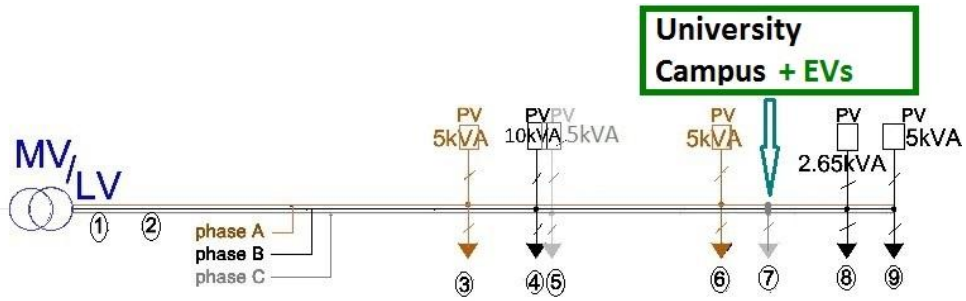

Figure 8.7: The simulated three-phase LV feeder incorporating the University building

Figure 8.8(i) and Figure 8.8(iii) show the statistical distributions of the half-hourly energy demand in a typical February day for three different configurations. The first configuration is the base scenario that considers no PHEVs connected to the building. The other two configurations apply the uncoordinated and the coordinated charging schedule, each one considering both scenarios of 10 and 20 PHEVs fleets. The cumulative distribution functions (CDFs) of probability in Figure 8.8(i) and Figure 8.8(iii), in blue and green color, practically illustrate the distribution of values that the energy demand could take in case the uncoordinated and coordinated PHEVs charging would be applied in the building. Determining an expected range of values is possible thanks to the use of the MC simulation. The reliability of the probabilistic estimation is reinforced with the use of the SM input for the respective month.

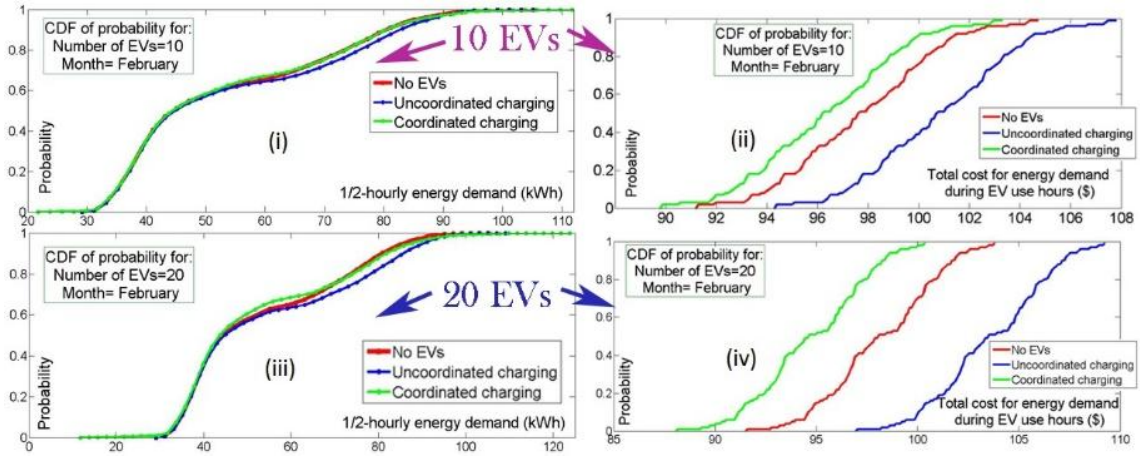

Figure 8.8: Half-hourly energy demand ((i) and (iii)) and total energy demand cost (((ii) and (iv))) during the PHEVs use hours, in a typical February day, considering 10 and 20 PHEVs fleets.

Basically, in this example, the optimization algorithm of paragraph 8.2.2 can determine the optimal schedule for PHEVs charging based on day ahead forecasted values and the probabilistic analysis can provide estimation on the possible range of values that the various parameters might take in reality.

Regarding energy demand, the CDFs of Figures 8.8(i) and 8.8(iii) demonstrate that in 85% of the simulated network states the optimal coordination of PHEVs charging implies half-hourly energy demand values that are almost equal to the ones of the configuration without PHEVs. In 15% of the simulated network states, the coordinated charging leads to energy demand that is lower than the ones of the case without PHEVs. Similarly, Figures 8.8(ii) and 8.8(iv) show that the optimal coordination of PHEVs charging reduces the daily cost for energy demand during PHEVs use hours in the total number of the simulated February days. This reduction is in the range of 2$ and 5$ in the 10 and 20 vehicles fleets' scenarios respectively, comparing to the case without PHEVs. Very similar outputs were obtained with the simulation of a typical day in May. The reduction in energy costs is even more decisive when one compares with the respective outputs for the uncoordinated PHEVs charging case (Figures 8.8(ii) and 8.8(iv)).

Regarding the impact of PHEVs integration on the operational indices of the feeder, the voltage variation snapshots of Figures 8.9(i), (ii) and (iii) show that both the coordinated and the uncoordinated charging strategies affect phase voltages at the PCC of the university building with the feeder (node 7), in a typical day in May, during a few time slots. The uncoordinated charging induced significant voltage dips during consecutive time slots in the morning. The coordinated charging pushes voltage magnitudes close to the lower acceptable limit of EN 50160 standard in the afternoon. Given the even higher energy demand in Febru-

ary, the added demand for PHEVs charging may lead to more frequent undervoltage events. For a set of consecutive simulated network states in February, Figure 8.9(iv) shows that the voltage dip at node 7 is bigger and longer in case of uncoordinated PHEVs charging while it can be avoided by applying the coordinated charging strategy, in morning hours. The coordinated charging leads to under voltage during one time slot in the afternoon.

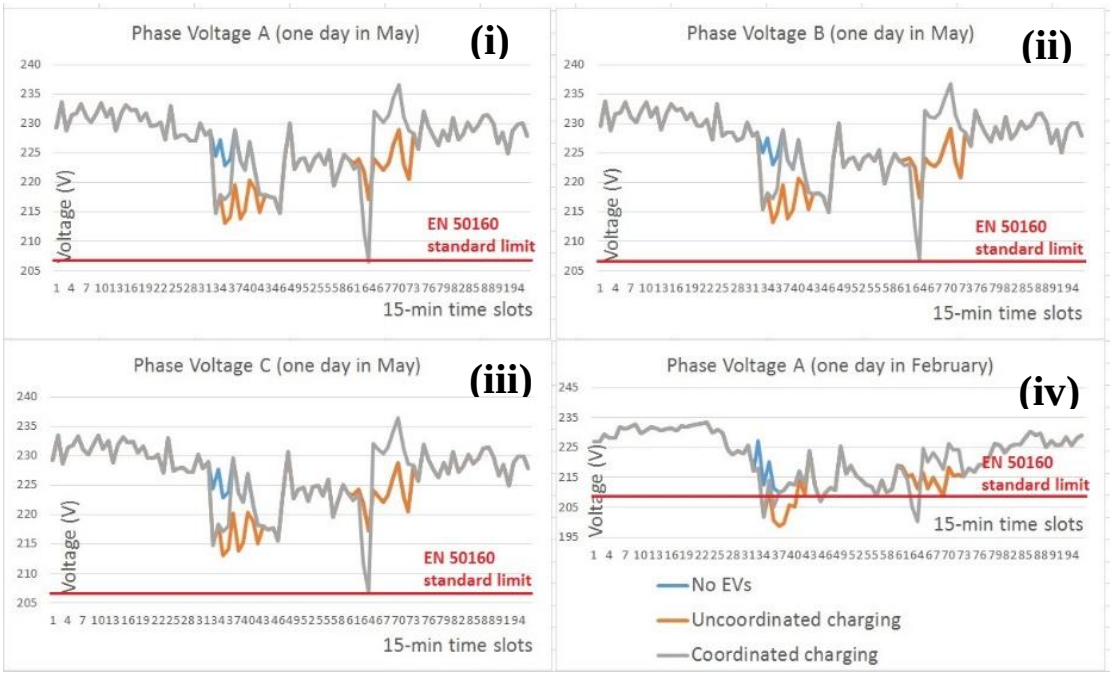

Figure 8.9: Phase voltage variation during a typical day in May ((i), (ii), (iii)) and EN 50160 standard violation (undervoltage) on a typical day in February (iv) at the PCC of the university building to the feeder

Concerning the impact on %VUF at the PCC of the university building with the network, the integration of EVs does not significantly affect this parameter (Figure 8.10). According to the EN 50160 standard, %VUF should not exceed the value of 2% during more than 5% of the operation time. This condition remains quite far from being violated before and after the integration of EVs. One should note that although all residential users are connected to the feeder in single-phase mode, the university building is connected in three-phase mode given its higher energy demand compared to them. As far as congestion risk is concerned, it has been computed that the integration of PHEVs only slightly increases line current values, given the three-phase connection of the university building.

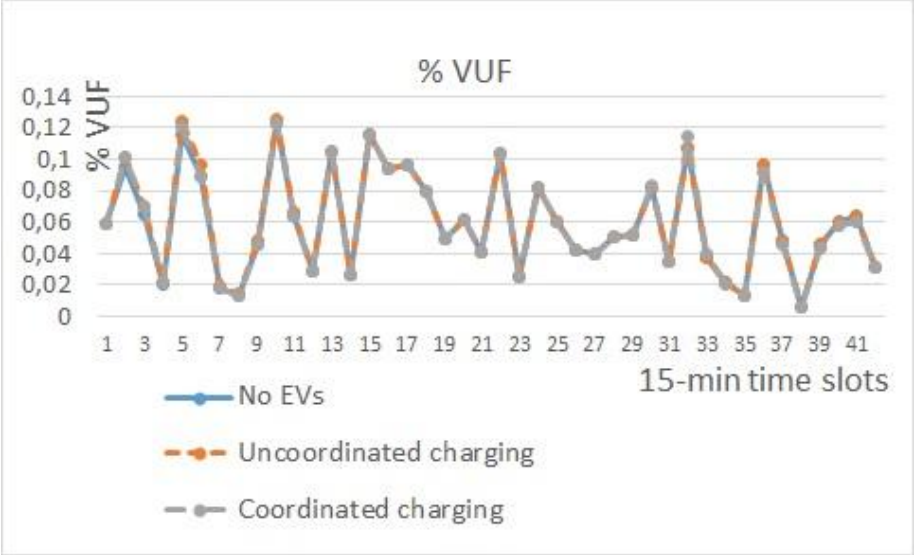

Figure 8.10: %VUF variation during a typical day in May at the PCC of the university building to the feeder

Based on the outputs of the probabilistic analysis, one can conclude with two principal outcomes concerning PHEVs integration in such a LV feeder. Firstly, the simulation of a large range of possible network states demonstrated that applying optimally coordinated charging is very valuable as it can ensure the cost-effectiveness of PHEVs integration for the respective network user. Secondly, the importance of including network operation parameters in the formulation of the problem is highlighted and greatly recommended. In such a way, PHEVs integration can be profitable for the respective user without inducing power quality problems to the other users and high operational expenses to the DSO.

8.2 Electric Bikes sharing system

This second paragraph of Chapter 8 presents the integration of an electric bike (e-bike) sharing system in a LV feeder. The modeled e-bike charging stations are equipped with PV panels and a PV battery to assist the charging process when there is no excess energy available in the network. The stochastic character of such distributed systems (PV units and e-bike charging stations), their interaction and their impact on network operation are studied with the use of the probabilistic framework. The developments presented in this section have also resulted from the collaboration of our research team with the "Net-Zero Energy Efficiency on City Districts" ERA chair of the Research Institute for Energy (University of Mons).

8.2.1 *E-bike sharing systems*

Bike sharing scheme is a transportation alternative system that has been rapidly growing in popularity across the world. Global concerns regarding climate change, environmental pollution, unstable fuel prices and energy security make bike sharing a mobility strategy that could assist in addressing many of these concerns [12] Many cities around the world have invested on bike sharing schemes in order to improve the sustainability of their transportation systems and in the same time reduce their dependency on the private motor vehicle [13]. Bike sharing can provide public transportation services, especially short trip demands that are frequently inadequately served by the fixed route public transit [14]. Bike share systems have been developing continuously over the last two decades aiming at evolving into fully automated, secure and cost-effective systems and have been installed in more than 100 cities worldwide.

Although the impact of EVs and PHEVs has been addressed explicitly in the literature [15–18], this is not the case with electric bikes. The main concept of vehicle-to-grid (V2G) applications which are only implemented through EV, is the potential ability of the vehicles to act as instantly available distributed energy storage devices allowing for a direct flow of power into the distribution network [19]. The high capacity of EV batteries along with the increasing purchase tendency of EV [20] have lead many electricity providers to evaluate and assess potential bidirectional interaction between EV and the electric network. However, this is not the case with the e-bikes. The reduced battery capacity, the lack of standard codes and most important the fact that e-bike market has not grown satisfactorily have held the research between e-bikes and the electric grid limited.

This section presents the design of an e-bike sharing system, in terms of system components and user mobility patterns, and simulates the integration of the

designed system in the LV network. The basic structure of the probabilistic algorithm presented in Chapter 4 is reformed such that it simulates the interaction of the e-bike charging stations with the network. Residential SM energy data, like the ones presented in Chapter 3, are used for simulating nodal power exchanges in the LV network. The e-bike charging stations are equipped with PV panels and a PV battery to assist the charging process when there is no excess energy available in the grid.

8.2.2 *System components*

A. *Electric Bike Technology*

E-bikes are split in two main categories; the 'throttle' type e-bikes or powered bicycles (PB) and the 'pedelec' e-bikes or power assisted bicycles (PAB). The PB bikes are equipped with a switch on the handlebar which allows the user to turn the motor on/off and/or vary its power. In 'pedelec' alternative system, the motor only works in response of user's pedaling. In many countries is it required by law that the user is pedaling for the motor to work. In Europe, e-bikes are classified as regular bikes only when they are equipped with an "auxiliary electric motor having a maximum continuous rated power of 250 W and of which the output is progressively reduced and finally cut-off as the vehicle reaches a speed of 25 km/h, or sooner, if the cyclist stops pedaling" [21]. The components of an e-bike can be categorized in four main groups: motors, bike parts, electrics and batteries [13]. In this section we focus mainly on the battery and the motor being the two components that determine the power consumption and the energy needs of an e-bike. The proposed configuration of the system is presented in Figure 8.11 and explained in the following paragraphs.

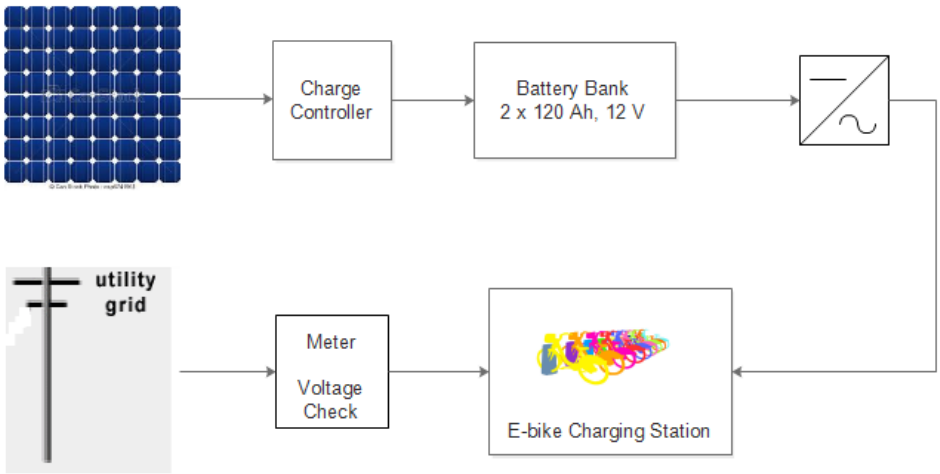

Figure 8.11: Proposed e-bike system implementation

Among the components of an e-bike, battery technology can be considered as the biggest technical burden. Batteries are very important for the e-bike's utilization mainly for two reasons. Their weight is added to the overall weight of the vehicle and their capacity places a limit on the distance over which the motor can provide assistance [22]. Three types are the most common battery technologies for e-bikes nowadays: the valve-regulated lead-acid battery (VRLA, also called SLA, Sealed Lead-Acid), the lithium-ion batteries (Li-ion) and the nickel-metal hydride batteries (Ni-MH) [22]. VRLA is the dominant battery technology in e-bikes mainly because they are cost effective, reliable and have a relatively long life. Their major disadvantage is their low energy density (30 Wh/kg) and their weight. On the other hand, Li-ion batteries provide better performance, are lighter and have higher energy density (140 Wh/kg) but their main disadvantage is their increased cost. VRLA batteries are more popular in e-bikes markets like China while Li-ion batteries are most dominant in Europe and the states [13, 22].

In this case, we have chosen the Bosch PowerPack 400 Lithium ion battery pack mainly due to its small weight and its satisfactory rated capacity. The technical data of the battery pack are presented in Table 8.2.

Table 8.2. E-bike battery parameters

Technical Data	Bosch Power Pack 400
Rated voltage	36 V
Rated Capacity	11 Ah
Energy	400 Wh
Weight, approx.	2.5 kg
Charging voltage	42 V
Charging current	6 A

B. Solar Supply System

The proposing e-bike charging stations are equipped with PV panels to assist the charging process when there is no excess energy available in the network. The size of the panels is calculated based on the size of the shelter used to protect the docking station. Assuming a maximum number of 16 e-bike parking spots per charging station (two parallel rows, 8 e-bikes spots each) and an individual spot of 1.5 × 0.75 m for each e-bike then the shelter should be able to cover an area of approximately 18 m2. In STC conditions (irradiance 1000 W/m2, module temperature 25 oC and AM = 1.5) and assuming a typical module efficiency of 15%, this area could host solar panels that are able to generate a maximum power of 2.7 kW. Actual measurements of a 2.65 kW residential PV installation, in Flo-

becq (Belgium), showed that the average energy production in the Walloon region of Belgium during 2014 was 11.43 kWh per day. The production varied significantly in different periods of the year. In a very sunny day (21/04/2014) the total PV production was 21.42 kWh while in a typical winter day (20/12/2014) the PV production was only 2.01 kWh.

The solar supply system includes also a solar charge controller and a battery bank for storing the generated energy. A charge controller or a charge regulator is a voltage and/or current regulator which prevents batteries from overcharging by regulating the voltage and current coming from the installed solar panels and going to the battery. In this study we assume that the charge controller provides the whole energy generated by the solar panels at any time to the battery bank. We consider that each station is equipped with two deep-cycle parallel connected 12V 120 Ah (capacity at the 1 hour rate) batteries which when fully charged can provide approximately 2.88 kW for one hour. On the AC side, considering a typical inverter efficiency of 85%, the maximum available power would be approximately 2.45 kW.

C. *Implementation Algorithm*

The proposed implementation algorithm is presented in Figure 8.12. The first part of the illustrated algorithm describes the demand – arrival process of an e-bike in a single station while the second part describes the recharging module. The first priority is at any moment, the plugged-in e-bike to charge using the potential excess energy generated from the network. A voltage check could indicate the availability of any excess energy. A higher voltage compared to the reference one (reference voltage = 1.05 × nominal voltage), indicates the injection of unutilized power to the network coming mainly from residential PV installations. The voltage check takes place every 15 minutes. If the network voltage value at the point of common coupling (PCC) of the charging station with the network is higher than the reference value, then all e-bikes that are actually plugged-in should charge using the network energy for the next 15 minutes. PV panels installed on the roofs of the charging stations are used as a secondary charging source to assist the charging process. In case the network voltage is lower than the reference value, a check to the state of charge (SoC) of the PV battery bank is performed. If the battery SoC is higher than 20 %, then all plugged-in e-bikes charge from the PV batteries. There is a direct relation between the discharge depth of a battery and the number of charge and discharge cycles it can perform [23]. Taking that into consideration and in order to achieve battery best lifespan we set the minimum SoC limit at 20%. If the battery SoC is lower than 20 %, the e-bikes charge from the network.

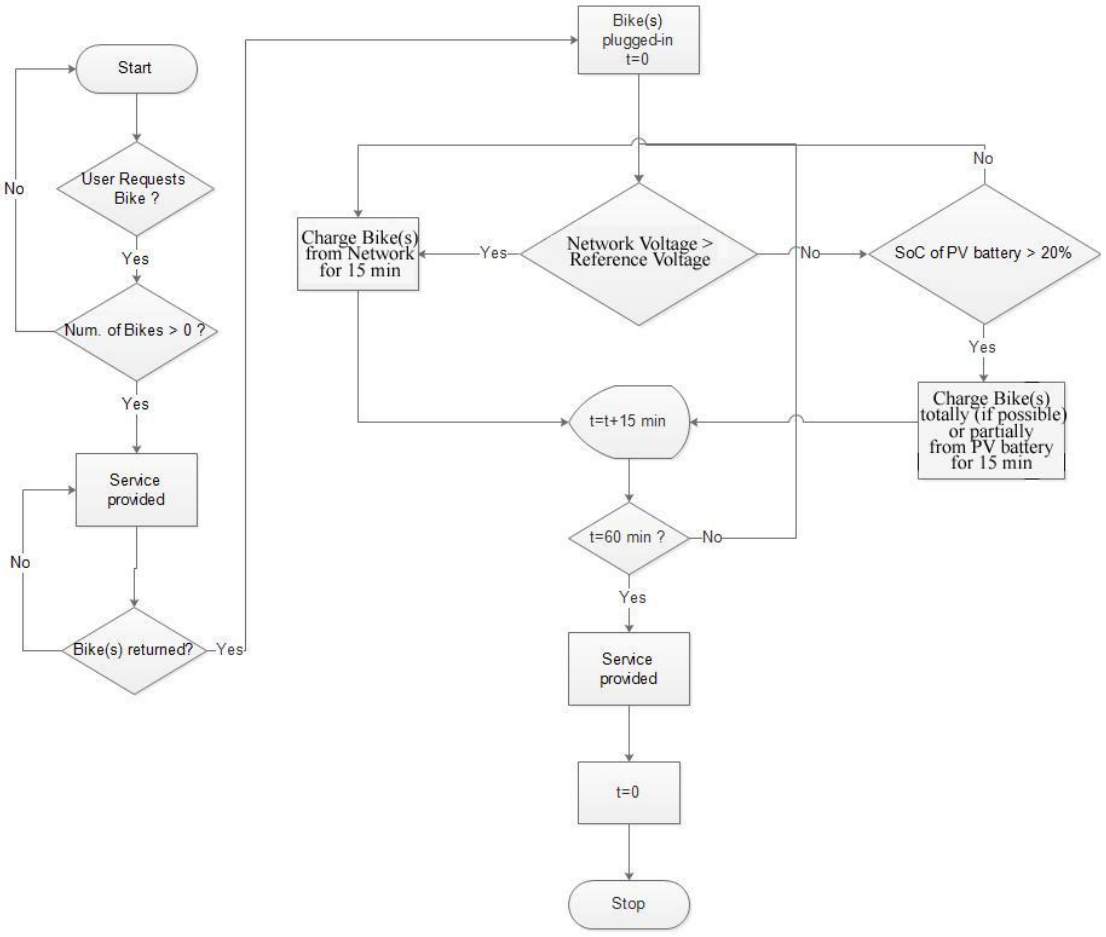

Figure 8.12: Operation algorithm of the e-bike charging station

The selection of ¼-hourly time steps for the voltage check has been decided for simulation reasons since the available energy flow data (consumption and PV injection) are recorded on a ¼-hourly basis. Given the lack of solid information for intra quarter-hourly PV intermittencies and load variations, the probabilistic modeling of the charging stations integration in the network is assumed to be more reliable when based on the real recorded total 15-min values. However, in the real implementation, voltage check and battery charging could absolutely take place in shorter time steps.

D. Charging Process

In [24] two methods for charging electric vehicles are described: the power scaling (constant time) approach and the time scaling (constant power) approach. In this section a combination of the aforementioned methods is used. More specifically, when an e-bike arrives to a dock station and it is plugged in for charging, it is assumed that its battery is at 30% SoC (approx. 120 Wh) and is charged

with a flat rate at nominal charging values for one 1h (42V x 6A x 1h = 252Wh) before it can be released for use. Lithium ion manufacturers recommend the batteries not to be further discharged after they reach 20% SoC [22]. The energy consumption rate can be estimated by multiplying trip distance by battery discharge rate. Previous research [14, 22] propose an energy consumption between 10 – 22 Wh per mile for e-bikes.

8.2.3 *Interaction of the system with the LV network*

The charging station model has been integrated in the basic structure of the probabilistic algorithm (Chapter 4). Therefore, its interaction with the LV distribution network can be evaluated in an extensive range of possible network states. Practically, the algorithm is adapted in order to be able to consider the operation of the charging stations during the period of the day during which they are available to users. This period is set by the planner in function of the implementation plan and the predicted use patterns for the installation. Therefore, during this set period, the operation of the charging stations is modeled within the probabilistic algorithm based on the flowchart of Figure 8.13 that is explained in the following paragraphs.

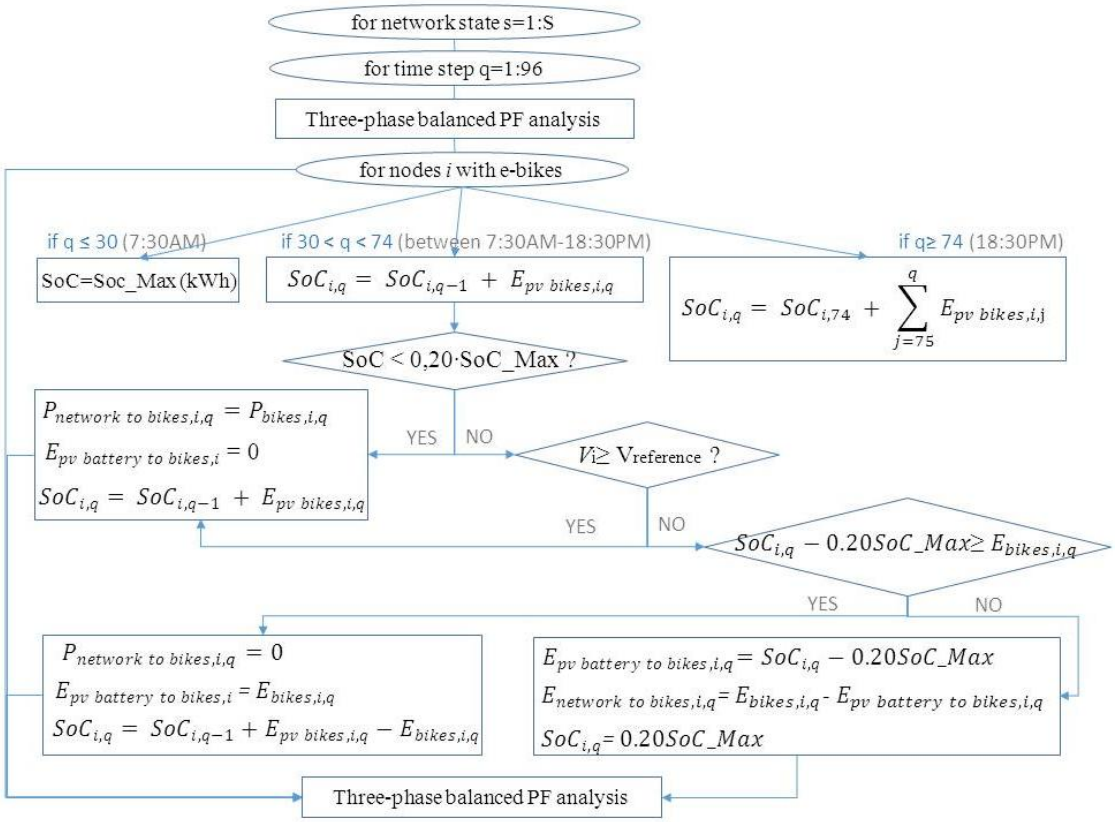

Figure 8.13: The operation of e-bike charging stations within the probabilistic tool

The probabilistic algorithm analyses as a first step each network state *s* without considering the operation of the charging stations but only the nodal power exchanges of the connected end-users (based on the considered SM datasets and the respective CDFs for each variable). When a network state coincides with the activity of the e-bike charging stations, the algorithm initially checks if SoC at every station is higher than 20% of the capacity of the PV battery. If the SoC of a PV battery in a station is lower than this value, then the currently plugged-in bikes are totally charged by the network, even if the network voltage at the PCC of the charging station is lower than the reference voltage (reference voltage = 1.05 × nominal voltage).

The exchanged power value $P_{load,i,q}$ at node *i* that is considered in the load flow analysis at node *i*, for network state *s* and time step *q*, becomes:

$$P_{load,i,q} = P_{load,MC,i,q} + P_{bikes,i,q} \tag{8.8}$$

where $P_{load,i,q}$ is the total net load demand (W) at the respective node *i*, $P_{load,MC,i,q}$ is the load demand that is sampled from the respective CDF of the end-user connected to node *i* (the one considered in relation (4.12), equal to

$E_{load_i}/0.25)$ and $P_{bikes,i,q}$ is the total required charging power for the currently present bikes at node *i* (in the considered time step *q*, see paragraph 8.2.4)).

In case the network voltage V_i at node *i* is higher than the reference value, the net power consumption is also determined with the same formula (8.8), since the total required power for the charging station is provided by the network. The SoC of the PV battery (after the load flow analysis in time step *q)* of the station connected to node *i*, is in both cases (SoC < 20% or V_i > reference voltage), equal to:

$$SoC_{i,q} = SoC_{i,q-1} + E_{pv\ bikes,i,q} \tag{8.9}$$

where $SoC_{i,q}$ is the available stored energy at node *i* after the analysis of the current time step *q*, $SoC_{i,q-1}$ is the available stored energy just before the analysis of the current time step *q* and $E_{pv\ bikes,i,q}$ is the ¼-hourly energy that has been locally generated by the roof PV panels of the station during the current time step *q*. This energy is directly stored into the PV battery.

In case the SoC of the battery at node *i* is higher than 20% and the respective network voltage at the PCC of node *i* is lower than the reference value, two cases are then possible. Either the PV battery has enough stored energy for feeding the station with the total required power, without reaching a SoC lower than 20%, or the PV battery has not enough stored energy (although its SoC is higher than 20%) and thus, power coming from the network is also necessary for providing the total required energy needs. In the first case, the whole energy, required by the charging station, is provided by the PV battery and the locally consumed power $P_{load,i}$, coming from the network, is the one that was initially defined in the MC simulation at node *i* (equal to $E_{load_i}/0.25$) for time step *q*. The SoC at node *i* becomes:

$$SoC_{i,q} = SoC_{i,q-1} + E_{pv\ bikes,i,q} - E_{bikes,i,q} \tag{8.10}$$

$$\forall\ SoC_{i,q} \geq 0.20 SoC\_Max\ \ \&\ \ SoC_{i,q-1} \geq 0.20 SoC\_Max$$

where SoC_Max is the maximum energy capacity of the PV battery (Table 8.2) and $E_{bikes,i,q}$ is the total required energy by the charging station at node *i* for time step *q*. $P_{bikes,i,q}$ in the flowchart of Figure 8.13 is computed by dividing $E_{bikes,i,q}$ with 0.25.

In case the stored energy of the PV battery $E_{pv\ bikes,i}$ is not sufficient for covering the total energy needs of the station, although its SoC is higher than 20%, a network contribution $P_{network\ to\ bikes,i}$ is then required. In this case, the exchanged power with the network $P_{load,i}$ (value considered in the power flow for the respective network state) is computed as follows:

$$P_{load,i} = P_{load,MC,i} + P_{network\ to\ bikes,i} \tag{8.11}$$

where:

$$P_{network\ to\ bikes,i} = \frac{E_{bikes,i} - E_{pv\ battery\ to\ bikes,i}}{0.25h(consumed\ over\ 15\ minutes)} \quad (8.12)$$

$$E_{pv\ battery\ to\ bikes,i} = SoC_{i,q} - 0.20SoC\_Max \quad (8.13)$$

Once these nodal values have been computed at each e-bike charging station, the probabilistic algorithm performs a new PF analysis considering them instead of the initially sampled values at the respective nodes. The computed operation magnitudes are saved so as to be compared with the initial computed indexes which did not consider the charging stations operation.

8.2.4 *Studied implementation*

A. Transportation and Mobility Patterns

In bike-sharing programs, a very important factor to success is the location and the distribution of bike stations [25]. Network coverage is very important and in general, the size and the configuration of the served area determine the distribution of the stations. This chapter assumes a small MV/LV substation feeding a set of residential customers and small enterprises, a university campus and student residences and a small train station. In such cases the network coverage is proposed only in city centers or higher-density areas [25]. For this reason, four e-bike docking stations located in zones with high population density have been considered: central station, city center, and University campus and university residences. The proximity of the docking stations to the public transport network is considered a key element to success of the program as the bicycle becomes a complementary transport mode extending route options [26].

A successful bike sharing system is highly dependable on how user demand is met. A number of studies in literature have addressed bicycle mobility planning and trend prediction related to bike-sharing transport systems [27], [28], [29]. However, this is not the main purpose of this study. Trip information and an approximate redeployment of the e-bikes at the four previously mentioned stations are needed in order to estimate the requiring energy that the e-bikes require when plugged-in to the charging stations and the electric load they add to the network.

Based on information and driven conclusions from the literature and taking into consideration individual human mobility patterns, a usual bicycle plan for a normal working day for a fixed number of e-bikes and charging docking stations (Table 8.3) [30]. The plan indicates the departures and the arrivals of the e-bikes in all four stations for a period of 12 hours (06:30 -18:30) divided in 1h intervals. It has been assumed that at 06.30 in the morning the e-bikes only depart from the docking stations and no bikes arrive. An initial number of 35 available e-bikes

have been considered. Table 8.3 presents the individual departures/arrivals for the four docking stations. A fixed number of total available e-bikes (35) distributed in the four docking stations has been considered. The initial e-bike allocation to the four stations is as following: 10 e-bikes in City Centre, 12 e-bikes in the Central Station, 15 e-bikes in the University Residences and 8 e-bikes in University Campus.

In Figure 8.14 the overall and individual requiring power of the charging stations during a normal working day is illustrated. The total requiring daily energy for a normal working day varies among the four stations. The lowest energy demand appears in the University Residences e-bike station (approx. 12 kWh per day) while the highest one in the University Campus station (16 kWh per day).

Table 8.3: E-bike arrivals and departures

	City Centre		Central Stat.		Univ. Resid.		Univ. Camp.	
Time	Arriv.	Dep.	Arriv.	Dep.	Arriv.	Dep.	Arriv.	Dep.
07:30	2	7	3	6	1	5	6	5
08:30	5	6	8	9	3	8	7	6
09:30	6	5	7	7	2	4	14	5
10:30	6	4	5	4	3	2	7	5
11:30	5	3	4	4	3	3	3	3
12:30	4	4	3	4	3	3	3	12
13:30	11	8	6	3	4	4	2	4
14:30	3	6	5	4	3	4	8	4
15:30	4	4	5	4	4	3	5	4
16:30	4	3	4	5	4	3	3	5
17:30	6	5	4	9	5	3	3	11
18:30	6	4	8	9	11	4	3	6

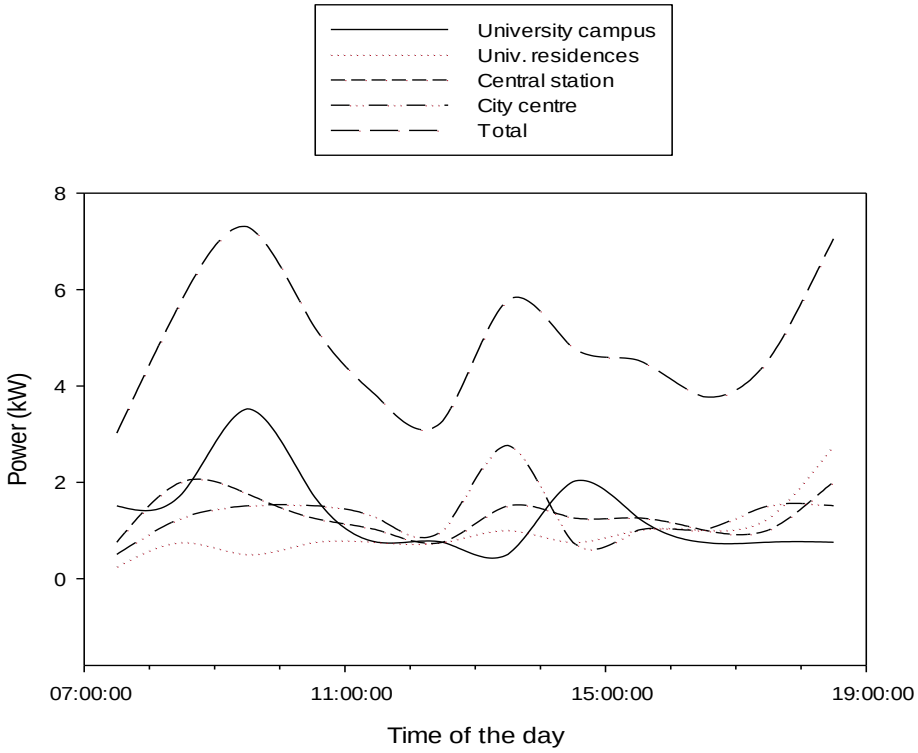

Figure 8.14: Power demand profile of e-bike charging stations

iii. *Integration in the LV Network*

To evaluate the operation of the four charging stations as part of a LV distribution feeder, the topology depicted in Figure 8.15 was simulated. This is practically the feeder that is analyzed in Chapter 5 however in this case it has been considered that the train station with an e-bike charging point is located at node 2 and the e-bike station serving the central square of the town has been considered connected to node 7. Similarly the students' residences with an e-bike station have been considered located at node 9 and the University campus at node 16.

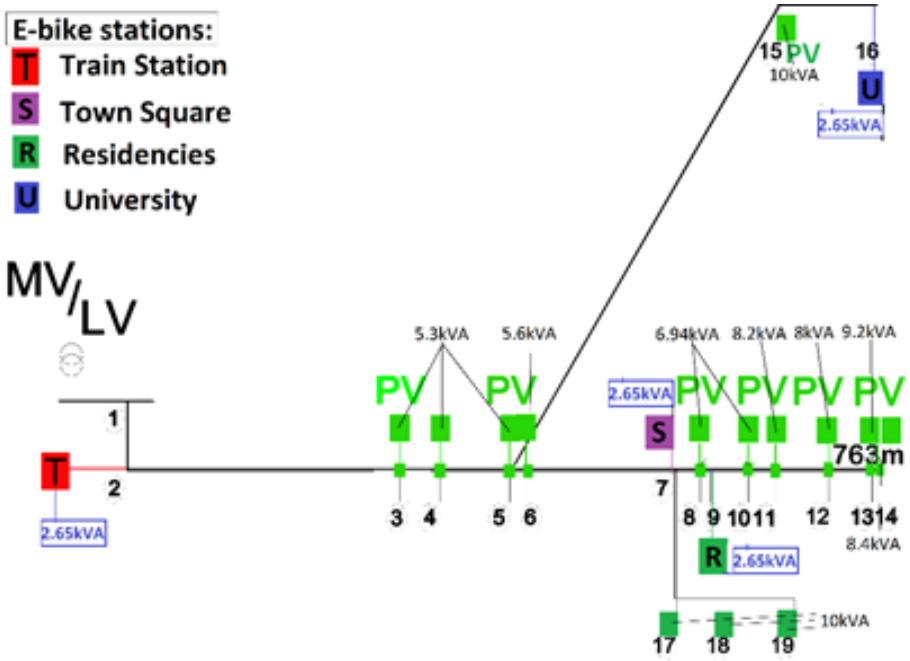

Figure 8.15: The simulated LV feeder

As far as used data are concerned, all residential end-users were simulated with data that were recorded by the DSO at the PCC of residential PV end-users connected to this feeder and other similar feeders in the same area (SM datasets like the ones presented in Chapter 3). The statistical profiles of consumption were created for the University campus and the residencies based on real consumption data measured over a period of one year in an existing University building and students' residencies building in Mons. These statistical profiles were created exactly in the same way as the ones for the residential end-users (as explained in Chapter 3). For the consumption profile of the train station, the same statistical profiles as for the students' residencies were used.

The PV generation statistical profiles of the rooftop PV panels of each station were based on real SM data recorded at a residential 2.7kVA PV installation in the same geographical area. In order to magnify PV injection so that big university building loads are partially compensated by local PV injection, bigger PV installations than the real ones have been considered at the existing residential PV nodes (4, 5, 12 and 14). For this reason, the bigger PV units have been considered connected in three-phase mode (since they are bigger than 5kVA) and the LV feeder has been analyzed as a three-phase balanced system, including the two laterals. Similarly, the PV units at nodes that do not currently have any PV generation were considered similar in size with the ones modeled at the existing PV nodes. Finally, the real technical parameters of the feeder (resistance and reactance of the lines, length of line segments…) were considered in the power flow

analysis. Since total PV integration (distributed over a big number of units) does not exceed the maximum acceptable PV hosting capacity computed in Chapter 6, while a perfectly balanced system is considered in this case, the consideration of bigger PV ratings should most possibly not lead to technical constraints' violation.

Figures 8.16 and 8.17 illustrate the variation of the SoC of all four charging stations on a ¼-hourly timescale during three consecutive typical days in April and in January. The SoC varies importantly not only in function of time but also in function of the position of each e-bike station in the feeder. It is worth mentioning that the time variation is partly induced from the Pseudo-Sequential configuration of the MC algorithm. Given that the latter is repeated for a big number of iterations, one can assume that the network states that represent realistic transitions of network states are taken into account.

However, a big amount of the battery SoC is affected from the time variation of the network states due to the stochastic character of PV injection and the randomness of consumption loads at all nodes. Indeed, the SoC of the train station charging point is quite stable over time (during e-bikes availability) although the rooftop PV installation is similar in size to the one of the other stations. This can be explained by the fact that this station is placed near the head of the feeder and therefore the power flow is not importantly affected by PV injection and loads' randomness. As a result, the network voltage at this node does not vary remarkably and therefore neither the charging process of the e-bikes station varies a lot over time. On the contrary with this remark, the charging process of the residences e-bikes station varies a lot over time since this station is located at node 9 which is importantly affected by reverse power flows and random load variations. Comparing the SoC time diagrams of April and January, similar assumptions can be made although in January all PV batteries are hardly fully charged due to the lower PV injection in winter.

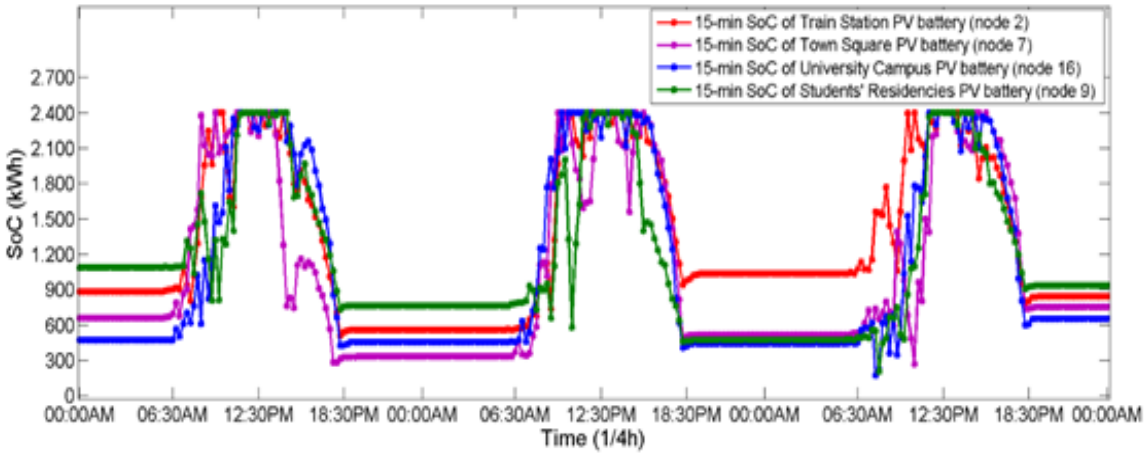

Figure 8.16: SoC of the PV batteries, installed at the e-bikes charging stations, computed on a ¼-hourly basis for three typical days in April

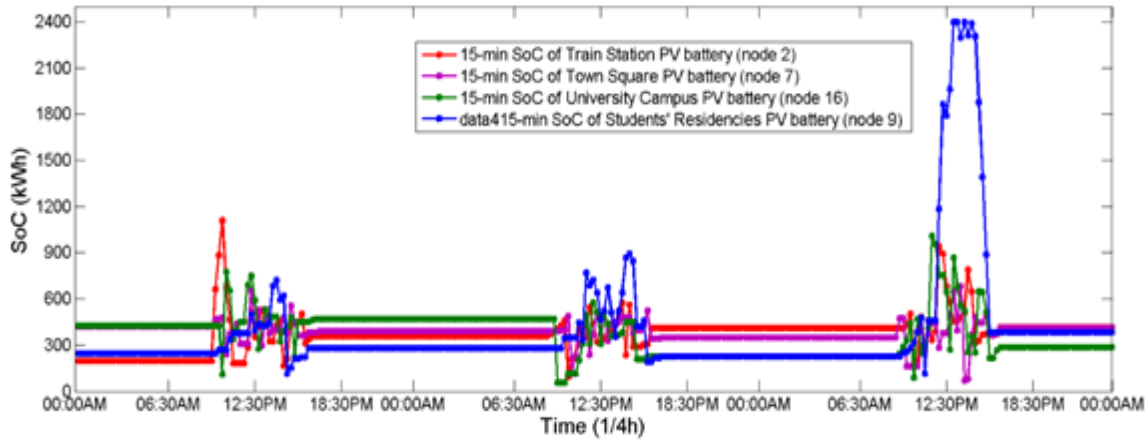

Figure 8.17: SoC of the PV batteries, installed at the e-bikes charging stations, computed on a ¼-hourly basis for three typical days in January

The above considerations demonstrate that the evaluation of distributed e-bike charging stations integrated in the LV network should take into account the time variability of network operation due to distributed PV units and random consumption loads. Figure 8.18 shows the ¼-hourly voltage variation at node 16 for the base scenario (no e-bikes in the feeder) and the "e-bikes" scenario for five consecutive time steps of a typical day in April. It is obvious that the integration of e-bikes charging stations does not affect the voltage profile along the feeder, given the increased energy use of the University campus and the student residencies compared to the PV installations in the feeder.

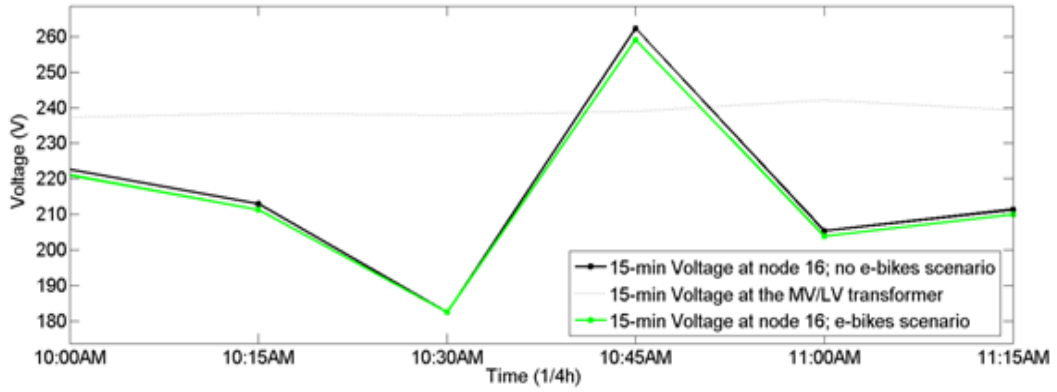

Figure 8.18: The ¼-hourly voltage profile at node 16 (e-bike station) for the period between 10:00AM and 11:15AM of a typical day in April for the scenarios with and without e-bikes in the LV feeder

The obtained output was expected given the small length of the feeder and the big consumption loads of the university campus and the students' residencies buildings. Therefore in this specific feeder the e-bikes charging stations do not contribute in mitigating the overvoltage risk by locally consuming PV injected power. On the other hand, the fact that the integration of such systems does not affect the existing conditions in the feeder can be also considered advantageous in terms of network voltage stability and reliability. It should be also mentioned that current results are driven based on mobility patterns of a normal working day. The mobility pattern for people is different during the weekends, a fact that could potentially affect the result.

8.3 Demand side management by residential end-users

In recent decades, the electric power system has seen major regulatory changes which gradually assigned a new role to it. This role is to provide a secure and reliable platform for the development of various business models concerning energy supply and integration of "green" energy resources. Even though transmission utilities, large energy users and producers, energy suppliers and aggregators can already visualize their steps in the upcoming years, for distribution utilities and small energy end-users tracing a path forward in the future is not so evident.

Lately, several authorities, regulatory bodies and research institutes worldwide [31]-[34] highlight the fact that distribution utilities seek to establish a new role in the currently evolving framework. At the same time, regulators and utilities agree that small energy users represent a large untapped potential for flexibility that could further enable the transition to a distributed generation model while rendering fair and cost-effective the overall energy business model. Indeed, although large grid users benefit from the competitive market, this is currently not the case for small end-users who are getting more exposed to the volatility of electricity prices, both consumption- and generation-wise.

Driven by these considerations, the third subsection of Chapter 9 presents a methodology for estimating, with a long-term statistical approach, the potential flexible load that small end-users connected to a given LV feeder can offer. The basic probabilistic algorithm previously developed in Chapter 5 is complemented for integrating DSM actions by individual end-users while accounting for LV network technical constraints. Furthermore, a distribution tariff scheme is designed for incentivizing small end-users engagement in DSM actions in LV feeders. The designed scheme is a capacity-based distribution network use tariff which aims at awarding low power withdrawal during peak demand periods. Both findings are interesting regarding the propagation of DSM in typical LV feeders like the studied one. As a future objective, such evaluation can be considered for comparing the incentivizing potential and the technical performance of distribution tariff reprofiling to the ones of real-time price-reactive schemes or other market-based DSM coordination schemes.

8.3.1 *Current Context*

The value that flexibility products can deliver to transmission utilities and to large users connected to the MV level has been widely discussed and demonstrated in several experimental and real implementations worldwide. Thus, this subsection focuses on the potential value that small end-users' participation in DSM actions could deliver to themselves and to the respective distribution utili-

ties in a long-term perspective. In this context, a set of simulation studies, experimental set-ups and pilot projects have been presented in recent years [35], [36]–[42]. All these studies demonstrate that a considerable amount of residential load can be shifted or curtailed inducing a clear benefit on LV network constraint management. Ref. [41] underlines the necessity of implementing a coordinated optimization approach, accounting for uncertainties, when integrating demand response (DR) strategies in residential feeders. Similarly, ref. [42] puts in evidence the effect of stochasticity in domestic appliances' use and in solar irradiation parameters.

Prompted by these recent findings, this chapter develops a simulation platform that estimates, with a long-term probabilistic approach, the potential flexible load of end-users in a given LV feeder. Compared to existing contributions, the chapter puts the focus on the uncertainty of total nodal power injections and consumptions. The latter is simulated based on user-specific SM energy flow measurements which are more easily accessible to distribution utilities compared to user-specific domestic appliances profiles and to solar irradiation patterns. The effect of LV network constant variability on the potentially generated flexibility, on the individual end-users cost savings and on the operation indices of the network is evaluated with a long-term observability approach.

Given the currently low electricity prices, some of the previously mentioned scientific contributions investigate possible schemes for incentivizing end-users to voluntarily participate in DSM strategies. The Energy and Power Research Institute (EPRI) concludes that a time-of-use (ToU) and critical peak pricing scheme with end-users controlled DSM events outperformed the other implemented schemes in [43]. According to the final report of the EU funded Linear Project [38], an adequate compensation mechanism for small users participation in the whole sale market is missing while DR actions could be promoted with a dynamic distribution grid tariff scheme. Besides, the European Distribution System Operators' Association (EDSO) for Smart Grids proposes that distribution tariffs should become more capacity-based, and less volumetric, in order to limit revenue uncertainty for DSOs (operating expenses reduction) and to motivate end-users to participate in demand response actions [31]. Ref. [32] thoroughly explains the importance of valuing capacity and energy as distinct elements in current energy markets.

For the above reasons, several distribution utilities have recently started visualizing or designing a reform of their distribution network use tariffs [33], [42]–[44]. In the EU context, there is currently a capacity component in the network use tariff scheme in 20 out of 25 countries. Nevertheless, the latter is only related to the contractual power of the end-user rather than to power withdrawal during peak periods, except from a Dutch case [45] which applies a dynamic pricing

scheme. In 14 out of 25 countries, there is a time of use component but mostly based on day/night or seasonal patterns or related to atypical or low-income users.

Based on these considerations and the EU recommendations on restructuring network tariffs [46], this chapter simulates with the presented probabilistic algorithm a specified distribution tariff scheme. The purpose is to statistically monetize the value of flexibility for small end-users, based on the considered tariff scheme. The simulated scheme is thoroughly explained in paragraph "*Simulating a capacity-based distribution tariff scheme*".

8.3.2 *Developments*

The presented methodology is developed for performing feeder-specific analysis and it consists of three overall simulation processes, the ones illustrated in Figure 8.19.

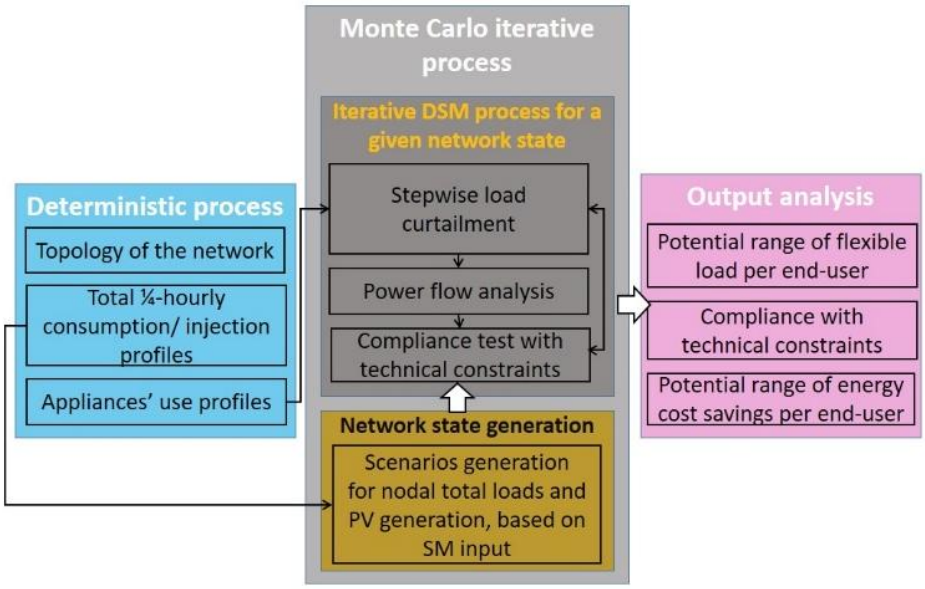

Figure 8.19: The work flow of the simulation

i. *Deterministic process*

The deterministic process comprises three models. The first one is the network topology model while the second one creates the statistical samples that characterize the total consumption and PV injection of end-users' at ¼-hourly intervals. Both models have been thoroughly explained in Chapter 4. As a first objective, chapter contributes the third model of the deterministic process which is the creation of different possible end-user types based on the daily load profiles of domestic electric appliances.

User-specific information concerning the load profiles of domestic appliances requires the deployment of energy audits and appliances' monitoring or questionnaires answered by the respective users. Although several pilot cases and experimental set-ups have taken place worldwide, these practices are not currently common which makes such information difficultly accessible. This chapter uses the load profiles of [41] because they match perfectly with the structure of the probabilistic framework. Indeed, such profiles can be easily adapted to a simulation that is updated at ¼-hourly intervals. Moreover, these load profiles can be randomly combined for creating different possible end-user types such that the variability of their behavior can be also accounted for.

In particular, this assessment considers five appliances with a high demand response potential, according to [41]. The selected household appliances are the electric AC system (AC), the clothes dryer (CD), the clothes washer (CW), the water heater (WH) and the dish washer (DW). Although these appliances often have similar load patterns for most households, the time of day at which they are used may vary a lot among different households. Based on this consideration, a set of different types of end-users has been created, by combining the appliances' load profiles of [41]. Indicatively, type E is illustrated in Figure 8.20. For all user types, the DW is considered to be used once per day while the CW and the CD are considered to be used three days per week, each time once per day. The days on which the CW and CD are used are randomly sampled with a MC process, considering the assigned probability of 3 out of the 7 week days.

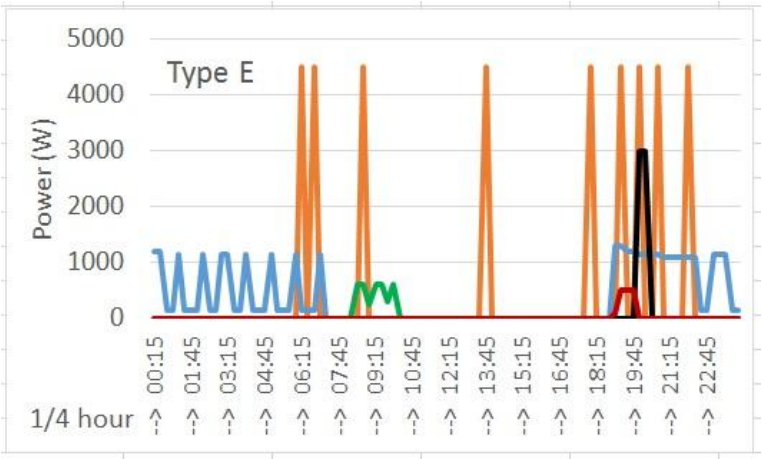

Figure 8.20: Daily profile of user type E (five electric domestic appliances)

Each end-user in the feeder is assigned to one of the created user types. The "peak hours" or LC period is deterministically defined in function of the overall context (purpose of the study, economic, sociological, and meteorological or other criteria). Based on the selected configuration, the initial objective of the long-term simulation is to estimate, in a statistical manner, the capacity that each end-

user could provide as flexible load during the defined LC period. The user-specific energy usage data (recorded SM datasets), the appliances' profiles (of the respective user type) and the necessary constraint management in the feeder are the input for such analysis.

For respecting the comfort level of end-users, the curtailed loads are considered to be entirely shifted in another period in the day which is also deterministically defined in function of the overall context. In a real case, this LS period could be refined to satisfy individual end-users' criteria. Based on this assumption, new user types are created for simulating the LS strategy. For example, type E^{DSM} is illustrated in Figure 8.21. Resuming the previous assumptions, the domestic appliances' use of each end-user *i* is characterized by two [*D*x96] sized matrices, U_i and U_i^{DSM}:

$$U_i = \begin{matrix} a_{1,1} & \cdots & a_{1,96} \\ \vdots & \cdots & \vdots \\ a_{d,1} & a_{d,q} & a_{d,96} \\ \vdots & \cdots & \vdots \\ a_{D,1} & \dots & a_{D,96} \end{matrix}, U_i^{DSM} = \begin{matrix} a_{1,1}^{DSM} & \cdots & a_{1,96}^{DSM} \\ \vdots & \cdots & \vdots \\ a_{d,1}^{DSM} & a_{d,q}^{DSM} & a_{d,96}^{DSM} \\ \vdots & \cdots & \vdots \\ a_{D,1}^{DSM} & \cdots & a_{D,96}^{DSM} \end{matrix} \quad (8.14)$$

where $a_{d,q}$ is the load of appliance *d* at time step *q*, without considering DSM actions (values based on [41]) and $a_{d,q}^{DSM}$ is the desired load of appliance *d* at time step *q*, in case LS is successfully applied by end-user *i*. For a given *q*, values $a_{d,q}$ and $a_{d,q}^{DSM}$ are different only if *q* falls within the defined LS and LC periods. The total number of appliances that take part in the DSM simulation is equal to *D* (in this case *D*=5). The number of ¼-hourly time steps in a day is equal to 96. Practically, each line *d* of matrices U_i and U_i^{DSM} describes the daily load profile, at ¼-hourly intervals, of the respective electric appliance *d*.

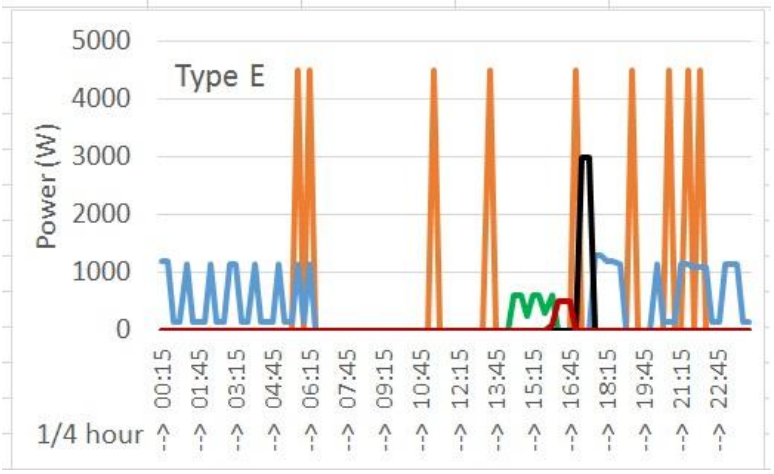

Figure 8.21: Daily profile of user type EDSM (considering shifted loads)

A challenging step in simulating the participation of residential end-users in DSM actions concerns the safe prediction and modeling of their electric appliances' daily use. Indeed, the simulated $a_{d,q}$ and $a_{d,1}^{DSM}$ values can be very different from the finally implemented ones given that the behavior of residential end-users is highly variable and unpredictable from day to day even in cases where remuneration for flexibility services is quite considerable. For example, a user might have consented to shift the usage of an appliance in the morning although he might also use it in the evening, during peak hours, due to an unpredictable everyday life event. Or, it might occur that the DR dispatcher decided not to curtail a certain load at a certain system state during peak hours due to constraint management issues. Such situations often induce important deviation from the expected system states. As a result, extra technical requirements might be introduced or loss of expected income might occur, depending on the applied business model.

For estimating such modeling errors and for setting boundary values for the parameters that are affected by the stochasticity of end-user behavior (or of distributed generation), probabilistic analysis is highly recommended. The following paragraph "*Monte Carlo iterative process*" presents the probabilistic methodology that is applied for simulating multiple possible network states and not just a set of static ones based on deterministically defined parameters. In this way, situations in which certain loads could not be curtailed due to technical constraints violation are also taken into account next to the "ideal" ones where LC and LS took place without encountering technical disturbances. Moreover, given that the different network states are assembled with real user-specific SM data, situations in which certain users consumed less or more than the expected values are also considered in the computation.

ii. *Monte Carlo iterative process*

The probabilistic process deploys a MC scenario generation process in the way described in Chapter 4. In this case, the historic measurements grouping and the simulation are also performed for monthly periods. The present implementation redefines the random variables of each network state such that the participation of end-users in DSM is also simulated in a probabilistic manner.

A given system state *s* in a LV feeder with *N* nodes is characterized by the following variables, as in relation (4.4):

$$E_{inj,pv,i} \quad , \; E_{load,i} \; , \; V_{MV\ LV} \quad , \qquad i = 1{:}N$$

and the instantaneous power value that represents the power flow at the PCC of each end-user *i* with the feeder is determined with expression (4.12):

$$P_{i=}\frac{E_{load_i}\text{-}E_{inj,pv_i}}{0.25}$$

If P_i is positive the respective end-user *i* is instantaneously consuming power from the grid, in the considered network state, whereas if P_i is negative, the end-user is instantaneously injecting power into the grid. For considering the integration of load curtailment, this subsection introduces an iterative process that performs (for each end-user *i*) stepwise load curtailments of loads $a_{d,q}$ (at each simulated network state *s)* in case *q* falls within the defined LC period. The curtailment order depends on the processes (appliances) that take part in the DSM actions and on the desired benefit. If for example, an end-user has an interest in curtailing the maximum possible load, at a certain time step, then the selection of curtailed appliances follows a descending order. Otherwise, if the function of a specific DW can be paused for some consecutive time steps and restart later while the respective end-user prefers to curtail DW in priority, then the algorithm follows such a predefined order.

Independently from the implemented priority order, the nodal LC are always performed in a stepwise manner for the following reason; after the completion of each LC step, the compliance with technical constraints is validated all along the feeder with the three-phase forward backward power flow method presented in paragraph 4.1.4.iii. If technical criteria (voltage limits and congestion risk) are not satisfied in a given network state, then the iterative LC process stops. This could be the case of an important simultaneous curtailment of many nodal loads coinciding with high PV injection along the feeder in the afternoon of a spring or summer day. Such situations often result in local violations of upper voltage limits and temporary cut-offs of distributed PV units. If a similar case is simulated with the probabilistic algorithm, then the last step of the LC iterative process is not considered in the final estimation of the potential flexible load that end-users can deliver for the considered network state.

Therefore, the LC iterative process practically modifies the P_i variables of relation (4.12). For a given state *s*, this modification can be expressed with the following relation for end-user *i*:

$$P_i^{DSM} = P_i - \sum_{1:d}^{q} a_{d,q} \qquad (8.15)$$

where P_i^{DSM} is the final curtailed load that can be applied without resulting in any technical parameters violation in the feeder, in the given network state, and $a_{d,q}$ is defined as in (8.14). In case the curtailment of the first appliance leads to the violation of an operation index in the feeder, then P_i^{DSM} and P_i are equal in the given network state (no LC can be applied). Focusing on DSM strategies, the potential modification of PV injection, as the one in chapter *8.1*, is not considered in this implementation.

As soon as the iterative LC process concludes to the P_i^{DSM} values for all end-users, a final (for the specific network state **s**) power flow analysis is performed such that all operation indices are computed. The LC iterative process and the LS process are illustrated in the flowchart of Figure 8.22. The appliances LC is performed in a descending order in this specific implementation.

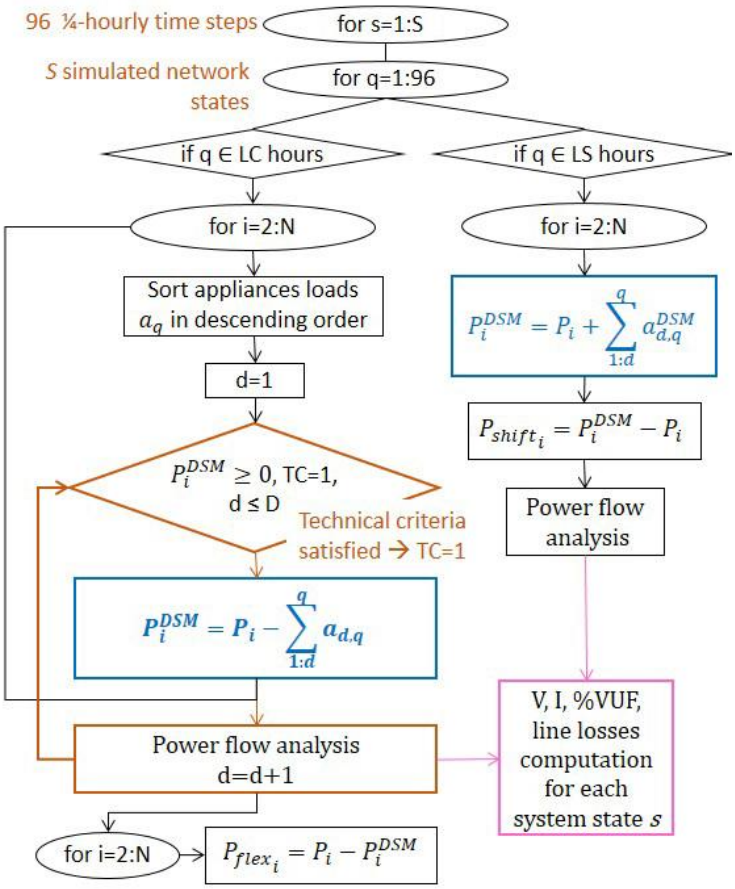

Figure 8.22: The load curtailment iterative process and the load shifting process for a given system state s

The iterative process for integrating DSM in the probabilistic simulation only concerns the LC process. All curtailed loads are considered entirely shifted to another period of the day. This means that, in a given system state that falls within the LS period, the presented algorithm does not restrict load shifting even if technical parameters are not satisfied. The purpose is to quantify the impact that such an uncoordinated LS strategy can have on the operation indices of a LV feeder during non-peak hours. The interest of such an option will be demonstrated in the feeder-specific simulation that is presented in the following paragraph 8.3.2.iii. Nevertheless, the probabilistic evaluation of a coordinated technical constraints-aware approach for both LC and LS actions is an interesting future objective.

iii. *Simulating a capacity-based distribution tariff scheme*

Once the boundary values of the technically potential nodal flexible load are defined, this study investigates whether implementing a capacity-based distribution tariff scheme could incentivize (in an economic sense) small end-users engagement in DSM actions. One should note that the periodical component of the network use tariff is the only one considered in the implementation since only this one is affected by the ToU.

The evaluated tariff scheme is predefined which means that a certain energy consumption tariff is fixed for every ¼-hourly time step in a day. The end-user is aware of the ¼-hourly tariffs and therefore takes DSM actions (reprofiles his consumption pattern over the day) in order to reduce his overall daily energy cost, in response to the price signal. This structure is much simpler than real-time price reactive mechanisms or other market-based schemes. Moreover, it allows distribution utilities to maintain their important role in technical control and to reduce revenue uncertainty, compared to market-based schemes. Thanks to a careful reprofiling of the network use tariff, distribution utilities can maintain unchanged or increase their revenues. This can be done by redistributing tariffs over the day based on a ToU principle such that higher values apply when network costs are higher. For example, a higher tariff during peak demand hours (critical peak load pricing) could allow for the compensation of line losses during peak evening periods. Based on the previous considerations, a tariff scheme that satisfies the following criteria is designed:

- Two parts tariff, comprising both a capacity-based and a volumetric component.
- The volumetric component relates to the ToU of energy. The capacity component relates to two or more capacity levels and to the ToU.
- Low power withdrawal during peak hours is awarded. This can be either based on forecasts (Structure *ex-ante*) or identified after-the-fact (Structure *ex-post*).

If the current periodical value of the network use tariff of a distribution utility is *A* (fee/kWh), then the proposed tariff scheme in this subsection considers three capacity levels and a whole day flat tariff (Figure 8.23). If the power withdrawal of an end-user does not exceed a defined limited value (P_{limited}), then the periodical part of the tariff is equal to B=0.5A (fee/kWh). If the power withdrawal exceeds this lower value, then the end-user pays a supplement that is function of the ToU. During non-peak hours and during PV injection hours, the tariff is equal to B=A. During peak hours, the tariff is equal to B=1.3A and during non-peak PV injection hours the tariff is equal to B=0.75A.

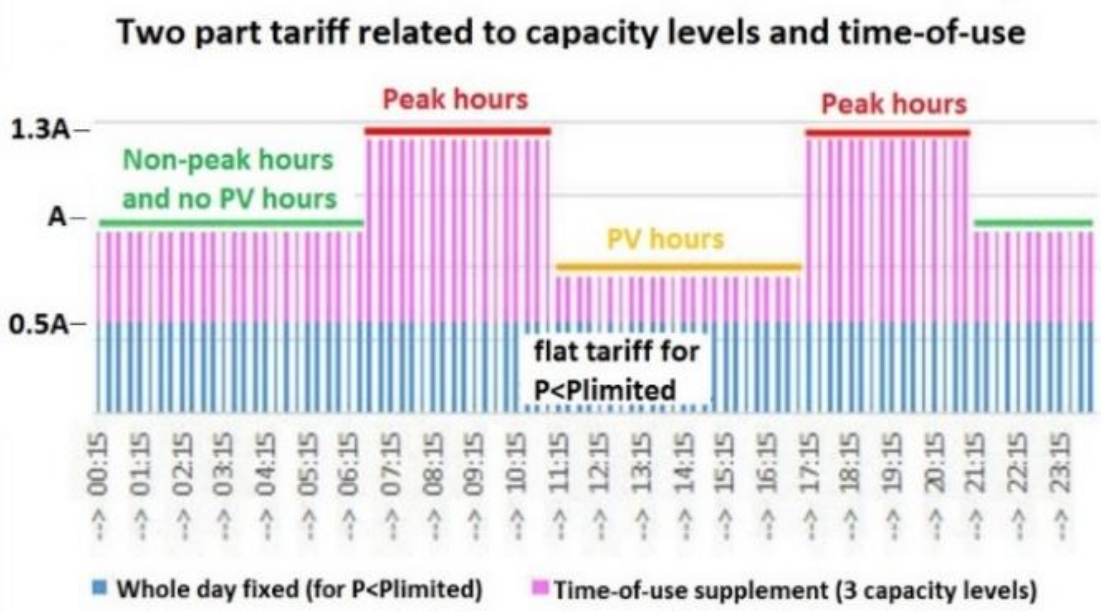

Figure 8.23: The simulated network use tariff

The tariff scheme of Figure 8.23 has been integrated in the probabilistic algorithm. Practically, in each analyzed system state, the cost of the ¼-hourly energy consumption of each end-user is computed for the base scenario (no DSM integration) and for the DSM scenario, considering the proposed tariff scheme. The outputs are statistically elaborated and explained in the following paragraph.

iv. *Statistical analysis of the outputs*

The presented probabilistic methodology is proposed for deploying long-term feasibility analysis of DSM integration in a given LV feeder. The sequentiality of the simulated system states is partly taken into account, not based on a mathematical sequentiality modeling approach but in the following two ways. First of all, each system state is simulated with values recorded at the respective ¼-hourly interval. Secondly, the matrices U_{i} and U_{i}^{DSM} are deterministically constructed such that the sequentiality of the use of the different appliances is accounted for. For example, the use of the CD in a day always follows the use of the CW. If the CW has been curtailed, then the use of the CD is not considered in the stepwise curtailment.

Given that the objective of the simulation is not a real-time or a day ahead estimation of the network but a long-term observability analysis, the different system states are regarded independently in a statistical manner. Each ¼-hourly time step is statistically characterized without considering its dependence on the previous and the following one with a mathematical approach but only thanks to the consideration of the time step-specific recorded values. The objective is to define boundary values for the variable parameters corresponding to each system state.

Such boundary values are very useful for long-term network planning studies or in the preprocessing phase of state estimation techniques for the overall distribution network. However, the algorithm also computes the difference between the total curtailed and shifted energy of each end-user on a daily basis. In case this difference is higher than a defined error value, it should be integrated with a statistical manner in the obtained outputs.

This chapter focuses on setting boundary values for the indices of Table 8.4, on a ¼-hourly basis or for longer periods (Peak hours, PV injection hours, daily and other). These values can be determined for each node or each line segment for the entire feeder. If for each ¼-hourly time step a total number of *S* states is analyzed, then the obtained outputs are structured in $3xS$ sized matrices as far as phase voltages and phase currents are concerned and in $1xS$ matrices as far as the rest of indices are concerned.

Table 8.4: Computed indices for ¼-hourly periods

Voltage	$3xS$
Current	$3xS$
%VUF	$1xS$
Power withdrawal	$1xS$
Flexible load	$1xS$
Line losses	$1xS$
Energy cost savings	$1xS$

The obtained output matrices are elaborated as statistical samples for the observed parameters. They are used to compute statistical distributions that characterize their possible variation and amplitude for each ¼-hourly period or for longer periods (daily periods, peak hours period etc.). As previously mentioned, the computed statistical distributions are computed with SM input corresponding to a specific month of the year.

8.3.3 *Simulation of a LV feeder*

The same three-phase LV feeder described in Chapter 5 is analyzed considering the load connections of Figure 8.24. Available SM historic measurements of energy flow are assigned to the connected end-users, recorded either in the studied feeder or in feeders in close proximity. The defined LC period, LS period and P_{limited} values are also illustrated in Figure 8.24. The periodical component of the distribution tariff (A) is considered equal to 0.125€/kWh which is the one currently applied in the area. The simulation was based on the principle that all end-

users fully participate in DSM whenever technical criteria in the feeder allow their participation.

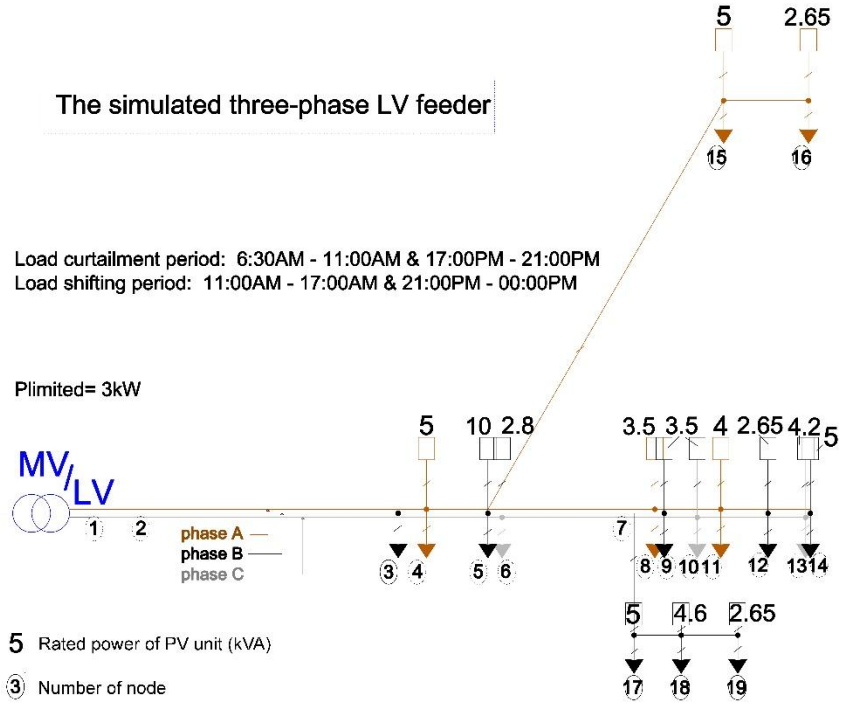

Figure 8.24: The simulated three-phase LV feeder

Regarding technical criteria, the integration of DSM decreased voltage magnitudes during the LS period all along the feeder. This effect is more decisive and advantageous for summer months which are generally characterized by higher overvoltage risk. As expected, voltage profiles slightly increased due to LC during peak hours. Voltage unbalance resulted negligible both before and after DSM integration. However, in certain network states during LS hours, the voltage unbalance factor (%VUF) at nodes at the end of the line had a significant (relative) rise because of many simultaneous single-phase power withdrawals in the feeder. Table 8.5 presents the amplitude of the effect of DSM integration (in %) on voltage magnitudes and unbalance at the PCC of 4 end-users, considering all the simulated network states for January. Table 8.5 should be read as follows; for example, in all simulated states, the deepest decrease of phase voltage V_a at the PCC of user 5 was of 5.35% after DSM integration. The decrease is computed by comparing the obtained V_a value for the same network state, in two scenarios: with and without DSM actions. The respective highest increase of V_a at node 5 was of 3.18%. All table's values are deduced based on the same principle. The

following tables 8.5 to 8.7 should also be read based on this "minimum-maximum" identified variation principle.

Table 8.5: Amplitude of DSM effect on voltage magnitude and unbalance

N	Va (%)	Vb (%)	Vc (%)	%VUF (%)
5	↓5.35 - ↑3.18	↓5.05 - ↑3.02	↓4.76 - ↑2.86	↓0.94 - ↑14
9	↓6.72 - ↑4.12	↓5.80 - ↑4.33	↓6.78 - ↑4.32	↓0.97- ↑84
11	↓7.22 - ↑4.56	↓5.78 - ↑4.51	↓6.44 - ↑4.73	↓0.98 - ↑90
14	↓7.83 - ↑5.20	↓5.91 - ↑4.58	↓6.37 - ↑5.21	↓0.98 - ↑87

In a few network states the uncoordinated LS strategy resulted in an important increase of current magnitudes or in a decisive decrease of the voltage profile. The power quality criteria were not violated in the specific feeder. Nevertheless, LS actions that are applied simultaneously by many end-users connected to the same feeder can be very disadvantageous for line losses and give rise to congestion risk in certain cases. Indicatively, Figure 8.25 shows the ¼-hourly variation of the current magnitude of line segment 2-3 during a simulated January day. Around midday hours, the current magnitude rises by almost 150% due to the simultaneous power withdrawal of many end-users as part of the LS strategy. Such system states should be carefully analyzed for achieving a lean integration of DSM.

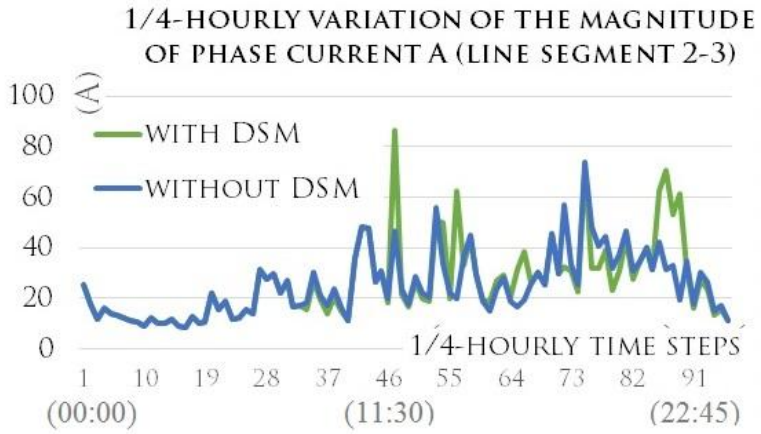

Figure 8.25: ¼-hourly variation of the magnitude of phase current I_a (line segment 2-3) and of the %VUF at node 14, during a typical January day

Table 8.6 presents the amplitude of the effect of DSM integration on current magnitudes of line segment 2-3 and of the daily line losses, in the entire feeder, for January. The upper thermal limits of the lines are not violated in any simulated state. However, in the extreme network states, the maximum simulated values

are quite close to the upper limit. Besides, an increase of current magnitudes in the order of 800% cannot be ignored, even if it corresponds to an extreme rare network state and to a small absolute value. Similarly, line losses over daily periods increase due to the integration of DSM. During PV hours the integration of DSM decreases total line losses in certain cases because the injected PV power is locally consumed thanks to the LS strategy. Nevertheless, in most simulated cases, the simultaneous shifting of loads without applying a coordinated approach can be very disadvantageous for line losses and induce high operational costs for the distribution utility. These outputs highlighted that a coordinated approach for integrating DSM is required both during peak and non-peak load periods.

Table 8.6: Amplitude of DSM effect on current magnitude and line losses

	Line segment 2-3
Ia (%)	↓90 - ↑317
Ib (%)	↓76 - ↑819
Ic (%)	↓90 - ↑829
	Entire feeder
Daily losses (%)	↑29-48
Losses during PV hours (%)	↓20 - ↑744

Table 8.7 presents the amplitude of the effect of DSM on end-users power withdrawal during 4 ¼-hourly periods in January. The potential effect of DSM on each end-user varies in function of his assigned appliances' user type, his SM measurements and the operation indices that characterize each ¼-hourly period. For example, end-user 5 is statistically more eligible for participating in DSM during early morning peak hours while end-user 14 is eligible for participating both during morning and evening peak hours.

Table 8.7: Amplitude of DSM effect on power withdrawal of end-users (%)

N	8:45 – 9:00	14:45 – 15:00	19:00 -19:15	20:00 – 20:15
5	↓0-99	0	0	0
9	↓0-92	0	↓0-98	0
11	↓9.43-69	0	↓0-78	↓0-99

14	↓0-100	↑0-67	↓0-80	↓6.9-100

Figure 8.26 presents the potential range of the daily energy that the same end-users can offer as flexible load in a typical January day. The respective energy cost savings (in %) that they can achieve have been statistically computed, over daily periods, considering the specified distribution tariff scheme. The computed percentage values correspond to the absolute cost savings of Table 8.8, for A=0.125€/kWh. The daily cost savings are not proportional to the potentially generated flexible energy because of the ToU character of the simulated tariff

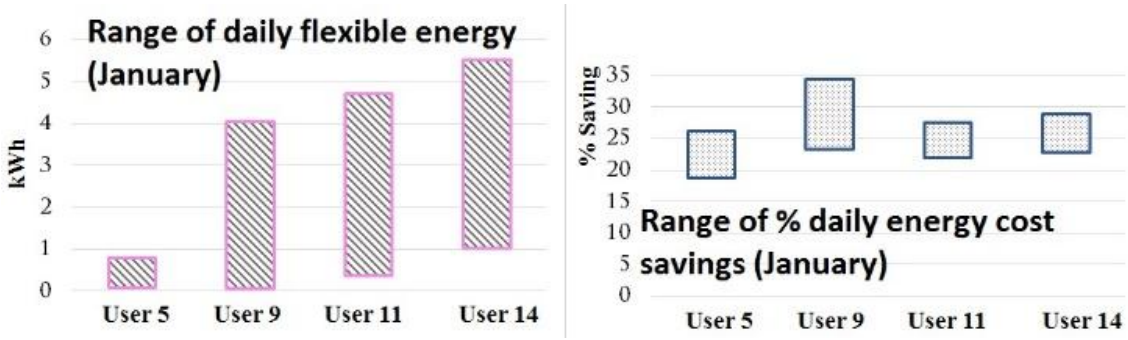

Figure 8.26: Statistical range of potentially generated flexible energy and cost savings (%) over daily periods in January, for 4 end-users in the feeder

Table 8.8: Absolute daily energy cost savings (€) for a=0.125€/kWh

N	5	9	11	14
min	0.39	0.98	0.94	2.34
max	0.63	1.11	1.40	3.44

Computed over one month, the energy cost savings for the same end-users would be within the range of 12-19€, 30-33€, 28-42€ and 70-103€ respectively for the month of January. These values correspond to the 30-70% of the total typical energy cost for electricity supply of residential end-users in the considered area (including both distribution network use tariff and energy tariff). Based on such findings, this study concludes that the application of a capacity-based distribution tariff scheme that awards low power withdrawal during peak hours can be sufficiently incentivizing for the residential end-users engagement in DSM action.

Chapter conclusions

Chapter 8 presented the restructuring of the basic probabilistic algorithm of Chapter 4 such that it can simulate three "load modification" strategies. The first two strategies concern the integration of EVs in LV feeders (one PHEVcharging station, in section 8.1, and several e-bike charging stations, in section 8.2). The third one concerns the integration of DSM actions, implemented by residential end-users, as a response to a specially tailored distribution tariff scheme. The probabilistic modeling of time-varying PHEV charging profiles and DSM actions in LV feeders allowed considering the volatility of the LV network state in the long-term evaluation of such schemes. Moreover, the use of feeder-specific historic measurements increased the accuracy of the assessment.

In this way, the study of the connection of one PHEV charging station to a University building (connected to the LV network) demonstrated that, in case of optimally coordinated charging-discharging control, the PHEVs batteries can contribute (as an alternative power source) to a significant reduction of the building's energy demand. This reduction can result in a considerable decrease of the electricity cost for the University building, if the considered pricing scheme is applied. Regarding the impact of the PHEV installation on the operation of the network, it has been concluded that undervoltage is more likely to occur in the case of uncoordinated PHEVs charging, while, to a countable extent (15%), the coordinated PHEVs charging-discharging control could result in lower total energy demand compared to the regular building load.

The study of the integration of an e-bike sharing system (including PV panels and storage for e-bikes charging) in a LV feeder gave an interesting insight on the impact of PV injection and loads stochasticity on the SoC of the e-bikes batteries. The power withdrawal of such systems from the main line strongly depends on the position of the system in the LV feeder and the volatility of nodal powers at the adjacent nodes. Given the big consumption loads of the University campus and the students' residencies buildings, which were considered connected to the studied feeder, the e-bikes charging stations did not affect voltage profiles along the feeder.

The simulation of a DSM strategy, accounting for LV network's technical constraints and considering a capacity-based distribution tariff scheme, resulted in two important findings. Firstly, the integration of DSM actions in LV feeders requires an optimized coordination both during peak and non-peak hours, for not stressing the operation of the network. Secondly, the implementation of a capacity-based distribution tariff scheme that awards low power withdrawal during peak hours can (economically) incentivize end-users to voluntarily participate in DSM strategies. Moreover, compared to real-time price-reactive schemes or other

market-based mechanisms, a carefully reprofiled network use tariff can ensure a more decisive role for distribution utilities in technical constraint management and revenue uncertainties related to DSM integration.

Apart from the separate conclusions mentioned above, the simulations of Chapter 8 highlighted one common point that is important for the future research perspectives of this work. The quasi-sequential configuration of the MC algorithm can affect the computation of parameters that need to be considered over daily periods, such as for example, the daily reduction of the electricity cost for a given end-user. Besides, the consideration of unrealistic transitions between successive network states (regarding, for example, the PV generation of a given end-user) could lead to an unrealistic computation of the SoC of e-bikes batteries, in the simulation of section 8.2. A similar problem can appear in the simulation of load curtailment and load shifting, in section 8.3, since the independency of MC samplings for nodal load demand (between successive network states) could result in an unrealistic estimation of the total curtailed or shifted load. In the specific simulation there has been an effort for eliminating such situations by integrating certain algorithmical actions or by absorbing the error in the final results. However, for increasing the accuracy of such computations, the use of a fully Sequential MC algorithm would be recommended.

On another hand, it is worth mentioning that the use of the Quasi-Sequential MC algorithm for computing indices that can be considered independently for each time step does not affect the accuracy of the results. For example, the statistical long-term computation of the flexible load that can be delivered by a given end-user in a given ¼-hourly time step can be reliably estimated with the Quasi-Sequential algorithm.

Chapter publications

The developments of Chapter 7 have been published in:

[1] D. Thomas, V. Klonari, F. Vallée, and C. S. Ioakimides, “Implemantation of an E-bike Sharing System: The Effect on Low Voltage Network using PV and Smart Charging Stations,” in 2015 International Conference on Renewable Energy Research and Applications (ICRERA), 2015, pp. 572–577.

[2] D. Thomas, V. Klonari, F. Vallée, O. Deblecker, and C. S. Ioakimides, “Effect of electric vehicles’ optimal charging-discharging schedule on a building’s electricity cost demand considering low voltage network uncertainties,” in IEEE PES Innovative Smart Grid Technologies Conference Europe, ISGT Europe, 2016.

[3] V. Klonari, A. Orfanos, J. Lobry, and F. Vallée, “Probabilistic assessment of a distribution tariff scheme for incentivizing demand side management in the small energy usage sector,” in IEEE PMAPS, Beijing, 2016.

[4] V. Klonari, J. Lobry, and F. Vallée, “Adapting Low Voltage distribution tariffs to peak demand Probabilistic assessment of a Low Voltage feeder in Belgium,” in BERA Workshop on Demand Response, 2016.

Chapter references

[1] D. B. Richardson, "Electric vehicles and the electric grid: A review of modeling approaches, Impacts, and renewable energy integration," Renewable and Sustainable Energy Reviews, vol. 19, pp. 247–254, 2013.

[2] P. Kadurek, C. Ioakimidis, and P. Ferrao, "Electric Vehicles and their impact to the electric grid in isolated systems," in 2009 International Conference on Power Engineering, Energy and Electrical Drives (POWERENG), pp. 49–54.

[3] E. Sortomme and M. A. El-Sharkawi, "Optimal Charging Strategies for Unidirectional Vehicle-to-Grid," IEEE Trans. Smart Grid, vol. 2, no. 1, pp. 131–138, 2011.

[4] L. Jian, Y. Zheng, X. Xiao, and C. C. Chan, "Optimal scheduling for vehicle-to-grid operation with stochastic connection of plug-in electric vehicles to smart grid," Applied Energy, vol. 146, pp. 150–161, 2015.

[5] J. Wang et al, "Impact of plug-in hybrid electric vehicles on power systems with demand response and wind power," Energy Policy, vol. 39, no. 7, pp. 4016–4021, 2011.

[6] S. Habib, M. Kamran, and U. Rashid, "Impact analysis of vehicle-to-grid technology and charging strategies of electric vehicles on distribution networks – A review," Journal of Power Sources, vol. 277, pp. 205–214, 2015.

[7] M. Sitterly, Le Yi Wang, G. G. Yin, and Caisheng Wang, "Enhanced Identification of Battery Models for Real-Time Battery Management," IEEE Trans. Sustain. Energy, vol. 2, no. 3, pp. 300–308, 2011.

[8] K. Clement-Nyns, E. Haesen, and J. Driesen, "The Impact of Charging Plug-In Hybrid Electric Vehicles on a Residential Distribution Grid," IEEE Trans. Power Syst, vol. 25, no. 1, pp. 371–380, 2010.

[9] K. M. Tsui and S. C. Chan, "Demand Response Optimization for Smart Home Scheduling Under Real-Time Pricing," IEEE Trans. Smart Grid, vol. 3, no. 4, pp. 1812–1821, 2012.

[10] D. Thomas, V. Klonari, F. Vallee, and C. S. Ioakimidis, "Implementation of an e-bike sharing system: The effect on low voltage network using pv and smart charging stations," in 2015 International Conference on Renewable Energy Research and Applications (ICRERA), pp. 572–577.

[11] New York Independent System Operator, NYISO. Available: www.nyiso.com (2013, Feb. 15).

[12] Z. Darabi and M. Ferdowsi, "Aggregated Impact of Plug-in Hybrid Electric Vehicles on Electricity Demand Profile," IEEE Trans. Sustain. Energy, vol. 2, no. 4, pp. 501–508, 2011.

[13] M.-H. Vandersmissen, P. Villeneuve, and M. Thériault, "Analyzing Changes in Urban Form and Commuting Time∗," The Professional Geographer, vol. 55, no. 4, pp. 446–463, 2003. [7] EDSO for Smart Grids, "European Distribution System Operators for Smart Grids Adapting distribution network tariffs to a decentralised energy future," no. September, 2015.

[14] S. A. Shaheen, S. Guzman, and H. Zhang, "Bikesharing in Europe, the Americas, and Asia," *Transportation Research Record: Journal of the Transportation Research Board*, vol. 2143, no. -1, pp. 159–167, 2010.

[15] G. Rose, "E-bikes and urban transportation: emerging issues and unresolved questions," *Transportation*, vol. 39, no. 1, pp. 81–96, 2012.

[16] S. Ji, C. R. Cherry, L. D. Han, and D. A. Jordan, "Electric bike sharing: simulation of user demand and system availability," *Journal of Cleaner Production*, vol. 85, pp. 250–257, 2014.

[17] S. Habib, M. Kamran, and U. Rashid, "Impact analysis of vehicle-to-grid technology and charging strategies of electric vehicles on distribution networks – A review," *Journal of Power Sources*, vol. 277, pp. 205–214, 2015.

[18] L. Jian, X. Zhu, Z. Shao, S. Niu, and C. C. Chan, "A scenario of vehicle-to-grid implementation and its double-layer optimal charging strategy for minimizing load variance within regional smart grids," *Energy Conversion and Management*, vol. 78, pp. 508–517, 2014.

[19] A. Kavousi-Fard, A. Abunasri, A. Zare, and R. Hoseinzadeh, "Impact of plug-in hybrid electric vehicles charging demand on the optimal energy management of renewable micro-grids," *Energy*, vol. 78, pp. 904–915, 2014.

[20] A. Marongiu, M. Roscher, and D. U. Sauer, "Influence of the vehicle-to-grid strategy on the aging behavior of lithium battery electric vehicles," *Applied Energy*, vol. 137, pp. 899–912, 2015.

[21] A. M. Haidar, K. M. Muttaqi, and D. Sutanto, "Technical challenges for electric power industries due to grid-integrated electric vehicles in low voltage

distributions: A review," *Energy Conversion and Management*, vol. 86, pp. 689–700, 2014.

[22] M. K. Hidrue and G. R. Parsons, "Is there a near-term market for vehicle-to-grid electric vehicles?," *Applied Energy*, vol. 151, pp. 67–76, 2015.

[23] Electric bikes - Legislation Directive 2002/24/EC relating to the type-approval of two or three-wheel motor.

[24] J. X. Weinert, A. F. Burke, and X. Wei, "Lead-acid and lithium-ion batteries for the Chinese electric bike market and implications on future technology advancement," Journal of Power Sources, vol. 172, no. 2, pp. 938–945, 2007.

[25] K. C. Divya and J. Østergaard, "Battery energy storage technology for power systems—An overview," Electric Power Systems Research, vol. 79, no. 4, pp. 511–520, 2009.

[26] J. C. García-Palomares, J. Gutiérrez, and M. Latorre, "Optimizing the location of stations in bike-sharing programs: A GIS approach," Applied Geography, vol. 35, no. 1-2, pp. 235–246, 2012.

[27] K. Martens, "Promoting bike-and-ride: The Dutch experience," Transportation Research Part A: Policy and Practice, vol. 41, no. 4, pp. 326–338, 2007.

[28] D. Chemla, F. Meunier, and R. Wolfler Calvo, "Bike sharing systems: Solving the static rebalancing problem," Discrete Optimization, vol. 10, no. 2, pp. 120–146, 2013.

[29] L. dell'Olio, A. Ibeas, and J. L. Moura, "Implementing bike-sharing systems," Proceedings of the ICE - Municipal Engineer, vol. 164, no. 2, pp. 89–101, 2011.

[30] J.-R. Lin and T.-H. Yang, "Strategic design of public bicycle sharing systems with service level constraints," Transportation Research Part E: Logistics and Transportation Review, vol. 47, no. 2, pp. 284–294, 2011.

[31] EDSO for Smart Grids, "European Distribution System Operators for Smart Grids Adapting distribution network tariffs to a decentralised energy future," no. September, 2015.

[32] Energy Power Research Institute, “Capacity and energy in the integrated grid,” 2015.

[33] NYS Department of Public Service, “Reforming the Energy Vision,” p. 85, 2014.

[34] Smart Grid Task Force, “2015 Regulatory Recommendations for the Deployment of Flexibility - EG3 REPORT,” no. January, 2015.

[35] M. Pipattanasomporn, M. Kuzlu, S. Rahman, and Y. Teklu, “Load Profiles of Selected Major Household Appliances and Their Demand Response Opportunities,” IEEE Trans. Smart Grid, vol. 5, no. 2, pp. 742–750, 2014.

[36] J. Dong, G. Xue, and R. Li, “Demand response in China: Regulations, pilot projects and recommendations – A review,” Renew. Sustain. Energy Rev., vol. 59, pp. 13–27, Jun. 2016.

[37] Energy Power Research Institute, “A Case Study on the SMUD Residential Summer Solutions Pilot Project,” 2014.

[38] EnergyVille, “LINEAR Final Report,” 2014.

[39] K. . Kessels, B. . Claessens, R. . D’hulst, and D. Six, “The value of residential flexibility to manage a BRP portfolio: a Belgian case study,” in Energycon, 2016.

[40] P. . Scott, S. . Thiébaux, M. . Van De Briel, and P. . Van Hentenryck, “Residential Demand Response under Uncertainty,” in Lecture Notes in Computer Science , Springer, 2013, pp. 645–660.

[41] R. Torquato, Q. Shi, W. Xu, and W. Freitas, “A Monte Carlo simulation platform for studying low voltage residential networks,” IEEE Trans. Smart Grid, vol. 5, no. 6, pp. 2766–2776, 2014.

[42] AF-Mercados; REF-E; Indra, “Study on tariff design for distribution systems,” 2015.

[43] Joint Committee on Telecommunications Utilities and Energy, “Bill. House No.4185,” 2014.

[44] J. McKinney and J. . Halligan, “Decision on residential rate reform for Pacific gas and electric company, Southern california edison company and San diego gas & electric company and transition to time-of-use rates,” 2015.

[45] P. Mandatova, M. Massimiano, D. Verreth, and C. Gonzalez, “Network tariff structure for smart energy system,” in CIRED, 2014.

[46] Eurelectric, “Network tariff structure for a smart energy system,” May, 2013.

Chapter 9 Global Conclusions and Prospects

9.1 Conclusions

In this thesis, we propose a probabilistic framework that is based on Pseudo-Sequential Monte Carlo (MC) simulation and uses Smart Metering (SM) energy measurements of end-users, connected to the Low Voltage (LV) network, for deploying long-term analytics and design studies of LV networks. **The main objective is to present a methodology and an algorithm that can simulate, in a reliable manner, the operation of LV networks by considering the stochasticity of nodal power exchanges (consumption- and generation-wise) in such networks. The second principal objective is to integrate, in the developed algorithm, models of strategies and technical solutions that could respond to problems currently met in LV networks, in order to evaluate, with a long-term techno-economic view, their possible benefit on the operation of the network and on the further integration of renewables.**

At first, a thourough review of existing methodologies, developed for studying, with a long-term view, the operation of LV networks, has been deployed. First of all, it has been concluded that long-term simulation models are subject to requirements similar to the ones for the real system, namely the ability to balance the trade-offs of the various end-users objectives and perspectives and the flexibility to evolve with the changing mix of resources. Secondly, **it has been noted that the accuracy of existing probabilistic models has been, up to now, restricted due to the lack of historic long-term measurements of end-users power (or energy) exchanges with the LV network**. Finally, it has been highlighted that existing probabilistic models do not integrate methods for evaluating strategies or distributed control schemes that are very important for the further integration of renewables and for the upcoming automation of the distribution network.

Followingly, the types of historic measurements that can be used for the development of the methodology proposed by this thesis have been presented. In this context, the configuration of the SM devices that ORES (a DSO in Wallonia, Belgium) has installed at the premises of several PV users (connected to the LV

network of the city of Flobecq, Belgium) since 2012 has been outlined. The procedure that has been implemented, by our research team, for collecting and treating the available SM recordings has also been explained step by step. **The treatment of the available PV energy injection and consumption historic measurements demonstrated that high variability applies, not only regarding the energy consumption of the same user over time, but also regarding the time-coincidence between the highest or the lowest amount of (¼-hourly) energy consumed by the different end-users.** This argument pointed out the interest of developing LV network modeling methodologies that can simulate the stochasticity of the loading parameters at the end-user level.

The main contribution of this thesis is a probabilistic algorithm that has been developed for deploying long-term observability analysis of the LV network with the use of historic SM measurements. It has been presented in Chapter 4.**The developed methodology can model LV network uncertainty and redirect long-term network design towards the most frequent network states rather than the extreme ones.** The simulation of a real LV feeder, with some available SM measurements, has also been presented. The purpose was to compare the voltage outputs from the probabilistic simulation with real-case phase voltage measurements at two PV nodes, during one winter and one summer month. The comparison demonstrated that the studied datasets (probabilistic simulation outputs and real measurements) are quite similar in certain cases while in other cases they are quite different. Regarding the worst-case (deterministic) computation, phase voltage values resulted higher than 80-90% of the values recorded with the SM devices. **These findings underlined that the worst-case approach can lead to conservative decisions regarding voltage margin and PV hosting capacity of a LV feeder. It was also concluded that for achieving higher precision in both approaches (probabilistic and worst-case), the monitored visibility in LV networks needs to increase or reliable methodologies should be developed for addressing the availability of sparse measurements**.

Subsequently, a study exploring the potential correlation of PV generation and energy consumption of PV users located in a close geographical area has been deployed. It has been demonstrated that the energy generation of all PV users is entirely correlated while no spatial correlation can be considered for their energy consumption on week days. Moreover, a method for LV load and generation modeling for systems with little or no metering devices has been presented. This method uses the available information of end-users located in a nearby area. The methodology was incorporated in the basic structure of the probabilistic algorithm, proposed by this thesis, and the results have highlighted the added value of this approach compared to current approaches, such as SLP.

The following step has been the implementation of the basic structure of the probabilistic methodology for simulating the operation of a three-phase LV feed-

er located in the city of Flobecq. This implementation gave a detailed statistical analysis of the values that the various network operation indices can take. In this way, extreme worst-case values were computed and probability functions were constructed for each studied time step at each node. Critical nodes have been identified and statistically characterized in terms of technical constraints' violation. For the studied feeder, it has been demonstrated that high voltage values can easily occur even during months with lower solar irradiation, during periods of low load demand and high PV injection. Nevertheless, the highest voltage rise has been computed in the summer months. Regarding voltage unbalance, it has been shown that single-phase loads have a bigger impact compared to single-phase generation units. The important time-variation and the variability among different locations in the feeder have been proved both for voltage magnitudes and voltage unbalance. Furthermore, it has been demonstrated that during summer months an important amount of injected PV power is not locally absorbed by end-users' loads which leads to frequent reverse power flows towards the head of the feeder. This fact increases line losses and gives an indication on the usefulness of integrating local storage technologies during such situations.

The analysis of a three-phase feeder (with several unbalanced single-phase connections of loads and PV units) assuming a perfectly balanced system and no coupling effects between phases, highlighted the importance of deploying detailed three-phase analysis of such feeders. **It was demonstrated that not considering phase loading unbalance or coupling effects between phases can lead to overestimation or underestimation of important operation indices. Finally, it was demonstrated that the overvoltage risk in a LV feeder with several PV users results higher when the correlation of their PV generation is taken into account.** Consequently, assuming that PV users, located in proximity, are independent concerning their PV generation might lead to an underestimation of the voltage rise in the feeder.

The basic structure of the proposed probabilistic algorithm has been used for developing a probabilistic methodology that can estimate the PV hosting capacity of a given feeder, considering a set of predefined PV location scenarios, with the use of models based on feeder-specific SM measurements. The application of a probabilistic methodology allows the consideration of the statistical constraints of the EN 50160 standard (for overvoltage, undervoltage risks and voltage unbalance violation), when assessing the voltage margin of a given feeder. Regarding line congestion, the probabilistic approach gives a more detailed mapping and quantification of the risk along the feeder so that local reinforcements can be considered instead of generalized ones.

The aforementioned PV hosting capacity computation methodology has been carried out in the previously studied LV feeder and the outputs have been compared to the ones of a typical deterministic approach that also uses feeder-specific

historic measurements. For the studied feeder, the probabilistic methodology led to much higher hosting capacities compared to the deterministically computed ones regarding voltage margin. **This finding is very important because it confirmed one of the principal hypothesis on which this thesis is based, namely the argument that the probabilistic analysis of LV networks leads to less restrictive results as far as the further integration of renewables is concerned** (second argument (II) of section 2.6). Concerning the impact of congestion risk on the hosting capacity, the probabilistic approach allowed identifying which would be the line segment to reinforce while the deterministic approach resulted in very high current magnitudes in all line segments. **Therefore, the probabilistic analysis led to a much more information-rich analysis that can result in a more refined and cost-effective design of the network** (fifth and sixth arguments (V and VI) of section 2.6). Finally, the reliability of the probabilistic hosting capacity review has been demonstrated since the consideration of 100-percentile limits for voltage constraints led to outputs very similar to the ones of the deterministic approach. **Finally, the probabilistic simulation demonstrated that the integration of several distributed PV units evenly distributed over the three phases led to much higher PV hosting capacities compared to the integration of less but bigger PV units.**

A further step has been taken for adapting the basic structure of the probabilistic algorithm in such a way that it can simulate the action of different distributed time-varying control schemes against voltage rise and voltage unbalance. Five control schemes have been modeled and compared. In this way, a reliable long-term assessment of the investigated control schemes, which considers an extensive range of possible system states rather than a set of deterministically defined ones, has been presented in Chapter 7. The stochasticity of nodal loads and generation and their interaction with the respective control schemes has been modeled, leading to a more refined design of each control strategy for a given feeder.

For the studied feeder, it was demonstrated that P/V droop control has indeed a decreasing effect on the voltage profile along the feeder while ensuring a gradual and network state-aware energy curtailment at every node, which is not the case with the application of the traditionally applied on-off control (hard curtailment for longer periods). The control parameters tuning with the use of the probabilistic framework, demonstrated that customizing the reference voltage (V_{up}) in function of the position of a node in the feeder and applying a small droop slope (k) is efficient in terms of overvoltage mitigation and more conservative in terms of PV energy curtailment. **This last argument validated the argument that the benefit of different control schemes and other technical strategies will be more direct if they are refined based on a probabilistic simulation that uses feeder-specific historic measurements (**sixth argument (VI) of section 2.6).

The simulation of the reactive power control scheme, the 3ph-DPC scheme and the 3ph-SI scheme demonstrated that distribution utilities would have a clear interest in considering the connection of new PV units in three-phase feeders, with the use of three-phase four-wire inverters integrating the three-phase damping control (3ph-DPC) scheme. The latter can decisively improve voltage magnitudes and unbalance without modifying the injected PV power and without inducing more line losses.

Finally, the restructuring of the basic probabilistic algorithm, presented in Chapter 4, so that it can simulate three "load modification" strategies has been presented. The first two strategies concern the integration of Electric Vehicles (EVs) in LV feeders (one charging station for Plug-in Hybrid Vehicles (PHEVs), in section 8.1, and several e-bike charging stations, in section 8.2). The third one concerns the integration of Demand Side Management (DSM) actions, implemented by residential end-users, as a response to a specially tailored distribution tariff scheme. **The probabilistic modeling of time-varying PHEV charging profiles and DSM actions in LV feeders allowed considering the volatility of the LV network state in the long-term evaluation of such schemes. Moreover, the use of feeder-specific historic measurements increased the accuracy of the assessment.**

In this way, the study of the connection of one PHEV charging station to a University building (connected to the LV network) demonstrated that, in case of optimally coordinated charging-discharging control, the PHEVs batteries can contribute (as an alternative power source) to a significant reduction of the building's energy demand. This reduction can result in a considerable decrease of the electricity cost for the University building, if the considered pricing scheme is applied. Regarding the impact of the PHEV installation on the operation of the network, it has been concluded that undervoltage is more likely to occur in the case of uncoordinated PHEVs charging, while, to a countable extent (15%), the coordinated PHEVs charging-discharging control could result in lower total energy demand compared to the regular building load.

The study of the integration of an e-bike sharing system (including PV panels and storage for e-bikes charging) in a LV feeder gave an interesting insight on the impact of PV injection and loads stochasticity on the State of Charge (SoC) of the e-bikes batteries. The power withdrawal of such systems from the main line strongly depends on the position of the system in the LV feeder and the volatility of nodal powers at the adjacent nodes. Given the big consumption loads of the University campus and the students' residencies buildings, which were considered connected to the studied feeder, the e-bikes charging stations did not affect voltage profiles along the feeder.

The simulation of a DSM strategy, accounting for LV network's technical constraints and considering a capacity-based distribution tariff scheme, resulted

in two important findings. Firstly, the integration of DSM actions in LV feeders requires an optimized coordination both during peak and non-peak hours, for not stressing the operation of the network. Secondly, the implementation of a capacity-based distribution tariff scheme that awards low power withdrawal during peak hours can (economically) incentivize end-users to voluntarily participate in DSM strategies. Moreover, compared to real-time price-reactive schemes or other market-based mechanisms, a carefully reprofiled network use tariff can ensure a more decisive role for distribution utilities in technical constraint management and revenue uncertainties related to DSM integration.

Finally, it is worth mentioning that the computational time that has been required for deploying the simulations of this thesis, with the developed probabilistic algorithm, is considered to be very satisfactory, given that a long-term time framework is addressed. The computational time for some of the simulations is presented in Table A.2 of Appendix A3.

9.2 Prospects

Beyond the original developments proposed by this thesis, it would be undoubtedly meaningful to consider and implement some further developments that could complement the utility of the proposed methodology and algorithms. A set of these prospects is presented as follows.

The aforementioned simulations of the "load modification" strategies in Chapter 8 highlighted one common point that is important for the future research perspectives of this work. **The quasi-sequential configuration of the MC algorithm can affect the computation of parameters that need to be considered over daily periods, such as for example, the daily reduction of the electricity cost for a given end-user.** Besides, the consideration of unrealistic transitions between successive network states (regarding, for example, the PV generation of a given end-user) could lead to an unrealistic computation of the SoC of e-bikes batteries, in the simulation of section 8.2. A similar problem can appear in the simulation of load curtailment and load shifting, in section 8.3, since the independency of MC samplings for nodal load demand (between successive network states) could result in an unrealistic estimation of the total curtailed or shifted load. In the specific simulation there has been an effort for eliminating such situations by integrating certain algorithmical actions or by absorbing the error in the final results. However, for increasing the accuracy of such computations, the use of a fully Sequential MC algorithm would be recommended. On another hand, it is worth mentioning that the use of the Quasi-Sequential (or Pseudo-Sequential) MC algorithm, for computing indices that can be considered independently for each time step, does not affect the accuracy of the results. For example, the statistical long-term computation of the flexible load that can be delivered by a given end-user in a given ¼-hourly time step can be reliably estimated with the Quasi-Sequential algorithm.

Therefore, the application of "load modification" and storage applications pointed out the interest of the transition of the scenario generation process, in the probabilistic algorithm, from a pseudo-sequential mode to a fully sequential mode. To this end, a review of existing scenario reduction techniques, such as "important sampling" methods, should be initially deployed. Subsequently, an appropriate scenario reduction technique should be developed and integrated in the scenario generation process of the algorithm for reducing the computational effort. The integration of time series in the MC samplings procedure could significantly increase the required computational effort for handling large SM databases and several variables with different statistical profiles. Appropriate clustering methodologies for load and generation modeling could facilitate and accelerate this process.

Another interesting prospect for the further development of the probabilistic algorithms presented in this thesis is the integration of models of renewable energy generation systems, other than PV generation, such as, for example, micro-Combined-Heat-Power (micro-CHP) units, small residential wind turbines or residential biomass units.

The use of forecasted values for nodal power exchanges, in parallel with the historic SM measurements, could render the probabilistic simulation more complete for long-term planning studies of the LV network. Moreover, a certain interest can be identified in integrating, in the probabilistic algorithm, and testing the accuracy and the required computational effort of three-phase power flow methodologies that apply a different approach than the one currently implemented.

Finally, concerning the techno-economic evaluation of strategies and technical solutions, the proposed probabilistic algorithm could be complemented with optimization techniques. Such techniques would allow an optimized design of technical solutions tailored for a given LV network, accounting for network-specific technical and economical parameters and considering, in an overall manner, operating and capital expenses of distribution utilities.

List of publications

The important developments of this thesis have resulted in five published journal papers, two book chapters and sixteen conference contributions that were or will be presented in international conferences such as the IEEE PES T&D Conference and Exposition, the IEEE Energycon Conference, the IEEE PMAPS (Probabilistic Methods Applied on Power Systems), the SMARTGREENS Conference, in which our contribution has been awarded the "*Best Student Paper*" award in 2016, the Solar Integration Workshop, the IEEE ICRERA (International Conference on Renewable Energy Research and Applications), the IEEE ISGT (Innovative Smart Grid Technologies) Conference and the CIRED (International Conference and Exhibition on Electricity Distribution). A list of these publications can be found in Appendix A4.

Appendix A1: Technical Parameters of the simulated feeder

Table A.1: Technical parameters of the simulated LV feeder

Sending node	Receiving node	Line length (km)	R (Ω/km)	X (Ω/km)
1	2	0.065	0.206	0.31
2	3	0.26	0.31	0.243
3	4	0.03	0.31	0.243
4	5	0.066	0.31	0.243
5	6	0.015	0.31	0.243
5	15	0.5	0.31	0.243
15	16	0.009	0.31	0.243
6	7	0.14	0.31	0.243
7	17	0.118	0.31	0.243
17	18	0.05	0.31	0.243
18	19	0.06	0.31	0.243
7	8	0.022	0.31	0.243
8	9	0.01	0.31	0.243
9	10	0.035	0.31	0.243
10	11	0.025	0.31	0.243
11	12	0.05	0.31	0.243
12	13	0.04	0.31	0.243
13	14	0.005	0.31	0.243

Appendix A2: Matlab code for the analytical computation of paragraph 4.2.1

```
Analytical Computation
E=230;
a=exp(j*2*pi/3);
l1=0.05;
l2=0.1;
Zd1=0.05*(0.32+j0.243);
Zd2=0.1*(0.32+j0.243);
Zd=Zd1+Zd2;
Zh1=3*Zd1;
Zh2=3*Zd2;
Zh=Zh1+Zh2;
Zl=-200+j*250;

% Calcul des courants des trois composantes
Id=E/ ((Zd+Zl) + ((Zd+Zl)*(Zh+Zl)/ (Zd+Zh+2*Zl)));
Ii=-Id*(Zh+Zl)/ (Zd+Zh+2*Zl);
Ih=-Id*(Zd+Zl)/ (Zd+Zh+2*Zl);

% Transormation Fortescue, courant par phase
Ia=0;
Ib=Ih+ (a^2)*Id+a*Ii
Ic=Ih+a*Id+ (a^2)*Ii

% Tension des composantes h, d, i au noeud 3
Vh3=-Zh*Ih
Vd3=E-Zd*Id
Vi3=-Zd*Ii
```

```
% Tension des phases a, b, c au noeud 3
Va3=Vh3+Vd3+Vi3;
Vb3=Vh3+(a^2)*Vd3+a*Vi3;
Vc3=Vh3+a*Vd3+(a^2)*Vi3;

Sb3=Vb3*Ib;
Sc3=Vc3*Ic;
Sb_3=Zl*(Ib^2);
Sc_3=Zl*(Ic^2);
```

Results obtained by the analytical computation for node 3:
Va3 = 229.999-j0.0029 (V) (voltage at node 3, phase *a*)
Vb3 = -114.96-j199.23 (V) (voltage at node 3, phase b)
Vc3 = -115.04+j199.14 (V) (voltage at node 3, phase c)

Results obtained by the *Hybrid Power Flow Method* for node 3
Va3=229.998-j0.003 (V)
(Difference with analytical method: 0.001-j0.0001 (V))

Vb3 =-114.97-j199.11 (V)
(Difference with analytical method: -0.01-j0.12 (V))

Vc3 = -114.99+j199.22 (V)
(Difference with analytical method: -0.05-j0.07 (V)

Appendix A3: Computational time required for the simulations

Table A.2. Computational time for *S*=1000

Chapter 5, simulation of the feeder (Figure 5.1) for on month (balanced power flow) & (consideration of correlation between PV units' generation)	≈ 90 seconds
Chapter 5, simulation of the feeder (Figure 5.1) for on month (balanced power flow) & (no consideration of correlation between PV units' generation)	≈ 80 seconds
Chapter 5, simulation of the feeder (Figure 5.1) for on month (unbalanced power flow)	≈ 300 seconds
Chapter 6, PV hosting capacity simulation of the feeder (Figure 5.1) for one month	≈ 8000 seconds
Section 7.1, simulation of the feeder (Figure 7.3) for one month	≈ 160 seconds
Section 7.2, simulation of the feeder (Figure 7.10) for one month (4 control strategies)	≈ 540 seconds
Section 8.3, simulation of the feeder (Figure 7.10) for one month	≈ 8000 seconds

A processor with the following characteristics has been used:
Intel (R) Core TM i7 -5600 CPU @ 2.60 GHz 2.59

Appendix A4: List of publications

Journal publications

[1] F. Vallee, V. Klonari, T. Lisiecki, O. Durieux, F. Moiny, and J. Lobry, "Development of a probabilistic tool using Monte Carlo simulation and smart meters measurements for the long term analysis of low voltage distribution grids with photovoltaic generation," Int. J. Electr. Power Energy Syst., vol. 53, pp. 468–477, 2013.

[2] V. Klonari, J.-F. Toubeau, Z. De Grève, O. Durieux, J. Lobry, and F. Vallée, "Probabilistic simulation framework for balanced and unbalanced low voltage networks," Int. J. Electr. Power Energy Syst., vol. 82, pp. 439–451, Nov. 2016.

[3] F. Vallee, F. Moutier, V. Klonari, J.-F. Toubeau, F. Lecron, Z. De Greve, and J. Lobry, "On The Correlation between Prosumers in Probabilistic Analysis of Low Voltage Distribution Systems," Int. Rev. Electr. Eng., 2016.

[4] V. Klonari, J.-F. Toubeau, T. L. Vandoorn, B. Meersman, De Grève, Zacharie, J. Lobry, and F. Vallée, "Probabilistic Framework for Evaluating Droop Control of Photovoltaic Inverters," Electr. Power Syst. Res., vol. 129, pp. 1–9.

[5] V. Klonari, B. Meersman, D. Bozalakov, T. L. Vandoorn, L. Vandevelde, J. Lobry, and F. Vallée, "A Probabilistic Framework for Evaluating Voltage Unbalance Mitigation by Photovoltaic Inverters," Sustain. Energy, Grids Networks, 2016.

Book chapters

[1] J.-F. Toubeau, V. Klonari, J. Lobry, Z. De Greve, and F. Vallée, "Planning tools for the integration of renewable energy sources in low and medium voltage distribution grids.," in Renewable Energy - Utilisation and System Integration, Intech Open Access Publisher, 2016.

[2] V. Klonari, J.-F. Toubeau, J. Lobry, and F. Vallée, "Estimating the Photovoltaic Hosting Capacity of a Low Voltage Feeder Using Smart Meters'

Measurements," in Smart Metering Technology and Services - Inspirations for Energy Utilities, , Intech Open Access Publisher, 2016.

Conference contributions

2013

[1] J. L. V.Klonari, F.Vallee, O.Durieux, "Probabilistic tool based on smart meters data to evaluate the impact of distributed photovoltaic generation on voltage profiles in low voltage grids," in Proc. 3rd SIW, 2013.

2014

[2] F. Vallée, V. Klonari, J. Lobry, and O. Durieux, "Study of the combined impact of auto-consumption behaviour and correlation level between prosumers on overvoltage probabilities in low voltage distribution grids," in IEEE PES T&D Conference and Exposition, 2014.

[3] V. Klonari, F. Vallée, O. Durieux, Z. De Grève, and J. Lobry, "Probabilistic Modeling of Short Term Fluctuations of Photovoltaic Power Injection for the Evaluation of Overvoltage Risk in Low Voltage Grids," in Energycon, 2014.

2015

[4] V. Klonari, J.-F. Toubeau, Z. De Greve, J. Lobry, and F. Vallée, "Probabilistic Analysis of Low Voltage Networks with Distributed Photovoltaic Generation Sources: Case study in Belgium," in MedICT, 2015.

[5] V. Klonari, J.-F. Toubeau, Z. De Grève, O. Durieux, J. Lobry, and F. Vallée, "Probabilistic Analysis Tool of the Voltage Profile in Low Voltage Grids," in 23rd CIRED, 2015.

[6] V. Klonari, J.-F. Toubeau, Z. De Grève, T. L. Vandoorn, B. Meersman, J. Lobry, and F. Vallée, "Probabilistic assessment of P/V droop control of PV inverters," in 23d CIRED, 2015.

[7] J.-F. Toubeau, V. Klonari, Z. De Grève, J. Lobry, and F. Vallée, "Probabilistic Study of the Impact on the Network Equipment of Changing Load Profiles in Modern Low Voltage Grids," in ICREPQ'14, 2014.

[8] F. Vallée, F. Moutier, V. Klonari, J. Toubeau, and J. Lobry, "Clustering of Photovoltaic Generation for the Consideration of Time Changing Geographical

Correlation in Probabilistic Analysis of Low Voltage Distribution Systems," in 5th Solar Integration Workshop, 2015.

[9] D. Thomas, V. Klonari, F. Vallée, and C. S. Ioakimides, "Implemantation of an E-bike Sharing System: The Effect on Low Voltage Network using PV and Smart Charging Stations," in 2015 International Conference on Renewable Energy Research and Applications (ICRERA), 2015, pp. 572–577.

2016

[10] V. Klonari, J.-F. Toubeau, J. Lobry, and Vall, "PV integration in smart city power distribution A probabilistic PV hosting capacity assessment based on smart metering data," "*Best student paper"* award in SMARTGREENS, 2016.

[11] V. Klonari, J. Lobry, and F. Vallée, "Adapting Low Voltage distribution tariffs to peak demand Probabilistic assessment of a Low Voltage feeder in Belgium," in BERA Workshop on Demand Response, 2016.

[12] V. Klonari, B. Meersman, D. Bozalakov, T. Vandoorn, J. Lobry, and F. Vallée, "Probabilistic Assessment of a Voltage Unbalance Mitigation Scheme implemented by Photovoltaic inverters," in Energycon, 2016.

[13] D. Thomas, V. Klonari, F. Vallée, O. Deblecker, and C. S. Ioakimides, "Effect of electric vehicles' optimal charging-discharging schedule on a building's electricity cost demand considering low voltage network uncertainties," in IEEE PES Innovative Smart Grid Technologies Conference Europe, ISGT Europe, 2016.

[14] J.-F. Toubeau, M. Hupez, V. Klonari, Z. De Greve, and Vallée, "Statistical Load and Generation Modelling for Long Term Studies of Low Voltage Networks in Presence of Sparse Smart Metering Data," in IECON, 2016.

[15] V. Klonari, A. Orfanos, J. Lobry, and F. Vallée, "Probabilistic assessment of a distribution tariff scheme for incentivizing demand side management in the small energy usage sector," in IEEE PMAPS, Beijing, 2016.

[16] V. Klonari, B. Bakhshideh Zad, J. Lobry, and F. Vallée, "Application of Voltage Sensitivity Analysis in a Probabilistic Context for Characterizing Low Voltage Network Operation," in IEEE PMAPS, Beijing, 2016.